HELLENIC REPUBLIC

UNIVERSITY OF IOANNINA

SCHOOL OF ENGINEERING

DEPARTMENT OF MATERIALS SCIENCE AND ENGINEERING

Durability of multi-scale reinforced epoxy composites

Baltzis Dimitrios, MSc Materials Engineer

Ioannina, Greece 2021

ΕΛΛΗΝΙΚΗ ΔΗΜΟΚΡΑΤΙΑ

ΠΑΝΕΠΙΣΤΗΜΙΟ ΙΩΑΝΝΙΝΩΝ

ΠΟΛΥΤΕΧΝΙΚΗ ΣΧΟΛΗ

ΤΜΗΜΑ ΜΗΧΑΝΙΚΩΝ ΕΠΙΣΤΗΜΗΣ ΥΛΙΚΩΝ

Ανθεκτικότητα Σύνθετων Υλικών Ενισχυμένων σε Πολλαπλή κλίμακα

Δημήτριος, Μπαλτζής, MSc Μηχανικός Υλικών

Ιωάννινα, 2021

«Η έγκριση της διδακτορικής διατριβής από το Τμήμα Μηχανικών Επιστήμης Υλικών της Πολυτεχνικής Σχολής του Πανεπιστημίου Ιωαννίνων δεν υποδηλώνει αποδοχή των γνωμών του συγγραφέα Ν. 5343/32, άρθρο 202, παράγραφος 2».

Application date of Mr. Dimitrios Baltzis: **03.02.2014**

Appointment date for the three-membered advisory committee: **12.02.2014**

Members of the three-membered advisory committee: **12.02.2014**

Supervisor

Alkiviadis S. Paipetis, Professor at the Dept. of Materials Science and Engineering, School of Engineering, University of Ioannina

Members

Angeliki Lekatou, Professor at the Dept. of Materials Science and Engineering, School of Engineering, University of Ioannina

Nektaria-Marianthi Barkoula, Professor at the Dept. of Materials Science and Engineering, School of Engineering, University of Ioannina

Subject appointment date: 12.02.2014

"Durability of multi-scaled reinforced composites"

APPOINTMENT DATE FOR THE SEVEN-MEMBERED ADVISORY: 19.05.2021

COMMITTEE:

1. **Alkiviadis S. Paipetis,** Professor at the Dept. of Materials Science and Engineering, School of Engineering, University of Ioannina,
2. **Angeliki Lekatou**, Professor at the Dept. of Materials Science and Engineering, School of Engineering, University of Ioannina
3. **Nektaria-Marianthi Barkoula**, Professor at the Dept. of Materials Science and Engineering, School of Engineering, University of Ioannina
4. **Theodoros Matikas,** Professor at the Dept. of Materials Science and Engineering, School of Engineering, University of Ioannina
5. **Nikolaos Zafeiropoulos**, Professor at the Dept. of Materials Science and Engineering, School of Engineering, University of Ioannina
6. **Leonidas Gergidis**, Assistant Professor the Dept. of Materials Science and Engineering, School of Engineering, University of Ioannina.
7. **Sotirios Grammatikos**, Professor at the Depart. of Manufacturing and Civil Engineering, Faculty of Engineering, National Technical University of Norway

The Ph.D. thesis was awarded with grade " **Excellent** " at **24/09/2021**

The Head of the Department	**The Secretary of the Department**
Apostolos Avgeropoulos, Professor	**Maria Kontou**

Ημερομηνία αίτησης του κ. Δημητρίου Μπαλτζή: **03.02.2014**

Ημερομηνία ορισμού Τριμελούς Συμβουλευτικής Επιτροπής: 12.02.2014

Μέλη Τριμελούς Συμβουλευτικής Επιτροπής: 12.02.2014

Επιβλέπων

Αλκιβιάδης Παϊπέτης, Καθηγητής του Τμήματος Μηχανικών Επιστήμης Υλικών της Πολυτεχνικής Σχολής του Πανεπιστημίου Ιωαννίνων

Μέλη

Αγγελική Λεκάτου, Καθηγήτρια του Τμήματος Μηχανικών Επιστήμης Υλικών της Πολυτεχνικής Σχολής του Πανεπιστημίου Ιωαννίνων
Νεκταρία-Μαριάνθη Μπάρκουλα Καθηγήτρια του Τμήματος Μηχανικών Επιστήμης Υλικών της Πολυτεχνικής Σχολής του Πανεπιστημίου Ιωαννίνων

Ημερομηνία ορισμού θέματος: **12.02.2014**

" Ανθεκτικότητα Σύνθετων Υλικών Ενισχυμένων σε Πολλαπλή κλίμακα".

ΔΙΟΡΙΣΜΟΣ ΕΠΤΑΜΕΛΟΥΣ ΕΞΕΤΑΣΤΙΚΗΣ ΕΠΙΤΡΟΠΗΣ: **19.05.2021**

1. Αλκιβιάδης Παϊπέτης, Καθηγητής του Τμήματος Μηχανικών Επιστήμης Υλικών της Πολυτεχνικής Σχολής του Πανεπιστημίου Ιωαννίνων
2. Αγγελική Λεκάτου, Καθηγήτρια του Τμήματος Μηχανικών Επιστήμης Υλικών της Πολυτεχνικής Σχολής του Πανεπιστημίου Ιωαννίνων
3. Νεκταρία-Μαριάνθη Μπάρκουλα Καθηγήτρια του Τμήματος Μηχανικών Επιστήμης Υλικών της Πολυτεχνικής Σχολής του Πανεπιστημίου Ιωαννίνων
4. Νικόλαος Ζαφειρόπουλος, Καθηγητής του Τμήματος Μηχανικών Επιστήμης Υλικών της Πολυτεχνικής Σχολής του Πανεπιστημίου Ιωαννίνων,
5. Θεόδωρος Ματίκας, Καθηγητής του Τμήματος Μηχανικών Επιστήμης Υλικών της Πολυτεχνικής Σχολής του Πανεπιστημίου Ιωαννίνων,
6. Sotirios Grammatikos, Professor, Department of Manufacturing and Civil Engineering, Norwegian University of Science and Technology/NTNU,
7. Λεωνίδας Γεργίδης, Αναπληρωτής Καθηγητής του Τμήματος Μηχανικών Επιστήμης Υλικών της Πολυτεχνικής Σχολής του Πανεπιστημίου Ιωαννίνων.

Έγκριση Διδακτορικής Διατριβής με βαθμό «ΑΡΙΣΤΑ» στις **24/09/2021**

Ο Πρόεδρος του Τμήματος **Η Γραμματέας του Τμήματος**

Απόστολος Αυγερόπουλος, Καθηγητής **Μαρία Κοντού**

Στην οικογένεια μου

Abstract

Epoxy resins have proven to be one of the most favourable polymeric materials in modern industrial and commercial applications. Versatility in final properties is the key reason behind such a widespread acceptance of this class of polymeric materials. However, their inherent hydrophilic and insulating nature still pose limitations associated with environmental exposure risks. The combined introduction of carbon conductive phases from different scale sizes, multi-scaled reinforcing approach, has exhibited promising beneficiary results in both the electrical conductivity and the environmental durability capabilities of epoxy based structures.

Based on the aforementioned, this thesis is concerned with the study of epoxy modification using the multi-scaled reinforcement approach. This approach involves the combined inclusion of two types of carbonaceous fillers that belong to different size scales. In the presented efforts, multi-walled carbon nano-tubes (MWCNTs) and milled carbon (MC) were selected as nano- and micron- scaled fillers respectively. The resulting ternary formulations were studied and compared to epoxy, MWCNTs and MC binary ones. Selected material properties were studied according to the end-user application, in both epoxy composites and fibre-reinforced composites (FRCs) composites levels. Hydrothermal exposure studies were conducted and the effect of the multi-scaled reinforcement on durability was benchmarked.

In a parallel study, the capabilities of metallic structures corrosion protection was assessed. Neat, binary and ternary formulations were employed as coatings on aluminium and steel substrates for electrochemical and galvanic current studies. Acoustic Emission measurements were coupled and corrosion monitoring capabilities were investigated.

In the vast majority of the results the ternary composites, outperformed both the neat epoxy and the binary composites. Improvements were observed in electrical conductivity, fracture toughness, tensile strength, shear strength, thermal degradation resistance and glass transition temperature. The detrimental effects of water absorption were less evident in the case of the ternary composites leading to a superior durability compared to neat and binary composites. The ternary composites exhibited greater corrosion protection capabilities regardless the metallic substrate in all electrochemical measurements and was manifested on all of the potential values. The observed results indicated a less active surface, capable of more stable and predictable performance, in the case of the ternary coatings, a pattern that can be associated to the improved durability. The overall performance of the ternary composites was attributed

to the formation of a 3D network of interconnected CNTs and MC particles. A network that was capable to facilitate electrical flow, hinder crack initiation and propagation, restrict chain mobility and more effectively mitigate hydrothermal degradation effects.

AE measurements revealed health monitoring capabilities in all coating formulations and specific indices were correlated with several corrosion phenomena.

Περίληψη

Η παρούσα διδακτορική διατριβή ασχολήθηκε με την μελέτη της επίδρασης της κλίμακας μεγέθους ανθρακικών πρόσθετων, στις τελικές ιδιότητες σύνθετων υλικών με εποξική μητρική φάση. Μέσω προκαταρκτικών μελετών επιλέχθηκαν οι νανοσωλήνες πολλαπλού τοιχώματος και ο άμορφος άνθρακας ως ενισχυτικά πρόσθετα, τα οποία είτε μεμονωμένα είτε συνδυαστικά εφαρμόστηκαν σε αναμείξεις υψηλών διατμητικών δυνάμεων. Πραγματοποιήθηκαν μετρήσεις για μελέτη της επίδρασης της μεθοδολογίας τροποποίησης (μίας ή πολλαπλής κλίμακας), σε εύρος ιδιοτήτων συναρτήσει πρωτόκολλων υδροθερμικής καταπόνησης. Επιλέχθηκε να μελετηθεί ένα εύρος μηχανικών, θερμομηχανικών, ηλεκτρικών και φυσικών ιδιοτήτων ώστε να μελετηθούν τα όρια και οι περιορισμοί της εκάστοτε μεθοδολογίας τροποποίησης τόσο σε επίπεδο ενίσχυσης εποξικού συνθέτου, αλλά και σε επίπεδο μητρικής φάσης σύνθετων υλικών με ινώδη ενισχυτική φάση.

Στην πλειοψηφία των αποτελεσμάτων, η τροποποίηση πολλαπλής κλίμακας, οδήγησε σε σημαντικές βελτιώσεις ιδιοτήτων, ενώ αποδείχτηκε ικανότερη στην μείωση φαινομένων υδροθερμικής καταπόνησης. Χαρακτηριστικά, στην περίπτωση της αντοχής σε διάτμηση τύπου-ΙΙ σε επίπεδο σύνθετου με τροποποιημένη εποξική μήτρα σε πολλαπλή κλίμακα, η αθροιστική αύξηση άγγιξε το 120%, η οποία ήταν και η υψηλότερη βελτίωση στη σχετική βιβλιογραφία κατά την περίοδο των μετρήσεων. Η σημαντικές βελτιώσεις ιδιοτήτων, αποδόθηκαν στην δημιουργία τρισδιάστατου δικτύου σωματιδίων με συνεργιστικά φαινόμενα μεταξύ των διαφορετικών νάνο- και μίκρο- κλίμακας πρόσθετων. Το υβριδικό δίκτυο σωματιδίων το οποίο αποτελείτο από μεμονωμένους νανοσωλήνες, συσσωματώματα νανοσωλήνων μίκρο- και νάνο- διαστάσεων, μικρό-ίνες άνθρακα και άμορφο γραφίτη, εμφανίστηκε πιο αποτελεσματικό συγκρινόμενο με τα μίας κλίμακας αντίστοιχα δίκτυα, στην ενίσχυση ιδιοτήτων όπως δυναμικό ιξώδες, δυσθραυστότητα τύπου-Ι και -ΙΙ.

Σε παράλληλη μελέτη, εφαρμόστηκε η τεχνική Ακουστικής Εκπομπής σε μετρήσεις ηλεκτροχημείας υποστρωμάτων αλουμινίου επικαλυμμένα με εποξικές επικαλύψεις τροποποιημένες σε μία και πολλαπλή κλίμακας μεγέθους, με στόχο τη μελέτη δυνατοτήτων της τεχνικής σαν εργαλείο ελέγχου διάβρωσης. Η τεχνική ακουστικής εμφάνισε ικανότητες σαν εργαλείο ελέγχου καθώς χαρακτηριστικοί δείκτες των σημάτων εμφάνισαν συσχέτιση με χαρακτηριστικές περιοχές και φαινόμενα διάβρωσης.

Acknowledgements

The following paragraphs are dedicated to those that contributed in the realization of this PhD thesis.

Alkiviadis Paipetis, Professor at the Dept. of Materials Science and Engineering (MSE) was my supervisor of my undergraduate diploma thesis back in 2009. 5 years to the future of 2014, he repeated his former mistake and accepted to supervise my PhD thesis thus giving me the opportunity to becoming a PhD student. During the four years of my thesis, I always received more information that I could have possibly requested both in research and career matters. I specially appreciated the freedom in exploring new ideas and research possibilities beyond the strict thesis scope. And last but not least, I will always remember fondly the exquisite British style anecdotes that we shared in front of the frozen faces of my colleagues. As Aretha Franklin and Snoop Dog would say: Respect and a Big Formal shout out Professor Paipetis.

Angeliki Lekatou, Professor at the Dept. of MSE for her participation in my advisory committee and her valuable information on corrosion related issues. I would like to also acknowledge her invaluable contribution to all the manuscript editing actions on our common publications.

Nektaria-Marianthi Barkoula, Professor at the Dept. of MSE for her participation in my advisory committee and her valuable information on thermomechanical related issues.

Nikolaos Zafeiropoulos sincere gratitude for granting me access to the Polymer Engineering Laboratory equipment.

My sincere gratitude to the members of my committee for honoring me with their participation: Leonidas Gergidis, Assistant professor at the Dept. of MSE.,

Bekas Dimitrios, PhD thanks for making me into a human.

Tsirka Kiriaki, PhD always appreciated and a formal thank you for all the assistance inside and outside the Lab environment. A beer is due for consumption.

My gratitude also extends to Apostolos Avgeropoulos, Professor at the Dept. of MSE, Alexandros Karantzalis, Assistant Professor at the Dept. of MSE and to all MSE professors that I had the honor of collaborating.

A formal shout-out to all of the undergraduate and graduate students of MSE that helped in the experimental procedures and especially to: Savvas Orfanidis, George Tzachristas, Spais Vasileios, Dionisis Petikaris, Orestis Evaggelou.

Mrs. Pagona Metou, you should receive the medal of honour form the Queen of England for tolerating me during those years. My wife, mother of my child, love of my life: Thank you.

Mr. Vasileios Baltzis, mrs. Galateia Fili and mrs. Fillitsa Baltzi, my father, my mother, my Sista: None of the presented would be possible without you: Ευχαριστώ.

The current Ph.D. dissertation was partially funded by the European project “Hipocrates” (FP7 2013-2016),

The current Ph.D. thesis was funded by the European project “HIPOCRATES” (FP7 2013-2016)

Project acronym: HIPOCRATES

Project full title: "Self-Healing Polymer for Concepts on self-Repaired Aeronautical composites"

Grant Agreement Number: ACP3-GA-2013-605412

SEVENTH FRAMEWORK PROGRAMME

HIPOCRATES PROJECT · EU

And by the Greek National Business Program “Human resources development, Training and Continuous Learning 2014-2020” supported by

ΕΣΠΑ 2014-2020

ανάπτυξη - εργασία - αλληλεγγύη

Contents

Contents

Nomenclature

Acoustic Emission ()	AE
Aluminum	Al
Aluminum 2024-T3 alloy ()	Al2024
Apparent mean molecular weight between cross links	Mc
Carbon black ()	CB
Carbon fiber ()	CF
Carbon fiber reinforced epoxy ()	CFRP
Carbon nano fibers ()	CNF
Carbon nano tubes ()	CNTs
Critical strain energy release rate,	Gic
Critical-stress-intensity factor ()	Kic
Direct Current ()	DC
Double walled CNTs	DWCNTs
Dynamic mechanical analysis ()	DMA
Dynamic Viscosity ()	DV
End notched fixture ()	ENF
Fiber Reinforced Composites ()	FRC
Flame ignition ()	FI
Flame out	FO
Friction coefficient ()	FC
Glass fiber reinforced composites ()	GFRP
Graphene nano-platelets ()	GNP
Impedance Spectroscopy ()	IS
Linear burning rate ()	LBR
Metal-to-composite ()	MtC
Metal-to-metal ()	MtM
Moed-I fracture toughness	K_{IC}
Mode-II interlaminar fracture toughness	G_{IIC}
Multi walled CNTs	MWCNTs

Rest potential	E_{REST}
Room temperature	RT
Room temperature on the specimen surface time	TR
Scanning Electron microscopy	SEM
Short carbon fibers	SCF
Single edge notched beam	SENB
Single lap-joint	SLJ
Single walled CNTs	SWCNTs
Specific wear rate,	Ks
Stainless steel SS304 alloy	SS304
Strain energy release rate	G_{IC}
Thermally reduced graphene oxide ()	TRGO
Ultimate Tensile Strength ()	UTS
Unidirectional	UD

1. Introduction – Theoretical background

1.1. Problem statement

It is a given fact that epoxy resins, have proven their engineering and commercial value in a wide range of industrial sectors. However, the hydrophilic and insulating inherent nature still pose limitations. High levels of water ingress, lead to plasticization and swelling effects which in turn can result to performance degradation and in extreme case failure of the structure. For example in the case of FRC structures, the absorbed water molecules favour the fibre/matrix interface thus compromising structural integrity. High electrical and thermal resistivity is associated with environmental and safety issues. Electrical insulation can be detrimental in cases of lightning strikes, for example in FRC wind turbine structures, where electrical flow dissipation is limited. Thermal conductivity can be beneficial in extreme weather exposure for de-icing of exposed surfaces.

1.2. Scope of the thesis

Based on the general remarks at the Problem statement section the scope of this thesis is the study of the multi-scaled reinforcing approach towards more durable epoxy composites. Reinforcing fillers that belong to different scale sizes, when simultaneously employed, have given promising results towards improved final properties. It is believed that hybrid networks of particles are formed which introduce a combination of reinforcing mechanisms from the different scale realms. Selection of carbonaceous fillers can simultaneously impart electrical conductivity in the epoxy composite thus tackling one of the most challenging limitations of epoxy resins.

Towards that end carbonaceous fillers from the nano- and micro- scale were introduced in an epoxy matrix for the development of conductive epoxy composites with improved durability and mechanical performance. More specifically, MWCNTs and MC fillers, were introduced in an epoxy resin using optimized dispersion parameters and weight content per filler. The optimized ternary and binary epoxy resins were studied using an extensive range of experimental procedures targeting mechanical, thermomechanical and physical properties in both of the epoxy composite and fibre reinforced composite levels. Selected procedures were repeated combined with hydrothermal exposure tests in order to gain insight on the capabilities for improved durability. In a parallel study, the binary and ternary epoxies were used as coating in metallic substrates. Uncoated and coated specimens were used in electrochemical measurements coupled with Acoustic Emission. This parallel study was focused on two axes.

(i) Explore the anti-corrosive capabilities of the multi-scale approach and (ii) explore the capabilities of AE as a corrosion monitoring tool.

The structure of the thesis is comprised of 7 chapters. Chapter 01 includes the problem statement, scope and the theoretical background of the thesis. Chapter 02 is dedicated to the introduction of all the experimental details including materials used, dispersion parameters and experimental procedures for the epoxy and FRC levels composites. Chapter 03 presents the reference dispersion study and the effect of filler content and dispersion approach on the final properties. The effect of the multi-scale reinforcement on the final properties at the epoxy matrix level, is presented in Chapter 04. On the subsequent Chapter 05, the effect of the multi-scale approach on the durability of epoxy composites is presented. Chapter 06 summarizes the results of the multi-scale approach on the FRC composite level. Finally, Chapter 07 presents the results of the side study concerned with corrosion resistance and corrosion monitoring capabilities of AE.

1.3. Theoretical background

Epoxy resins belong to the class of thermosetting polymeric materials and are defined as low-molecular weight pre-polymers containing more than one epoxide group. Cured epoxy polymers can be found in a wide range of applications spanning from electronic encapsulating materials and protective coatings to matrices for Fibre Reinforced Composites (FRC) for marine or aeronautics structures [1–5]. Their wide range of application fields, stems from the variety of properties that can be achieved by combining several types of epoxy monomers and curing agents [6]. Diglycidyl ether of Bisphenol-A (DGEBA), cycloaliphatic, novolac, tri- or tetra- functional, phosphorous or silicon containing epoxy pre-polymers can be cured by using amine, alkali or anhydride curing agents [7–14]. Depending on the epoxy/hardener pair, flame retardancy, abrasion and/or impact resistance etc. can be achieved [15–23].

In most of the application fields, epoxies are required to operate in demanding and diverse environments enduring sudden temperature variations, water or moisture exposure, particle erosion or magnetic discharge phenomena [24–26]. Consequently, the overall performance of epoxies, would depend on several material properties like abrasion resistance, modulus, toughness, moisture absorption to name few. Despite their extended use in demanding engineering fields their poor electrical and thermal conductivities, still pose limitations. High electrical conductivities can lead to multi-functionality via strain and damage monitoring [27].

Dispersing of conductive nano, micro or macro fillers in epoxy matrices, has proven to be a reliable route towards conductive epoxy based composites. Improved mechanical performance can be simultaneously achieved in most of the cases [28,29]. The introduction of conductive reinforcing fillers can lead to epoxy based composite materials that are simultaneously capable of performing a non-structural and a structural role [30]. Randomly dispersed short carbon fibres, [31] or oriented textile carbon fabrics are some micro and macro scaled alternatives [32]. Single, Double or Multi Walled Carbon Nano Tubes (SWCNTs, DWCNTs, MWCNTs respectively) [33–35] or Graphene (Gr) [36] are some of the nano-scaled fillers [37–39] (**Figure** 1-1).

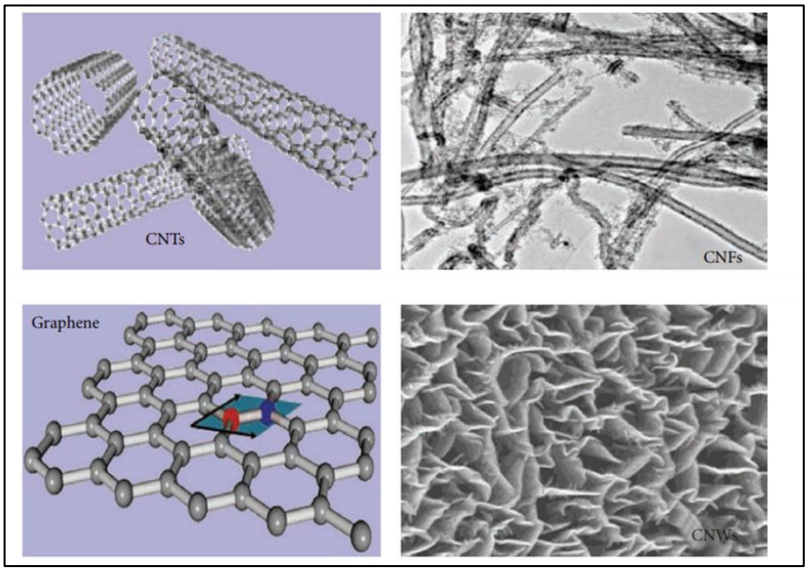

Figure 1-1 Carbon allotropes used as reinforcing fillers in epoxy based composites [40].

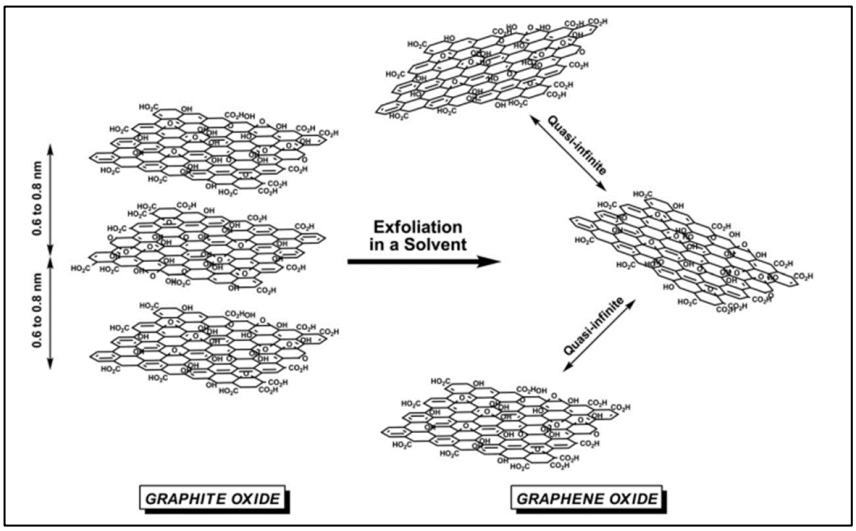

Figure 1-2 Schematic illustrating the chemical structure of graphite oxide (GO) and the structural difference between layered GO and exfoliated graphene oxide (GeO) platelets [41].

Graphene is essentially one sheet of carbon atoms connected in a hexagonal lattice. It is derived from exfoliated graphite structures (**Figure** 1-2). Many research efforts have employed pristine, oxidized and/or functionalized grades towards conductive composites [41]. Vetruccio et. al. [42] developed a flexible graphene film and embedded it to a carbon fibre reinforced epoxy (CFRP) laminate for improved de-icing capabilities. The flexible graphene heater exhibited high thermal and mechanical properties and reduced energy consumption compared to traditional resistance based heating pads. Ahmadi-Moghadam and Taher employed functionalized graphene nano-platelets (GNP) as a reinforcing phase of an epoxy matrix of glass fibre reinforced composites (GFRP) [43]. The functionalized GNP led to

significantly improved interfacial strength in all shear modes. In a similar research effort, Chandrasekaran et.al. performed a comparative study of three different nano-fillers. Fracture toughness and failure mechanisms of epoxy based nano-composites were studied [44]. The thermally reduced graphene oxide (TRGO) filler led to the most pronounced toughening effect followed by GNP and MWCNTs fillers.

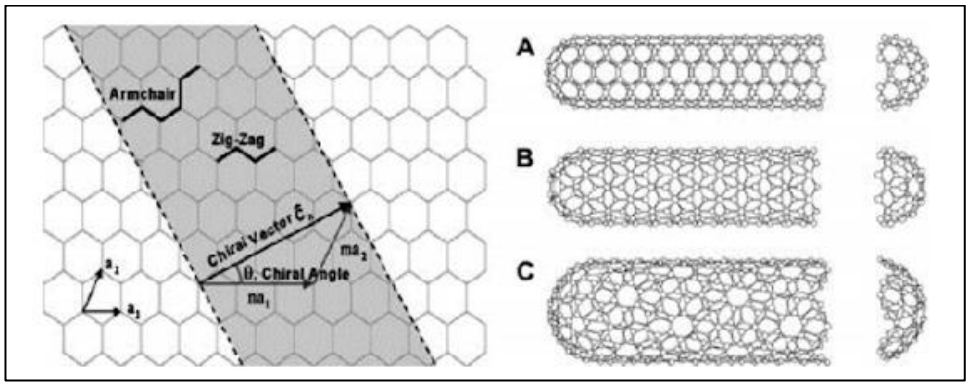

Figure 1-3 Left, one graphene sheet with the chiral vectors and right, types of CNTs based on different vector orientations [1].

Carbon nano tubes (CNTs) were first produced by Sumio Ijima [45] and can be considered as cylinders of rolled graphene sheets, terminated at both ends by fulllerene hemispheres [46]. Various types of CNTs can be obtained depending on the indices of the chiral vectors stemming from the different orientations of the tube axis in respect to the carbon network [29] (**Figure** 1-3). CNT types can be classified in relation to the number of carbon layers in their sidewalls, as single (SW), double (DW) and multi walled (MW) CNTs. Gojny et.al. performed a comparative study amongst the three different types and their effect on the mechanical properties of epoxy based nano-composites [47]. All mechanical properties were affected by the introduction of pristine and functionalized CNTs and the most pronounced increases were seen in the MWCNTs based case. Tensile strength, stiffness and fracture toughness were enhanced by 10%, 15% and 43% respectively. These significant improvements were attributed to the combination of micro- and nano- mechanical toughening mechanisms that are inherited by the matrix phase and CNTs respectively. Plastic matrix deformation, nucleation of voids and crack deflection were attributed to the matrix epoxy phase. MWCNTs introduced crack bridging, particle pull-out and fibre breakage thus enhancing the energy absorption capabilities of the nano-composite. Jakubinek et.al. [48] employed SWCNTs at 0.5%w.w. and 1%w.w, in order to impart electrical conductivity to an aerospace grade epoxy system while maintaining structural bonding performance. Significantly higher conductivities were achieved for the nano-composite with 1%w.w SWCNTs with a simultaneous 30%

increase in peel-strength. Gojny et. al. [49], introduced SWCNTs and carbon black (CB) (**Figure** 1-4), separately in an epoxy matrix in order to enhance the mechanical properties of the epoxy matrix. The results showed that even small amounts of DWCNTs (0.1%w.w.) can lead to improved tensile strength, young modulus and fracture toughness resistance. The effects of MWCNTs on fire retardation and char formation of epoxy coatings under thermal exposure, were studied in [50]. At 0.5%w.w. of MWCNTs loading, the resulting nano-composites exhibited increased char weight with higher carbon content but with lower oxygen. The nano-composites were also found to release less gaseous products during pyrolysis providing an additional safety related advantage.

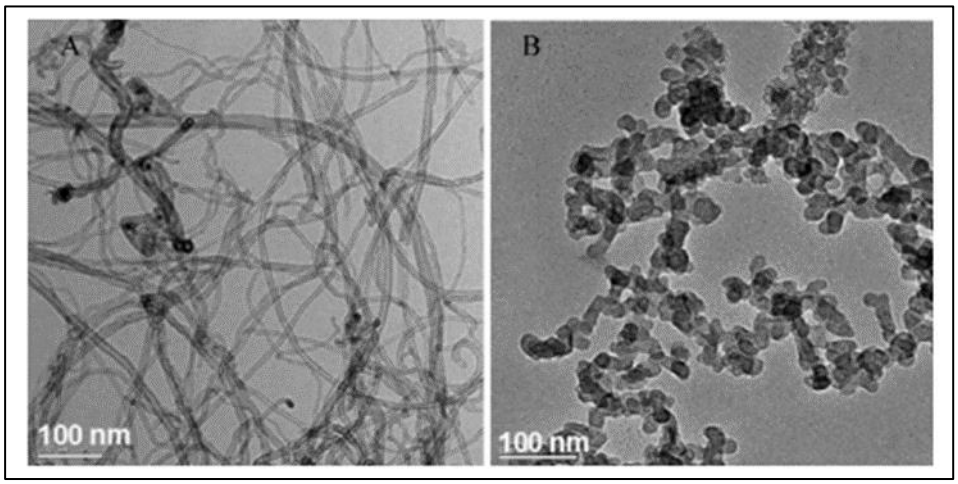

Figure 1-4 Transmission electron microscopy images of MWCNTs (left) and CB (right) agglomerates [51].

Several other filler types have been studied for their feasibility towards epoxy based reinforced composites like graphite or inorganic fillers like alumina particles, rubbers spheres etc, [52,53]. The resulting beneficiary effect is greatly dependent on the dispersion efficiency of the fillers which, in its turn, is dependent on various factors like the dispersion method, duration and intensity [54–56]. An effective dispersion technique, should be able to break down the agglomerates, preferably down to the level of individual particles but without inducing any degradation to the matrix or reinforcing phase. Various techniques like ultra-sonication [57], ball milling [58], roll milling [59] or high shear force mixing [60] have been successfully employed in order to provide homogeneous mixtures. Each one has unique advantages and disadvantages depending on the final application. Ultra-sonication can provide significantly even and stable suspensions, but high intensities and durations can lead to matrix thermal degradation or particle breakage at the sonication tip especially for high viscosity mixtures. Three roll milling has also been successful in providing even deagglomaration and distribution

however due to roll gap limitations, multiple passes are required for nano-scaled dispersion results.

Due to the inherent hydrophilic nature of epoxies, moisture and water ingress uptake has always been a disadvantage. It is generally accepted that epoxies tend to absorb water within the free volume of the polymeric network [61]. In general, two types of water can be observed in epoxies upon absorption: (i) unbound free water, which fills the nano-voids not inducing swelling referred to as type-I water and (ii) hydrogen-bonded water, which causes swelling of the polymers and referred as type-II water [62]. In most of the epoxy formulations, the moisture absorption follows a Fickian pattern where two stages of absorption behaviour are observed [63–66]. During the initial absorption stage, the ingress of water increases linearly with time until a saturation point, related to the free volume of the polymer. At this point, stage-2 absorption is initiated and the ingress of water slows down mainly due to swelling effects. During stage-2, type-II water molecules create hydrogen bonds with unreacted epoxy rings resulting in further swelling of the polymer thus leading to performance degradation [61]. In FRP composites water absorption takes place either at the locus of the matrix micro-cracks or at the fibre-matrix interface. Diffusion to the surrounding polymer network through unreacted polymeric chains is the latter mechanism [67,68]. The increased free volume in highly cross-linked epoxy systems tends to result in higher type I water absorption at the early stages of exposure[69][70]. The ingress of water ultimately, leads to detrimental effects on both of the mechanical and physical properties. It has been observed that water uptake can cause secondary curing reactions, also known as pseudo-cross-linking, leading to improved or unaltered properties depending on the absorption stage [71].

The introduction of carbonaceous fillers, has been shown to be beneficiary in both reducing the water ingress and mitigating the detrimental effects of water ingress [72–74]. It is believed that, the reinforcing fillers, tend to fill the free volume of the polymeric chain network, thus introducing more tortuous paths for the water molecules ingress [75]. CNTs or graphene, can facilitate epoxy cross linking reactions by bridging unreacted polar molecules thus toughening the epoxy matrix and counterbalancing the detrimental effects of water ingress [76].

In recent years, a multi scale reinforcing approach has been introduced to the epoxy based nano-composites field [77–80]. This approach involves the introduction of multiple reinforcing phases of different scales exploiting the benefits of all scales [81]. It has been assumed that the combined inclusion of the different fillers lead to a more dense and robust 3D

particle network. Especially in cases with conductive fillers, the interconnections provide additional current flow paths and effectively hinder and delay crack initiation and propagation [51].

Following this approach, Ravidan et.al. used carbon nano fibers (CNF) and short carbon fibers (SCF), independently or in combination, and studied their effect on fracture properties [82]. Both fillers were effective in enhancing the fracture toughness but the combination led to a 20 fold increase in mode-I fracture toughness. The results were attributed to intrinsic and extrinsic toughening mechanisms like fibre/matrix interfacial debonding, fibre crack bridging, snubbing (for the SCFs), fibre pull-out and rupture.

Synergistic effects amongst fillers particles have been observed in the electrical conductivity of multi scaled composites. Introduction of small amounts of GNP in MWCNTs epoxy resins, have led in electrical conductivity values superior to the binary composites, (binary composite is a composite with a matrix and only one reinforcing phase) [83]. The combination of CNTs and GNPs, have also proven to be effective in providing superior mechanical properties [84]. In [85], improved tensile and flexural were achieved by exploiting synergistic effects between the 1D GNPs and 2D MWCNTs. A multi-scaled reinforced epoxy was used in CFRP laminates and interlaminar shear strength was assessed. It was found that GNPs were entangled by the CNTs particles and effectively filled the interlayer gaps. A denser 3D particle network capable of deterring and delaying crack initiation and propagation was observed. Combining of alumina nano particles with short carbon and glass fibre have resulted to superior wear and friction resistance by promoting matrix/fibre bonding interactions [86]. Novel nano-composites reinforced with CNTs and CB, with enhanced electrical conductivity and balanced mechanical properties, were developed in [87]. Wichmann et.al., introduced SW- and DW- CNTs in the epoxy matrix of GFRP laminates manufactured via resin transfer molding. The laminates exhibited an almost unaffected interlaminar toughness but increased interlaminar shear strength and relatively higher electrical conductivity [88].

2. Experimental Methods

2.1. Materials

Primer coating over chromate anodized aluminium alloy 2024-T3 (Al 2024) and stainless steel SS304 strips were used for the single lap-joint metal to metal, metal to composite specimens and as substrate material for electrochemical measurements.

Al2024 substrates were used in as received, anodized and epoxy coated forms. The as received state indicate that the aluminium substrates were sanded, cleaned and tested. In the anodized state, as-received specimens were surface treated according to ASTM D 3933 without the surface sealing step. The substrates were then tested so as to simulate a "failure type" scenario where a protective coating is ruptured exposing the underlying anodization film. In the epoxy coated specimens, anodized specimens were further coated with a series of epoxy coatings. More specifically, the epoxy coatings were neat epoxy and reinforced with CNTs, MC and Ternary at 0.5%, 2.0 and 0.5-2.0% w.w. respectively denoting the neat, CNTs, MC and ternary specimens respectively.

A two part low viscosity epoxy resin was used, i.e. resin LY5052 and hardener Aradur 5052, both provided by Huntsman Advanced Materials at a mix ratio of 100:38 %w/w. According to the manufacturer, a typical curing cycle for optimum final mechanical properties consists of curing at 23^0C for 24 hours and post curing at 100^0C for 4 hours.

Graphistrength C100 MWCNTs provided by Arkema, France, were selected as the reinforcing phase for the nano-composites. The diameter of the MWCNTs ranges between 10 to 15nm while the length ranges from 1 to 10μm. The nanotubes were provided in the form of agglomerated bundles with average diameter of 400μm ranging from 50 to 900μm.

MC was selected as the secondary reinforcing filler comprising of spherical graphite particles and chopped micro-carbon fibres. Unidirectional (UD) carbon fabrics (CF) with an aerial density of 210 gr/m^2 and UD glass fabrics with aerial density of 180 gr/m2 were employed for the FRC laminates manufacturing.

2.2. Dispersion methods

The nano- and micro- scaled fillers were introduced in the host resin using a Dispermat AE dissolver (**Figure** 2-1). The apparatus was equipped with a double walled steel bucket with water circulation for stable temperature within $\pm3^0$C. All dispersions were conducted under vacuum conditions. Two dispersion modules were used (i) a bead mill module and (ii) an

impeller disk shaft. For detailed presentation of the modules, the reader is referred to the appendix section.

Figure 2-1 Dissolver Dispermat mixer (top left), the bead mill module (top right) and the impeller disk module (bottom).

2.3. Test methods - Epoxy resin composite level

The epoxy formulations in all presented test methods, were processed using the following steps:

(i) Filler dispersion in the epoxy resin

(ii) Hand mixing of the hardener and epoxy formulation at 38:100 weight ratio.

(iii) Degassing for 10'in a vacuum oven at 30^{O}C.

(iv) Application of the degassed mixture as adhesive, coating, or matrix material for specimen production.

(v) Curing (24hrs @ 25^{0}C).

(vi) Surface and edge processing in a laboratory grinding apparatus (up to 1000grit) in order to ensure dimensional stability and eliminate any surface defects

(vii) Post curing for 4hrs at 100^{0}C.

2.3.1. Adhesive shear strength

The effect of CNTs on the adhesion efficiency was studied using the SLJ specimen geometry, according to on ASTM D 5868-01 and ASTM D 1002. Strips of either metallic or FRC substrates were bonded in a SLJ configuration employing neat and nano modified LY5052 resin as adhesive films approximately 0.20±0.01mm thick. After the application of the thin films on the strips, the assembled specimens were cured at the recommended curing cycle on heated pressure plates under 5bars of pressure using spacers to ensure a uniform thickness on the entire bonded area (25x25mm). Subsequently the specimens were tested under tensile loading on an Instron universal machine, series 5900 using 1.3mm/min extension rate till fracture (**Figure** 2-3).

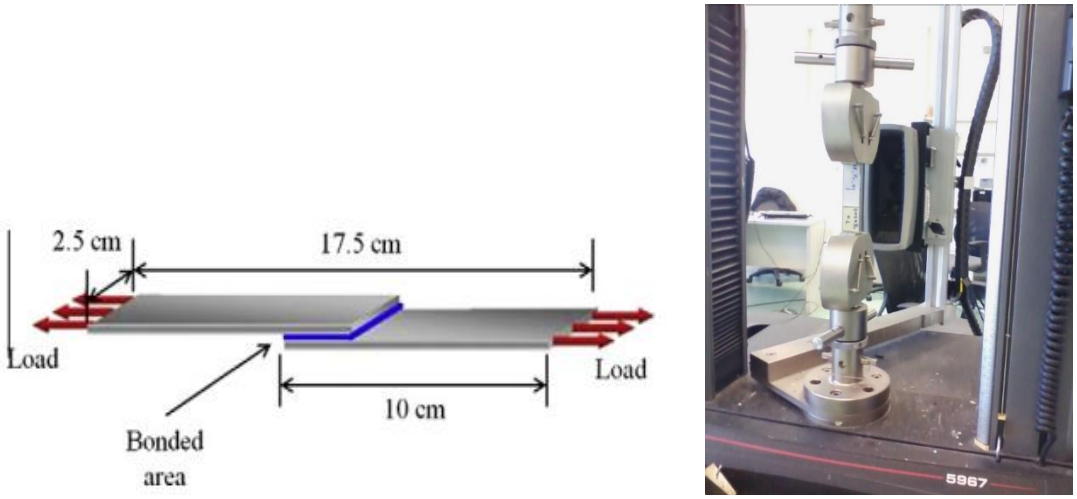

Figure 2-2 Specimen configuration for the adhesive strength measurements (left) and the tensile testing machine (right). .

2.3.2. Single edge notched beam (SENB) mode-I fracture toughness

In this study, the 3 point bending on SENB fracture toughness test according to ASTM D 5045 [89] was adopted. Extension rate was set at 1mm/min while the starter crack length was 5.70±0.20 mm (**Figure** 3-2). Critical-stress-intensity factor, K_{Ic}, and energy per unit area of crack surface or critical strain energy release rate, G_{Ic}, at fracture initiation values were calculated, according to **Equation**s (3-1) and (3-2), for all dispersion specimens.

$$K_{IC} = \frac{P_{max}}{B\,W^{\frac{1}{2}}} f(x) \qquad \textbf{Equation } (3\text{-}1)$$

$$G_{IC} = \frac{U}{BW\varphi} \qquad \textbf{Equation } (3\text{-}2)$$

Where: P_{max} is the maximum load in N, B is the specimen thickness in mm, W is the specimen width in mm, U is the corrected energy under the load vs deflection curve and f(x) and φ are calibration factors dependent on the a/W ratio where a is the crack length.

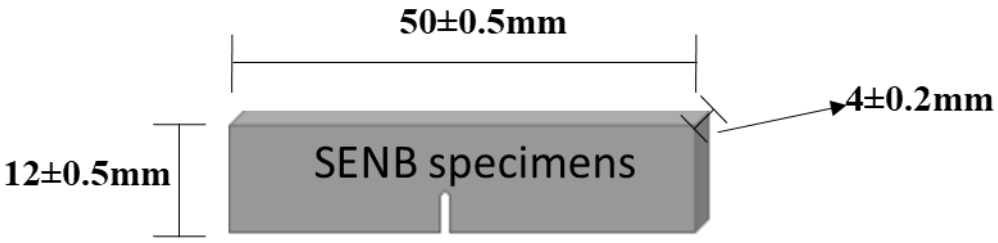

Figure 2-3 SENB specimens' dimensions

2.3.3. Sliding wear rate

Dry tribological measurements were conducted on pristine and aged specimens (**Figure** 2-4) employing the CSM ball-on-disk tribometer with sliding distance of 1000 m, AISI 5210 counter-body steel ball with Ø6 mm, sliding speed of 10 cm/s, normal load of 4 N and absence of lubricating agent. The specific wear rate, K_s (cm^3/Nm), was calculated according to **Equation** 3-3 [90].

$$K_s = \frac{\Delta m}{\rho} \; x \; F_N \; x \; L \qquad \textbf{Equation } 3\text{-}3$$

where Δm, ρ, F_N and L are the mass loss (mgr), density (gr/cm^3), normal load (N) and total sliding distance (m), respectively. FC mean values were obtained from FC vs sliding distance curves. The roughness of the worn surfaces was measured using a Tesa-Rugosurf 20 profilometer, along various lines perpendicular to the wear track.

Figure 2-4 Sliding wear rate specimen shape and dimensions (left) and the CSM ball-on-disk tribometer apparatus (right).

2.3.4. Scanning Electron microscopy (SEM).

All SEM images that are presented, were obtained using a JEOL JSM 5600 Scanning Electron Microscope equipped with an EDS (Energy Dispersive Spectrometry) detector. All specimens were coated by a thin layer of Au/Pd (5 nm) prior to the SEM analysis to limit charging.

2.3.5. Dynamic Viscosity (DV)

A Brookfield DV-1 type viscometer was used with a set of spindles capable of measuring a dynamic viscosity range of 0.001Pa.s to 100000Pa.s (**Figure** 2-5). The measurement process involved application of the appropriate spindle on the viscometer according to the expected viscosity range. Subsequently, the viscometer spindle was submerged to the liquid suspension inside the dispersion bucket so as to ensure temperature stability. DV measurements in mPa.s., were recorded for 1' at each shear rate to ensure repeatability of values.

Preliminary measurements were taken for the neat epoxy resin at three different temperatures (23^0C, 28^0C, 31^0C) and will be presented. The recorded values were compared to the materials technical datasheet for measurement repeatability and Newtonian fluid characteristics validation.

Figure 2-5 Brookfield DV-1 type viscometer.

2.3.6. Impedance spectroscopy

2.3.6.1. Theoretical considerations (IS)

Impedance Spectroscopy (IS) is a non-invasive electrochemical technique where a monochromatic signal $V_t = V_o cos\ (\omega t)$, involving the single frequency f=ω/2π, is applied to the material under test and the resulting output signal of the same frequency is measured. This resulting steady state current is described by the function, $I_t = I_o cos\ (\omega t + \varphi)$, where φ is the phase difference between the voltage and the current. In detail, the total impedance of the system (Z) can be calculated using a form similar to Ohm's law for Direct Current (DC): $Z = V_t/I_t$. The impedance can be represented as a complex number with a real and an imaginary part: with $Z' = |Z|co(\varphi)$ and $Z'' = |Z|sin\ (\varphi)$ where Z' and Z'' is the real and the imaginary parts of the complex impedance respectively. It is evident that at a given frequency range, phase difference φ is directly affected by the nature of the dominant conductive element. For a purely resistive material φ=0 and the total impedance is then represented only by the real component. On the other hand, when the material's response is that of a capacitor, φ = -90^0 while the total impedance lacks real part ($Z = Z''$).

When an electric field is applied across a parallel plate capacitor containing a dielectric material, several atomic and molecular charges in the dielectric are displaced from their equilibrium positions resulting in a polarized material. There are several polarization mechanisms that may occur during this interaction including electrode polarization (EP), dipole orientation, free change migration (intrinsic and/or extrinsic), and the interfacial polarization in heterogeneous or composite systems. The interfacial polarization mechanism occurs due to the accumulation of free charges at the interface between two phases with different dielectric properties and its manifested by a single peak at intermediate frequencies of the imaginary part spectra. Therefore, the principle objective of this study was to monitor and accesses the effect of the dispersion conditions, of the conductive fillers (CNTs and MC), on the interfacial polarization mechanism that take place within the composite during its interaction with an external electric field.

2.3.6.2. IS measurements

IS was performed at room temperature using a dielectric spectrometer-frequency spectrum analyzer (DETA SCOPE L1 provided by Advise Ltd.). For the purposes of the impedance measurements, specimens (52x12x4mm) were placed between two aluminium plates so that the plates completely covered the sides of the nano-composites (**Figure** 2-6). The aluminium (Al) plates with dimensions of 14 x 12 x 1 mm^3 were held on the specimen sides using mechanical grips, thus eliminating any entrapped air between the electrodes and the material.

The spectrometer applied a sinusoidal electrical excitation waveform of varying frequency while the induced current waveform was recorded. The excitation frequency ranged from 10^{-1} Hz to 0.5 MHz while the voltage amplitude was set at 10 V. The selection of a relatively high voltage amplitude was based on the increased resistivity of the epoxy resin and the relatively high thickness of the materials under test. During the IS measurements, a thermocouple was attached to the specimen surface in order to ensure that the employed high voltage did not result in temperature increase.

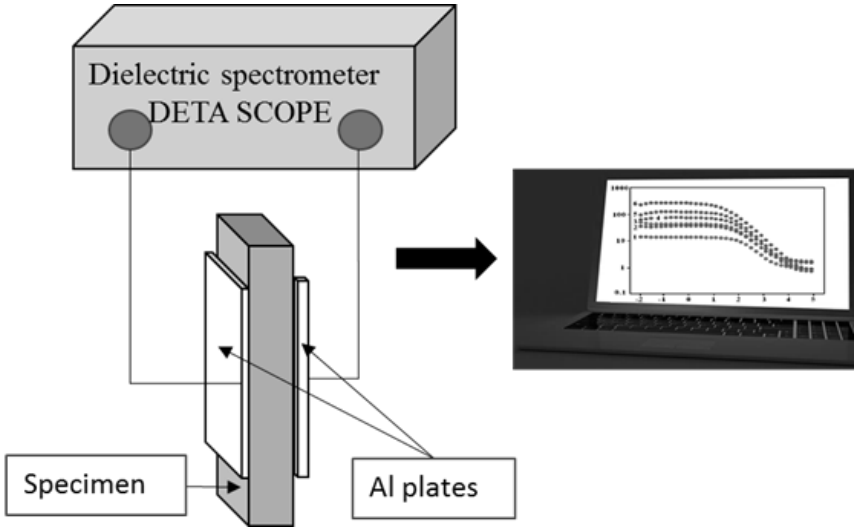

Figure 2-6 Experimental setup for the Impedance spectroscopy measurements.

2.3.7. Dynamic mechanical analysis (DMA)

DMA tests were performed on a Q800 DMA (TA Instruments) in dual cantilever mode. Rectangular specimens (60 mm x 10 mm x 3 mm, **Figure** 2-7 DMA rectangular specimens dimensions.) were prepared with the same group types as in 2.3.4, and tested using a frequency of 1 Hz and an amplitude of 15 mm. A temperature range from 25^0C to 185^0C with a heating rate of 2 ^{0}C /min was studied and determine, storage modulus (E') and tangent delta (tand) vs temperature plots were made for all specimens. From the plot analysis the glass-transition temperature (Tg) and apparent mean molecular weight between cross links (Mc) was calculated for all specimen types according to **Equation** 3.5 [19,91].

$$\mathbf{E_R = 3(d/Mc)RT_{ER}} \qquad \textbf{Equation } 3\text{-}5$$

Where E_R, d, Mc, R and T_{ER} is the rubbery plateau modulus, density of the epoxy, universal gas constant and temperature of the E_R plateau according to **Figure** 3-13.

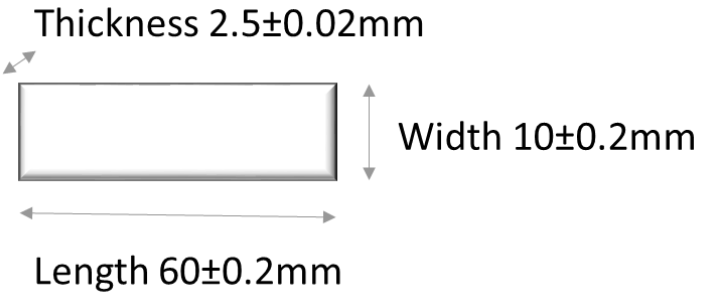

Figure 2-7 DMA rectangular specimens dimensions.

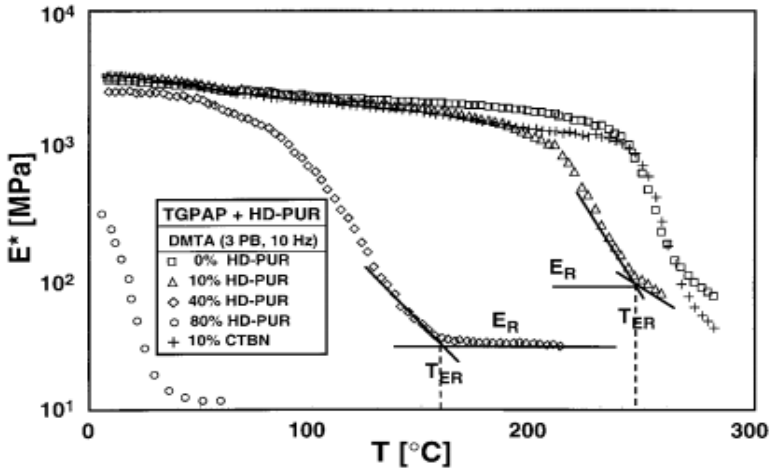

Figure 2-8 Storage modulus vs temperature curve and the charastectic values for the Mc calculation [91].

2.3.8. UL 94 Linear burning rate (LBR)

LBR testing according to ASTM D 635 was conducted on an in-house manufactured device a schematic of which is shown in **Figure** 2-9. Temperature profiles for the specimens were recorded with a FLIR IR E50 thermal camera and the testing procedure involved the following process: An open propane flame was brought in touch with the tip of a rectangular specimen in the horizontal position for 60'' or until the flame reached mark a. At this point the propane flame was removed from the combusted specimen and time measurements ended when flame was out. After the measurements, the IR videos were analyzed in order to note the "flame ignition" (FI), "flame out" (FO), "room temperature on the specimen surface" (T_R) time signatures for all specimens. The total specimen burned length was also recorded so as to calculate the LBR values in cm/min. A low LBR is preferred as it indicates that a small length of specimen has been charred for an extended amount of time.

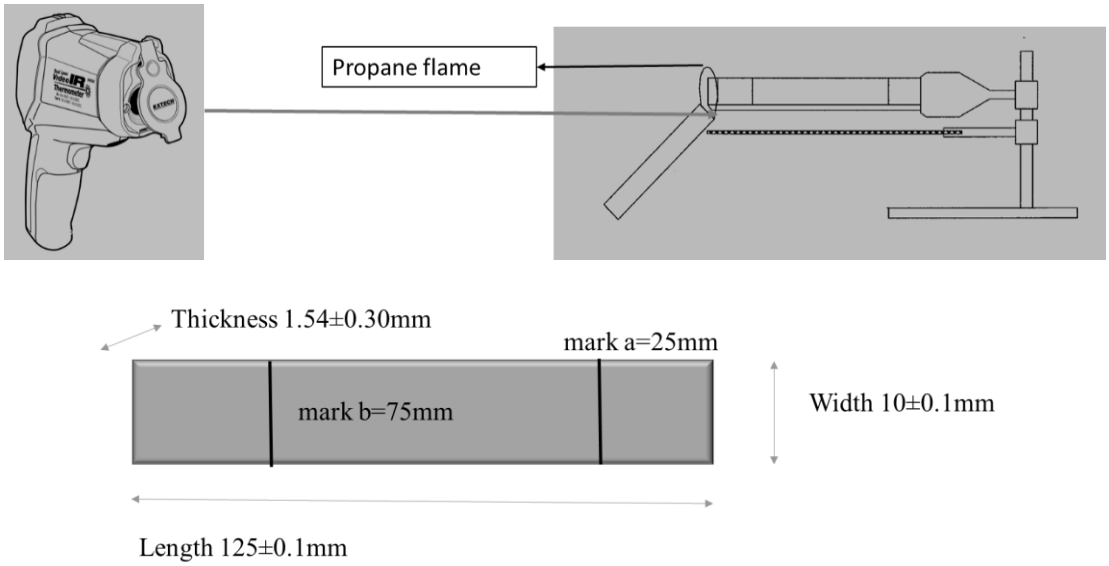

Figure 2-9 Linear burning rate time and temperature schematic representation (top) and specimen dimensions (bottom).

2.3.9. Electrochemical

2.3.9.1. Specimens.

Small rectangular metallic coupons were cut with a diamond saw under wet conditions. The rectangular coupons, were either, anodized or coated with neat and nano modified resins and after curing, a copper wire was attached on the back surface. the assembly was encapsulated in vacuum bag sealant tape and PTFE, leaving a front side surface area of approximately 1 cm^2 to be exposed to aerated 3.5%w/w NaCl solution, at room temperature (RT) (**Figure** 2-10).

2.3.9.2. Potensiodynamic cyclic polarization

All electrochemical tests were performed using the Gill AC potensiostat/ galvanostat by ACM Instruments. A standard three electrode cell was employed, with Ag/AgCl (3.5 M KCl, E_{AgCl} = E_{SHE} 200 mV) as the reference electrode and a platinum gauge as the counter electrode. The specimens were connected to the working electrode of the instrument while potensiodynamic polarization tests were carried out at a scan rate of 10 mV/min ranging from -1500mV to +1500mV in regards to the recorded rest potential, E_{rest}. E_{rest} was determined after 2 h of immersion in 3.5% NaCl, at room temperature (RT). Reverse polarization tests were conducted to study the susceptibility of the systems to localized degradation. Corrosion current densities were determined by Tafel extrapolation, as described in [29].

2.3.9.3. Galvanic current density

In addition, the galvanic current density values were recorded. for pairs of were measured and used as baselines for the two types of metallic substrates. The measurement involved the connection of the reference specimen (anodized Al2024 or sandblasted SS304) to the working electrode 1 (WE1) input of the galvanostat and the connection of the modified coated specimen to the working electrode 2 (WE2). The positive or negative galvanic current values, indicated the anodic or cathodic behaviour of WE1 on the WE2. The electrolyte provided a means for ion migration, whereby metallic ions moved from the anode to the cathode. Positive current density denoted the movement of the metallic ions from the anode to the cathode.

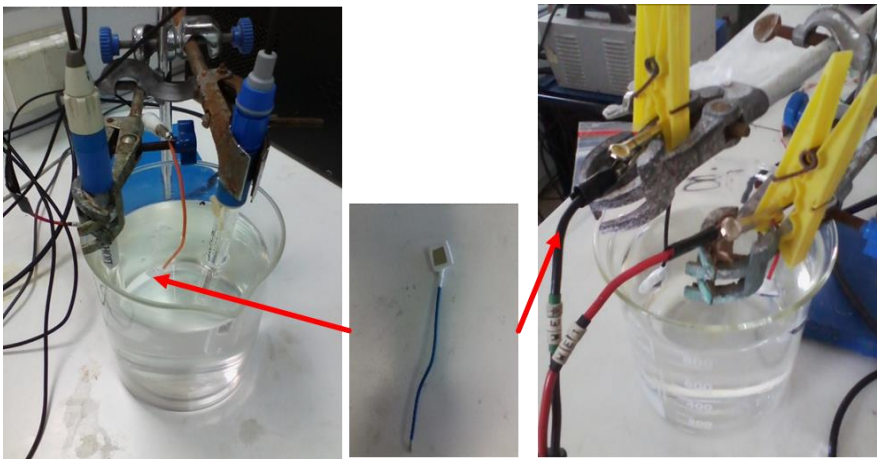

Figure 2-10 Cyclic potentiodynamic sweep set-up (left), electrochemical measurements indicative specimen (middle) and galvanic current set-up (right).

2.3.9.4. AE emission and Electrochemical coupled tests.

The electrochemical test methods were also conducted coupled with AE measurements. At the back side of the specimens, a Pico Acoustic emission (AE) sensor provided by Enviroacoustics was placed using ultrasound coupling gel (**Figure** 2-11). The sensor was connected to a Mistras group preamplifier with 40db pre-amplification and threshold. AE was recorded and post processed using the AEWin software. A schematic representation of the experimental set up can be found in **Figure** 2-12

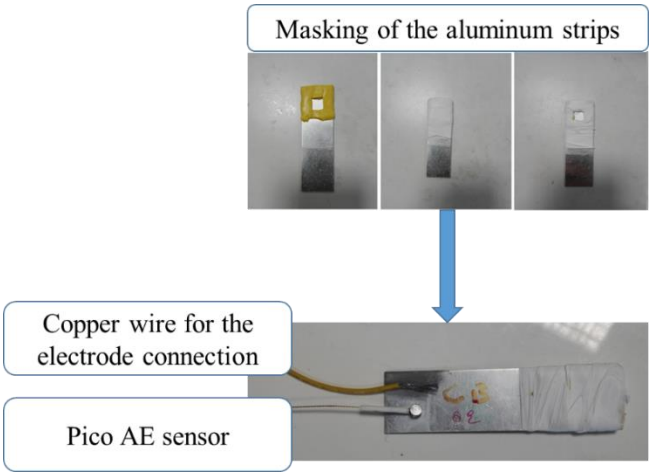

Figure 2-11 Aluminium strips process towards specimens manufacturing

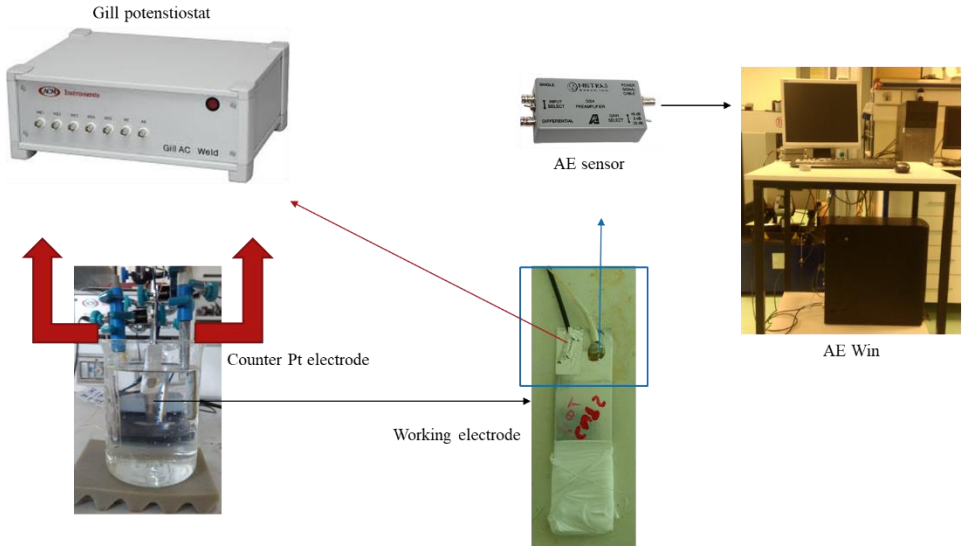

Figure 2-12 Experimental set up.

2.3.10. Water immersion

Neat and modified specimens were immersed in a water bath at a controlled temperature of 50 ± 2^0 C. Periodically the specimens were removed from the water bath, wiped with a cotton cloth and weighed at a high precision scale (±0.0005g) in order to monitor the water ingress Water immersion was terminated after 66 d, where a stabilization of the mass increase was observed and all specimens were extracted from the water bath. A first group of neat and modified specimens were wiped with a cotton cloth, weighed and sealed by a polyethylene stretch film until testing. A second group was wiped, weighed and then treated in an oven at 25 ^{O}C while being periodically weighed for 30 d, so as to record the water desorption profiles. All specimens that were not subjected to water immersion will be denoted hereafter as

"Pristine"; those tested after water immersion as "Aged" and those treated in an oven as "Conditioned". From the early stages of the absorption profiles, where the diffusion process is described by Fick's law, the diffusion coefficient D_F was calculated based on **Equation** 3-6 [19,92].

$$D_F = slope^2 \, x \, (\frac{\pi a^2}{16 W_\infty^2})^{1/2} \qquad \textbf{Equation } 3\text{-}6$$

Where a and W_∞^2 are the thickness (in mm) of the specimen and the % water uptake after saturation, respectively, while the slope is calculated from the initial linear part of the water absorption profile.

2.3.11. Anodization process

All aluminium substrates that were used in the as-received and coated states, were processed according to ASTM 3933 [93] in order to create anodization films of aluminium oxide (Al_2O_3). A 5% NaOH at 40±1^{0}C and a HNO_3 50%w.w. at room temperature ±1^{0}C solutions were used for the alkaline and nitric acid surface cleaning in order to eliminate surface contaminations and prepare the surfaces for the anodization process. Multi rack phosphoric anodization process involved submersion of the specimens (positive electrode) in a metallic bath (negative electrode) with a H_3PO_4 10%w.w. solution at 43±1^{0}C. A current generator was used to apply a 15V potential for 30' in order to create films of 25±1μm thick. For the cases of the coated specimens, the anodized strips where cleaned using deionized water, dried in an oven at 80±1^{0}C for 30', left to cool to room temperature and subsequently were coated using neat and modified epoxies. For the cases of the anodized specimens, anodized strips were immersed in fresh clean water at 43±1^{0}C so as to seal the surface oxide film pores, towards improved weathering resistance. A summary of the preparation and the anodization of the aluminium substrates can be found in 2.3.11.

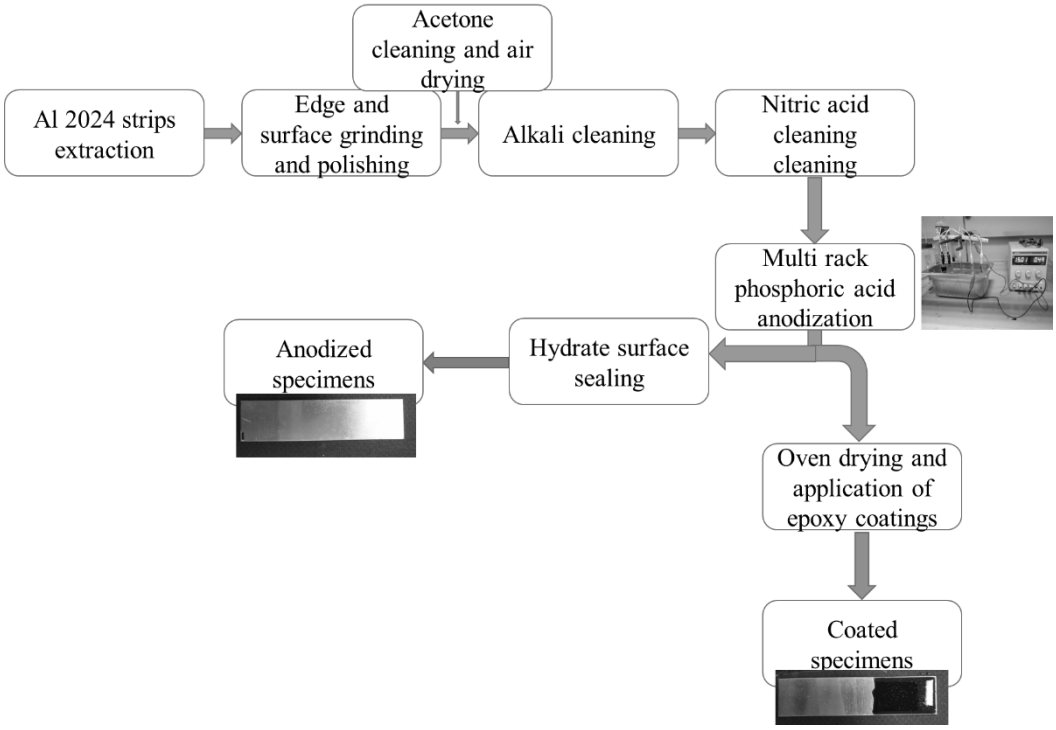

Figure 2-13 Manufacturing process step flow for the preparation of the aluminium substrates

2.4. FRC level test methods

2.4.1. Tensile strength (ASTM D3039)

Tensile testing was conducted according to ASTM D 3039 using an extension rate control of 2.0mm/min for all specimen configurations on a universal tensile tester (**Figure** 2-15). Rectangular specimens with 25x150mm dimensions (**Figure** 2-14) were cut from the manufactured laminates. 25mm end tabs were bonded on each side of the specimens for stress concentration reduction at the grip areas, leaving an effective specimen length of 100mm.

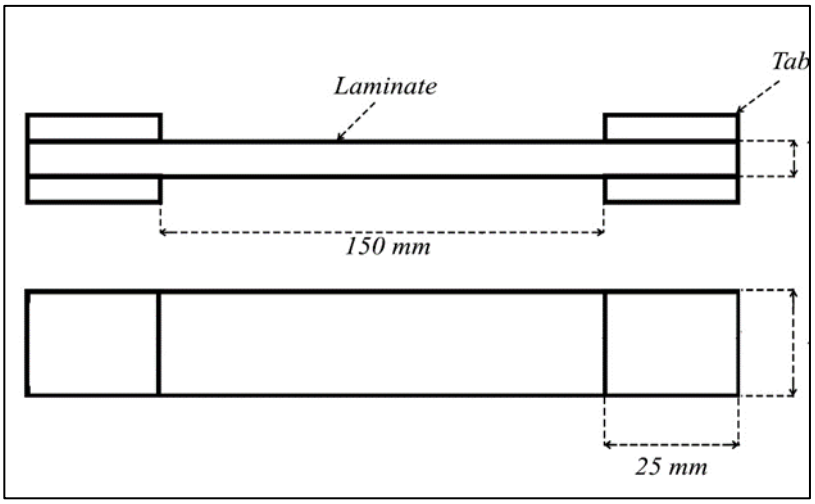

Figure 2-14 Schematic representation for the tensile strength specimens with the end tabs bonded.

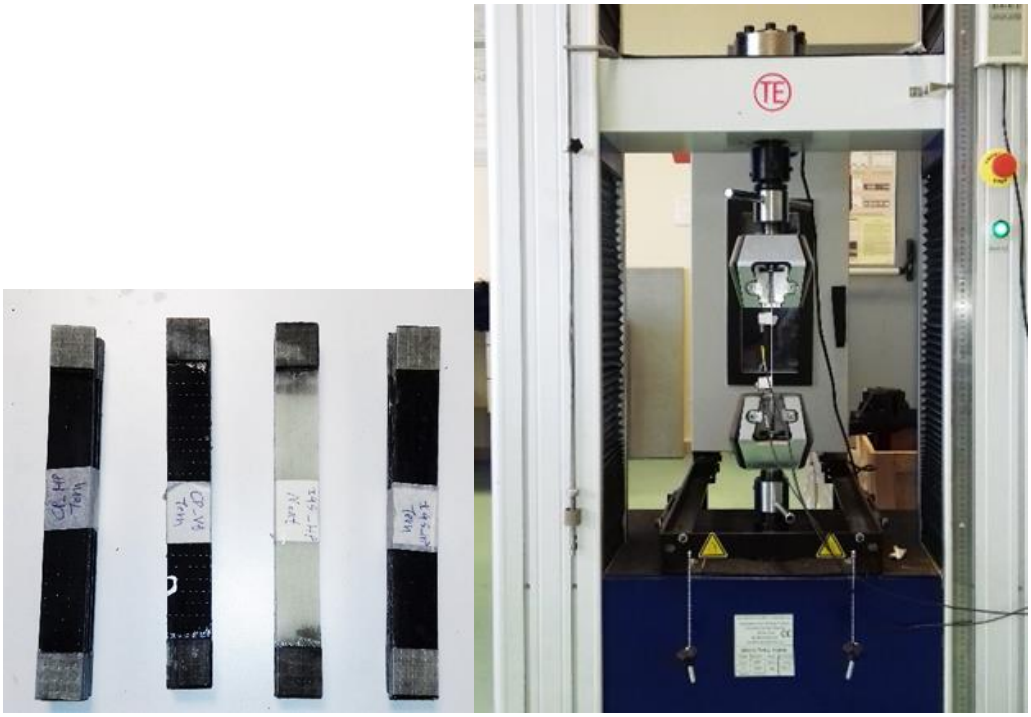

Figure 2-15 GFRP tensile specimens with neat and ternary modified epoxy matrix (left) and the tensile testing machine (right).

2.4.2. Mode-II fracture toughness

All mode-II tests were conducted using the ENF specimen configuration [4–8]. The ENF specimen (**Figure** 2-16), is comprised of UD glass fibres with a 125μm Teflon insert placed at the edge mid-plane of the laminate to act as stress concentration point. The specimen was positioned in a 3-point bending fixture and load is applied. During loading shear stresses build up at the Teflon insert tip up to a critical mode-II crack initiation load. Load vs displacement data were recorded and mode-II interlaminar fracture toughness (GIIC) was calculated according to **Equation** 3-4.

$$G_{IIC} = \frac{9P^{c}\delta\alpha^{2}}{2W(2L^{3}+3a^{3})} \qquad \textbf{Equation } 3\text{-}4$$

Where:

- P_c = load at crack initiation
- δ = displacement at crack initiation
- a = crack length
- W= specimen width

- L = specimen half-span

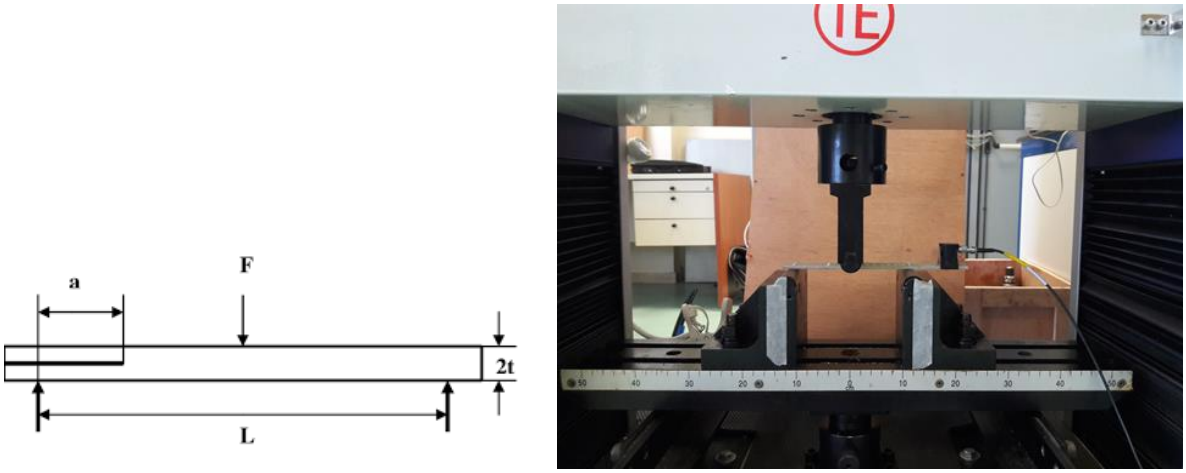

Figure 2-16 Schematic representation of the mode-II ENF set-up (lefta0 and Mode-II 3-point-bending machine fixture (right).

2.4.3. Laminates manufacturing procedure

CFRPs and GFRP laminates were manufactured using neat, binary and ternary matrices with a cure and post cure cycle according to section 4.1.

In the CFRPs laminates case, two constructions were used using UD or biaxial (BA) plane weave carbon fabrics with aerial density of 218 gr/m^2 and 200gr/m^2 respectively.

1. Quasi:16layer $[0,\pm45, 90]_{2s}$.
2. ±45: 12 layer $[,\pm45]_{6.}$

In the GFRPs laminates case three laminate constructions were manufactured using either unidirectional (UD) or BA glass fibre fabrics with aerial densities of 220 g/m^2 and 310gr/m^2:

1. Cross ply: 10 layer $[0,90]_5$ using BA fabrics.
2. ,±45: 6 layer $[,\pm45]_3$ using BA fabrics.
3. UD: 10 layer $[0]_{10}$ for the tensile testing and 16 layers $[0]_{16}$ for the mode-II testing, using UD fabrics for both cases.

The lamination process involved cutting of the appropriate number of layers from the fabrics at specified dimensions 300x300mm. The fabrics were then stacked on a glass substrate coated with polyvinyl alcohol (PVA) release agent were the impregnation with the epoxy resin took place (Subsequently, the auxiliary peel, bleeder, breather and vacuum bag plies were positioned on the collated fabric layers and vacuum sealing at 0atm was conducted to remove any entrapped air during hand lay-up (**Figure** 2-17).

Post curing was conducted in a laboratory oven at 100^0C for 4hrs with subsequent slow cooling to room temperature for both of the FRPs categories in order to alleviate any residual stresses from curing. At the next step, the laminates were cut in the appropriate specimen dimensions using a table disk saw equipped with a diamond cutting disk. All cuts were conducted using water lubrication in order to avoid any overheating of the FRPs that would compromise their structural performance.

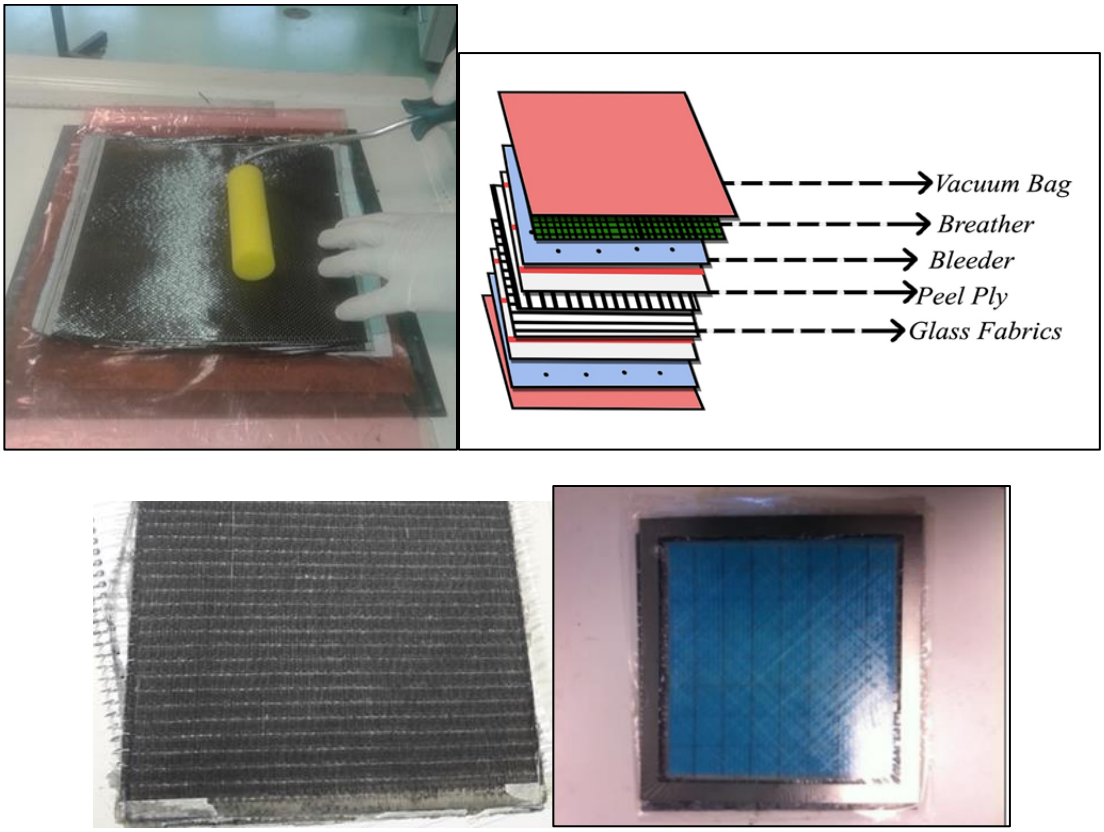

Figure 2-17 FRPs laminates vacuum preparation stages.

Table 2-1 FRP laminates construction and grade per mechanical test

Fiber reinforcement:Glass		Matrix				Mechanical test	
Laminate construction	Cross ply	Neat			Ternary	Tensile strength	
	(+-45)	Neat			Ternary	Tensile strength	

	UD	Neat	binary MC	binary CNTs	Ternary	Tensile strength	Mode II
Fiber reinforcement:Carbon		Matrix				Mechanical test	
Laminate construction	Quasi	Neat			Ternary	Tensile strength	
	(+-45)	Neat			Ternary	Tensile strength	

3. Effect of MWCNTs filler content on the epoxy matrix performance.

Part of the presented results have been published in [94].

3.1. Scope of the study

The following efforts are focused with the establishment of MWCNTs content of the fillers for optimum final properties. Towards that end various weight contents were used using constant dispersion parameters. Changes in mechanical, thermal and thermomechanical properties were examined using shear strength, LBR and DMA tests. The tests were selected targeting an end-user application where the modified epoxies were used as adhesives.

3.2. Introduction

Fibre reinforced bonded patch repairs for metallic and CFRP structures, are increasingly gaining trust as a viable and safe repair option in various demanding industrial sectors like aeronautics or marine [95]. Ease of application even on the field, reduction of induced stresses when compared to riveted repairs [96], infinite versatility in terms of shape complexity [97] and increased fatigue resistance [98], are some of the advantages of adhesively bonded repairs. Additional benefits associated with safety regulations in the oil and gas industries, classify bonded repairs as viable and well established alternatives to traditional welding repair methodologies [99–102].

The performance of the bond between the repair patch and the repair surface is primarily governed by the adhesive strength of the joint [103]. In the cases of bonded joints, stresses along the entire area of the composite-substrate interface are uniformly transferred while stress concentrations are minimized when compared to riveted joints [104]. However many concerns may arise when fibre reinforced composites (FRCs) are selected as the choice for repair. Differences in the mechanical and physical properties of the majority of metallic alloys and FRCs create difficulties in ensuring a strong bond and reducing the possibility of delamination, particularly in the presence of severe temperature fluctuations [105–108].

A significant factor that affects the joint strength and durability, is the metallic substrate surface morphology. Established techniques for high joint strength, include primer coatings, grit blasting and chemical etching of the metallic surface, for promoting either chemical bonding or mechanical interlocking [109]. The selection of the appropriate surface modification, depends mainly on the metallic substrate type in combination with specific to the application [110]. In addition to surface morphology, the thickness of the adhesive layer is a well-known

factor that greatly affects the bond repair shear strength, as too thick or too slim adhesive layers can greatly reduce the bond performance [111,112].

The interfacial area between the defected part and the patch is of key importance since this interface is responsible for stress distribution. Epoxy resins are the most widely used materials for creating the desired interface mainly due to their wide range of curing and operational temperatures [101], their application to CFRPs as matrix material [113,114] and versatility of material properties tuning. However when metallic parts of aluminium or steel alloys are to be bonded, galvanic corrosion phenomena can occur between the metallic substrates and the insulating epoxy resin [112,115]. Sealing of the joint with specially formulated coatings has proven to be a reliable route towards elimination of such concerns, although in the case of coating cracking galvanic cells can be created thus leading to premature failures [116].

It is generally accepted that in CFRP bonded patch repairs, the epoxy matrix properties govern the overall performance of the joints. The physical properties of the matrix will affect the performance in terms of water absorption while the mechanical properties will affect the adhesive shear strength of the joint. It has been shown in various publications that a reliable route for simultaneously improving the physical and mechanical properties of epoxies, is that of introducing carbonaceous fillers as reinforcements [117][118]. Single walled and multi walled nano tubes (SWCNT, MWCNT) are amongst the most frequently used nano fillers. CNT modified polymeric matrixes offer increased interfacial area assisting for better interlock between the bonded surfaces [119]. Especially MWCNTs may be incorporated in the adhesive layer in order to improve the shear strength of the interface and reduce the probability of delamination and failure of the joint [120,121]. An additional advantage for CNTs modified polymers is that they offer greater protection in corrosive environments by reducing the water uptake in the polymer mass resulting in better performance in terms of durability [122] or even improving the cross-linking of the epoxy [123]. However, the galvanic corrosion is again an issue for the nano-modified adhesives since in some cases the new conductive phase, i.e. CNTs, can accelerate galvanic corrosion in some metallic systems like aluminium [124].

One significant disadvantage of epoxy based composites or coatings in commercial or industrial applications, is that of high flammability, and toxic gas emissions when ignited [125]. When epoxy based composites are exposed to moderate temperatures, composites soften, creep and distort which can result in buckling and failure. At even higher temperatures the organic matrix decomposes with the release of heat, smoke, soot and toxic volatiles [50,126].

Improving the fire retardant behaviour of epoxy composites pose a major challenge towards a broader range of applications [127,128].

Halogenated compounds are widely used as additives with epoxy resins towards fire-retardant materials. Flame retardant epoxy resins that contain bromine or chlorine additives, however can produce poisonous and corrosive smoke and may give toxic halogenated dibenzodioxins and dibenzofurans [129,130]. Compounds with phosphorus like 9,10-dihydro-9-oxa-10-phosphaphenanthrene-10-oxide (DOPO) have shown promising results as halogen-free, flame retardants in epoxy resins [131,132]. One major issue regarding the use of traditional flame retardants though, is the high weight contents, which in some cases can be as high as 50%w.w. and can negatively affect both of the epoxy process ability and degrade the mechanical and/or durability properties [133–135].

Recent research efforts have combined traditional flame retardant compounds with carbonaceous fillers like CNTs towards improvements in flame retardancy and materials properties as well [29,136–138]. By the combination of traditional flame retardants fillers like montmorillonite (MMT) with MWCNTs, Im et. al. managed to significantly improve the flame retardancy of the matrix epoxy. The exfoliated MMT and CNTs acted as energy storage mediums as a result of their high thermal conductivity, thus leading to double activation energy, reduced degradation rate and increased char yield [139].

The magnitude of any performance enhancement mentioned above, heavily relies on many factors like the selected type of carbon nano tubes (single wall, multi wall, functionalized or not etc.) [140], epoxy system [141], the weight content of the CNTs in the epoxy [142] or the employed dispersion methodology. The dispersion methodology holds the most critical role in the manufacturing process, because at this step an effective deagglomaration and even distribution should be accomplished. Dispersing the nano fillers via various methods such as sonication[57], shear mixing etc [143] or three-roll milling[144] can be conducted either with as received CNTs or functionalized ones [54]. Each of the dispersion approaches, carries advantages and disadvantages and most frequently, a compromised solution is the best route. For example, the sonication method despite being a very effective dispersion method, requires a very accurate and reliable cooling system for temperature control and cannot be scaled up to the industrial level. High speed shear mixing (HSSM) on the other hand, is free of such limitations although in some variations like bead milling, breakage of the carbonaceous filler can occur [145,146].

Under the aforementioned considerations, the scope of this chapter, is to present the study on the effect of MWCNTs dispersion in an epoxy resin used as an adhesive for bonding two commercially available metallic alloys, namely aluminium 2024-T3 (Al-2024) and stainless steel 304 (SS304). These specific alloys were chosen due to their applicability in the aeronautics and oil marine industries respectively were epoxy based coatings and/or composite patch repairs are frequently applied. MWCNTs were dispersed in various contents using an industrial dissolver equipped with a vacuum assisted ball mixing module under controlled temperature and vacuum conditions. This specific dispersion approach was selected firstly due to its capability of accurate temperature control and secondly due to its industrial level scalability. The nano-modified epoxy resins were used as adhesives in single lap-joint specimens under tension to study the nano fillers effect on the maximum shear strength. Scanning electron microscopy was used to qualitatively assess the fracture surface morphology and the dispersion quality. In addition the nano-modified epoxies were used in dynamic mechanical analysis (DMA) and linear burning rate (LBR) tests so as to study their thermomechanical performance and fire resistance respectively.

3.3. Experimental

The effect of filler content on mechanical, thermal and thermomechanical properties has been studied via SLJ shear strength, LBR and DMA tests respectively. Details for the experimental methods can be found in 2.3.1, 2.3.8 and 2.3.7 respectively.

Neat and modified with 0.4%, 0.5% and 0.6% w.w MWCNTs were used as adhesives in metal-to-metal (MtM) SLJ specimens using AL2024 and SS304 metallic substrates. Additional metal-to-composite (MtC) SLJ specimens were tested using SS304 and CFC substrates. The CFC substrates were extracted from laminates according to 2.4.3 and bonded with the SS304 substrates using the same adhesives as in the MtM case.

3.4. Results

3.4.1. CNTs effects on the adhesive strength – Aluminum substrates

The effect of the CNTs on the adhesion properties of the epoxy resins, was evaluated by using single lap-joint shear specimens under tensile loading. **Figure** 3-1 depicts typical load vs extension diagrams obtained from the neat and nano modified resin adhesives. As can be seen, all the systems exhibited a brittle material behaviour. The non-linearity up to 0.25mm of extension, can be attributed to slippage of the end tabs and to machine slack.

It is seen that the nano modified resins exhibited higher failure loads when compared to the neat ones. In addition it is observed that the nano modified adhesives failed in greater extension values than the neat ones. The most significant enhancement was present for the 0.5%w/w CNTs adhesives. Specimens of this particular CNT content loading, failed at maximum load of 8.99kN with maximum average shear stress of 12.81 MPa, as presented in **Figure** 3-1. For comparison reasons, it should be noted that the maximum failure load of the neat resins peaked at 7.57 kN while maximum shear stress peaked 10.88 MPa.

The aforementioned behaviour is also depicted in **Figure** 3-2 where average maximum shear stress strength values of neat and nano modified resins are presented. Compared to the neat resins, the nano modified resins exhibited higher shear strength and the effect is greater for the 0.5%w/w CNTs content reaching a limit of 25% enhancement. The 0.5%w/w content exhibits the highest shear strength compared to the 0.4% and 0.6% w/w contents indicating that the CNTs addition effect in the epoxy resins shear strength reaches a plateau for the 0.5%w/w content. Further addition of MWCNTs in the resin adhesive (0.6%ww), led to a decrease in average shear strength. The deviation in the average shear strength values for the 0.5%ww 0.6%ww indicate variations within experimental errors.

a.

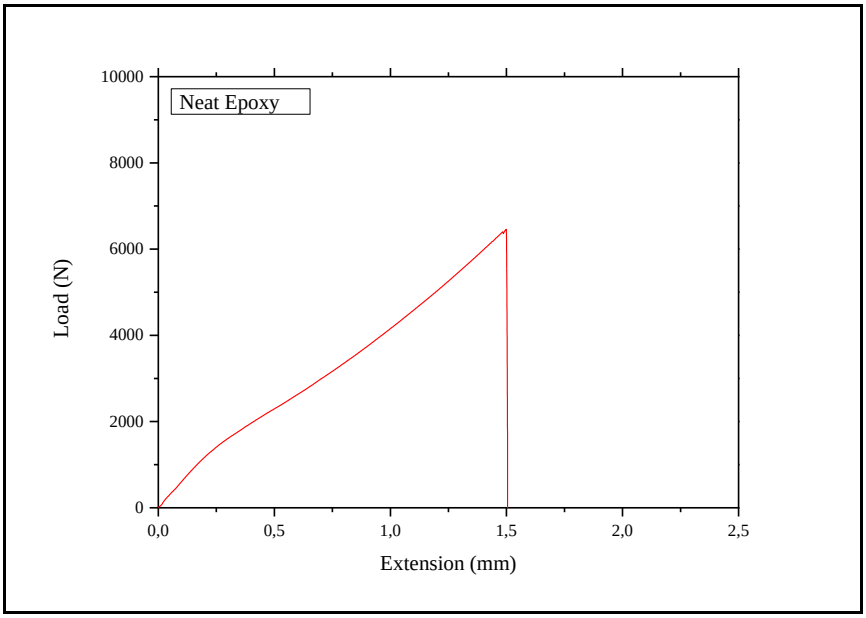

b.

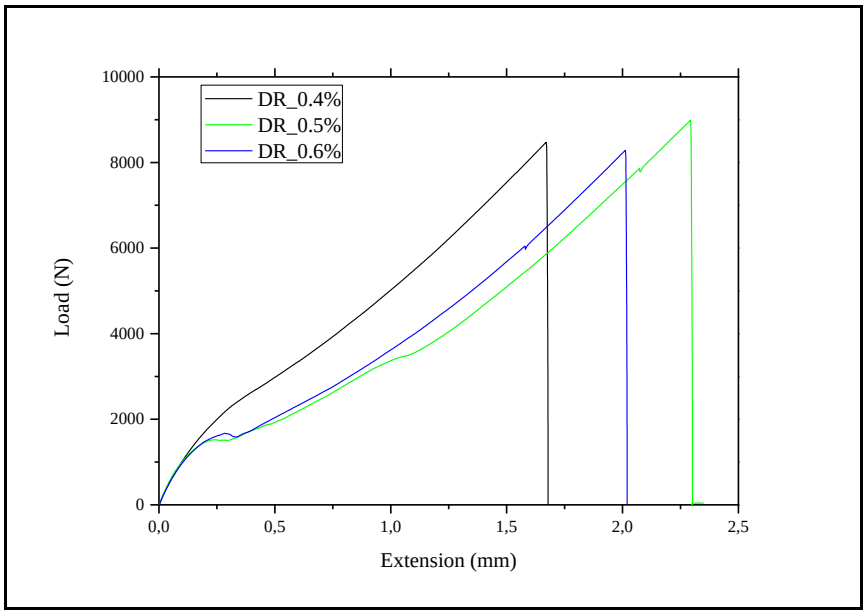

Figure 3-1 Typical Load=f(Extension) diagrams of the neat (top) and nano modified adhesives (bottom).

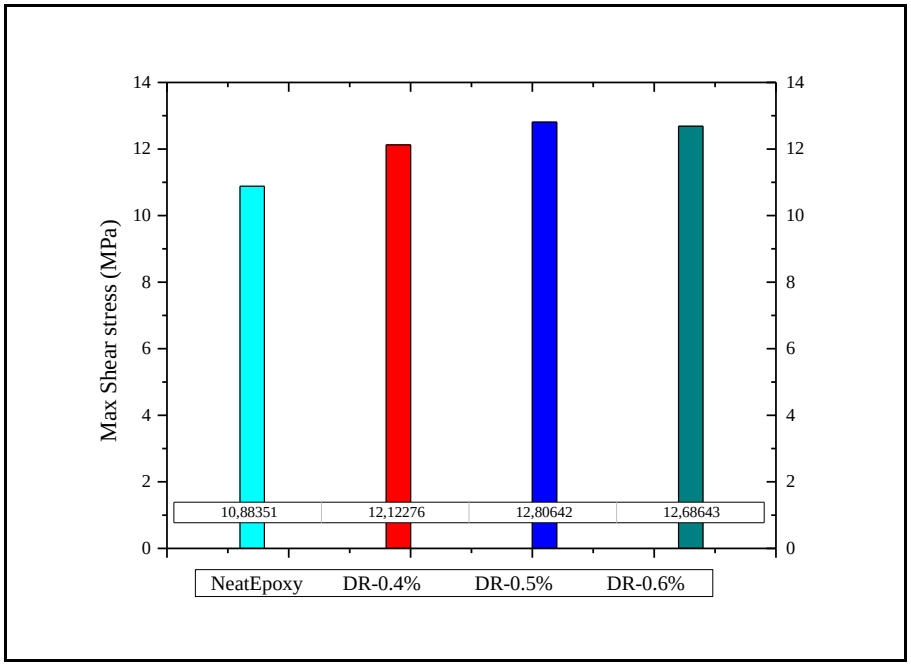

Figure 3-2 Bar chart depicting average maximum shear stress values for the neat and nano modified resins.

In **Figure** 3-3, single lap joint fracture surfaces SEM photographs are depicted for the nano enhanced adhesives. Higher magnification photographs, indicate that the dispersion procedure broke the agglomerated MWCNTs quite well reducing the average agglomeration size from 400μm to 30μm (**Figure** 3-3). Based on observations from the SEM images, it is safe to say that the dispersion managed to de-agglomerate the MWCNTs bundles down to the single nanotube level. The SEM images, reveal the in the case of the DR04 composites bundles with average dimensions in the range of 10-50μm are intermixed with individual CNTs. In the case of the D05 and D06 composites though the CNTs bundles are not present and only individual CNTs form the reinforcing network. It can be postulated that the CNTs reinforcing network in these cases, was more effective in providing mechanical interlocking with the primer substrate. The reduction in shear strength in the case of the D06, could be linked to either reverse percolation phenomena or CNTs fracture during dispersion. Especially for the latter case, it can be observed in **Figure** 3-3 d and f, that some CNTs were present with lengths smaller than the average length of single CNTs.

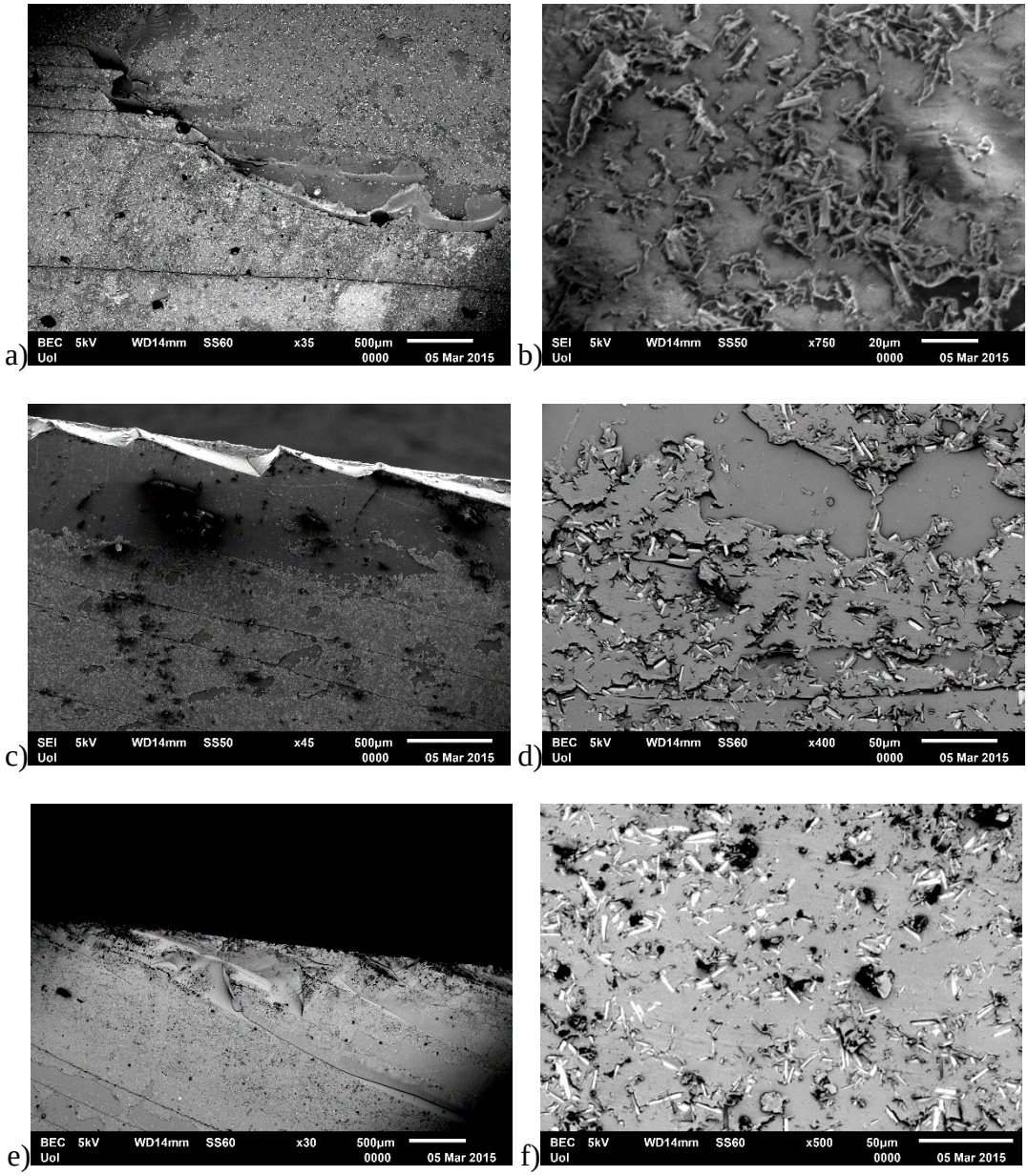

Figure 3-3 SEM photographs from fracture surfaces of single lap joint specimens for the (a-b) 0.4%w/w, (c-d) 0.5%w/w and (e-f) 0.6%w/w MWCNTs doped resin.

Most of the single lap-joint specimens failed in an adhesive manner where failure occurred primarily at the primer/anodization interface. Some parts of the bond area failed at the primer/adhesive interface especially in the cases for neat and 0.4% content resins. The 0.5% and 0.6% contents fracture surfaces exhibited a mixed failure mode. While most of the fracture surfaces appear to have failed in an adhesive way, fracture in some areas appears to jump from one interface to another. In addition failure predominately occurred at the primer/anodization interface with small areas failing at the primer/adhesive interface.

3.4.2. CNTs effects on the adhesive strength – Stainless steel substrates

Table 3-1 Nomenclature of the lap shear specimens.

Epoxy Resin configuration	Neat epoxy resin	Epoxy Resin + 0.4%w/w CNTs	Epoxy Resin + 0.5%w/w CNTs	Epoxy Resin + 0.6%w/w CNTs	CF reinforced epoxy	CF reinforced Epoxy + 0,6%w/w CNTs
Specimen nomenclature	Neat	NE0.4	NE0.5	NE0.6	NECF	NECF0.6

As mentioned before, two different single lap-joint specimen configurations were used, metal to metal (MtM) and metal to composite (MtC) in the case of the stainless steel substrates. **Figure** 3-4 depicts a cumulative bar chart with the average shear strength for the two groups, derived from data of five test specimens for each configuration and CNTs loading. As can be seen, the case of (MtM) configuration, exhibits a significant increase in shear strength after the addition of the CNTs in the host matrix. Shear strength for the doped adhesives, was improved by 35%, 43% and 47% for the NE04, NE05 and NE06 adhesives respectively when compared to the neat adhesives. The results indicate that the shear strength is CNT loading dependent as in the case of the aluminium substrate based specimens. A linear relation between CNT loading and shear strength was observed with similar values in standard deviation, which is an indication of even MWCNTs distribution on all doped adhesives. Such behaviour is in agreement with the literature where improvements in shear strength are observed for nano-enhanced epoxy adhesives [109]**.**

The highest adhesive shear strength was achieved for 0.6% CNT loading hence this CNT loading was used for the doped CFRP specimen manufacture. Two CFRP plates were manufactured, one with neat resin (nCFRP) and one with 0.6% doped resin (dCFRP) as the matrix material. As can be seen in **Figure** 3-4 and **Table** 3-2, nCFRP specimens exhibit better shear strength when compared to the dCFRP specimens. The doped resin matrix degraded the shear strength of the adhesive bond, possibly due to reduced wettability of the modified resin on the steel surface. It has been shown that in some cases, the increased viscosity of CNT doped resin matrices could lead to degraded mechanical properties as a result of reduced wettability [110,120].

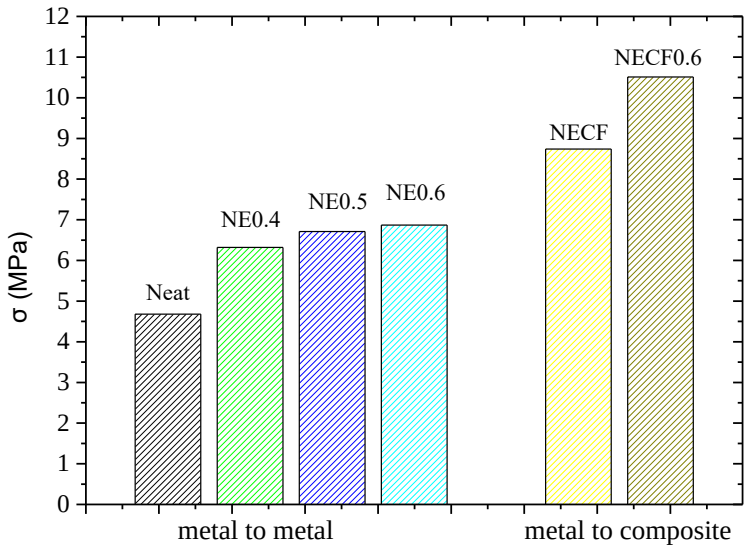

Figure 3-4 Lap shear strength for two groups (MtM) (MtC)

Table 3-2 Results from Single Lap-Joint testing

Specimen configuration	**neat**	**NE0.4**	**NE 0.5**	**NE 0.6**	**NE CF**	**NECF0.6**
Avg shear strength (MPa)	4.68	6.32	6.71	6.87	10.51	8.74
Highest value (MPa)	4.77	7.17	7.88	7.24	15.23	10.26

3.4.3. Linear Burning rate

Based on the lap-shear and electrochemical results from the aluminium based specimens, it was decided to employ the D05 modified epoxy in LBR testing. In addition, an additional modified with 1.0%w.w. of CNTs (namely D10) epoxy was also used in order to investigate further the filler concentration effect on the final properties.

As it can be observed in **Table** 3-3 and **Figure** 3-5, the introduction of the CNT filler resulted to significantly improved fire resistance in both of the studied cases. LBR was significantly reduced by 350% and 302% for the D05 and D10 composites respectively while an increase in the maximum combustion temperature was also seen. It has been shown that the incorporation of carbonaceous fillers like CNTs results to improved fire resistance via

improvements in thermal conductivity and heat dissipation phenomena [125]. In [134], inorganic montmorillonite and CNTs were incorporated in an epoxy matrix and the thermal properties of the resulting composites were compared. The results indicated that the continuous network of filler particles formed a protective layer on the surface of the tested specimens thus improving the fire resistance. CNTs were more effective than the inorganic filler in reducing the flammability of the composites and in a significantly lower weight contents. It has to be noted though that the increased heat-transfer capabilities of the CNTs network, increased the mass loss rates at the initial pyrolysis stages. In a similar effort [128], functionalized CNTs were introduced in an epoxy matrix in various contents and the thermal properties of the resulting composites were studied. The results revealed that the presence of 9%w.w. CNT improved the thermal properties of the composites and upgraded the epoxy matrix from a HB to a V-0 UL 94 classification. It is generally accepted that the thermally conductive CNTs, promote energy absorption and char formation on the surface of the composites. The formation of the hybrid CNTs containing char plays a protective role and is more effective in reducing flame spreading by hindering oxygen supply.

It has to be noted though, that the magnitude of the effect on flame retardancy for CNT modified epoxies, is significantly lower when compared to traditional flame retardants [127,147]. However the combination of traditional flame retardants with CNTs can lead to a multifunctional flame retardant composite with superior mechanical, electrical and mechanical performance [148].

In terms of comparison between the two modified epoxies, only marginal differences in the LBR values were observed despite doubling the filler weight content. The higher maximum combustion temperature values in the case of the modified epoxies, indicate improved thermal energy capabilities due to the thermally conductive nature of the fillers. As in the case of the lap-shear results from the aluminium based specimens, it is seen that the increase of the weight content is not linearly related to a property improvement. In fact the results suggest that increasing the filler weight content beyond a certain value, can lead to minimizing of the beneficial effects in the material properties.

Table 3-3 LBR testing extracted and calculated values

Specimen formulation	**LBR (cm/min)**	**Burned specimen length (cm)**	**Average burning time (min)**	**Maximum combustion Temperature (^{0}C)**	**UL 94 classification**

Neat epoxy	1.33 ± 0.52	54±2.5	4’	212±15	N/A
D05	0.38 ± 0.07	6.8±0.6	1’35’’	240±5	HB / V-2
D10	0.44 ± 0.01	7±1	1’25’’	260±6	HB

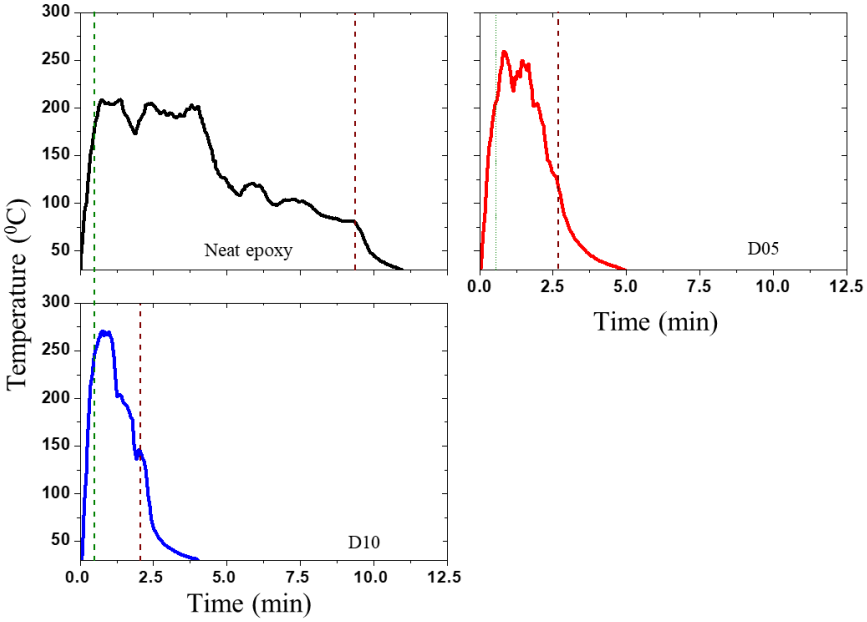

Figure 3-5 Temperature vs time curves from the LBR tests.

3.4.4. DMA

Table 3-4 summarizes all characteristic values extracted for the DMA curves that are depicted in **Figure** 3-7. As can be observed in **Figure** 3-7, the introduction of the CNT filler has been beneficial on the E’ values even though in a marginal manner. It is generally accepted that the incorporation of stiff CNT particles in epoxy matrices leads to reduction in polymeric chain mobility manifested as higher E’ values.

It has been reported [149] that the structure of the interface in epoxy composites mostly affects the height of the tan d peak and, therefore, this variable is recommended for characterizing the interfacial structure of the composites. As can be seen in **Figure** 3-7, the height of the tan d peak was decreased when compared to the neat epoxy. This decrease in the tan d peak could be attributed to the stiffening effect as a result of the CNTs inclusion. The reduction in the D10 E’ values compared to the D05 one, could be attributed to the dispersion methodology. The principle of bead milling dispersion, lays on the employment of spherical

ceramic beads towards introduction of high shear impact forces that will lead to de-agglomeration of the MWCNTs. Given that the dispersion duration was the same for both of the composite groups, two root causes can be hypothesized. (i) The bead milling was ineffective in reducing the agglomerates size for such a weight content due to excessively high viscosity or (ii) the bead milling duration was excessively long thus leading to CNTs fracture via aspect ratio reduction [150]. The results from the SEM analysis, advocate towards the latter hypothesis as in some areas CNTs with lengths smaller than the average values were observed.

The width and position of the tan d peak is also a parameter for the assessment of polymer heterogeneity. As seen in **Figure** 3-7, the tan d width was decreased in the case of the D10 when compared with the neat epoxy. The height was shifted towards lower temperatures, thus indicating a less heterogeneous network. On the other hand, the D05 tand height was maintained in the same levels with neat epoxy but shifted towards lower temperatures thus indicating a more heterogeneous network [151].

Crosslink density was also affected by the introduction of the CNTs. The inclusion of the CNTs, which were close in dimensions to the polymeric chains, may have facilitated crosslinking reactions. It has been reported that the inclusion of CNTs results to increased cross-linking via bridging of unreacted polymeric chains thus leading to stiffening of the polymeric chain network [76]. The drop in the Mc values that was observed for the D10 composites when compared to the D05 ones, could be associated to percolation type phenomena.

Table 3-4 DMA characteristic values for the studied specimens

	E' (MPa)	**Tg (^{0}C)**	**Mc (gr/mol)**	**Er (Mpa)**	**p (gr/cm3)**	**T_{ER} (^{0}C)**
Neat	2755.5±23.3	128.2±0.8	427.11±1.58	17.03 ±0.5	1.105±0.001	122±1
D05	2836.5±51.6	121.8±0.3	481.87±1.09	15.78±0.5	1.103±0.001	122±1
D10	2790±76.6	127.1±1.6	446.57±2.98	16.35±0.5	1.088±0.001	130±1

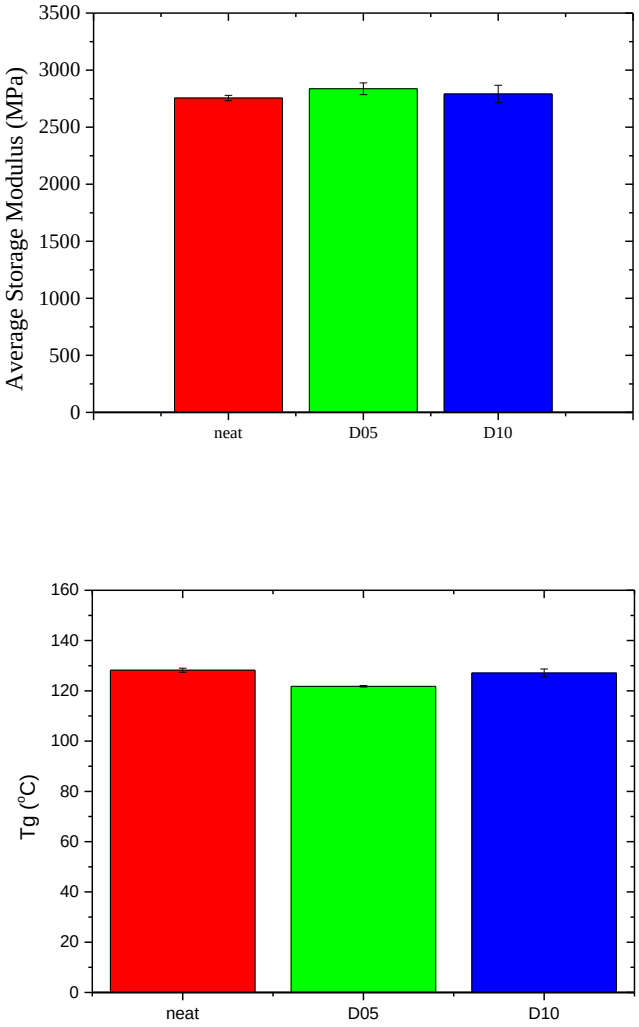

Figure 3-6 Average storage modulus for all tested specimens

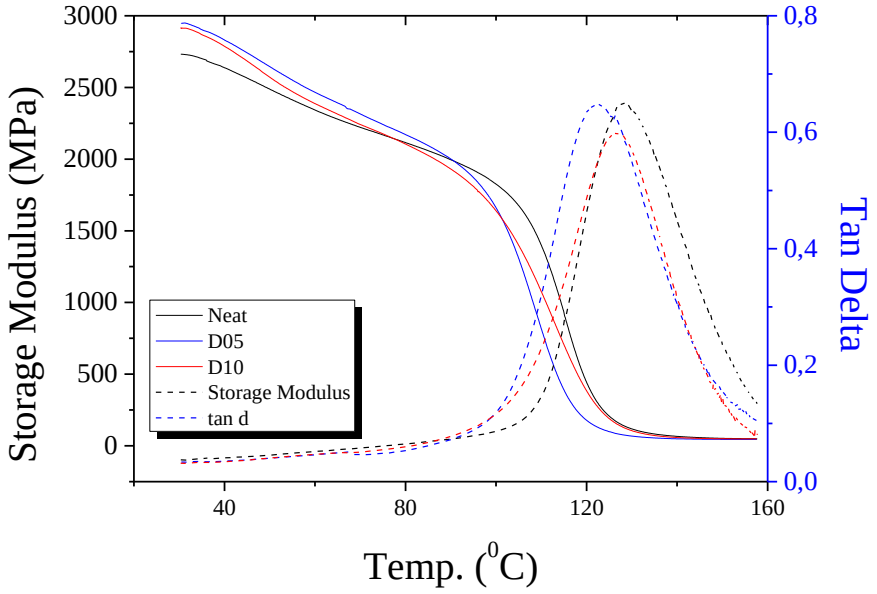

Figure 3-7 Storage modulus and tand vs temperature curves for the neat and doped nano composites.

3.5. Conclusions

The overall assessment of the nano-reinforcement, indicated that the inclusion of CNTs leads to beneficial results, both for the electrochemical and mechanical properties.

The incorporation of CNTs in the epoxy magnifies the galvanic effect between epoxy and metallic substrates, either aluminium or steel. Nevertheless, it promotes corrosion resistance from both a kinetic and thermodynamic standpoint, whilst it magnifying the resistance to localized corrosion.

The inclusion of CNTs lead to significant improvement of the adhesive properties as was verified by lap shear tests. The CNT loading with highest shear strength was the 0.5%w.w. and 0.6% w.w. for the aluminium and steel based substrates respectively. SEM imaging analysis revealed good de-agglomeration and even distribution of small CNTs bundles engulfed in the majority of individual CNTs.

Improvements were observed fire resistance properties of the CNTs reinforced epoxies. In the case of LBR, the inclusion of CNTs led to significant enhancement in fire resistance manifested through reduction of burned length and combustion duration. The observed performance was attributed to the thermal conductivity of CNTs, imparting thermal energy absorption

capabilities to the composites. In addition, CNTs promoted char formation on the surface of the specimens thus sealing the flame from the environmental oxygen.

DMA analysis revealed that the inclusion of CNTs in epoxies can be beneficial but dependencies on the weight content were evident. D05 composites exhibited the highest E' and Mc values with the D10 composites at the second place. The analysis indicated that the CNTs weight content highly affects the final properties and should be carefully selected for optimum performance.

The overall observations and postulations of the conducted research, advocates towards the effectiveness of epoxy modification via CNTs dispersion. The results revealed the effect of dispersion procedure and CNTs weight content indicating the weight content threshold exist which when surpassed, a reduction in properties is observed.

4. Effect of Multi-scale reinforcement on the epoxy matrix

Part of the results presented in this chapter were published in [152,153].

4.1. Scope of the study

The results in this chapter are focused on the study of (i) the effect of the dispersion parameters and (ii) the effect of the multi-scale reinforcing approach on the final properties. Towards both ends, dispersions with variable time and temperature were conducted using the one-filler and multi-scale approach. The dispersions were coupled with dynamic viscosity measurements to gain insight on changes related to the filler type/types. Binary composites with either MWCNTs or MC and ternary epoxy resins were used for the manufacturing of specimens for IS, fracture toughness and DMA tests. The DMA tests were selected so as to have a cross correlation with the results from Chapter 04 where a different dispersion module was used.

4.2. Introduction

Epoxy resins can be found in an extensive range of applications due to their wide range of physical and mechanical properties and with the ability to tailor material properties according to specific operational prerequisites [154,155]. However, the dielectric nature of epoxy resins, is not compatible with functional roles such as strain and damage monitoring especially in cases where electrical conductivity is of interest can provide significant information [156–159].

Dispersing a conductive nano, micro or macro filler in an epoxy matrix, has proven to be a reliable route towards conductive epoxy based composites with simultaneous improvements in mechanical and electrical properties [160]. Hernandez-Perez et. al, achieved an almost two-fold increase in impact strength and fracture toughness while increasing electrical conductivity by 10 orders of magnitude when introducing Multiwalled carbon nano tubes in an epoxy matrix [161]. The most widely used carbonaceous fillers towards functional epoxy composites are randomly dispersed short carbon fibres, Carbon Black (CB) [162] are macro and micro scaled alternatives [163]. Single, Double or Multi Walled Carbon Nano Tubes (SWCNTs, DWCNTs, MWCNTs respectively)[164], Graphene (Gr) [165] and nano diamonds [166]. Depending on the filler type and weight content, material properties like fracture toughness, shear strength, corrosion resistance or electrical properties, can be beneficially affected [167–169]. The resulting beneficiary effect is greatly dependent on the dispersion efficiency of the fillers which, in its turn, is dependent on various factors like dispersion method, duration and intensity along with the filler type and weight content [170–173]. SWCNTs and graphene result in conductive composites even for very low weight contents,

while MWCNTs and CB require higher weight contents in order to match the electrical conductivity values attained by the employment of the former two nanostructures. However, the high cost of SWCNTs is a significant drawback, especially when a scale-up to industrial processes is of importance [174,175].

Achievement of multifunctionality in epoxy resins via the incorporation of carbonaceous fillers [176], comes with a compromise though as it has been shown that high aspect ratio fillers can lead to significantly high viscosities after dispersion [177]. In applications where the rheological characteristics of the epoxy resin are the single controlling factor, increased viscosity can prove to be either a favourable or not factor [87,140,178]. In such an application, Siddiqui et. al. studied the effect of CNTs in the rheological performance of an epoxy resin matrix of pre-preg Fibre Reinforced Composites (FRC) [179]. They observed that optimization of the pre-preg processing parameters was necessary to reduce the adverse effect of CNTs on the viscosity of epoxy and FRP pre-preg characteristics. The magnitude of the effect on the resin viscosity is directly associated to the amount of interconnected fillers that reduce resin chain mobility [180] which in turn is directly related to the dispersion quality in the epoxy suspension [181][182].

There is a trend in the recent years to modify epoxy resins via the inclusion of more than one filler in order to exploit synergistic effects between the fillers. Especially when these are of nano or micro scale, it is possible to exploit and combine the dominant fracture mechanisms from both worlds [183,184]. Ternary epoxy based composites i.e. epoxies with two different fillers, may exhibit improved performance when compared to the respective binary i.e. epoxies with one filler type, systems [185–187]. In [51] et.al., employed CNTs and CB fillers in various contents towards the production of binary and ternary epoxy composites and the assessment of their electrical and mechanical properties. It was shown that in the majority of the cases, the ternary composites outperformed the binary ones. The authors attributed the observed behaviour to the distinct geometric shapes and aspect ratios as well as to the different dispersion characteristics of the CB and CNTs particles. Spherical CB effectively filled the gaps among the long aspect ratio CNTs thus leading to a more effective network which in turn resulted to significant improvements in electrical and mechanical properties.

Apart from the improved properties, the coexistence of different fillers can also provide multifunctionality. Multifunctionality in materials engineering can be defined as the

combination of different properties in one material so as to make it suitable for the use in applications in which different loading conditions must be sustained [188,189]. An example of such a multifunctional material can be a glass fibre reinforced structural component with an epoxy based nano-reinforced matrix. The macro-scaled fibres are responsible for the structural integrity of the component while the conductivity of the matrix can be employed as strain and structural health monitoring sensors [31,190,191].

The effective exploitation of the beneficiary effects of the dispersed nano or micro fillers strongly depends on the proper selection of the dispersion protocol i.e. method of dispersion, temperature, duration and intensity. Dispersion methods like sonication [170], calendering [165] and high shear mixing [192] either employed individually or in combination are the methods of choice for the majority of research efforts [193]. It is known that with increasing dispersion duration, the viscosity of CNTs-epoxies tends to increase significantly [194]. The increased viscosity can result to increased attenuation of the ultrasounds energy which can result to ineffective dispersion, degradation of the epoxy matrix around the sonication tip and possibly to extensive breakage of the fillers thus degrading their reinforcing capability. Shear mixing on the other hand is not affected by the increased viscosity, cannot induce any matrix degradation and additionally shear mixing is a viable technique for industrial upscale [173][195]. Sandler et. al., have successfully employed high shear mixing either as a stand-alone technique [196] or in combination with well-established dispersion methodologies like ultrasonic[197], towards improved electrical conductivity for epoxy based antistatic coatings.

The selected dispersion protocol strongly affects the dielectric properties of the final composite, as the impedance of the system changes dynamically when a conductive filler is being dispersed in an insulating matrix [198–200]. A novel tool for monitoring changes in the dielectric profile of a material is impedance spectroscopy (IS). IS has been extensively utilized as a non-destructive evaluation technique in the context of thermosetting polymer cure [201,202] for the study of the dielectric properties of nano-reinforced composites [203–206] as well as for damage state analysis in composite materials [201,207,208]. IS involves the monitoring of the phase delay and amplitude of the resulting current as a function of frequency. A spectrum is generated by either a frequency sweep or by Fast Fourier Transform (FFT) of the recorded transient time series.

The research effort that will be presented in thischapter, is focused on the development of a ternary epoxy based composite containing MWCNTs and micro-scaled milled carbon

particles using high speed shear mixer with an impeller disk module as the dispersion approach. A comprehensive study on the dispersion conditions, in terms of duration and dispersion temperature, filler weight contents and type was conducted in order to fine tune the controlling factors and reach optimum material properties. Concurrently, IS was utilized as a tool for the study of the influence of the dispersion parameters on the dielectric properties of the composite as well as to study how the synergy effect of CNTs/MC influences the impedance of the final composite over a wide frequency spectrum. The synergy effect on the fracture toughness and the thermomechanical behaviour (storage modulus, tan(delta) and glass transition temperature was evaluated through three point bending on single edge notched beam specimens (SENB) and dynamic mechanical analysis (DMA) measurements respectively. In addition, Scanning Electron Microscopy (SEM) was also employed to study the SENB fractured surfaces and examine the effect of the multi-phase reinforcement.

4.3. Experimental

The effect of multi-scaled vs binary reinforcement on the properties of epoxy composites has been studied. The dispersions were conducted as a function of duration according to 2.3 using an impeller module. Dispersions were performed for 1,2,3 and 4 hours at 3000rpms and 25^0C for both binary and ternary systems. Between each time interval DV measurements were recorded according to 2.4.5. Reference values from the epoxy resin without the hardener were recorded at three temperatures for validation and repeatability purposes. Additional dispersion protocols were performed for the binary CNTs systems for 1,2 and 3 hours at 3000rpms and 5^0C, so as to monitor temperature induced variations. Neat and modified specimens for IS, fracture toughness and DMA measurements were manufactured. SEM analysis was conducted on the SENB specimens' fractured surfaces to study the fracture mechanisms. MWCNTs and CB binary composites at 0.5%w.w. and 2.0%w.w. filler loadings respectively were used. Ternary composites were manufactured using MWCNTs and CB at the aforementioned weight contents.

Table 4-1 Summary of specimen formulations and Nomenclature.

Filler Material	**Filler content (%w.w)**	**Dispersion duration (hr)**	**Temperature (^{O}C)**	**Nomenclature**
None				Neat
MWCNTs	0.5	1	25	CNTs-(1)
MWCNTs	0.5	2	25	CNTs-(2)

MWCNTs	0.5	3	25	CNTs-(3)
MWCNTs	0.5	4	25	CNTs-(4)
MWCNTs	0.5	1	5	CNTs(f)-(1)
MWCNTs	0.5	2	5	CNTs(f)-(2)
MWCNTs	0.5	3	5	CNTs(f)-(3)
MC	2.0	1	25	MC-(1)
MC	2.0	2	25	MC-(2)
MC	2.0	3	25	MC-(3)
MC	2.0	4	25	MC-(4)
MWCNTs/CB	0.5/2.0	1	25	ternary-(1)
MWCNTs/CB	0.5/2.0	2	25	ternary-(2)
MWCNTs/CB	0.5/2.0	3	25	ternary-(3)
MWCNTs/CB	0.5/2.0	4	25	ternary-(4)

4.4. Results and Discussion

4.4.1. Viscosity measurements

Table 4-2 presents the neat epoxy resin dynamic viscosity recorded values, while **Figure** 4-1 depicts the dynamic viscosity vs shear rate profile of the neat epoxy resin at three different temperatures. **Figure** 4-2 and **Figure** 4-3 exhibit the dynamic viscosity profiles of the modified epoxy suspensions at 1hr of dispersion duration intervals in a log-log and linear axes respectively.

Table 4-2 Neat epoxy dynamic viscosity at various temperatures

Dynamic Viscosity (mPa)	**at 5^0C**	**at 23ºC**	**at 28ºC**	**at 31ºC**
neat epoxy	2500	1820	1170	757

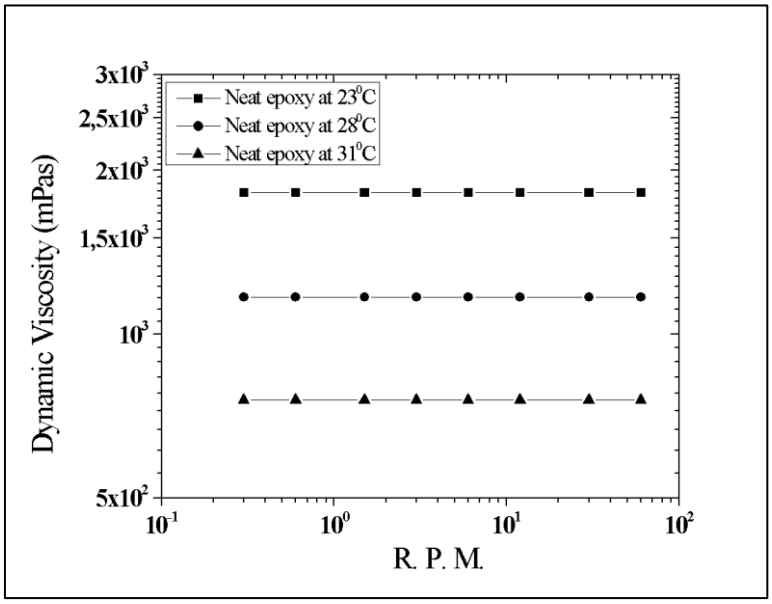

Figure 4-1 Viscosity vs rpm curve for the neat epoxy at three different temperatures

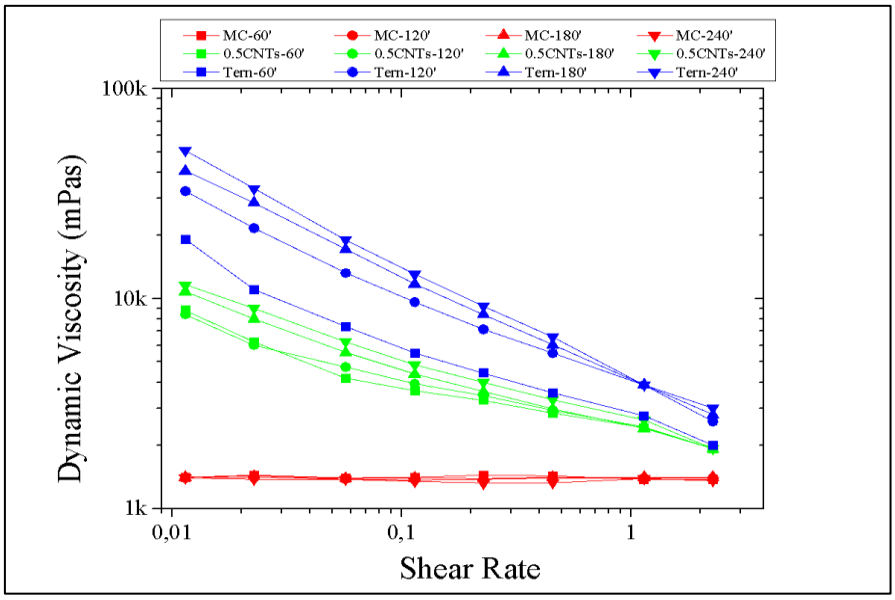

Figure 4-2 Viscosity vs rpm logarithmic curve for all modified epoxies for all dispersion duration increments.

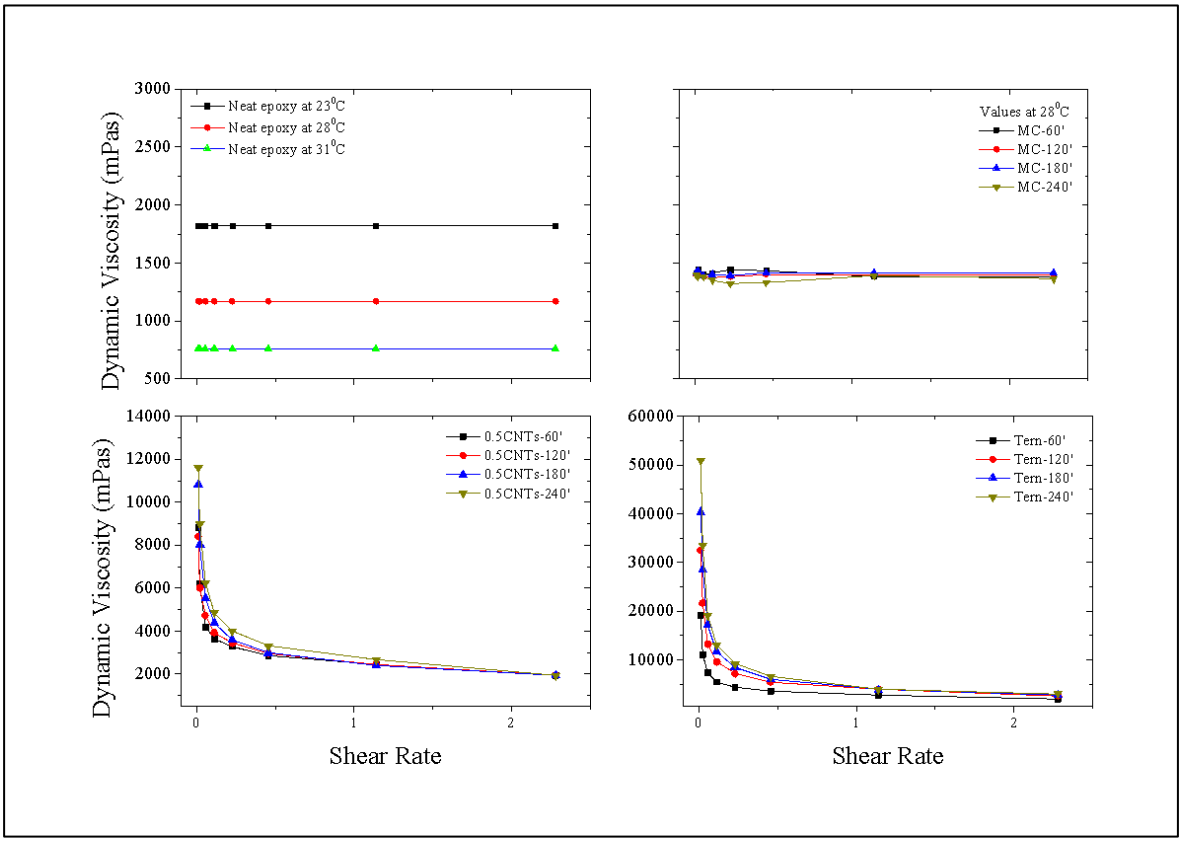

Figure 4-3 Dynamic viscosity vs rpm curves for neat and modified epoxies. All modified epoxies were measured at 23^{0}C.

As expected, the neat epoxy dynamic viscosity did not exhibit any shear rate dependence thus confirming the expected Newtonian fluid behaviour [87]. As it can be seen in **Figure** 4-1, the dynamic viscosity was sstable around one value and only temperature dependence was evident as expected. In the case of the modified suspensions and according to the literature, shear thinning rheological characteristics were expected to arise [209]. An inverse dependency of the dynamic viscosity over the shear rate is the phenomena of shear thinning. At low shear rates, the modified suspension behaves like a thick highly viscous liquid while in high shear rates the suspension 'thins' thus exhibiting decreased resistance to flow. The 'shear thinning characteristics of modified epoxy suspensions, are correlated with the reduction of particles interconnections which lead to improved flow [209]. It has been shown, that in low filler concentrations, the modified suspensions follow the resin matrix Newtonian characteristics, but above a critical concentration that depends on the dispersion approach, resin and filler types [210], shear thinning is observed [211] and dramatically increased viscosities are experienced.

As seen in **Figure** 4-2 and **Figure** 4-3, shear thinning is observed in the CNTs and Ternary where the shear rate dependency is evident. At low shear rates, both systems exhibit

significantly increased values, by orders of magnitude, when compared to the neat suspensions. With increasing shear rates, the viscosity values tend asymptotically to the neat suspension value. The viscosity profiles of the CNTs and Ternary suspensions, also exhibited a linear dependency with the dispersion duration as well. Increasing of the dispersion duration, promoted particles deagglomaration and even distribution thus leading to increased interconnections amongst the filler particles. Similar observations have been made for MWCNTs suspensions with other dispersion approaches like sonication. In such an approach, Fan and Advani, employed MWCNTs in order to study the effects of dispersion state in the final properties. They observed a strong correlation between sonication duration and viscosity indicating the continuous deagglomaration of the MWCNTs bundles down to individual CNTs [194].

At this point it is interesting to note that in the case of the MC suspensions, neither shear thinning nor significant dynamic viscosity increases were observed when compared to the neat resin. The MC suspensions, exhibited identical rheological characteristics with the neat resin indicating that the filler particles concentration and type (graphite spherical particles and micron carbon fibers) were not capable of producing an interconnecting network. It has been shown that high aspect ratio fillers like CNTs tend to have a greater impact on the viscosity and shear thinning effect when compared to low aspect ratio fillers like carbon nano fibers [211].

Taking into account the MC suspension characteristics, synergy effects in the Ternary suspensions can be supported. As evident in **Figure** 4-2 and **Figure** 4-3, the combined inclusion of CNTs and MC particles, even after only one hour of duration (Tern-(1)) led to a more than double dynamic viscosity values at low shear rates, when compared to the CNTs-(1) suspension. Further dispersion resulted to the highest observed dynamic viscosity at low shear rate at 51Pa.s. for the Tern-(4) suspension. It can be postulated that the MC particles acted as connection bridges among the MWCNTs thus leading to the formation of a network which greatly restricted resin chain mobility. The pronounced increase between Tern-(1) and Tern-(2) suspensions, may also indicate that the MC particles could have facilitated a more rapid CNTs deagglomaration by acting as shear stress inducing particles.

4.4.2. Impedance Spectroscopy

In general, when a conductive phase is dispersed within an insulating matrix, the response of the material to an external alternating field is highly affected. In detail, as the conductive

network is forming, the total impedance of the system is decreasing while the DC conductivity of the composite tends to increase. Consequently, both real and imaginary components of the impedance could provide useful information about the effect of several dispersion parameters (i.e. duration, temperature) and the type of the inclusion (i.e. CNT, MC) on the dielectric response of the final material.

Table 4-3 DC conductivities of all studied composites

Sample	**Filler**	**σ_{DC} (S/m)**
CNTs-(1)	MWCNTs	$2.39*10^{-8}$
CNTs-(2)	MWCNTs	$1.33*10^{-7}$
CNTs-(3)	MWCNTs	$2.80*10^{-7}$
CNTs-(4)	MWCNTs	$9.58*10^{-7}$
CNTs(f)-(1)	MWCNTs	$1.04*10^{-6}$
CNTs(f)-(2)	MWCNTs	$1.09*10^{-6}$
CNTs(f)-(3)	MWCNTs	$2.34*10^{-6}$
ternary-(1)	MWCNTs + MC	$2.55*10^{-8}$
ternary-(2)	MWCNTs + MC	$9.29*10^{-7}$
ternary-(3)	MWCNTs + MC	$1.25*10^{-6}$
ternary-(4)	MWCNTs + MC	$1.90*10^{-6}$

4.4.2.1. Binary system

The IS results for the CNTs-(1-4) system can be seen in **Figure** 4-4. As can be observed, the real part of the impedance was highly affected by the dispersion duration. In detail, the real part of the impedance values at low frequencies exhibited a significant decrease with increasing dispersion duration. The most pronounced decrease can be observed between the CNTs-(1) and CNTs-(2) composite where the real component showed a decrease of approximately one order of magnitude. After dispersing the MWCNTs in the epoxy matrix for 4 hours, the real part decreased from 1.14 $10^8\Omega$ (1st hour) to $2.85x10^6\ \Omega$. This behaviour can be attributed to the de-

agglomeration of the CNTs within the epoxy and the formation of a conductive network. The CNTs interconnected network, provided conductive paths for the charged carriers within the insulating polymeric matrix, thus leading to the conductivity increases of the nanocomposites as seen in **Table** 4-3. This increase also caused the Ohmic (linear) to a non-Ohmic (non-linear) transition to shift towards higher frequencies (**Figure** 4-4a). This change is denoted by the shift of the transition of the values of the real part of the impedance vector from a quasi-stable value to decreasing values as a function of frequency.

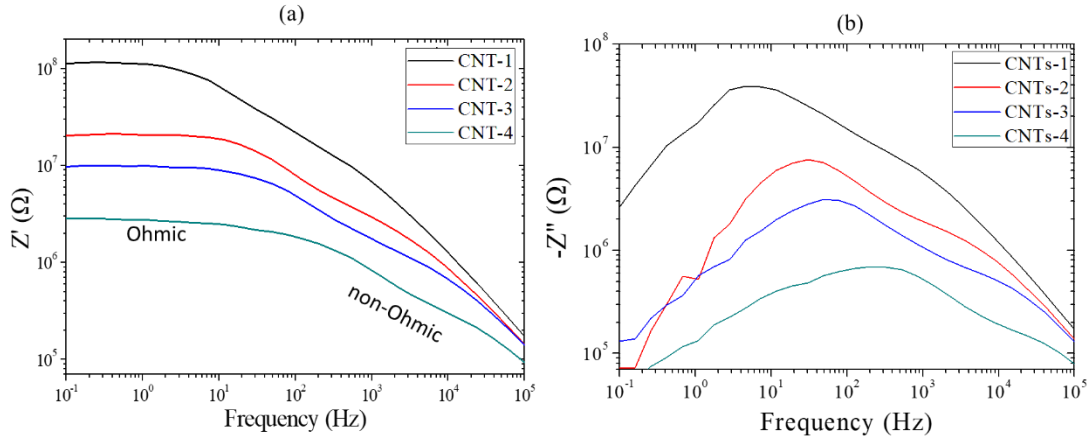

Figure 4-4 Real (a) and imaginary (b) parts of the impedance versus frequency for the CNTs reinforced composites.

Figure 4-4b depicts the evolution of the imaginary part in the frequency domain as a function of dispersion duration. In general, the imaginary part of the impedance or the reactance is characteristic of the ability of the system to store energy and is related with the capacitance or inductance properties. In this case, the shape of the curves was close to that of a semicircle which in its turn was indicative of a strong capacitive behaviour. This capacitance behaviour was observed to scale according to the duration of dispersion. Additionally, it potentially denoted the existence of an interfacial polarization mechanism, which was manifested by a single peak at intermediate frequencies of the imaginary part spectra [200,212,213]. Summarising, the continuous de-agglomeration of the MWCNTs resulted in an increase to the conductivity of the nanocomposite. This affected the imaginary part in a dual fashion: (i) the maximum of the imaginary component of the impedance decreased due to the reduction of the effect of the interfacial mechanism and simultaneously (ii) the peak of the imaginary spectra shifted to higher frequency due to the fact that the charged carriers were able to follow the alterations of the external field at higher frequencies.

4.4.2.2. Low temperature protocol – CNTs(f)- (1-3)

Figure 3-6 presents the real and imaginary components of the impedance for the low temperature dispersion protocol. As stated in the experimental section, the low temperature dispersion was conducted so as to ascertain whether the increased viscosity induced by the low dispersion temperature would affect the composites electrical properties.

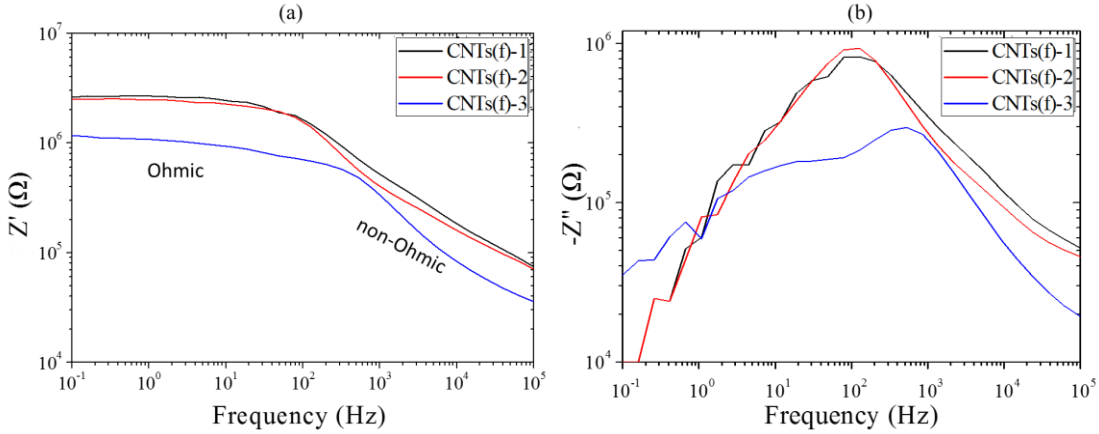

Figure 4-5 Real (a) and imaginary (b) parts of the impedance versus frequency for the CNTs (f)-(1-3) system

In this case, the real part of the impedance (**Figure** 4-5a) exhibited a more pronounced reduction to its values at low frequencies, after 1 h of dispersion, when compared with the dispersion protocol at 25 °C. The aforementioned behaviour can be attributed to the increased viscosity of the system during the dispersion process, which enhanced the shear forces induced by the impeller rotation. This enhancement, evidently resulted in improved deagglomaration of the MWCNTs and a more effective particle distribution in the epoxy matrix. As can also be observed in **Table** 4-3, the DC conductivity between the two dispersion protocols after 1 dispersion hour, reached a two orders of magnitude of increase. After 2 h of dispersion the real part of the impedance remained unaffected while after the third dispersion hour, the impedance values were reduced to less than half the previous values (from 2.52 MΩ to 1.15 MΩ). Similar to the 25 °C dispersion, the continuous formation of the conductive CNT network forced the transition frequency, where the hysteric phenomena occur, to shift towards higher values.

As can be seen in **Figure** 4-5b, in the case of the CNT (f)-3 composite, the imaginary impedance spectrum exhibited a peak which is significantly broader than that observed in the case of the CNTs (f)-(1) and CNTs(f)-(2) composites. It is evident that the dispersion duration and the capacitive behaviour of the nanocomposite are `inversely proportional. This can be

observed by the decreased contribution of the interfacial mechanism to the total polarization of the system at higher dispersion duration. This behaviour can be attributed to a greater amount of conductive "paths" within the matrix that allowed charged carriers to follow the changes of the external alternating field at even higher frequencies resulting in a notable decrease in maximum imaginary values in the case of CNT (f)-(3).

4.4.2.3. Ternary

Figure 4-7 illustrates the real and imaginary parts of the impedance for the ternary composites as affected by the dispersion duration.

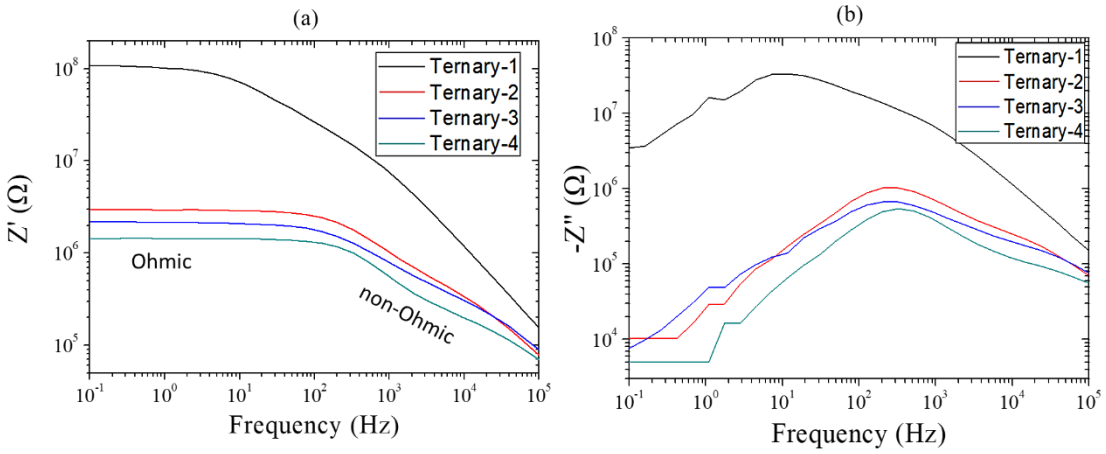

Figure 4-6 Real (a) and imaginary (b) parts of the impedance versus frequency for the Ternary-(1-4) system.

It is evident that the dielectric properties of the final composite were highly affected by the addition of the MC to the nano-modified MWCNT/epoxy mixture. The most noticeable difference was the abrupt decrease in Z' values at the Ohmic region by almost two orders of magnitude after only two hours of dispersion. At the same time, the transition frequency from linear to non-linear behaviour shifted towards significantly higher values indicating an increased conductive behaviour. After 3 hours of dispersion, no major alterations in the dielectric profiles of the ternary composites were present with the values of the real part of the impedance at low frequencies to exhibit a relative stabilization. At this point the obtained results indicated that the formation of the CNT network was fully completed after only 2 hours.

The synergy effect between CNTs and MC was also evident in the case of the imaginary part, since there was a significant reduction to its maximum values after only 2 hours of dispersion by almost one order of magnitude (**Figure** 4-6b). The aforementioned behaviour was not present in the case of the binary system where a smoother reduction in Z'' values with

increasing dispersion duration was recorded. This difference can be attributed to a more rapid conductive CNT/ MC network formation as the MC particles created small interconnections between individual CNT and/or CNT agglomerates that enhanced the total conductivity of the system and decreased the effect of the interfacial polarization mechanism [214].

4.4.3. Fracture toughness

Figure 4-7 summarizes all K_{IC} and G_{IC} mean values that were extracted from the binary and ternary composites SENB fracture toughness tests.

a.

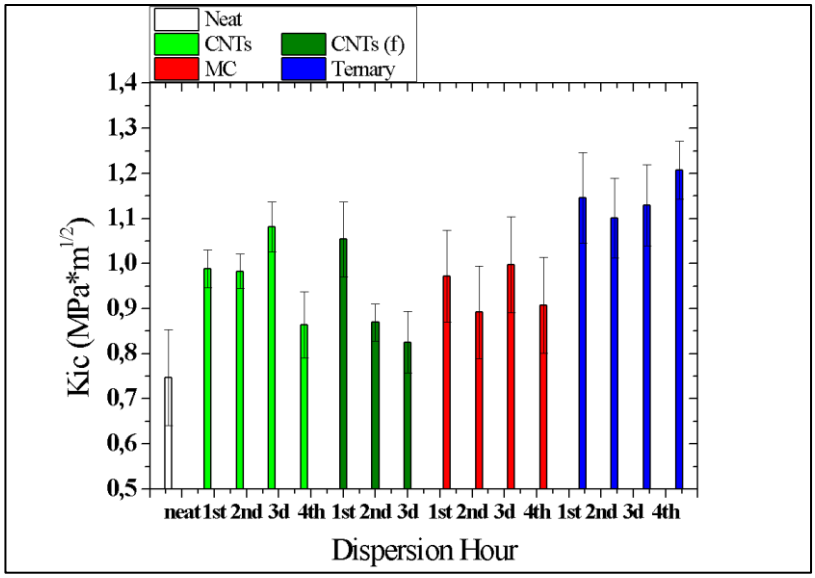

b.

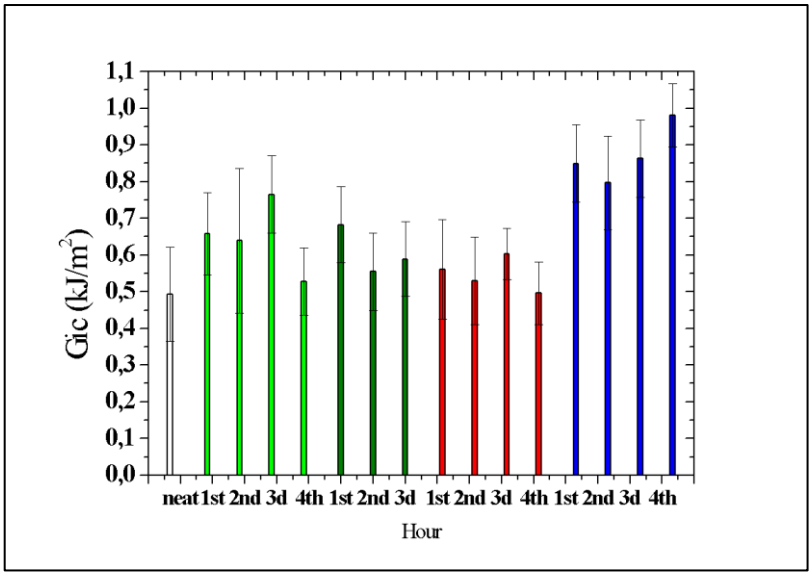

Figure 4-7 (a) K_{IC} and (b) G_{IC} fracture toughness results obtained from all manufactured composites

It can be observed that the selected fillers, either in the binary or the ternary systems, resulted in improved fracture toughness and the K_{IC} and G_{IC} values were dependent on the

dispersion variables and reinforcing approach (binary vs ternary). In detail, CNTs-(1-3) composites exhibited intermediately increased K_{IC} values by 32, 32 and 45%, respectively. Interestingly enough, the fourth hour of dispersion resulted in a relative increase of fracture toughness values (13%) for the CNTs-4 composites when compared to the neat epoxy. It can be postulated that there was a dispersion duration and applied energy threshold, which when overpassed, any obtained improvements are being diminished. This observed behaviour may be also related to the formed network in the nano-composites. It can be postulated that the excessive dispersion time, could have led to such small particles average size that the formed network was ineffective in restricting and hindering crack propagation.

In the case of the low temperature dispersion, K_{IC} value of CNTs(f)-(1) appeared improved by 25% however the consequent two hours of dispersion (CNTs(f)-2 and -3), led to lower relative increases of 12.8% and 5.9%, respectively compared to the neat epoxy values. As similarly observed in the CNTs-(1-4) composites, a dispersion time an energy threshold was present, which when surpassed, a diminishing trend in the relative improvements in fracture toughness values will be manifested. In the case of the low temperature dispersion, this trend was evident in a more rapid manner.

The binary MC composites, exhibited moderately increased values, similar to the CNTs binary composites. The highest observed K_{IC} value obtained after three hours of dispersion, was improved by 30% when compared with neat epoxy. The obtained fracture toughness results didn't show any pattern which can be correlated to the dispersion duration as in the case for the CNTs composites.

All ternary composites possessed significantly improved K_{IC} values when compared both with neat, MC and CNTs composites. Ternary-(4) composites exhibited the maximum increase in K_{IC} values of 61.0% while the other three ternary-(1-3) composites exhibited increased values by 52, 48, and 49% respectively. In addition, it was observed that the standard deviation in the calculated values was decreased, indicating that the combination of the two fillers resulted in more reliable results (clustered closely around the mean). Taking into account the aforementioned behaviour of the binary composites, it can be postulated that the observable improvements could be attributed to synergistic effects between the two employed fillers which resulted to the formation of a hybrid 3D network of particles capable of more effectively hindering micro-crack propagation.

In terms of G_{IC} performance, the CNTs composites exhibited the same behaviour as in the case of K_{IC} with increasing values up to the third dispersion hour. This time however, the fourth hour of dispersion not only eliminated any improvement, but resulted in degraded performance when compared with the neat epoxy. The low temperature dispersion resulted in intermediate improvements in G_{IC} terms but in this case the mean values seem to be unaltered by the increasing dispersion duration. The ternary composites, exhibited the same behaviour as with the case of K_{IC} with the ternary-(4) composites possessing the highest increase at 96% while the remaining ternary-(1-3) composites increase ranged from 60 to 72.0%.

4.4.4. SEM fracture surface analysis.

Figure 4-8, **Figure** 4-9 and **Figure** 4-10 present SEM images obtained from the SENB fracture surfaces of the MC-(3), CNTs-(3) and ternary-(4). These specific specimens exhibited the highest observed fracture toughness values of their respective classes. Inside the noted circles and ellipses (sites), different fracture phenomena are enclosed while the direction of crack propagation is indicated with the green arrow.

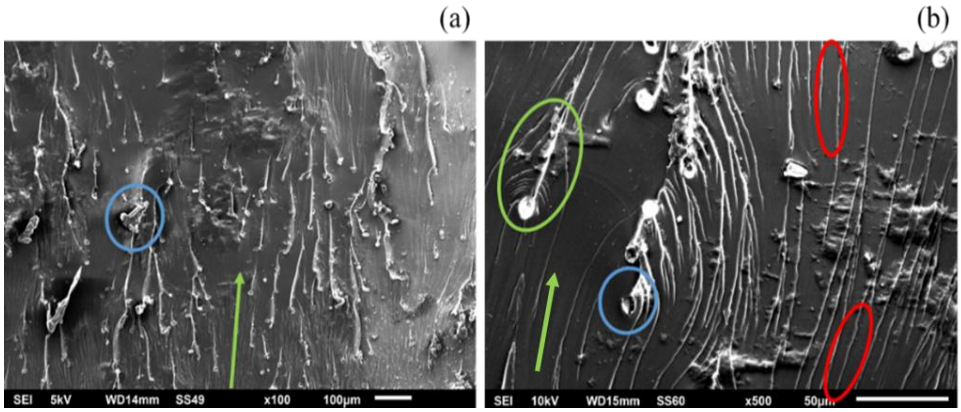

Figure 4-8 SEM photographs obtained from a MC-(3) SENB specimen fracture surface at (a) x100 and (b) x500 magnification.

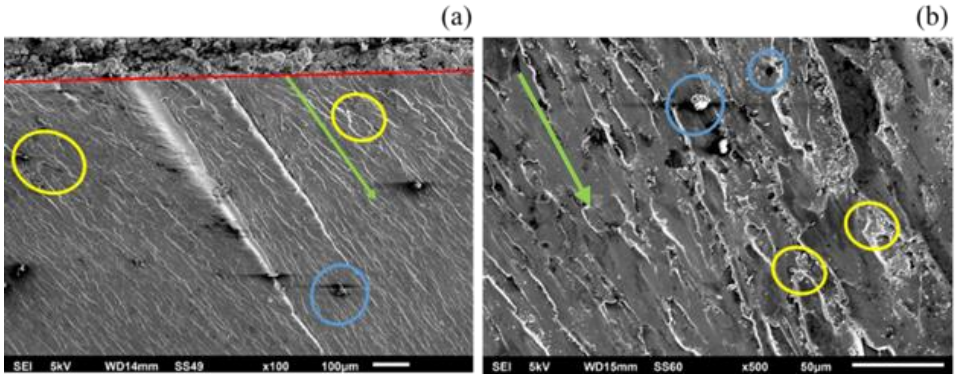

Figure 4-9 SEM photographs obtained from a CNTs-(3) SENB specimen fracture surface at (a) x100 and (b) x500 magnification. The red vertical line represent the pre-crack tap.

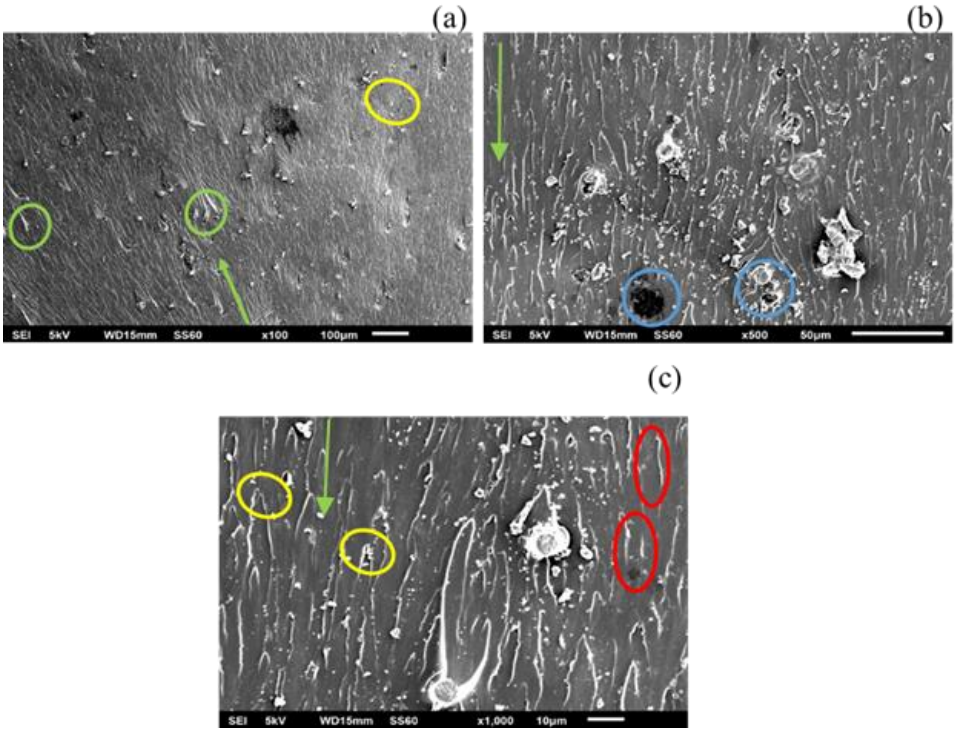

Figure 4-10 SEM photographs obtained from a ternary (4) SENB specimen fracture surface at (a) x100,(b) x500 and (c) x1000 magnification.

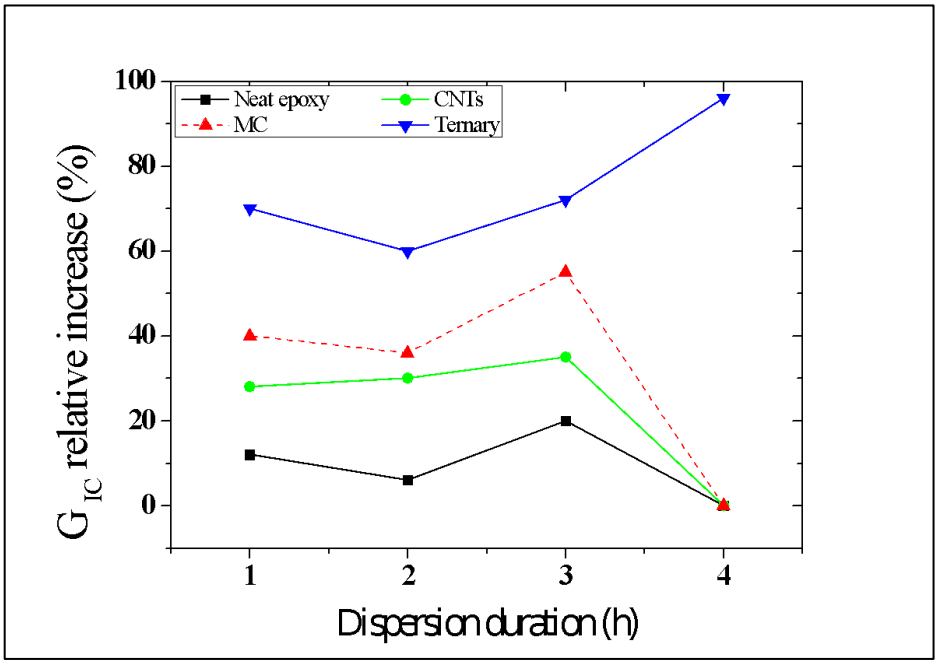

Figure 4-11 G_{IC} relative increase vs dispersion hours for the binary and ternary composites. The sum of the MC and MWCNTs binary composites is also depicted.

In the previous sections it was shown that the combination of the selected carbon micro and nano scaled fillers resulted in the formation of a hybrid 3D network with improved mechanical and electrical performance when compared to the binary systems. This hybrid network was comprised of long aspect ratio MWCNTs, either in agglomerated or disentangled state, and micro-scaled MC particles which can effectively increase fracture toughness with simultaneous significant decrease in the electrical impedance of the final composite. According to a very resent comprehensive review by Quaresimin et. al. [183] on thermosetting composites fracture mechanisms, the micro and nano scale, can be associated with distinctive but sometimes overlapping fracture phenomena. Both micro and nano fillers can act as stress concentration sites from which crack initiation can occur. Deflection and pinning of a generated micro crack can be achieved via the presence of micro particles while secondary generated nano cracks, known as tails, can be subsequently deflected or pinned by nano particles. Apart from crack deflection and pinning phenomena, it is possible that the released concentrated energy will result to particle pull-out, which along with crack initiation and propagation, are the dominant fracture mechanisms in CNT modified epoxy systems like the CNTs binary composites in this study. However, similarly to micro carbon fibers, long aspect ratio CNTs, tend to break rather than pull-out from the matrix when a critical length is surpassed [215].

As it can be observed, all composites exhibited a very good distribution of the filler particles all over their entire respective surfaces. In all composites, striations indicative of matrix cracking (red sites), are observed throughout the scanned surfaces, though on the MC -(3) specimen, large matrix areas with clear fracture surface areas are evident indicating that the weight content of the MC could not effectively 'fill' most of the epoxy resin matrix. However, the fracture toughness results indicated that the MC micro particles can effectively increase the amount of absorbed energy.

The main fracture mechanisms that were present in the MC -(3) binary composites, were that of crack deflection and pinning (green sites) and particle pull-out (blue sites). In the case of the CNTs-(3) binary composites, it is observed that fracture phenomena like crack bifurcation or initiation, especially at sites with increased particle agglomeration, (yellow sites), along with particle pull-out, breakage and void creation (blue sites) phenomena, were mostly present. In the micrographs obtained from the ternary-(4) composites, it is evident that a dominant fracture mechanism could not be clearly distinguished. In fact, all the observed fracture mechanisms of the binary composites, could be identified, in various extents, on the fracture surface of the ternary composite. The combination of the micro scaled MC, MWCNTs agglomerates, the nano-scaled MWCNTs agglomerates and the fully disentangled MWCNTs, resulted in a creation of a 3D hybrid micro/nano-network, capable of hindering crack initiation and propagation more effectively when compared to the binary counterparts as was evident in the fracture toughness results.

The co-existence of the micro and nano scaled conductive fillers, is associated with the formation of the hybrid 3D network with decreased electrical resistivity and improved fracture toughness. The effectiveness of the hybrid network, can also be supported by the G_{IC} relative increase results found in **Figure** 4-11. It is observed that most of the composites exhibited a linear increase up to the third dispersion hour. The fourth hour though, had detrimental effects on G_{IC} for both binary composites, where the relative increase plummeted to 0%. However, the ternary-(4) composite, benefited even more from four hours of dispersion, peaking at 96% which was the highest observed increase in this study.

4.4.5. DMA results

The obtained storage modulus, loss modulus and loss factor as a function of scanned temperature curves for the neat epoxy and the binary and ternary composites can be found in **Figure** 4-12 and **Figure** 4-13 respectively. **Table** 4-4 summarizes all glass transition

temperature (T_g), tand and tand width while **Table** 4-5 presents storage modulus in the glassy (E'_g) and rubbery (E'_r) region along with the calculated Mc values for all studied composites.

Table 4-4 Values of glass transition temperature and tand of the studied composites

Material	T_g (^{o}C)	tand at T_g	tand peak (^{o}C)
Neat epoxy Resin	131	0.83	33
MC -composite	135	0.74	31
CNTs-composite	136	0.73	30
Hybrid-composite	134	0.72	28

Table 4-5 DMA values used for the calculation of the apparent cross link density for the studied composites

	Neat Epoxy	MC -(3)	CNTs-(3)	Ternary-(4)
E'_g (MPa) (at 30^{0}C)	2668±5	2711±5	2910±5	3029±4
E'_r (MPa) (at ^{0}C)	17.0±0.3	17.0±0.3	21.5±0.3	21.9±0.3
M_c (gr/mol)	655.5±0.5	654.7±0.5	522.4±0.5	509.9±0.5

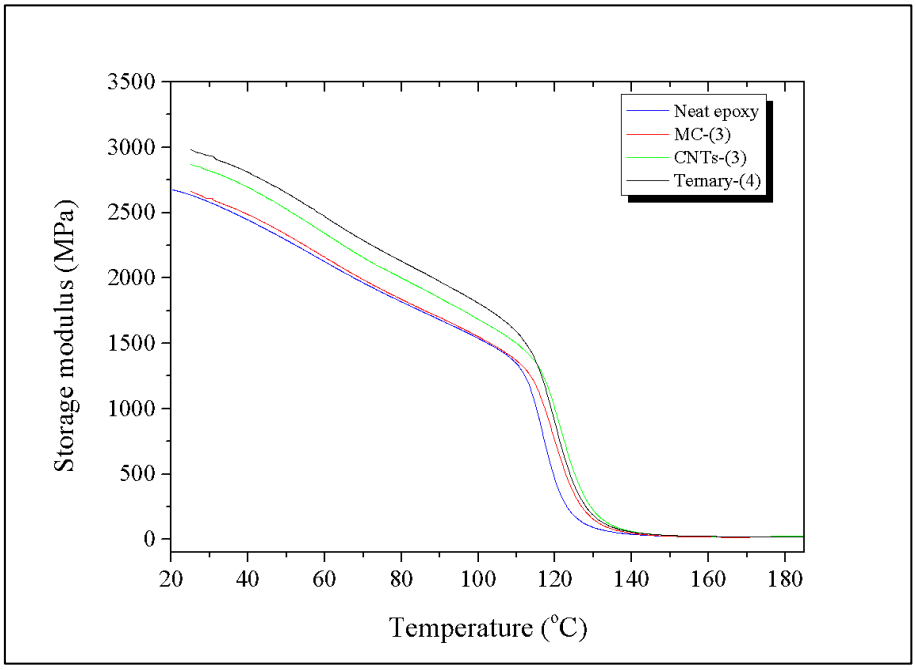

Figure 4-12 Storage modulus E' vs temperature curves for the neat epoxy, the binary and ternary composites.

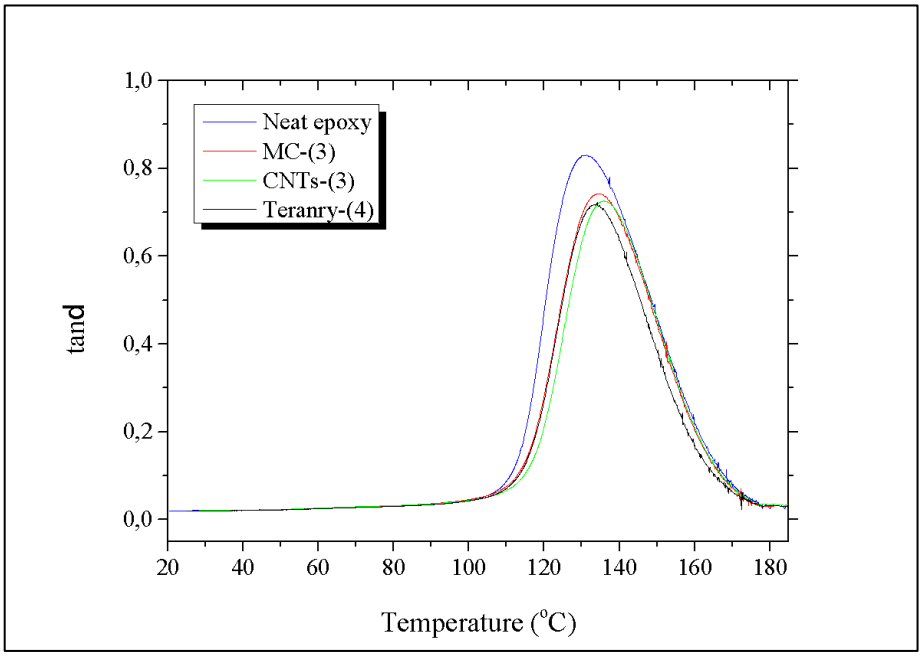

Figure 4-13 Curves of the tand versus temperature of the neat epoxy resin and composites

As shown by DMA the Ternary composite material with the different types of carbon fillers exhibited increased mechanical properties as compared to neat epoxy resin and binary composites. As expected, at a given frequency, the curves of E' exhibited a glassy region (below 100°C) followed by a large decrease in the glass transition region (100-140°C) and a plateau in the rubbery state (above 140°C). The incorporation of different types of carbon fillers to neat epoxy resin led to an increase of the storage modulus values both in the glassy and in the glass transition region. In the glassy region, the elastic modulus for the ternary composite are higher (3029 MPa at 30°C), followed by the CNTs-composite (2910 MPa) and finally by MC -composite (2710 MPa) and by neat epoxy resin (2668 MPa). The incorporation of MC particles or/and CNTs into the neat epoxy appeared to restrict the epoxy chains' mobility. The combination of micro and nano scaled fillers exploited synergistic effects between the two types of carbon fillers. When MC particles were added into the composites containing nano-tubes CNTs, the gaps between the CNTs were effectively filled and the CNTs were linked together, resulting in the formation of a network with increased stiffness [38] On the contrary, in the rubbery state, no significant difference of the studied materials' stiffness was observed.

In terms of glass transition temperature, it can be seen that Tg has shifted from 131°C for the neat epoxy resin to higher temperatures for the composites. However, it has been reported [216] that the feature that is most sensitive to the structure of the interphase is the

height of the tand at the Tg and is recommended as the best parameter for characterizing variations in interfacial structure of composites. It can also be observed that the height of the tand peaks of the composites remained unaffected to the filler type but decreased compared to that of the neat epoxy resin. The decrease of tand can be attributed to the stiffening effect due to the filler inclusion. The low value tand at the Tg indicates better interfacial adhesion between filler and matrix. In the present study, the ternary-composite showed the lowest value. Therefore, it can be inferred that the combination of micro and nano scaled carbon fillers, yields better interfacial adhesion between filler and matrix and contributes to a more uniform dispersion of particles in epoxy network.

A parameter for characterizing the heterogeneity of polymeric network is the tand peak width. Simultaneously the amplitude of the tand was decreased while its half-width was increased, evidencing a distribution of relaxation times of the polymer chains [217]. This effect can be considered as a measure of the network heterogeneity evidence, thus, denoting that these composites displayed a more heterogeneous distribution of relaxation times as compared to the neat epoxy matrix. In this study, the ternary composite showed the less heterogeneity (**Table** 4-4), as a result of the synergistic effect between the two fillers.

As previously stated, the best performing binary and ternary composites, in terms of fracture toughness, were studied in DMA so as to compare the fillers effect on the thermomechanical performance of the composites. The M_c was calculated according to the basic equation of rubber elasticity and is the inverse of cross link density [92], (equation 3.5). The values of storage modulus in the glassy (E'_g) and rubbery (E'_R) region along with the calculated values of Mc for the studied CNTs-(3), MC-(3) and ternary-(4) composites can be found in **Table** 4-5.

As can be seen, the filler particles in the CNTs binary and ternary composites led to decreased M_c values with the MC-(3) possessing almost identical $M_{c.}$ when compared to the neat epoxy. This behaviour indicates that the CNTs filler particles interfered with the crosslinking process resulting to the formation of greater amount of cross links in the epoxy matrix a behaviour that is in cross relation to the relevant literature [92,218]. Overall it was observed that the CNTs and ternary composites exhibited improved thermomechanical performance when compared with the neat epoxy in agreement with the observed improvements in the fracture toughness.

4.5. Conclusions

The scope of this work was to study the effect of different dispersion duration and selected filler on the final mechanical and electrical properties of epoxy based composites. IS and SENB tests were performed in order to access the electrical and mechanical properties of the composites respectively.

IS results indicated a direct correlation between the dispersion duration and real and imaginary parts of the impedance. In all cases the real component exhibited significant decrease to its values with increasing dispersion duration due to the formation of the CNTs or CNTs/ MC conductive network. The influence of the dispersion parameters and the synergistic effect between the two fillers was evident in the imaginary component as well. This influence was manifested by the decrease in maximum imaginary impedance values followed by a concurrent shift of the observed peaks towards higher frequencies with increasing dispersion duration. A behaviour that can be attributed to a more rapid formation of conductive CNT/MC network as the MC particles created small bridges between individual CNT and/or CNT agglomerates that enhanced the total conductivity of the system

The inclusion of the fillers resulted also in improved fracture toughness. The binary CNTs systems exhibited increased fracture toughness for increasing duration up until 4 hours of dispersion. The ternary systems exhibited significant improvements even after only one hour of dispersion. The formation of the hybrid micro/nano particle network was also evident in the DMA results where the ternary composites exhibited increased storage modulus and glass transition temperatures when compared with the neat epoxy and the binary composites. The overall observations in the fracture toughness and the thermomechanical performance of the binary and ternary systems, indicated that the combination of the micro and nano scaled fillers resulted in synergistic effects between the two carbon fillers, leading to the formation of a hybrid 3D micro/nano scaled hybrid network which was more effective for hindering crack propagation. The co-existence of the micro and nano scaled particles effectively resulted in increased energy absorption capabilities by imposing more tortuous paths in the crack front tip. The macro scaled MC particles effectively ‘arrested’ the micro cracks effectively branching them to smaller nano cracks which in turn were arrested by the nano scaled CNTs agglomerates and individual CNTs.

5. Effect of multi-scale reinforcement on the durability – Epoxy composites level

Pat of the results of the following chapter have been published in [152,219,220]

5.1. Scope of the study

This chapter includes the results of the study of the multi-scaled reinforcing approach on the durability of epoxy composites. Towards that end, the formulations from Chapter 04 that led to the optimum final properties, were reproduced and were used for the manufacturing of specimens for DMA, wear resistance and IS measurements. All measurements were coupled with hydrothermal exposure protocols in order to study the effects of the reinforcing approach on environmental durability.

5.2. Introduction

Epoxy resins can be found in a wide range of applications spanning from electronics as encapsulating materials, to marine applications as protective coatings and as matrices for Fibre Reinforced Composites (FRC) for aeronautics structures [221]. In most of these modern engineering applications, epoxies are required to operate in demanding and diverse environments enduring sudden temperature variations, water or moisture exposure, particle erosion or magnetic discharge phenomena [222–225]. As can be understood, the overall performance of the epoxies, would be dependent on several material properties like abrasion resistance, modulus, toughness, moisture absorption to name few.

However, due to their hydrophilic nature, epoxies tend to absorb water within the free volume of the polymeric network, i.e. the unoccupied volume in between the polymeric chains. It is generally accepted, that two types of water can be observed in epoxies upon absorption: (i) unbound free water which fills the nano-voids but do not induce swelling, frequently referred to as type-I water and (ii) hydrogen-bonded water, which causes swelling of the polymers and is referred as type-II water [226]. In most cases, the moisture absorption follows a Fickian pattern where a stage-1 and a stage-2 absorption patterns are observed [227,228]. Fickian-like behaviour, can also be observed in particulate epoxy matrix composites during immersion in aqueous chloride solutions as seen in [229,230].

Stage-1 absorption is related to the filling of the free volume of the polymer, where the ingress of water increases linearly with time until a saturation point. At this point, stage-2 absorption is initiated and the ingress of water slows down mainly due to swelling effects. In general, during stage-2, type-II water molecules create hydrogen bonds with unreacted epoxy

rings resulting in further swelling of the polymer thus leading to degradation of material properties [231]. In FRCs, water absorption takes place either at the locus of the matrix micro-cracks or at the fibre-matrix interface leading to diffusion to the surrounding polymer network through unreacted polymeric chains [232,233]. It has been shown, that the increased free volume in highly cross-linked epoxy systems tends to result in increased type I water absorption at the early stages of exposure while the lower percentage of unreacted polymeric chains leads to reduced type-I water absorption at the latter absorption stages [115,234].

The ingress of water leads to detrimental effects in both the mechanical properties, i.e. fracture toughness or tensile strength, and the physical properties, i.e. glass transition temperature of both neat and modified epoxies [235]. Although, it has been observed that water uptake can cause secondary curing reactions, also known as pseudo-cross-linking, leading to improved or unaltered properties depending on the absorption stage [236]. For instance, in [237] the hydrothermal aging behaviour of a Carbon FRP laminate and its epoxy matrix in bulk form were investigated at various immersion temperatures. The studied aged bulk epoxy, i.e. epoxy after water absorption, exhibited an almost identical storage modulus but decreased Tg when compared to the unaged one, while the mode-I interlaminar fracture toughness increased after immersion of 4 weeks at 30^0C.

Since moisture absorption is mainly controlled by type-I water ingress, it is reasonable to postulate that reducing the polymeric free volume could lead to the reduction in water uptake levels. The introduction of nano-sized inclusions into an epoxy matrix has been demonstrated as an effective method for controlling the stage-1 moisture uptake [60,238]. Such an approach has also led to improved mechanical performance with mitigation effects of the water induced degradation [178,239,240]. It has to be noted though, that nano fillers like carbon nano tubes (CNTs), can lead to changes in the crosslink density of the polymeric matrix network as well, resulting to accelerated cure kinetics with higher number of open polar sites [241–243]. Type-II water exploit these open polar sites thus forming hydrogen bonds leading to swelling and plasticization effects [244]. These detrimental effects, nevertheless, are counterbalanced by the stiff nature of the CNTs thus resulting in a more rigid polymeric network and counterbalancing effects.

A combined inclusion of fillers at different length scales as reinforcing phases has recently gained attention in the scientific community in order to exploit synergistic effects in mechanical, physical or electrical properties [81,245]. By exploiting the multiscale reinforcing

approach, it was shown that the combination of Multi Wall CNTs (MWCNTs) with milled carbon (MC), leads to composites with significantly improved fracture toughness and reduced electrical resistivity compared to binary ones (i.e. composites comprised of the matrix and one filler type) [152]. Such a multi-scale reinforcing approach has also been shown that can result in composites with improved tribological properties as well thus resulting in multi-functional composites [246,247].

Considering all of the above, this chapter focuses on the effect of the multi-scaled reinforcement approach on the water absorption behaviour in epoxy resins. In detail, MWCNTs and MC were introduced into an epoxy matrix so as to fabricate specimens for dynamic mechanical analysis (DMA), Impedance Spectroscopy and sliding wear experiments. Specimens were immersed in a water bath in order to study the effect of the hydrothermal exposure on the overall performance of the neat and modified specimens.

5.3. Experimental

The effect of water ingress effect on the final properties was assessed. Binary MWCNTs, binary CB and ternary composites were prepared following the procedures in 2.22.3. The dispersion was conducted according to 2.3 with 3000rpms intensity at 25^{O}C for 3hr for all composites.

Specimens for sliding wear resistance, DMA and IS according to 2.4.3, 2.4.7 and 2.4.6.2 were manufacture and tested in “pristine”, “aged” and “conditioned” referring to specimens as produced, after water aging and after water desorption respectively. The “aged” and “conditioned” specimens were processed according to 2.4.10.

Table 5-1 Nomenclature and dispersion conditions for the studied specimens

Filler Material	**Filler content (%w.w)**	**Dispersion duration (hr)**	**Temperature (^{O}C)**	**Nomenclature**
None				Neat
MWCNTs	0.5	3	25	CNTs
MC	2.0	3	25	MC
MWCNTs/CB	0.5/2.0	3	25	ternary

5.4. Results and Discussion

5.4.1. Water absorption

Figure 5-1 and **Figure** 3-2 depict the absorption and desorption profiles respectively for all the tested specimens (neat and modified), while **Table** 5-2 summarises the absorbed water at saturation W_∞, the maximum desorbed water W_{DES} and the calculated Fick coefficients (D_F).

Table 5-2 Moisture uptake and Fick coefficient D, after exposure till saturation for all systems.

	W∞ (%)	**W_{DES} (%)**	**D_F (mm^2/h)**
Neat	4,95± 0.07	-1,655±0.01	0,210±0.00
MC composites	4,31±0.04	-1,504±0.01	0,208±0.01
CNTs composites	4,33±0.05	-1,899±0.05	0,204±0.005
Ternary composites	4,34±0.02	-1,545±0.03	0,204±0.03

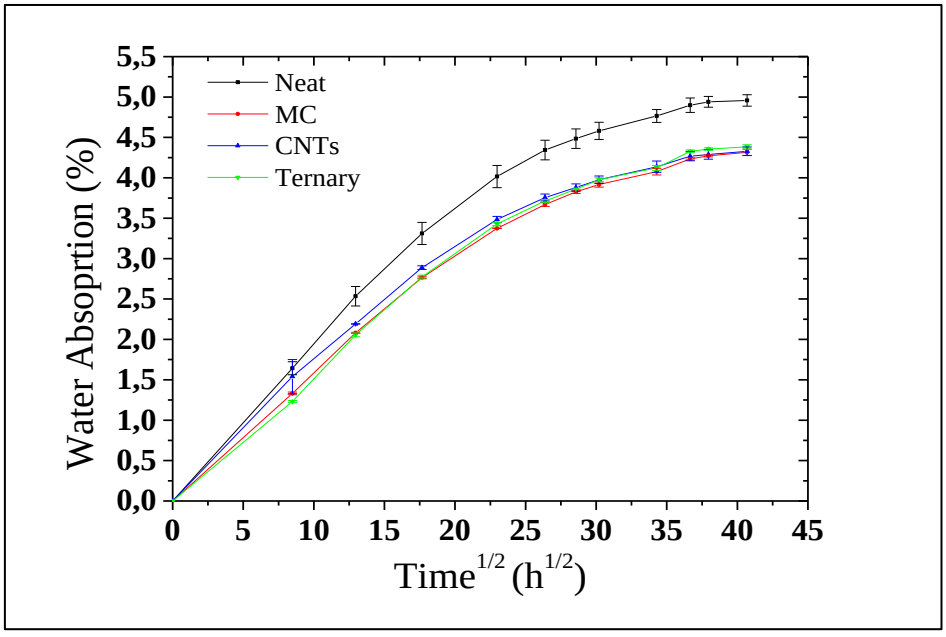

Figure 5-1 Water absorption profiles for all studied composites.

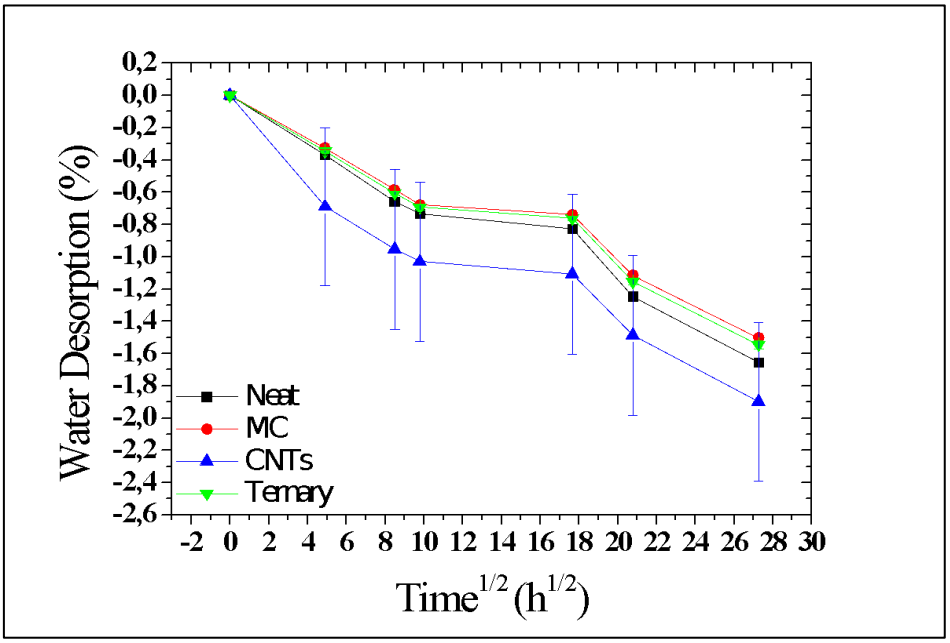

Figure 5-2 Water desorption profiles for all studied composites.

As observed by other researchers [248–251], D_F was marginally affected by the presence of the reinforcing phases. The minor variations in the D_F values could be attributed to the reinforcing particles that could have led to a decreased free volume and slower water uptake. In terms of water ingress, it was observed that for all the systems, the curves presented a linear part at the early stages while they tended asymptotically to the saturation point approximately at 1600 h of immersion. This pattern is indicative of a Fickian absorption behaviour and can also be observed in similar research efforts [252]. In detail, at the early stages of the measurements, all the carbonaceous reinforcements resulted in decreased water absorption when compared with the neat epoxy, leading to an overall 12% reduction in the water absorption at saturation. This phenomenon was associated with the reduction of the polymeric matrix free volume and with the introduction of more tortuous paths for the movement of the incoming water [73]. It is interesting to note, that for all composites minor differences both in the evolution of their absorption profiles and to the maximum absorbed water at saturation were observed (**Figure** 5-1).

Interesting differences were also observed in the desorption profiles of the aged specimens. As **Figure** 3-2 depicts the desorption process was controlled mainly by the matrix phase for all the specimens, while three distinct stages were identified in each profile. At the first stage up to 4 days, all specimens desorbed water with a linear desorption rate, with the CNT composites

exhibiting the highest rate. It can be postulated that during this stage, type-I water from the surface layers quickly evaporated. The water release was more pronounced for the case of CNTs composites, a phenomenon that could be associated with the CNTs-matrix interface. MC and Ternary composites exhibited similar desorption profiles with variations within experimental error indicating a counterbalancing synergy between MC and CNTs particles. During the second desorption stage from 5 to 13 d, a stabilization was observed followed by a second sharp increase in water desorption in stage three. This last stage could be associated with the diffusion of water molecules from sub-surface layers, which, after migrating to the surface, evaporated.

5.4.2. DMA

5.4.2.1. Pristine specimens

Figure 5-3, **Figure** 5-4 and **Figure** 5-5 present the storage modules and tand curves for all pristine, aged and conditioned specimens respectively. **Table** 5-3 summarizes all E', Mc and Tg extracted values from the aforementioned DMA curves for all studied composites.

Table 5-3 Apparent mean molecular weight between cross links (Mc), cross-link density (n), storage modulus (E'), and glass transition temperature (Tg) variations for all tested conditions.

		n (mol/cm^3)	
Neat	1,792	1,931	1,617
MC composites	1,779	1,848	1,982
CNTs composites	2,150	1,645	1,961
Ternary composites	2,346	2,017	2,098
		E' (Mpa)	
Neat	2667±30	2975±25	2265±25
MC composites	2707±25	2724±25	2659±20
CNTs composites	2920±35	2632±50	2157±30

Ternary composites	3026±20	2850±40	2718±20
		Tg (^{0}C)	
Neat	131±1	123±1	122±2
MC composites	134±1	123±1	123±2
CNTs composites	135±2	122±1	121±2
Ternary composites	135±1	124±1	123±2

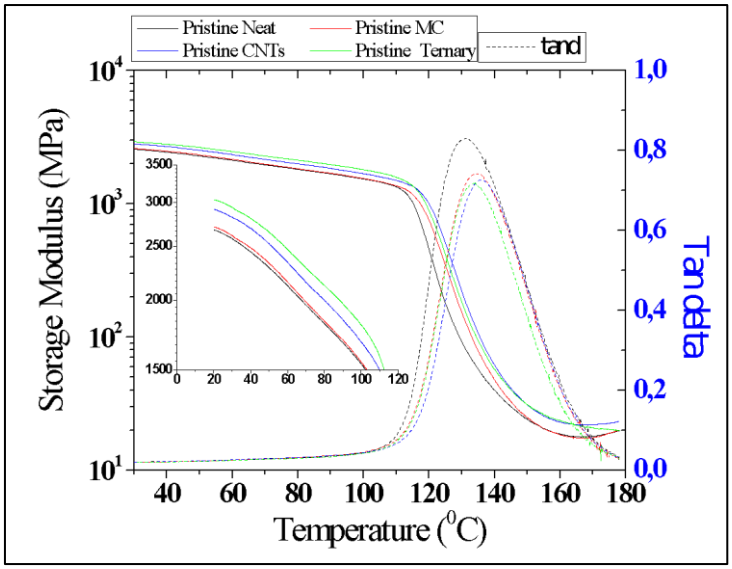

Figure 5-3 Storage modulus and tan d vs temperature curves from pristine specimens.

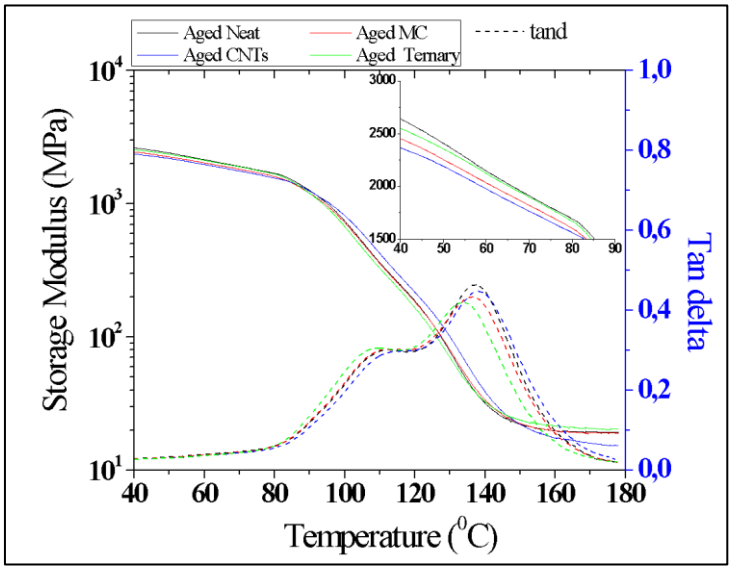

Figure 5-4 Storage modulus and tand vs temperature curves from aged specimens.

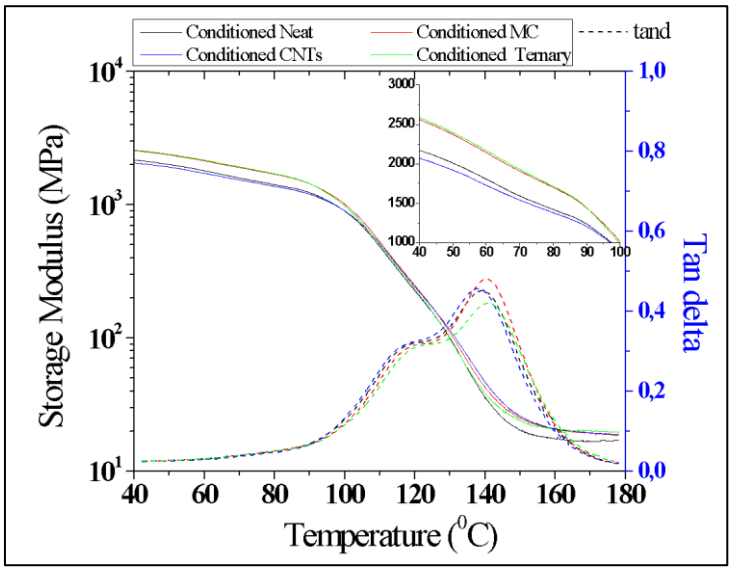

Figure 5-5 Storage modulus and tand vs temperature curves from conditioned specimens.

In terms of pristine condition, it was observed that the combination of CNTs and MC led to the most pronounced increase in the storage modulus (3026 MPa). The CNT composites followed with (2900 MPa), while the MC fillers only marginally increased the E' values (2707 MPa) when compared with the neat epoxy (2667 MPa). Furthermore, the ternary composites were found improved throughout the whole tested temperature range. From the observed results, it could be postulated that the combined introduction of MC and CNTs into the epoxy matrix, resulted in a more restricted polymer chain mobility indicating more effective filler

inter-connection when compared to the binary CNT and MC systems. In terms of Tg, it can be seen in **Table** 5-2, that Tg shifted from 131^{o}C for the neat epoxy to 134 ^{o}C, 135 ^{o}C, and 133 ^{o}C for the binary (MC, CNTs) and ternary composites, respectively.

It has been reported [149] that the structure of the interface in epoxy composites mostly affects the height of the tan d peak and, therefore, this variable is recommended for characterizing the interfacial structure of the composites. As can be seen in **Figure** 5-3, the height of the tan d peak was decreased for all composites when compared to the neat epoxy. This decrease in the tan d peak could be attributed to the stiffening effect as a result of the carbonaceous fillers inclusion. Furthermore, given that the ternary composites exhibited the lowest tan d peak values among all the systems, it can be inferred that the combination of micron and nanoscaled particles led to a more effective filler network with more uniformly dispersed particles. The width of the tan d peak is also a parameter for the assessment of polymer heterogeneity. The tan d width was decreased for all composites when compared with the neat epoxy, with no significant variations between the three composites, thus indicating more heterogeneous networks.

Cross link density ‘n’ was also found dependent to the different types of fillers. MC composites exhibited slightly decreased values in comparison to the neat epoxy composites while the CNT composites and the ternary composites showed significantly increased values. It could be postulated that the introduction of MC particles, caused this small decrease in the crosslink density by impeding the molecular motions during the resin polymerization. Conversely, the inclusion of the CNTs, which were much closer in dimensions to the polymeric chains, facilitated crosslinking reactions due to their significantly higher surface area, leading to a remarkable increase in the crosslink density. It has been reported that the inclusion of CNTs results to increased cross-linking via bridging of unreacted polymeric chains thus leading to a stiffening of the polymeric chain network [76]. The combined inclusion of MC and CNTs also increased ‘n’, led to the most pronounced increase in ‘n’ values indicating a synergy between the two filler types. It could be inferred that the simultaneous introduction of CNTs and MC particles in the epoxy matrix, led to “a cooperation” between the fillers resulting in a more effective bridging of unreactive polymeric chains.

5.4.2.2. Aged composites

As stated in the Introduction section, water absorption could result in ‘secondary’ cross-linking phenomena (pseudo crosslinking) and/or stiffening effects in epoxy polymers, which could be

attributed to type-I and type-II water [236]. This phenomenon was observed in the aged neat epoxy as an increase in E' to 2975 MPa, a value which approached the corresponding value of the pristine ternary composites (**Figure** 5-4). The presence of water molecules in the free volume of the polymer along with the bound water molecules resulted in restricted chain mobility and stiffening effects. On the other hand, it was observed that the absorption of water, led to decreased E' (by 10%) for the case of the CNT composites. As has been reported, moisture or water absorption in CNT modified epoxies, occurred both through epoxy matrix microcracks and at the CNT/epoxy interface [252,253]. The observed E' values for the aged binary CNT composites, which almost coincided with that of the pristine neat epoxy, indicated that the ingress of water deteriorated the interfacial strength leading to softening effects. The observed decrease could also be induced by swelling stresses in the interfacial areas due to the aforementioned phenomena. This postulation could be further supported by the calculated decreased (almost by 25%) 'n' values of the aged binary CNTs specimens when compared to the pristine CNTs composites ones. In the case of the MC aged specimens, a slight increase was observed indicating matrix dominating properties. Finally, in the case of the ternary composites, a decrease was also observed in the E' values (by 6%) but in this case to a smaller percentage in comparison with the CNT composites, further indicating synergistic effects between the MC and CNTs fillers.

Out of all studied thermo-mechanical properties, (E', tan d and n), tan d curves were mostly affected by the ingress of water. The most pronounced difference between the pristine and aged specimens is the existence of a double peak for the latter ones, in the temperature range from 80 ^{0}C to 140 ^{0}C. The first peak could be associated with the evaporation of type-I water, while the second one with the relaxation of the polymeric chain network. The presence of water resulted in almost identical heights and widths for all systems (neat and modified), with the ternary composites slightly deviating and exhibiting the lowest values among all specimens. Water absorption had detrimental effects on Tg values as well. All systems exhibited decreased Tg values by almost 10^{0}C with the aged CNTs composites experiencing the most pronounced deterioration with Tg values being reduced by 13^{0}C. It was further inferred that the combined inclusion of micron and nanofillers gave rise to synergistic effects leading to a more effective and stable reinforcing effect, therefore, mediating the detrimental consequences of the water ingress.

In terms of 'n', the pseudo crosslinking was evident in the calculated values for the aged neat and MC specimens. As seen in **Table** 5-2, the aged specimens exhibited increased

'n' values indicating the ingress of type-II water led to bridging of unreacted polymeric chains. On the other hand, in the cases of CNTs and ternary composites, the aged specimens exhibited decreased 'n' values (30% and 16% respectively), with the CNTs composites having the most profound deterioration amongst all studied specimens exhibiting. It could be inferred that the weak interface between the epoxy matrix and the inert CNTs surfaces, was not effective enough to impede the deteriorating effects of water ingress. Interestingly though, in the case of the ternary composites, a synergy effect between the two filler types, led to a more controlled deterioration thus further indicating synergy effects.

5.4.2.3. Conditioned composites

The 'conditioned' study was conducted so as to investigate the effect of type-I water in the materials properties. More specifically, it was expected that the evaporation of type-I water, that took place at the early stages of desorption, would result in even more pronounced thermomechanical performance deterioration. In detail, it can be seen in **Figure** 5-5, that all systems exhibited similar curves when compared with the aged ones. More specifically the tan d curves of the conditioned specimens exhibited the double peak and in terms of E' values at 30 ^{0}C, all systems exhibited reduced values when compared with the aged and pristine specimens, with the MC and ternary ones being less affected. For the case of the conditioned neat specimens, it was observed that the E' values dropped at levels below those of the pristine ones, thus confirming the pseudo-cross-linking postulation. What was more interesting though, is the fact that the evaporation of type-I water resulted in the most pronounced deterioration for the case of the conditioned CNTs composites. Not only the conditioned CNT specimens exhibited E' values below those of the pristine and aged CNTs specimens, but the observed values were also even lower than those of the conditioned neat ones. Such behaviour indicated that type-I water was preferably absorbed in the CNT-matrix interface and with subsequent evaporation, led to further deterioration of the materials properties.

In terms of 'n' values, it was seen that the evaporation of the water molecules led to a reversible effect in the cases of the CNTs and MC conditioned composites as manifested to the increased 'n' values when compared to the aged specimens. It can be postulated that the desorption of water left open polar groups, where the CNTs and MC particles could have interconnected. However, the decreased conditioned E' values suggested that the thermomechanical deterioration and plasticization of the epoxy matrix, could not be counterbalanced by the presence of the stiff CNTs and MC fillers. This effect was also evident

in the ternary composites ‘n’ values and as in the case of the E’ values, the combined inclusion of the two fillers was manifested in a more controlled manner.

5.4.3. Wear

In **Figure** 5-6 and **Figure** 5-7, the K_S and FC average values from the wear tests from pristine and aged specimen groups are depicted, while **Table** 5-4 summarizes all the extracted values. **Figure** 5-8 presents representative FC vs sliding distance diagrams while **Figure** 5-9 depicts the surface roughness vs measuring distance plots from the profilometry measurements. Finally, **Figure** 3-10 11 depicts representative SEM micrographs obtained from the wear tracks of the pristine and aged specimens.

Table 5-4 Specific wear rate and friction coefficient for all pristine and aged specimens.

	K_s (cm^3/Nm)		**FC (μ)**	
	Pristine	**Aged**	**Pristine**	**Aged**
Neat	0.142±0.011	0.062±0.015	0.588±0.063	0.496±0.079
MC composites	0.070±0.019	0.060±0.010	0.540±0.021	0.463±0.068
CNTs composites	0.181±0.032	0.154±0.030	0.455±0.097	0.340±0.093
Ternary composites	0.139±0.031	0.125±0.015	0.568±0.068	0.467±0.014

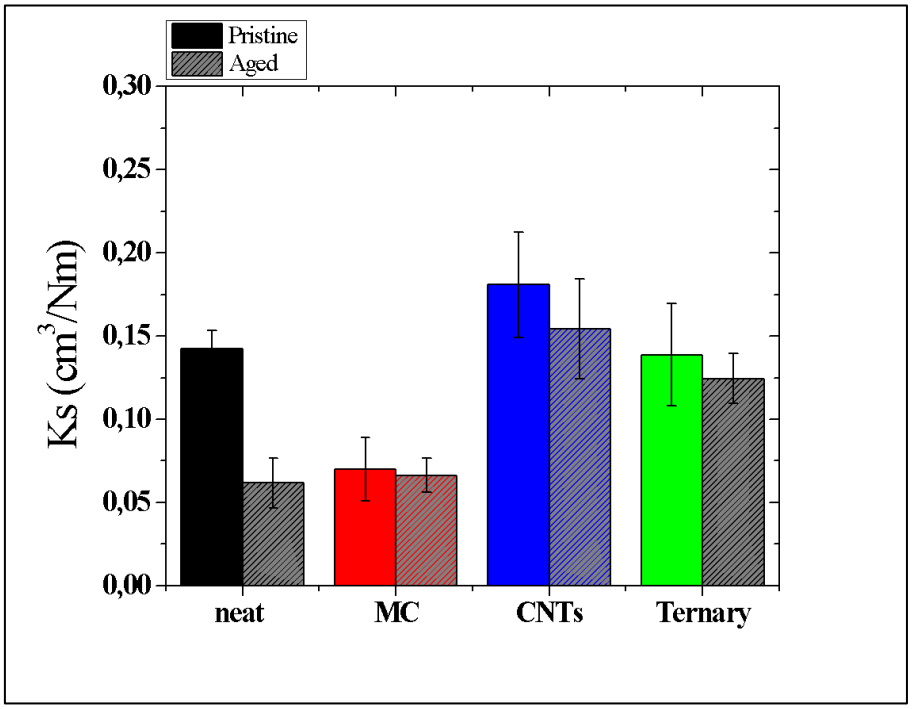

Figure 5-6 Specific wear rate average values for pristine and aged specimens.

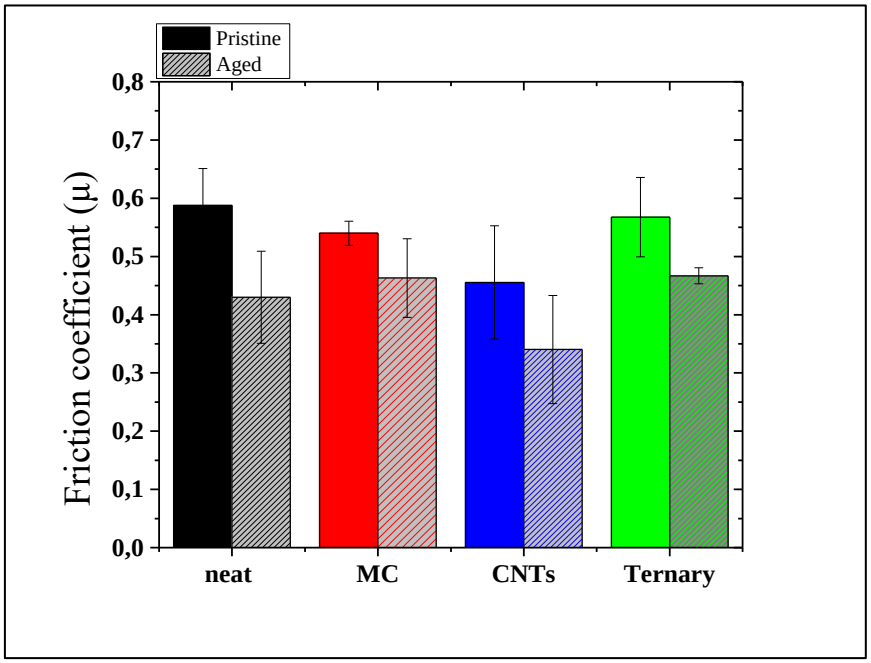

Figure 5-7 Friction coefficient average values for pristine and aged specimens.

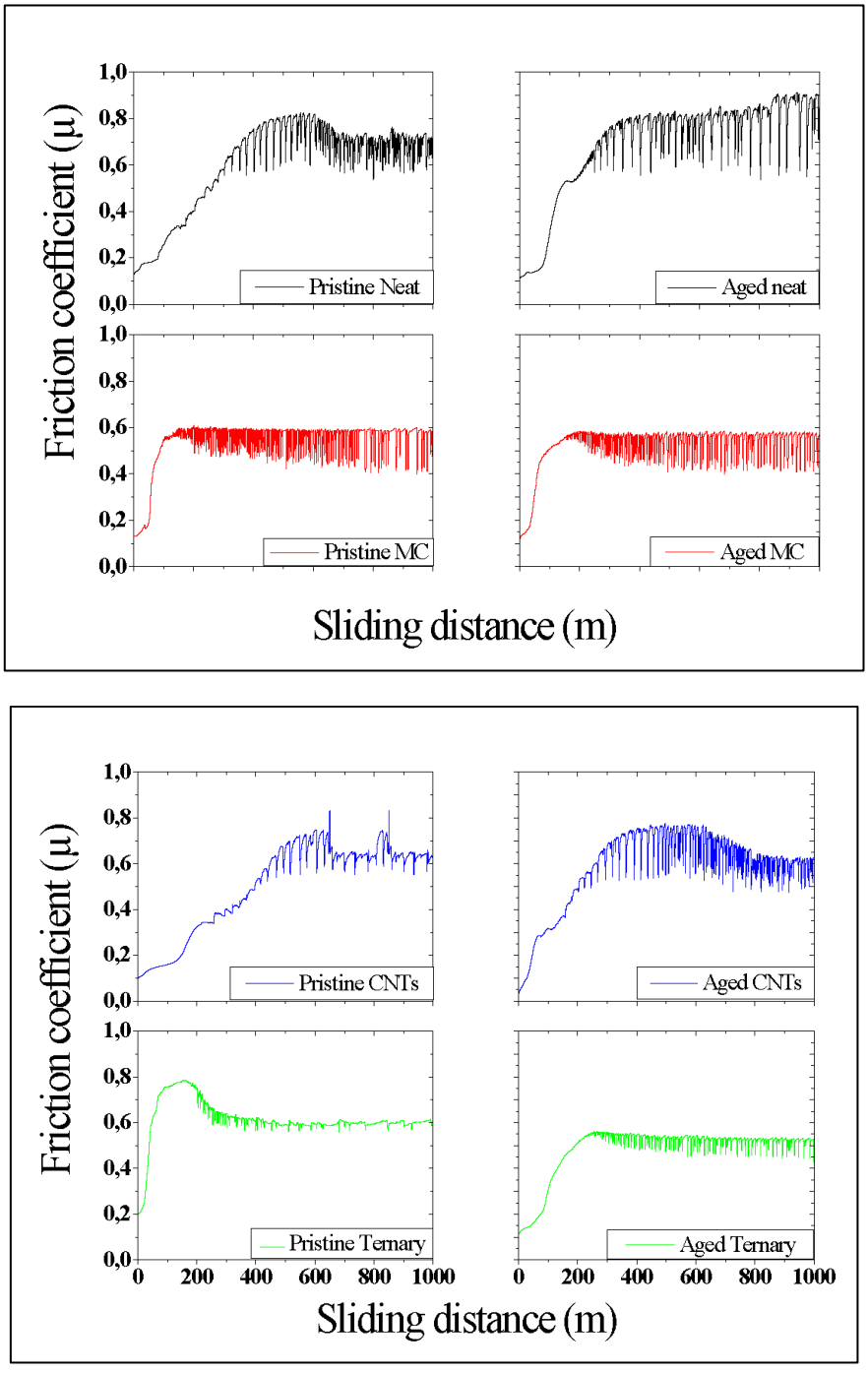

Figure 5-8 Friction coefficient vs sliding distance variations for all the pristine and aged specimens.

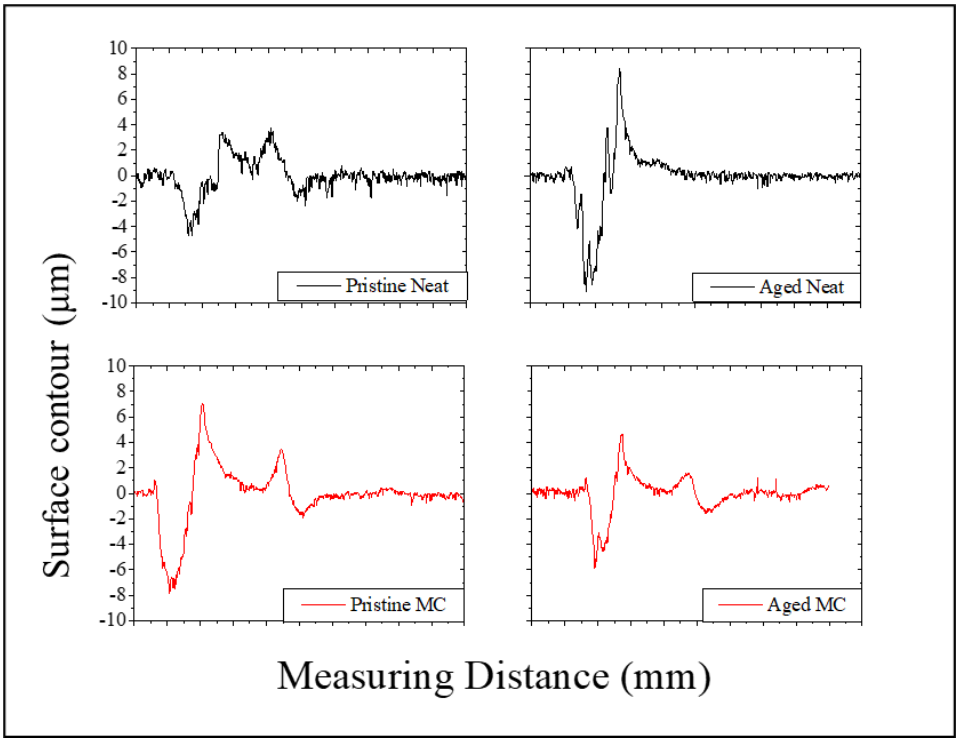

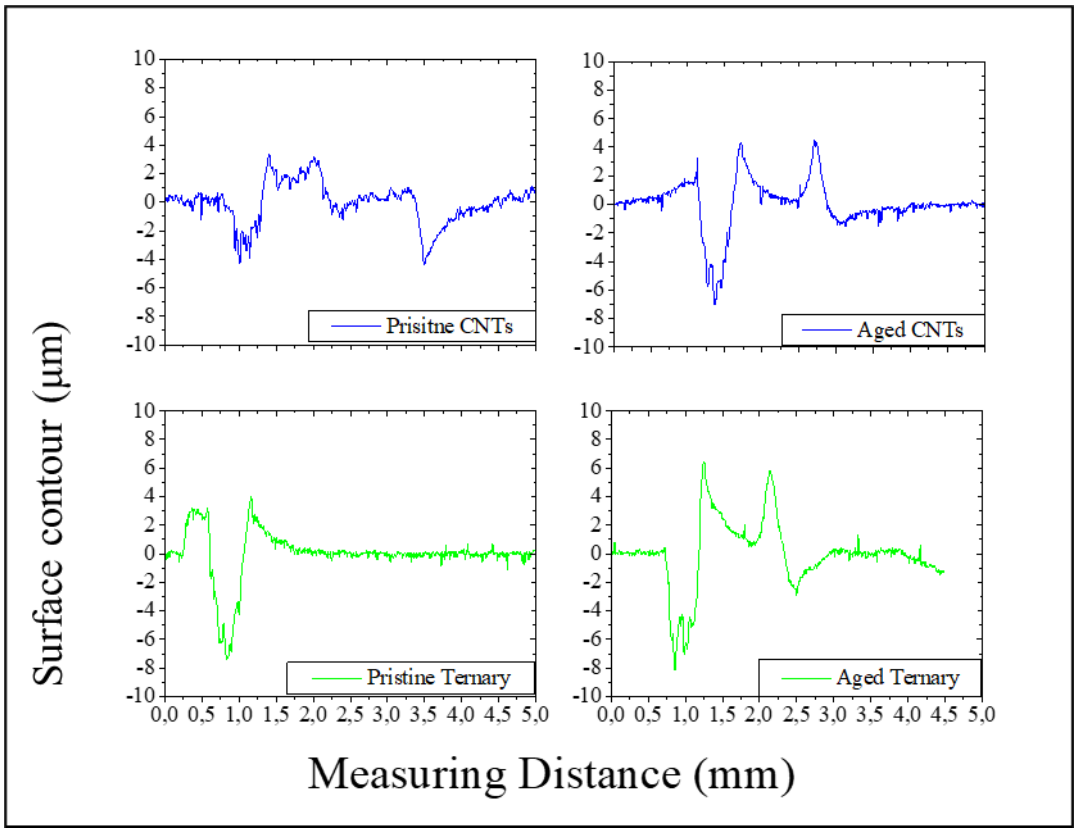

Figure 5-9 Surface roughness vs measuring distance for pristine and aged specimens.

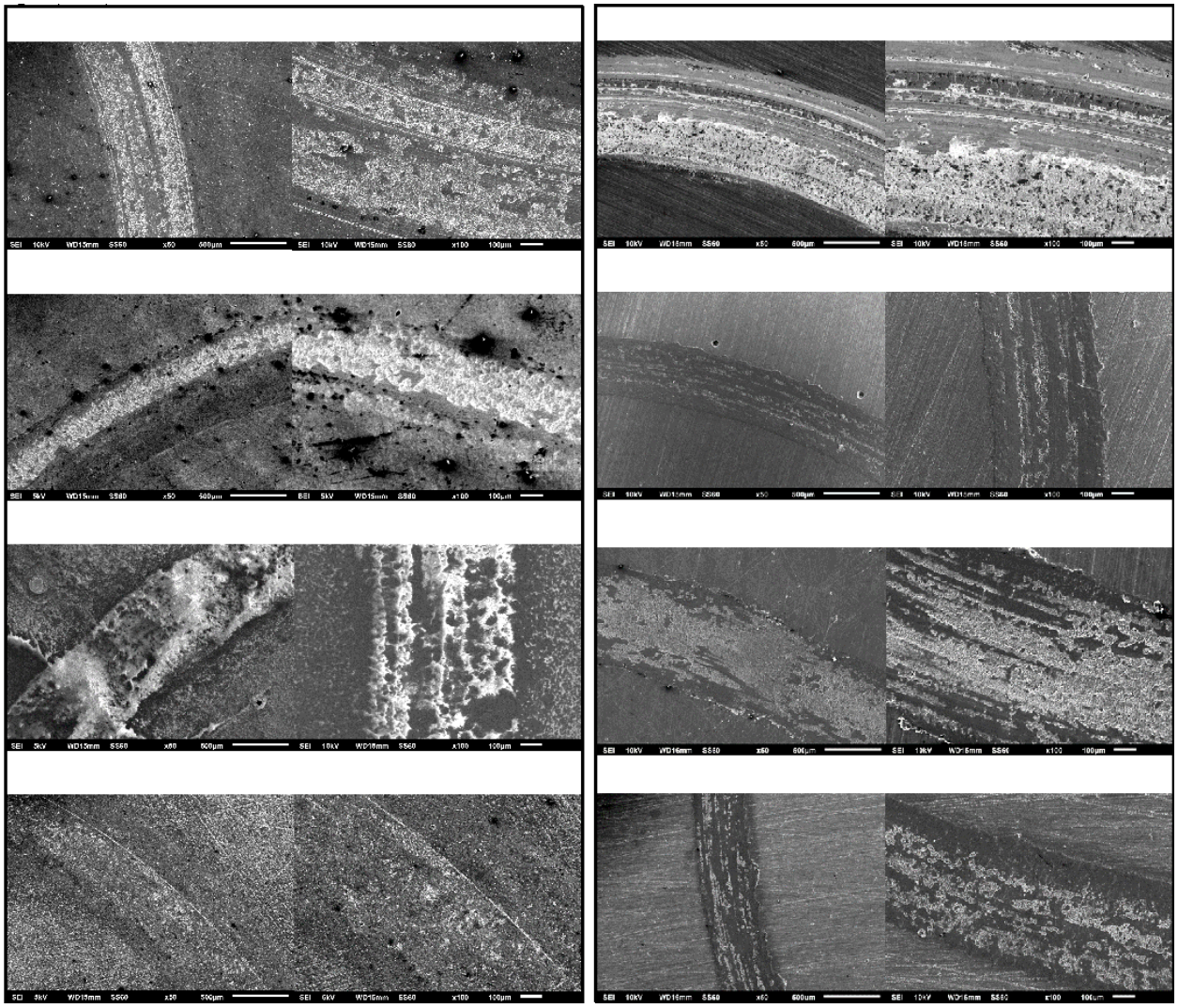

Figure 5-10Wear track SEM micrographs from pristine and aged specimens.

5.4.3.1. Pristine specimens

In terms of K_S, it can be observed that the MC and CNT composites exhibited the most pronounced beneficial and detrimental effects, respectively, on the recorded values. The presence of the MC particles reduced K_S by as much as 50%, while CNTs resulted in a 27% increase when compared to the pristine neat ones. It is possible that the spherical and cylindrical shape of the graphite particles and chopped carbon fibers affected the friction interface by providing a smoother surface. It has been observed elsewhere that carbon nanofibers and spherical fillers like alumina or silica can lead to significantly improved wear resistance [78,246]. On the other hand, the observed decrease in the K_S values of the CNT composites do not agree with the published literature. In [254], where untreated and functionalized CNTs were introduced amongst other reinforcing fillers in an epoxy matrix, the resulting composites

exhibited the lowest K_S values. In a similar work, CNTs led to almost half K_S values when compared with neat epoxy [255]. The observed behaviour in this work could be attributed to the weak interface between the epoxy and the inert surface of the employed CNTs. The weak interfacial bond could have led to easier CNT pullouts from the epoxy. This postulation could further be supported by observing the wear track surfaces in **Figure** 5-10. As can be seen, the CNT composites exhibit the widest wear track amongst the neat and modified specimens. Furthermore, the surface of the CNT composites appears quite rougher and with more cavities, indicative characteristics of massive material flow and particle pull out, respectively. In addition, shearing of CNT agglomerates could have also added up to the significant mass loss. In the case of the ternary specimens, it was observed that K_S was almost identical to the neat specimens (**Figure** 5-6**, Table** 5-3). It could be postulated that the detrimental effects of the CNTs were counterbalanced by the beneficial effects of the MC particles leading to a very mild wear performance as compared to the neat epoxy.

This counterbalancing synergy between the two carbon filler types was also observed in the FC average values. As can be seen in **Table** 5-4 and **Figure** 5-7, the ternary composites exhibited a marginally reduced value (within experimental error) when compared with the neat specimens varying by a mere 3.5%. A higher reduction (8.8%) was also found in the case of the MC composites, whereas the CNT composites experienced the greatest reduction in the FC values (29%), with respect to the neat epoxy. However, it should be noted that the FC values of the CNT composites exhibited large standard deviation values with some specimens exhibiting FC values very close to those of the neat ones. This fluctuating effect of the CNTs on FC has also been observed in [254] , where FC fluctuated depending on the sliding distance and not on the employed reinforcing particles.

None-the-less, a somewhat unexpected observation is that the CNT composites present the lowest mean FC values despite the roughest wear tracks. It has been suggested that CNTs form a friction-due film on the sliding interface that can act as a lubricating agent [78,231,255], thus reducing FC and KS. This film is not adherent with the substrate, but it comprises CNTs and matrix particles, which are detached from the specimen surface and adhere to the steel ball; as a consequence, specimen mass loss is greater but friction is lower due to the lubricating properties of the tribo-layer covering the counter-ball. The above postulations can be supported and further analyzed by the respective FC vs sliding distance curves. More analytically, the CNT composites exhibit similar linearly increased curves with those of the neat specimens, up to approximately 400 m. Beyond this point, both specimens exhibit a hump with great

fluctuations. At approximately 600 m, a sudden drop in the FC of the CNT composite is observed, followed by stabilization. The decrease in the FC increasing rate, as manifested by the formation of a hump in the respective curve of **Figure** 5-8, corresponds to the formation of a film on the CNT surfaces. The high fluctuations may correspond to the alternating sliding over areas free of film and areas with film and/or the alternating detachment/reformation on the underlayer process. The abrupt drop of the FC can be attributed to the adherence of the detached film on the counter-ball surface, leading to a reduced friction action. The increased friction activity after 800 m that eventually leads to a spike can be explained by the film detachment from the steel counter-ball and subsequent film reformation phenomena on the steel surface. The fluctuating effect in the recorded FC values can additionally be attributed to the varied three-body abrasion effect, depending on whether the detached tribo-layer has stuck on the steel counter-face or has been removed as debris.

In the case of the ternary composites, FC peaks much quicker when compared to the neat and CNT composite specimens with an almost identical increase rate to the MC ones. In the case of the MC specimens, FC was stabilized just after 100 m of sliding distance. It is postulated that during the initial stages of the measurements, CNT particles were continuously removed from the wear track leading to an MC rich surface. As sliding progressed, CNTs created the aforementioned self-lubricating film on the steel ball surface thus contributing to the observed reduced rate of FC increase. The sharp drop of FC that follows can be justified by the adherence of the film on the steel ball. The observed friction behaviour of the pristine ternary composites suggest synergistic effects of the CNT self-lubricating film acting on the MC rich (low friction) surface.

5.4.3.2. Aged specimens

The ingress of water resulted in reduced wear rates for all specimen types. It is reasonable to suggest that type-I water on the surface of the specimens acted as a lubricant thus reducing the wear rate; moreover, the pseudo-crosslinking stiffening effects that were observed in the aged DMA results, could have further contributed to the obtained reduced Ks values. The low Ks values could be associated with the filler particle shape, as mentioned in 3.3.1. Moreover, the lubricating action of water seems a much less significant factor on the wear rate reduction than the smooth surface due to the filler particle shape, thus leading to slightly less Ks values as compared to those of the pristine composites.

In the case of the CNT composites, both Ks and FC were found reduced after water absorption, indicating that the absorbed water from the surface layers acted as a lubricant. For the aged ternary specimens, the water ingress affected mostly the FC results. As in the case of the pristine ternary specimens, the friction and wear characteristics of the aged specimens were the result of the MC fillers counterbalancing the detrimental effects of the CNTs.

Both the employed filler and the moisture absorption affected the wear tracks in all cases. As the images in **Figure** 5-10 depict, the pristine wear surface of the neat specimen exhibits significant damage with delamination areas along with abrasive wear grooves from sliding debris. In the case of the aged MC composites, the wear surface exhibits characteristics of higher wear abrasion (grooving) and less delamination as compared to the pristine groups. In the aged composites, the overall surface profile appeared distinctly smoother when compared to the pristine MC composites In the case of the pristine CNT composites, the observed wear surfaces evidenced significant amount of cavities indicative of particle pull-out. On the other hand, the aged CNT composites, exhibited considerably altered wear surface characteristics, with notably less cavities and smoother profile compared to the pristine CNT composites.

A combination of the aforementioned patterns was observed in the pristine ternary composites wear surfaces. In the case of the aged ternary specimens, the ingress of water greatly affected the wear surface characteristics. The similarity in the shapes of the surface roughness vs. distance curves of the aged CNT composites and aged ternary composites suggests that CNT pullout is the governing process during wear of the aged ternary specimens.

5.4.4. Impedance Spectroscopy

Figure 5-11 and **Figure** 5-12present the real and imaginary parts of the impedance for the pristine and ternary composites as a function of water immersion duration while **Figure** 5-13 depicts the DC conductivity values versus immersion duration for the CNTs and Ternary composites.

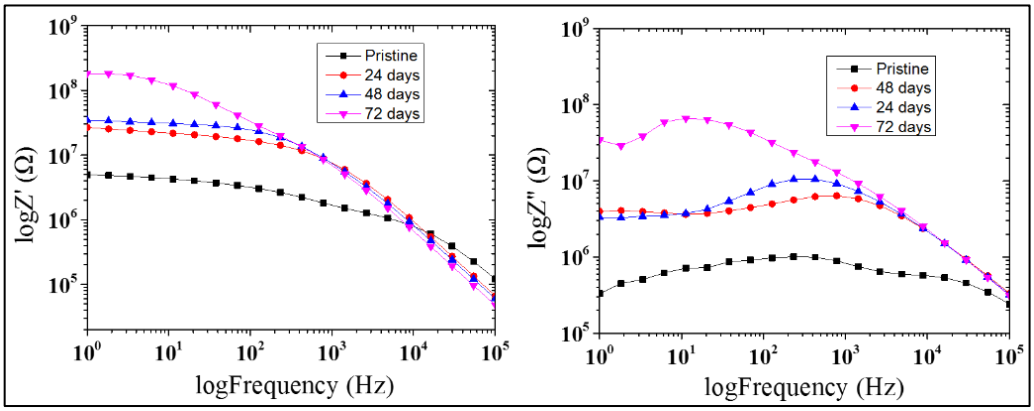

Figure 5-11 Real (left) and imaginary (right) parts of the impedance for the CNTs composites

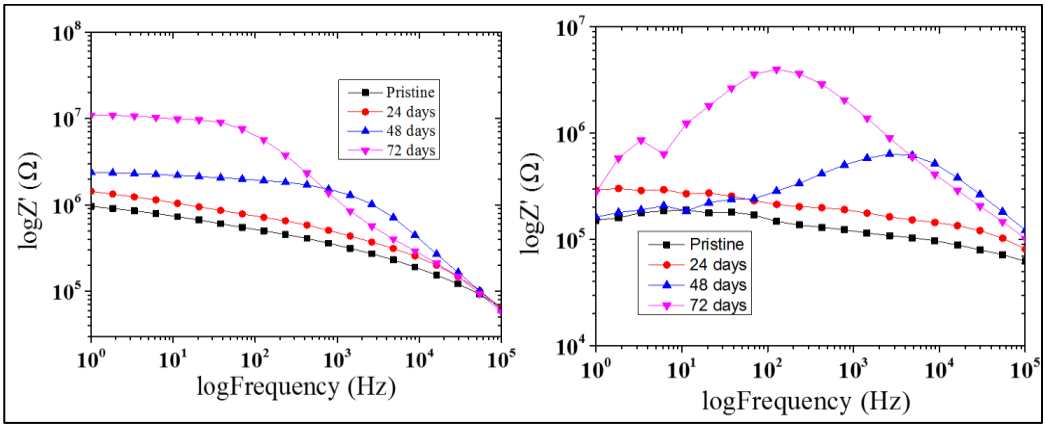

Figure 5-12Real (left) and imaginary (right) parts of the impedance for the ternary composites.

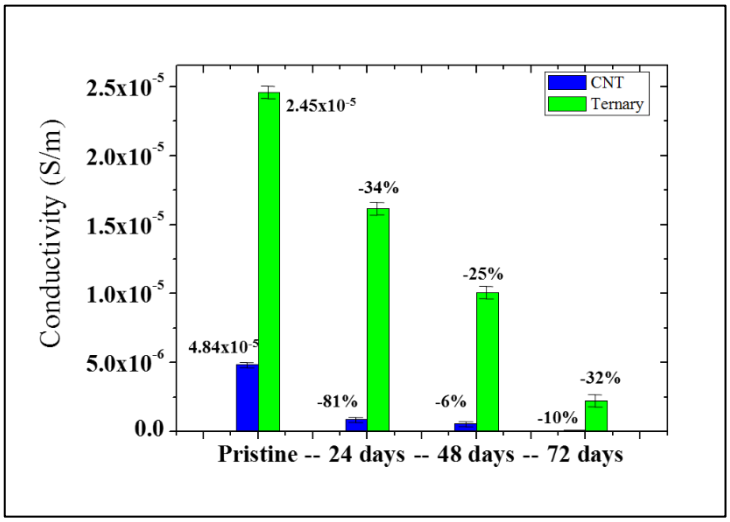

Figure 5-13 DC conductivity values versus hydrothermal exposure duration for the CNT composites - and ternary composites.

The quantities that were expected to be highly affected by the hydrothermal exposure and therefore provided useful information about the dielectric behaviour of the material were the real (Z') and the imaginary (Z'') components of the impedance. The Z' and Z'' are the resistance and the reactance, respectively, of a system that is subjected to an external MC field. As is well known, hydrothermal exposure introduces another phase to the material, that of water, which causes swelling, plasticization and in some cases softening of the epoxy matrix [256–258]. Thus, the conductive network of CNTs or CNTs/MC could be partially disrupted and both Z' and Z'' would be affected in different ways. It can be seen in both types of composites (**Figure** 5-11 and **Figure** 5-12), that with increasing hydrothermal exposure duration, the Z' at low frequencies increased, especially for the specimens that remained in the water tank for 72 h. In addition, the transition from Ohmic (linear) to non-Ohmic (non-linear) behaviour was shifted towards higher frequencies. This change is denoted by the shift of the transition of the values of the Z' vector from a quasi-stable value to decreasing values as a function of frequency.

In more detail, the Z' values of the pristine CNT composites at 1 Hz increased significantly from $4.97*10^6\Omega$ to $2.68*10^7\Omega$ after 24 d of hydrothermal exposure, followed by a minor increase at $3.46*10^7\Omega$ after 48 d in the water tank. The second abrupt increase was measured for the specimen that remained submerged in the water for 72 d. This behaviour clearly indicated that the hydrothermal exposure disrupted the conductive CNT network after only a 24 d stay in the water. On the other hand, the Z' of the ternary composites showed a more stable behaviour. In this case, the Z' values at 1 Hz showed a minor increase from $9.63*10^5\,\Omega$ to $1.44*10^6\,\Omega$ and then further to $2.39*10^6\,\Omega$ after 24 d and 48 d of hydrothermal exposure, respectively. The most significant increase in Z' values (by one order of magnitude) was recorded for the ternary composites that remained in the water tank for 72 d, indicating that the water intake highly affected the electrical performance of the specimens.

The imaginary part of the impedance (Z''), or the reactance, is characteristic of the ability of the system to store energy and is related to the capacitance or inductance properties. The imaginary component can be expressed via **Equation** 4:

$$X = 2\pi fL - \frac{1}{2\pi fC} \qquad \textbf{Equation } 4$$

where X is the total reactance, L the inductance and C the capacitance. The first term of the right-hand side of Eq. (4) is the inductive part of the reactance and the second term is the capacitive part of the reactance. When the phase of voltage leads the phase of the current, the reactance is positive and implies inductance while a negative reactance implies a capacitive behaviour (voltage phase lags the phase of the current).

As can be seen in **Figure** 5-11 and **Figure** 5-12, the Z'' values (CNTs composites and ternary composites) were negative, which is indicative of a capacitive behaviour. The capacitance in this case can be expressed as:

$$C = \frac{1}{2\pi f Z''}$$ **Equation** 5

In addition, the Z" values showed a maximum at intermediate frequencies that is scaled according to the hydrothermal exposure duration. As stated, the hydrothermal exposure introduces another phase to the material, thus the number of the interphases within the nano-composite increase. This behaviour enhances the effect of interfacial polarization on the total polarization of the system. This polarization mechanism occurs due to the accumulation of free charges at the newly created interfaces and is manifested by the increase in the maximum of the Z'' curves at intermediate frequencies [152,258,259]. The most profound increase was found in both cases after subjecting the specimens to a 72 d hydrothermal exposure.

It is also interesting to examine the effect of hydrothermal exposure on the DC conductivity of the composites as presented in **Figure** 5-13**.** The DC electrical conductivity measurements were performed using a digital multimeter. As can be seen, the conductivity of the CNT composites was significantly affected by the hydrothermal exposure, exhibiting a reduction of 81.7% (almost one order of magnitude) after 24 d of hydrothermal exposure. This reduction was followed by a second minor drop of 6.25% for the specimen that remained in the water bath for 48 d. The DC conductivity of the CNT composites, which were immersed for 72 d in water reached $1.83*10^{-8}$ S/m showing a total decrease of 97.35% when compared with the pristine one ($4.84*10^{-6}$ S/m). This reduction in conductivity indicated that the electrical performance of the composite was severely undermined due to the hydrothermal exposure.

On the other hand, the conductivity reduction in the case of the ternary composites followed a different trend. After a 24 d stay in water, the ternary composite conductivity exhibited a 34.11% reduction compared to its initial value. This significantly lower reduction in comparison to the CNT composite could be attributed to the synergy effect between the

different fillers that provided additional conductive paths/bridges between the AC and the CNTs. A second reduction of 24.78% in the specimen conductivity was measured for the composite subjected to hydrothermal exposure for 48 d. The total conductivity reduction after 72 d in water was 90.9% reaching at $2.21*10^{-6}$ S/m.

5.5. Conclusions

The research effort that was presented in this chapter, was focused on studying the effect of water absorption on a wide range of epoxy material properties. A multi-scaled reinforcing approach was selected based on a previous study in order to further explore its capabilities towards synergy of different filler types [34]. The synergy between the two carbon fillers, was evident in all obtained results while the detrimental effects of water ingress were mediated.

The analysis of the impedance data indicated that the hydrothermal exposure had a significantly lower effect on the electrical properties, and more specifically the electrical conductivity, in the case of the ternary composites compared with the binary ones. This behaviour was attributed to the synergy effect between the fillers that provided additional conductive paths/bridges between the MC and the CNTs.

The carbonaceous fillers resulted in increased E' values in all studied composites, while the combined inclusion of fillers in the ternary composites led to the most pronounced increase in E'. In addition, water-induced degradation on the thermo-mechanical performance of the aged and conditioned ternary composites was evident in a more controlled manner when compared with the neat and reinforced respective specimens. The E' values were found to decrease much less in the ternary composites when compared to the neat, MC and the CNT specimens. The synergy amongst the fillers was evident in the 'n' values of the aged and conditioned specimens indicating that each filler can provide counterbalancing effects thus leading to a more controlled deterioration.

The beneficial synergy of the carbon fillers was also evident in the wear characteristics of the pristine and aged ternary specimens. CNT composites exhibited the highest wear rate amongst the tested specimens, which could be attributed to the weak CNTs-epoxy interface. On the other hand, the MC composites were found to be the most resistant to wear. The presence of the MC fillers in the ternary composites, resulted in a low friction surface with reduced wear rates counterbalancing the detrimental effects of the CNTs and suggesting synergistic effects between the two carbon fillers.

All the obtained results, favor the effectiveness of the multi-scaled reinforcing approach for the future production of tailor-made epoxy composites. Low friction and wear rate MC particles combined with highly–conductive stiff CNTs could result in conductive materials with improved thermo-mechanical characteristics capable of operation in a wide range of operating conditions.

6. Effect of multi scale reinforcement on final properties – FRC level

6.1. Scope of the study

Chapter 06 includes the results of the application of the multi-scale reinforcing approach on matrices for FRCs. Ternary, MWCNTs and MC binary resins were produced using the dispersion parameters that led to the optimum observed performance in chapters 04 and 05. The formulations were subsequently employed as matrix materials in GRFC and CFRC specimens for tensile and mode-II fracture toughness tests,

6.2. Introduction.

Fibre Reinforced Polymeric Composites (FRPs) belong to a class of engineering materials that have proven to be a reliable choice towards tailored properties and application performance. Combining the versatile polymeric thermoset or thermoplastic materials with stiff and light weight fibrous reinforcements, result to material properties that can be tailored to specific application prerequisites. High specific mechanical properties combined with significantly lower weight, higher fatigue resistance, extremely higher corrosion resistance and environmental durability [104] when compared to metallic or ceramic materials are amongst the many advantages of FRPs [116,260].

Amongst the many polymeric material choices, epoxy and polyester resins are the most widely employed as matrices in FRPs mainly due to their wide range of physical and thermal properties. Combined with Carbon or Glass (CFRPs, GFRPs) fibrous reinforcement, the resulting composites exhibit superior fatigue resistance, environmental durability, duration of healthy operation combined with relatively lower weight when compared with metallic materials [74,225,261–263]. CFRPs are mostly consumed at high end sectors like aerospace, motorsport and competitive sports were cost is not a significant factor and ultimate mechanical performance is the sole goal. GFRPs on a parallel path, are mainly employed to sectors with more cost driven applications like marine, oil and civil infrastructure spanning to applications like load bearing structures, patch repair materials, etc [264].

The overall performance of FRPs is controlled by the properties of the fibre–matrix interface and evidently the properties of the matrix. An effective interfacial bonding ensures efficient load transfer from the matrix to the fibrous reinforcement, which in turn leads to even spread and distribution of mechanical stresses [265,266]. An effective epoxy matrix phase, should be capable of smooth load transferring and possess high fracture toughness for efficient crack hindering [267]. Due to their inherent design characteristics, the matrix phase also

controls the majority of the out of plane (or through thickness, TT), mechanical, electrical and thermal properties as well [268]. For example, the electrical conductivity between the fibre and TT orientations, can vary even multiple orders of magnitude in CFRPs structures. Extremely low TT conductivities are solely connected to the insulating nature of the polymeric matrix which impedes structural health monitoring based on electrical properties [31]. Several research efforts have been focused on mitigating the electrical anisotropy of FRPs employing the matrix nano-modification approach. Gojny et.al [269], dispersed carbon black (CB) and Carbon Nano Tubes (CNTs) as matrix nan-reinforcements and manufactured nano GFRPs (nGFRPs) via resin transfer moulding (RTM) technique. The resulting nGFRPs, exhibited improved matrix dominated properties like interlaminar shear strength or electrical conductivity. Tensile strength was in cases practically unaffected by the nano-fillers due to the fibre-reinforcement dominating effect.

Interfacial strength on FRPs have always been their Achilles heel and several efforts have been published towards improved interlaminar toughness [270]. Introduction of nano-sheets [271,272], nano-fibre veils [273], mats [274] or polymeric films [275] between laminae, layer nano-stitching [276–278], carbon fibre interleave layers [279], or fibre surface treatment [280] are some of the approaches that can be found in relevant published journals. Complicated manufacturing or demand for specialized materials render most of these approaches commercially non-viable yet.

Similarly to epoxy based nanocomposites [152,160], the dispersion of conductive nano, micro or macro fillers in the matrix phase [113,281–283] towards hybrid FRP structures, have shown promising results. The resulting hybrid FRPs comprise of nano-modified matrices and traditional fibre reinforcements like carbon and glass [284,285], exhibit significant enhancements in mechanical performance. Chaudhry et. al. introduced Multi walled CNTs (MWCNTs) at several weight contents in epoxy resins that were used as matrices in woven CFRPs laminates. The experimental results indicated that small amounts of CNTs can lead to increased Mode-I fracture toughness and the optimum performance is directly related to the selected manufacturing parameters. The increased energy consumption during fracture was attributed to the MWCNTs particles 3D network observed under scanning electron microscopy (SEM). The MWCNTs particles introduced several distinctive fracture mechanisms like crack bridging, particle pull-out, particles fracture etc, that are known as energy consuming mechanisms [281]. In [286], (i) grafting of CNTs on either Carbon of Glass fibre surfaces and (ii) directly dispersing of CNTs in the matrix, were employed as fibre/CNTs interaction

approaches. The grafting approach favoured tensile strength improvement via good compatibility with carbon fibres while dispersion favoured flexural strength in the case of sandwiched CGFRPs. Ahmadi-Moghadam et. al., introduced various grades of graphene nano-platelets (GNPs) in the matrix epoxy phase of UD GFRPs laminates and studied the effect on the principal fracture modes [43]. The results revealed that functionalized GNPs resulted in the most pronounced improvements in mode-I, -II and –II fracture energies. GNPs functionalization improved the surface energy characteristics and facilitated stronger matrix/filler and matrix/fibre bonding.

The combination with fibre reinforcement fracture mechanisms like particle pull-out, shear of tensile fibre fracture, greater amounts of energy are demanded for structural failure in the cases of hybrid FRPs [287,288]. In [289], MWCNTs were introduced in the matrix phase of GFRP laminates and a detailed mechanical properties characterization was conducted. Ultimate tensile and flexural strength were increased by 35% and 40% in the hybrid GFRPs when compared with the neat ones. In [290] MWCNTs were incorporated in a GFRP laminate towards the study of mechanical properties at various temperature environments. Interlaminar shear strength (ILSS), flexural strength and storage modulus were examined for the hybrid GFRPs in several MWCNTs weight contents. Optimum mechanical performance was achieved in specific MWCNTs weight content and crack pinning and deflection were identified as the prevalent matrix fracture mechanisms.

Hybrid matrix FRPs property enhancement [176], often comes with a compromise `as it has been shown that high aspect ratio fillers can lead to significantly high viscosities after dispersion [177]. In applications where the rheological characteristics of the epoxy resin are the single controlling factor, increased viscosity can prove to be either a favourable or not factor [87,140,178]. In such an application, Siddiqui et. al. studied the effect of CNTs in the rheological performance of an epoxy resin matrix of pre-preg Fibre Reinforced Composites (FRC) [179]. They observed that optimization of the pre-preg processing parameters was necessary to reduce the adverse effect of CNTs on the viscosity of epoxy and FRP pre-preg characteristics. The magnitude of the effect on the resin viscosity is directly associated to the amount of interconnected fillers that reduce resin chain mobility [180] which in turn is directly related to the dispersion quality in the epoxy suspension [181][182].

Several efforts have been published regarding modifications of epoxy resins via the inclusion of more than one filler type in order to exploit synergistic effects between the fillers

[117,185,186]. Especially when these are of nano or micro scale, it has been shown that capabilities to exploit and combine the dominant fracture mechanisms from both worlds are presented in mechanical, electrical and thermal properties [183,185–187,291]. To the knowledge of the author and up to the date that this magnificent manuscript was composed, very few efforts have been published towards the development and study of hybrid FRPs with a multi-scaled reinforced epoxy matrix and carbon or glass fibrous reinforcements. In [85] Wang et. al. combined graphene nano platelets and CNTs in order to manufacture epoxy based nanocomposites and hybrid CFRPs. The experimental results showed that the hybrid CFRPs tensile strength, flexural strength and interlaminar shear strength were increased when compared to the neat ones.

Continuing with the investigation of the multi-scaled reinforcing approach, this chapter will present an effort towards the development of hybrid FRPs laminates using the ternary epoxy that has been presented in the previous chapters. In the following chapter, the ternary epoxy was employed as a matrix materials along with CFs and GFs fibres in the form of unidirectional and biaxial fabrics, towards the manufacturing of hybrid CFRPs and GFRPs and tensile strength investigation. In the GFRPs case, Mode-II interlaminar shear strength.

6.3. Experimental

The effect of the multi-scale reinforcement on the properties of FRCs has been studied. CFRC and GFRC laminates were manufactured according to 2.5.3 using neat and ternary epoxy matrices. The FRC laminates were cured and post cured under vacuum conditions of 0 atm. Specimens for tensile and mode-II interlaminar fracture toughness tests according to 2.4.1 and 2.4.2 respectively, were extracted.

6.4. Results and Discussion

6.4.1. Tensile strength

6.4.1.1. CFRPs

Table 6-1 summarizes the Ultimate tensile strength (UTS), Young's modulus and strain at fracture obtained from the quasi isotropic and ±45 CFRP specimens. **Figure** 6-1 and **Figure** 6-2 depict the bar chart representation of the aforementioned values including the maximum strain property with indicative stress strain curves obtained from quasi and ±45 CFRP specimens respectively.

Table 6-1 UTS, Young's Modulus, strain at fracture and maximum achieved strain for the quasi isostropic and ±45 CFRPs laminates.

	Ultimate Tensile Strength (MPa)	**Young's Modulus (MPa)**	**SaF (%)**
Quasi			
Neat	422.50±29.22	130.10±5.90	2.31±0.13
Ternary	428.09±11.36	111.87±2.46	2.23±0.05
±45			
Neat	96.95±5.72	32.99±2.09	6.59±0.31
Ternary	174.72±10.93	49.80±1.13	7.74±0.26

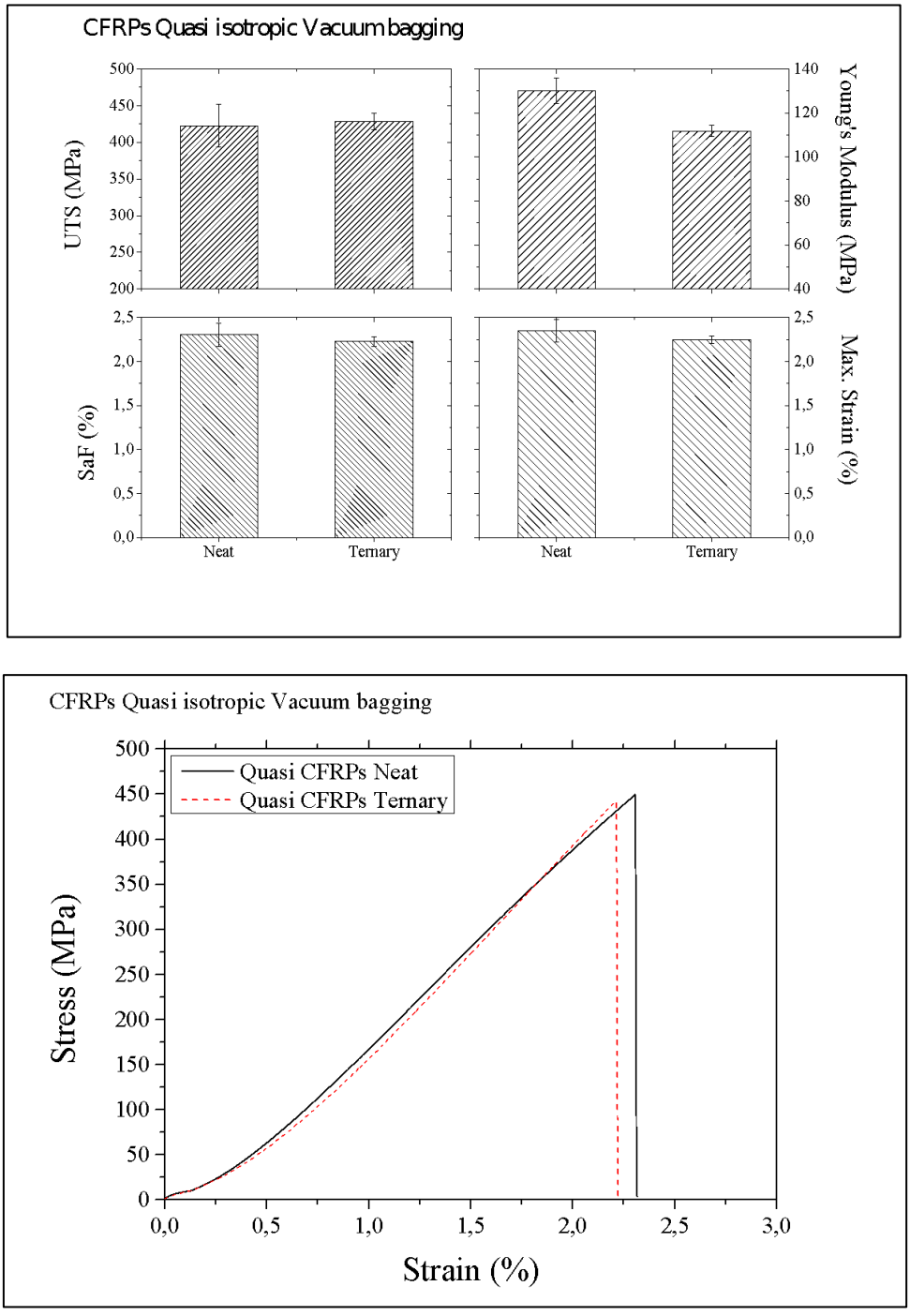

Figure 6-1 (Top) Bar chart of the UTS, Young's Modulus, strain at fracture and maximum achieved strain and (bottom) indicative stres vs strain curves for the quasi isostropis CFRPs laminates.

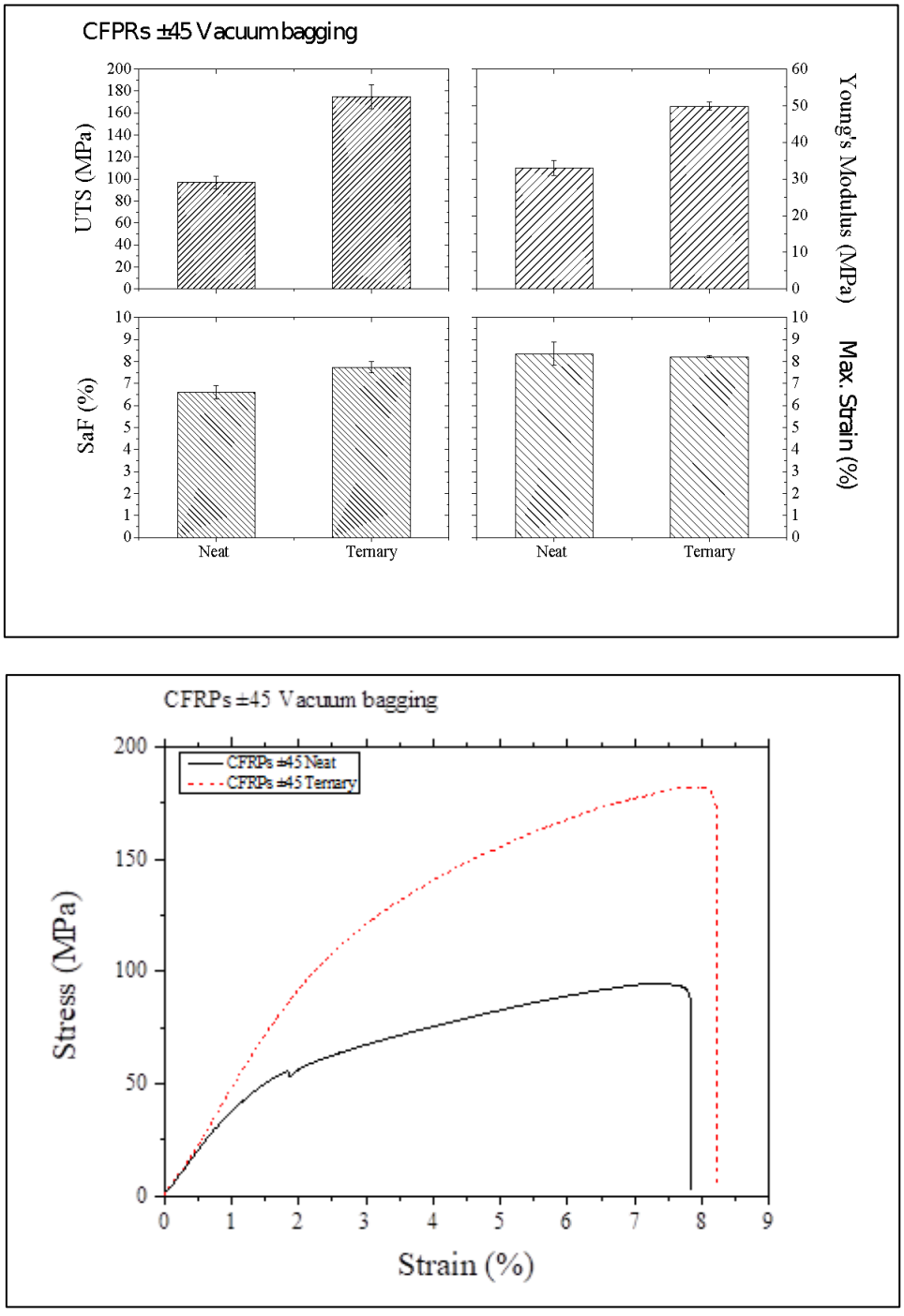

Figure 6-2 (Top) Bar chart of the UTS, Young's Modulus, strain at fracture and maximum achieved strain and (bottom) indicative stres vs strain curves for the ±45 CFRPs laminates.

As it can be observed, in the case of the cross ply laminates, both specimen types exhibited curves indicative of brittle materials and the hybrid specimens exhibited marginally reduced UTS, Youngs' modulus and SAF, within experimental deviations when compared with the neat specimens. Due to the fact that in cross ply laminates UTS is mainly controlled by the fibre reinforcement properties, the ternary matrix in the hybrid CFRPs did not have any effect

on the UTS. This postulation can be further supported by Young's modulus values of the cross-ply neat and hybrid specimens. As it can be seen, both values where found in the same ball park indicating similar if not the same material formulations.

On the other hand, in the case of the ±45 laminates, the hybrid CFRP specimens outperformed the neat CFRPs. As it can be seen, hybrid CFRPs exhibited significantly increased UTS (80%) while both Young's Modulus and SAF values were increased when compared with the neat specimens indicating 'different' material formulations. In terms of the stress vs strain curves, both materials exhibited curves indicative of plastic materials with elastic deformation, plastic deformation and neck formation stages. The observed patterns can be explained by considering that, in the ±45 laminates UTS is controlled by the matrix properties rather than the fibre reinforcements since all fibrous reinforcements, do not run through the entire length of the specimen. Hence in ±45 laminates, a matrix modification could be far more effective towards improved mechanical performance. Based on these premises, it can be postulated that the observed UTS results can be solely attributed to the ternary matrix of the hybrid ±45 CFRPs. The ternary matrix was tougher and stronger when compared to the neat one [152,219] leading to better stress distribution and superior load handling capabilities when compared to the neat CFRPs specimens. The ternary epoxy matrix, was capable for increased tensile load bearing capabilities, possibly via the introduction of additional energy absorbing fracture mechanisms accompanying the traditional primary fracture modes in FRPs like matrix cracking and fibre pull-out [292].

6.4.1.2. GFRPs

Table 6-2 summarizes the Ultimate tensile strength (UTS), Young's modulus and strain at fracture obtained from the UD, cross ply and ±45 GFRP specimens. **Figure** 6-3, **Figure** 6-4, and **Figure** 6-5 depict the bar chart representations of the aforementioned values including the maximum strain property and indicative stress strain curves obtained from the UD, cross ply and ±45 GFRP specimens respectively.

Table 6-2 UTS, Young's Modulus, strain at fracture and maximum achieved strain for the UD, cross ply and ±45 GFRPs laminates.

	UTS (Mpa)	Young's Modulus (MPa)	SAF (%)	Max. Strain (%)
UD				

Neat	532.23±58.17	65.44±10.60	14.02±0.74	14.66±0.68
Ternary	429.20±69.32	78.01±5.75	14.50±0.85	14.70±0.83
Cross ply				
Neat	409.39±43.34	67.52±12.78	7.85±0.60	8.02±0.68
Ternary	454.51±15.37	74.46±3.69	7.89±0.23	7.97±0.31
±45				
Neat	86.35±24.16	45.41±11.61	17.06±2.06	19.00±2.37
Ternary	96.46±8.76	45.03±1.75	18.56±2.46	19.78±3.60
Ternary 1/2	106.32±5.09	50.12±1.00	18.53±1.73	20.59±1.69

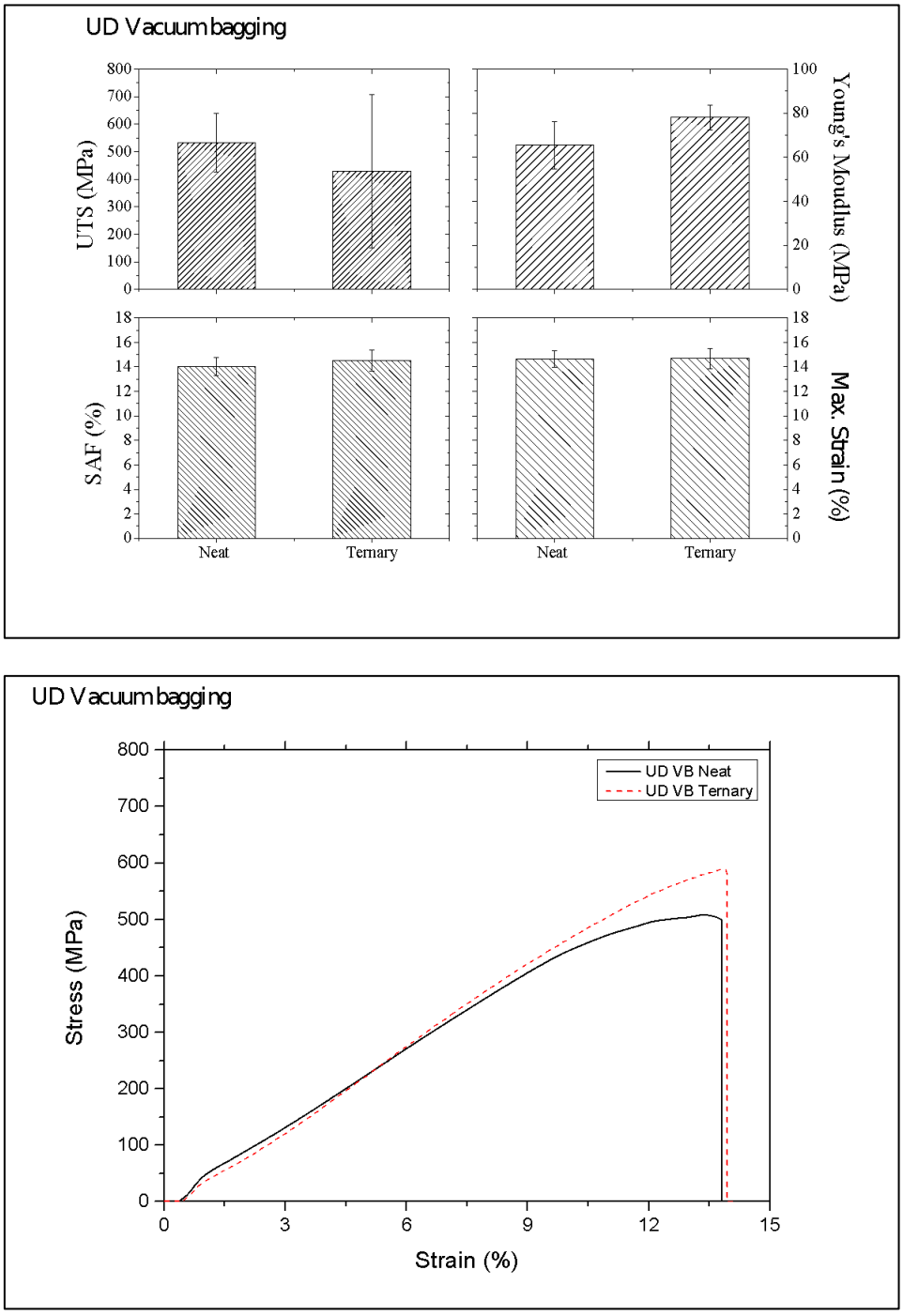

Figure 6-3 (Top) Bar chart of the UTS, Young's Modulus, strain at fracture and maximum achieved strain and (bottom) indicative stres vs strain curves for the UD GFRPs laminates.

In the case of the UD GFRPs, the matrix modification did not result to any improvements and was even found reduced (19%). It is possible that the reinforcing fillers particles acted as stress concentration sites thus leading to reduced load bearing capabilities. These results come in disagreement with some of the public research efforts. In [293], MWCNTs were introduced in UD GFRPs composites via vacuum assisted hand lay-up and

aligned by the application of external electrical field in the periphery of open-hole tensile specimens. An enhancement of 27% in the tensile strength was observed for the specimens with MWCNTs aligned perpendicular to the fibre axis. The alignment of the CNTs can be considered a governing factor for the observed results. In terms of stress strain curves, both of the specimen groups exhibited curves indicative of brittle materials with abrupt and sudden fractures.

In the case of the ±45 GFRPS the hybrid GFRPs exhibited increased UTS values but not in such a pronounced manner as in the case of the CFRPs counterparts. The hybrid GFRPs had a 25% increased UTS compared with the neat ones and the Young's modulus and SAF values being almost identical for both specimens groups. It is generally seen in published research efforts that GFRPs laminates with non-continuous fibre reinforcements like chopped strand matt or ±45 woven layers, tend to be more affected by the introduction of hybrid matrix phases [294] As a side study, a third specimen group was manufactured employing the ternary matrix but with half filler weight content denoted hereafter as ternary1/2 matrix (1.0%ww MC + 0.25%ww CNTs). This side study was conducted in order to investigate any patterns that could be associated with the matrix viscosity. As it has been shown, the multi-scaled epoxy reinforcing approach can lead to significantly increased viscosities that could present manufacturing issues like filler filtering, reduced wettability etc.

As it can be seen, the hybrid GFRPs with the ternary1/2 matrix, exhibited higher UTS values compared to both of the neat (23%) and ternary (10%) GFRPs. It can be postulated that the lower viscosity of the ternary1/2 matrix, led to better fibre wettability and in turn to higher load bearing capabilities and reduced filtration effects [295].

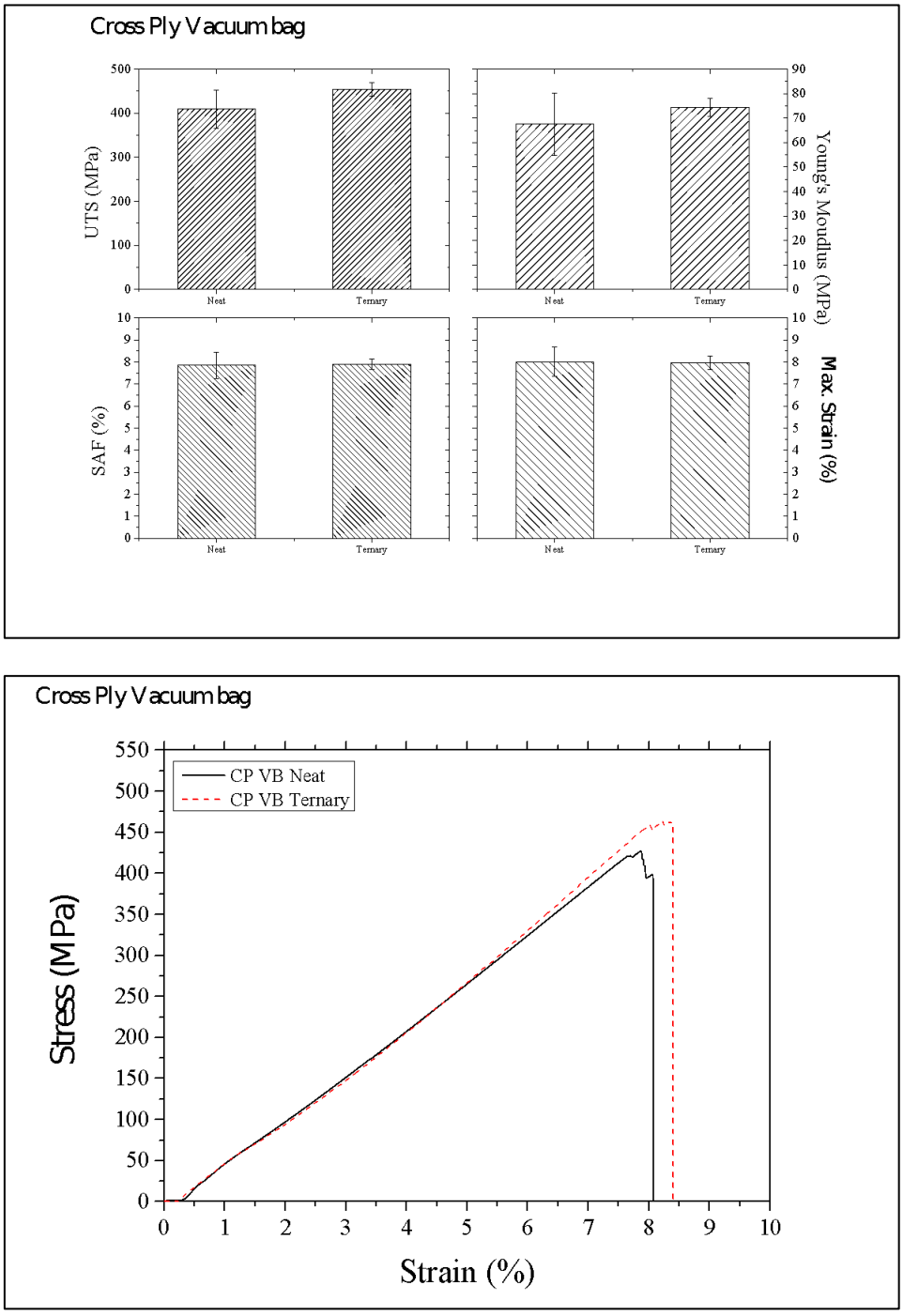

Figure 6-4 (Top) Bar chart of the UTS, Young's Modulus, strain at fracture and maximum achieved strain and (bottom) indicative stres vs strain curves for the cross ply GFRPs laminates.

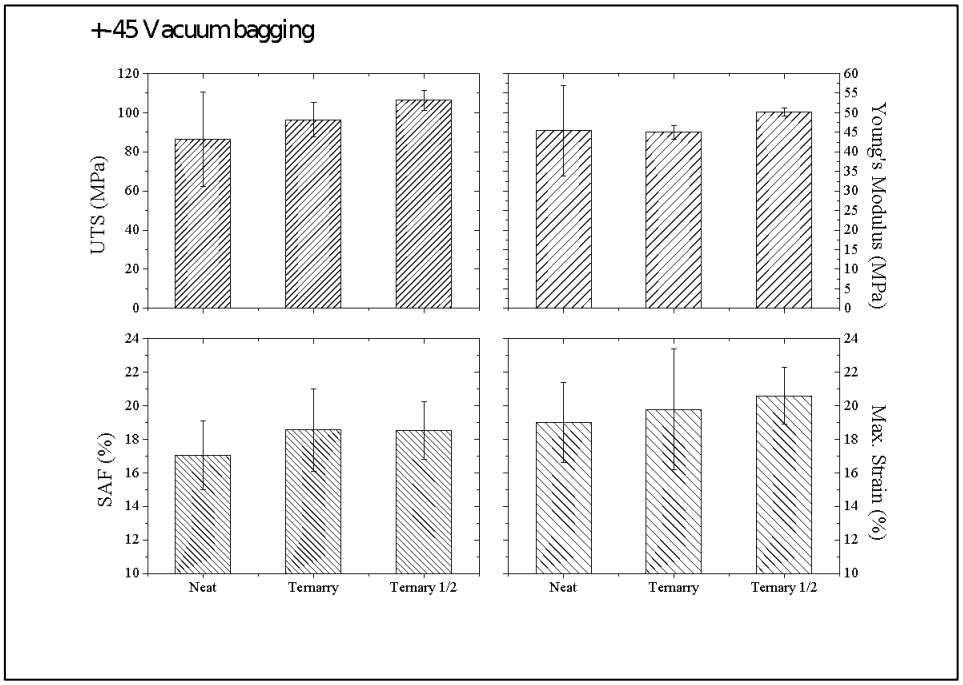

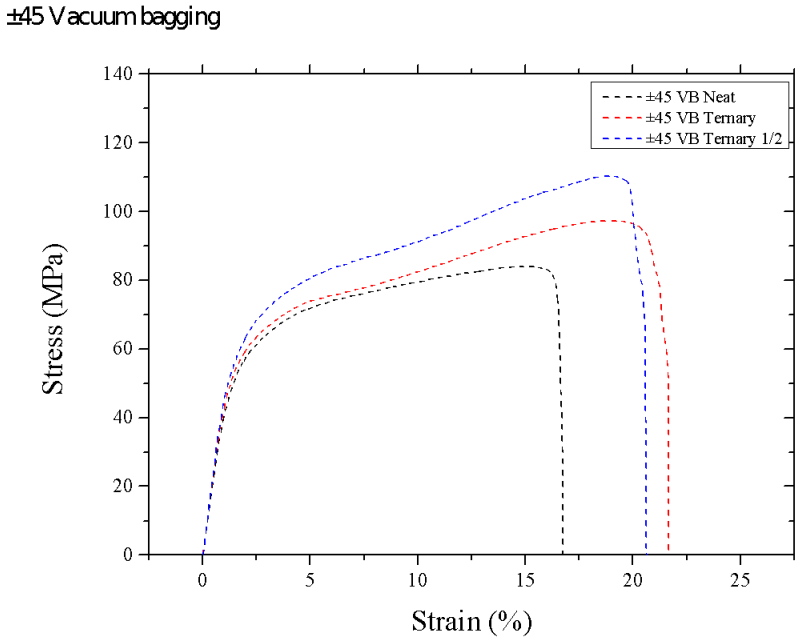

Figure 6-5 (Top) Bar chart of the UTS, Young's Modulus, strain at fracture and maximum achieved strain and (bottom) indicative stres vs strain curves for the ±45 GFRPs laminates.

6.4.2. Mode II fracture toughness

Figure 6-6 presents indicative load vs deflection curves obtained from the mode-II fracture toughness tests for the UD GFRP with neat, binary and ternary matrices. **Figure** 6-7 depicts the bar chart representation of the calculated mode-II interlaminar fracture toughness.

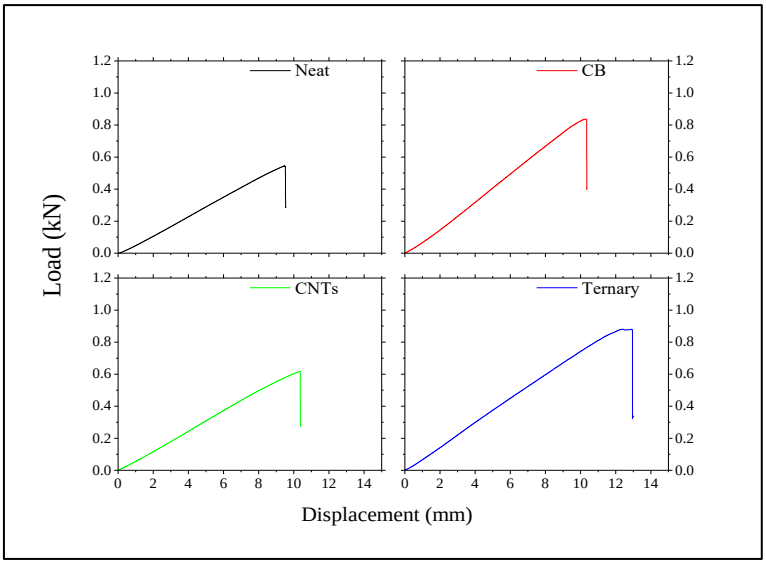

Figure 6-6 Indicative load vs displacement curves from mode-II fracture tests.

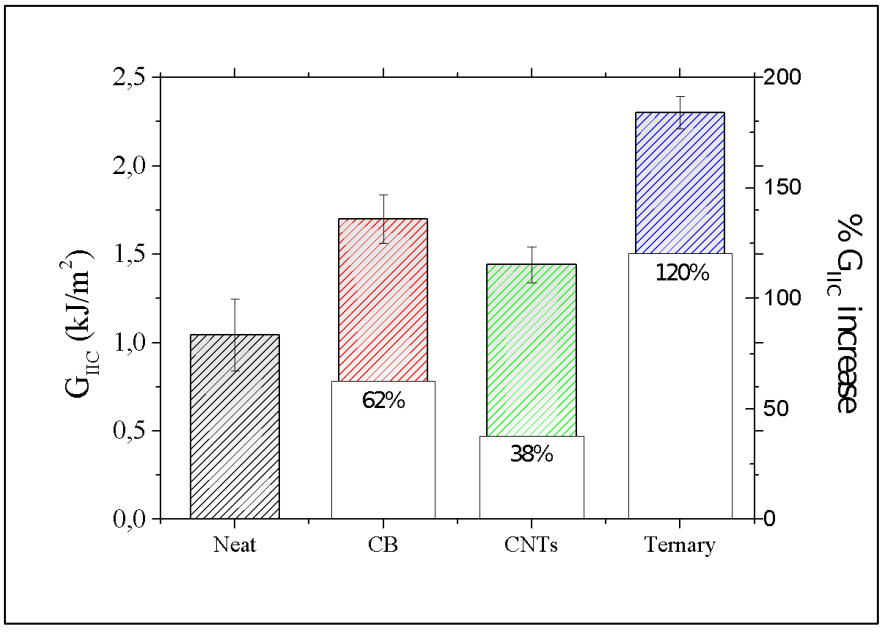

Figure 6-7 Mode-II fracture toughness results for the GFRPs UD specimens.

Similar to other efforts on hybrid GFRPs [296], the introduction of the carbonaceous fillers in the epoxy matrix led to significantly improved G_{IIC}. It has been shown that the incorporation of stiff filler particles in epoxy matrices, leads to tougher composites via the introduction of additional energy absorption fracture mechanisms like particle pull-out, fibre fracture, crack arresting and bifurcation etc. [270]. In the case of the MC binary GFRPs, it is

observed that the micro scaled carbon fibers and graphitic particles were more effective as reinforcing fillers when compared with CNTs. It has been observed elsewhere [297] that resin rich areas in FRPs, exhibit higher delamination toughness compared to high fibre content areas. Thick interlaminar layers can extend plastic deformation in a greater volume when compared with high-fibre content slim interlaminar layers. Both of the MC and ternary specimens exhibited relatively higher thickness values when compared to the neat and CNTs ones.

Synergistic effects amongst the different fillers were evident in the ternary GFRPs values. As it is observed, the ternary GFRP fracture toughness was far greater when compared with both of the binary ones with higher relative values. These results come in agreement with similar research efforts on GFPRs with multi-scaled reinforced matrices [37,80]. It can be postulated that the combined presence of the MC and CNTs particles resulted in a more robust 3D particles network capable of absorbing greater amounts of stress energy thus leading to the highest observed G_{IIC} values. Smaller cracks in the nano-scale were effectively handled by the CNTs particles, while micro-scaled cracks were hindered by the micro-scaled MC particles. In addition the micro-scaled fibers of the MC filler, could have introduced further interlayer connections between the middle laminas thus leading to the significant improvements [37].

6.5. Conclusions

Incorporation of a ternary multi-scaled epoxy matrix towards manufacturing of hybrid FRPs, have been studied. Milled carbon and carbon nano tubes were dispersed in an epoxy pre-polymer using high shear forces mixing, at pre-defined parameters. Glass and carbon fibre fabrics were employed as principal reinforcements for the manufacturing of neat and hybrid laminates with several stacking sequences, in order to extract rectangular and edge notched fracture specimens for tensile and mode-II fracture toughness testing. Additional hybrid ±45 GFRPs laminates were manufactured using diluted ternary matrix with half the original weight content, in order to investigate the effect on the tensile strength.

Significant improvements have been observed in matrix dominated properties like mode-II fracture toughness in all cases of matrix modifications, binary or teranry. More specifically, G_{IIC} was found significantly enhanced in the hybrid GFRP specimens by 120% compared with the neat GFRPs. Tensile strength was also beneficiary affected in the cross ply and ±45 GFRPs and CFRPs specimens where the ±45 GFRPs exhibited the highest affect. Given the stacking sequence and the direction of the applied load, additional energy consuming

fracture mechanisms were introduced by the carbonaceous nano and micro fillers thus greatly affecting shear fracture resistance

On the other hand, tensile strength was marginally affected in the cross ply CFRP and UD GFRP specimens. In these case, fibre domination effects on the mechanical performance hindered any beneficiary effects thus leading to unaffected of deteriorated tensile strength. Especially in the UD GFRPs case, where decreased values were seen, the filler particles could have acted like stress concentration areas thus resulting to premature epoxy/matrix interface debonding and reduced load bearing capabilities.

7. Corrosion protection studies

Part of the results in the following chapter have been published in [94,298]

7.1. Scope of this study.

The scope of this study was (i) to study the effect of the reinforcing approach on the anti-corrosive properties of epoxy coatings and (ii) to study the capabilities of the AE technique as a corrosion monitoring tool. Towards both ends, the formulations from Chapter 03 and 05 were used as protective coating on metallic substrates. The coated and non-coated substrates were used as electrodes in galvanic current and potensiodynamic polarizations tests coupled with AE measurements.

7.2. Effect of filler content

The effect of MWCNTs content on the anti-corrosive performance of epoxy coatings was studied. Electrochemical measurements in aerated NaCl solution (potensiodynamic polarization and galvanic current measurements) were conducted according to 2.3.9.2 and 2.3.9.3. Al2024 and SS304 metallic substrates were used for specimen manufacturing according to 2.3.9.1 using neat and modified with 0.4%-05% and 0.6% w.w. of MWCNTs epoxy coatings. Details on specimen configuration and employed nomenclature for both metallic substrates categories can be found in table 7-1.

Table 7-1 Nomenclature for the potensiodynamic measurements employing Al2024 substrates.

Specimen configuration	**Nomenclature**
Chromate anodized Aluminum2024	Anodized Aluminium
Primer coating over chromate anodized Al2024	Primer coated
Epoxy coated Al2024	NeatAl2024
Epoxy+0.4%CNTs coated Al2024	D04Al2024
Epoxy+0.5%CNTs	D05Al2024
Epoxy+0.6%CNTs	D06Al2024

Table 7-2 Nomenclature for the couples used in the galvanic current measurements employing Al2024 substrates.

Nomenclature	**AlPr**	**Aluneat**	**AluD0.4**	**AluD0.5**	**AluD0.6**
Working Electrode 1	Al 2024 primer coated	Al 2024 primer coated	Al 2024 primer coated	Al 2024 primer coated	Al 2024 primer coated
Working Electrode 2	Al 2024 primer coated	Al 2024 coated with neat epoxy	Al 2024coated with 0.4% CNTs nano composite coating	Al 2024 coated with 0.5% CNTs nano composite coating	Al 2024 coated with 0.6% CNTs nano composite coating

Table 7-3 Electrochemical values of the materials immersed in 3.5% NaCl. All potentials are cited against Ag/AgCl.

Material	**E_{corr} (mV)**	**E_b (mV)**	**E_b - E_{cor} (mV)**	**E_{cp} (mV)**	**E_{cp}-E_{corr} (mV)**
ss304	-362	350(E_{b2})	712	-56	306
SSNeat	-656	-47	609	-47	609
SSD0.6	-497			-280	217
SSCF	-170	797	967	-54	116

7.2.1. Aluminium substrate polarization curves

Figure 7-1 shows the cyclic polarization behavior of anodized, primer coated, neat resin coated and doped resin coted aluminum in 3.5% NaCl at room temperature while *Table 7-4* lists all extracted electrochemical values for all the measured coatings.

Based on these values we can see that all coatings (primer, neat and doped resin), shifted the rest potential values to less negative values. The steep flattening of the gradient at the corrosion

potential (E_{cor}) which is maintained for more than five orders of magnitude, indicates that the anodized aluminum is prone to localized corrosion. The lower anodic-to-cathodic transition potential as compared to the corrosion potential is an indication of a more active surface during the reverse polarization.

The polarization curve in Figure 7-1b, shows that the primer coating application was beneficial for the aluminum substrate. This behavior is indicated from the less negative rest potential, corrosion potential, breakaway potential and anodic-to-cathodic potential values. In addition the steep flattening of the gradient at the breakaway potential is maintained only for approximately three orders of magnitude and the higher anodic-to-cathodic potential as compared to the corrosion potential indicates a less active surface than in the case of anodized aluminum. Furthermore, we can see that the current density values are significantly lower (two orders of magnitude) when compared to the uncoated anodized aluminum.

Similar behavior to the primer coated aluminum, is observed for the neat and doped resin coatings (Figure 7-1 c to f). All the doped resin coatings demonstrate a conductive behavior attributed to the conductive nature of the CNTs. The differences on the respective curves (primer coatings vs neat and doped resin coatings), indicated that the electrolyte didn't penetrate the resin coatings. All resin coatings present nobler anodic-to-cathodic potential as compared to the corrosion potential and the current density values are significantly lower when compared to the anodized aluminum. The slightly higher current density values during the reverse polarization may be attributed to water adsorption [19].

Among the doped resin coatings, the best behavior is present for the 0.5% content (Figure 7-1-c) where as we can see the curve is uniformly (forward and reverse polarization) indicating general corrosion and good CNTs dispersion. In addition, as indicated from the values of Table 7-4, this coating exhibits the lowest current density values three and four orders of magnitude smaller when compared to the 0.4% and 0.6% coatings respectively.

Table 7-4 Electrochemical values of the materials immersed in 3.5% NaCl, R.T. (Erest: Open circuit potential after immersion for 2 hrs)

Material	E_{rest} (mV)	E_{corr} (mV)	E_b (mV)	$E_{a/c/tr}$ (mV)	E_b - E_{cor} (mV)	$E_{a/c/tr}$ - E_{cor} (mV)	i_{cor} *10^{-3} (mA/cm^2)
Anodized Aluminum	-918.26	-684.19		-819.96		240.34	0.41

Primer coated	-699.15	-735.9	-302.34	-508.34	396.81	227.56	0.12
NeatAl2024	-699.89	-705.02	31.79	-435.9	736.81	269.12	0.0009
D04Al2024	-684.58	-1096	87.3	-719.89	1183.3	376.11	0.014
D05Al2024	-706.71	-704.96	235.4	-702.97	940.36	1.99	0.0043
D06Al2024	-608.80	-608.4	-158.59	-114.85	449.81	493.55	0.13

a.

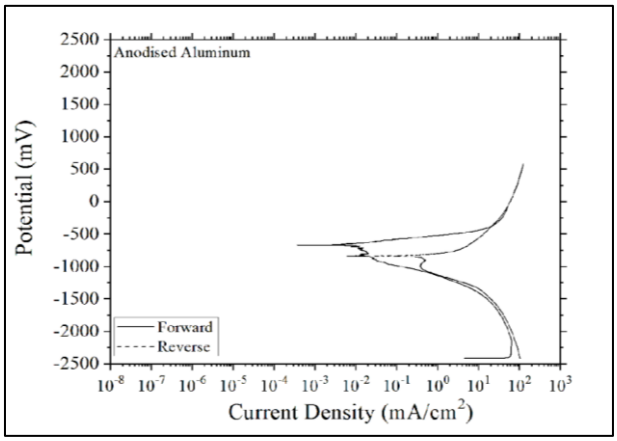

b.

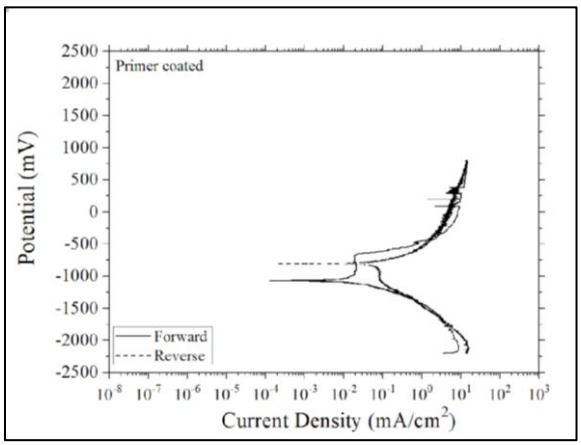

c.

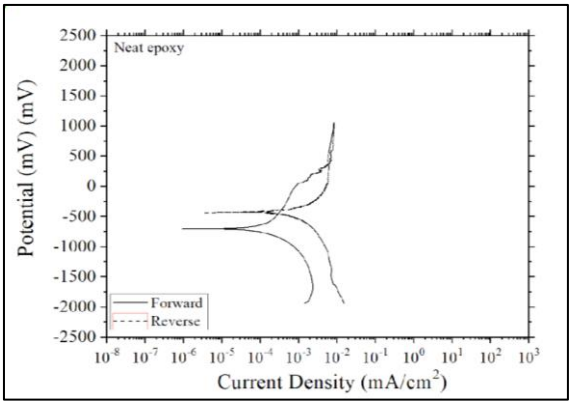

d.

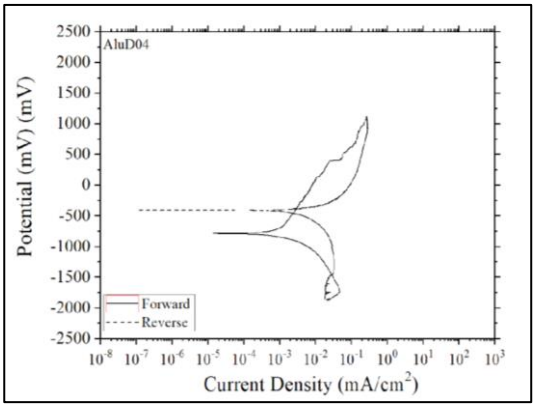

e. 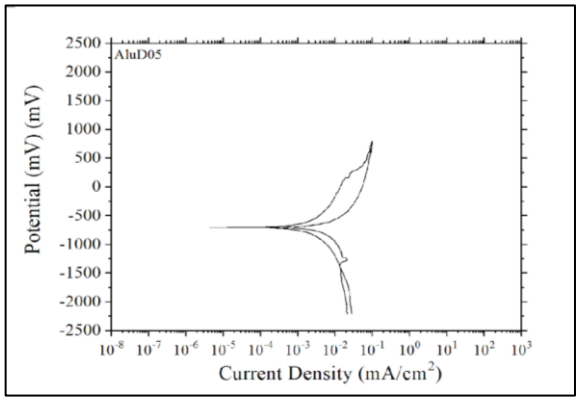

f. 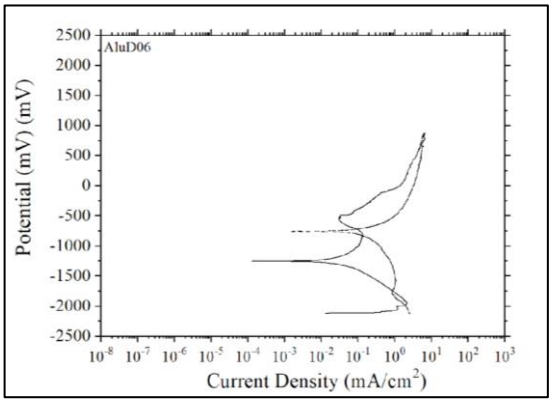

Figure 7-1 Potential vs Current density curves for (a) anodized Al2024-T3, (b) primer coated Al2024-T3, (c) neat epoxy, (d) doped epoxy with 0.4%, (e) 0.5% (c) and (f) 0.6%) w/w MWCNTs.

7.2.2. Aluminium substrate galvanic current curves

Figure 7-2 presents the galvanic current vs. immersion time plots for the couples presented in Table 2-2. As can be seen apart from the couple AlPr, all the other couples exhibit positive current density values suggesting that the primer coated Al2024 electrodes are anodic to the opposite ones in compatibility with the rest potential and corrosion potential measurements observed behavior.

It is observed that the AlPr_AlPr couple exhibits negative current density values. However it is expected that the current density should be equal or close to zero. According to optical observations on the specimen surfaces, small holes were present on both specimens. Meaning that the primer coating failed and the electrolyte reached the aluminum substrate promoting galvanic corrosion greater to the specimen connected to the WE 2 input. Current density current values lay in the range of -0.015 to -0.005 mA with current oscillations maybe associated to pit corrosion phenomena and re-passivation areas underneath the primer coating.

As far the couples containing primer coated Al 2024 and Al 2024 coated with either neat or nano-composite epoxy coatings are concerned, the trend is similar to the aforementioned couple (AlPr_AlPr), but with an opposite sign. The D_0.5 coating appears to be the more stable one with current density values in the range of 0.015 to 0.020 mA. The other two nano composite coatings (D-0.4 and D-0.6) and the neat coating, exhibit pikes and values in their values suggesting areas with large activity of pitting corrosion and repassivation. Neat epoxy and D-0.6 coatings current density values range in the area between 0.005 and 0.030 mA while D-0.4 has a slightly lower upper limit of 0.025 mA.

As the data indicate, all the epoxy coatings appear to enhance the galvanic corrosion activity between them and the primer coating. However they offer grade protection to the layers beneath them as no visual proof was found of electrolyte penetrating the epoxy coatings either in the galvanic corrosion or the cyclic voltammetry measurements.

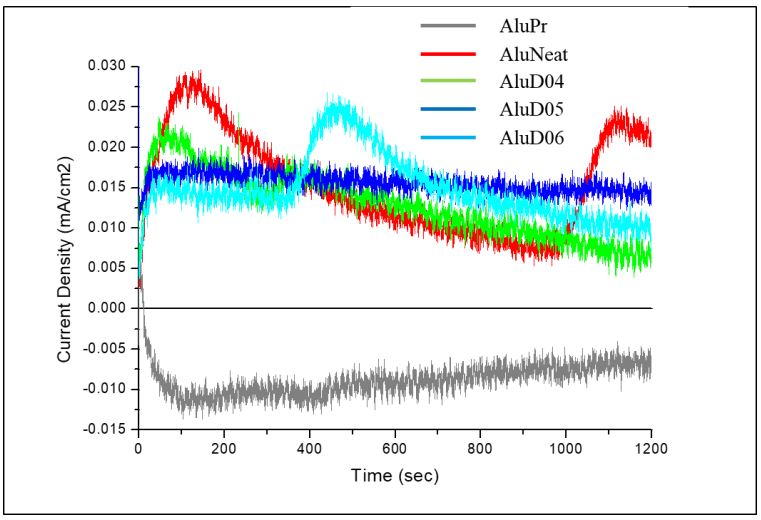

Figure 7-2 Galvanic Current Density vs Immersion time plot.

7.2.3. Stainless steel substrate polarization curves

Table 7-5 Nomenclature for the couples used in the galvanic current measurements employing an stainless steel substrate.

Nomenclature	SS304	SSNeat	SSD0.6	SSCF
Working Electrode 1	SS304 sand blasted	SS304 sand blasted	SS304 sand blasted	SS304 sand blasted
Working Electrode 2	SS304 sand blasted	SS304 coated with neat epoxy	SS304 coated with 0.6% doped epoxy	SS304 coated with CFRP patch with neat epoxy

Table 7-6 Electrochemical values of the materials immersed in 3.5% NaCl. All potentials are cited against Ag/AgCl.

Material	**E_{corr} (mV)**	**E_b (mV)**	**E_b - E_{cor} (mV)**	**E_{cp} (mV)**	**E_{cp}-E_{corr} (mV)**
ss304	-362	350(E_{b2})	712	-56	306
SSNeat	-656	-47	609	-47	609
SSD0.6	-497			-280	217
SSCF	-170	797	967	-54	116

Figure 7-2 depicts the polarization behaviour of all stainless based specimens after immersion in 3.5% NaCl, at room temperature while **Table** 7-6 lists the extracted electrochemical values. As can be seen, SSD0.6 nano modified epoxy and ss304 exhibited the highest current density differences in compatibility with the galvanic effect data while the CF reinforced epoxy exhibited the noblest corrosion potential most likely due to the noble nature of the graphite reinforcement. The conductive behaviour of SSNeat can be attributed to the water sorption by the free volume of the polymer and the hydrogen bonding of water molecules into hydrophilic sites, which increases the inherent low conductivity of the epoxy. The very low conductivity of the 0.6% CNT doped epoxy was compatible with the galvanic effect measurements and it can be explained, as aforementioned, by the existence of polymer tunneling barriers between

CNTs in the form of sheathing layers around the nanotubes. Two other reasons for the observed very low corrosion kinetics of the 0.6% CNT doped epoxy coating are: the hydrophobic nature of CNTs and the uniform distribution of CNT into the polymer matrix. The latter may limit transport of water through micro cracks or other forms of micro damage, such as pores or small channels already present in the neat polymer or generated by water attack since CNTs can act as crack deflectors. The CF reinforced polymer exhibits an intermediate kinetic behaviour; CFs may also limit water transport by the free polymer volume by acting as crack deflectors.

The anodic polarization curves of the neat epoxy coating and the 0.6 CNT coating presented stabilization current regimes at the high anodic potentials. The anodic polarization curve of the neat epoxy reinforced by CF exhibits a "passive" regime starting at -54 mV and sustained for about 870 mV. These regimes can be explained by the saturation of the polymer with water and the deposition of unstable polymer oxidation products. In the case of the CNT and CF reinforced polymers these current stabilization regimes start at E_{cp} potentials that are much closer to the corrosion potential in comparison with the neat polymer coating, because a) they present a polymer free volume that is smaller than that of the neat polymer and b) the reinforcements may limit water transport through defects of the polymer structure, as mentioned in the previous paragraph.

It can also be observed that the forward anodic curves of the neat epoxy and the CF reinforced epoxy present breakaway potentials (i.e. flattened gradients) suggesting the localized presence of deficient cross-link density regions. In the case of CF reinforced epoxy, an additional reason for the localized degradation can be the localized existence of weak matrix/CF interfaces that induce preferential water adsorption at the fibre/matrix interfaces. The 0.6% CNT doped epoxy did not present deviation from a uniform corrosion behaviour indicating a uniform CNT distribution that has densified localized poor cross-link density regions.

The positive hysteresis in **Figure** 7-2a (namely higher "reverse" currents than the "forward" ones at the same potential in the anodic scan) suggests that bare SS304 was susceptible to pitting in aqueous NaCl. The neat epoxy and the CF reinforced epoxy coatings present negative hysteresis indicative of localized degradation phenomena in compatibility with the aforementioned breakaway behaviour upon forward polarization. The only system presenting a positive hysteresis is the CNT doped coating due to the absence of localized

degradation phenomena that can cause irreversible damage as in the case of the neat polymer and the CF reinforced polymer.

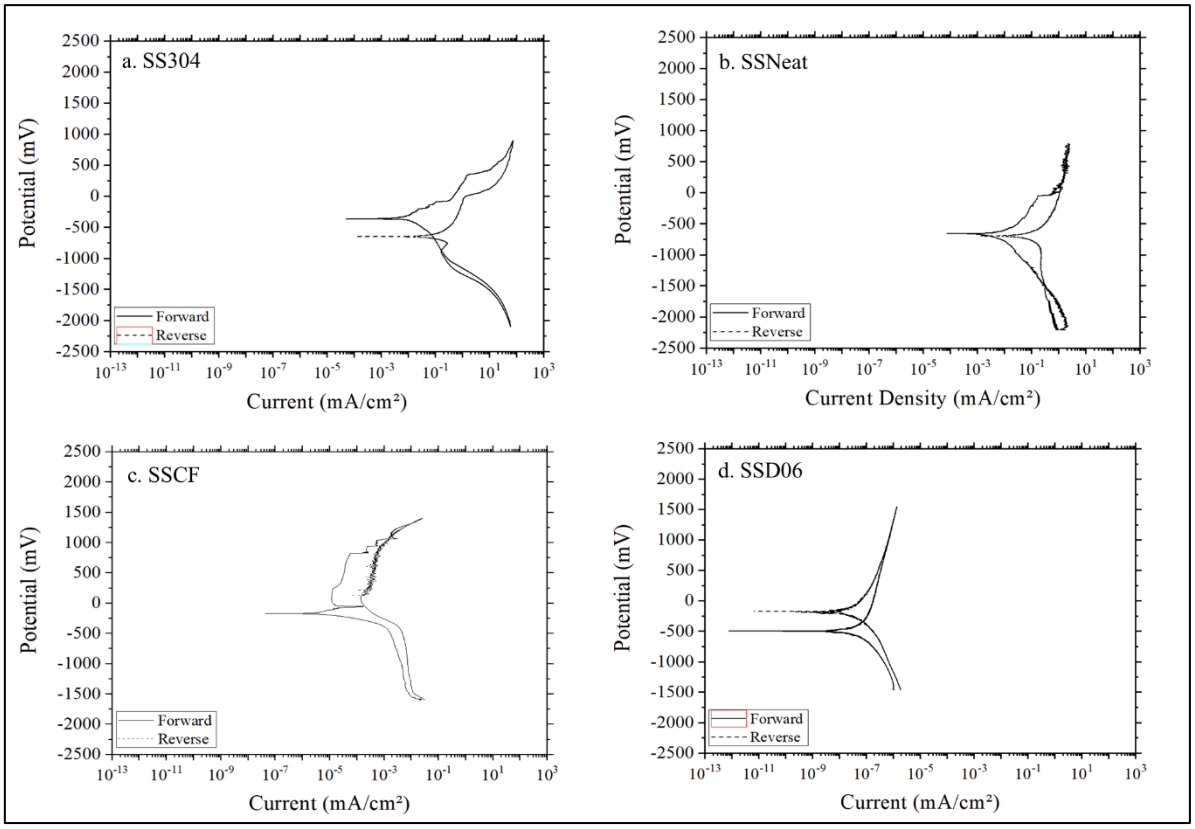

Figure 7-3 Cyclic polarization behaviour of (a) bare ss304L, (b) neat epoxy film on ss304L, (c) 0.6 wt.% CNT doped epoxy film on ss304L and (d) neat epoxy carbon fiber composite on ss304L (aerated 3.5% NaCl, R.T.). All potentials are cited against Ag/AgCl.

7.2.4. Stainless steel substrate galvanic effect

Figure 7-3 presents the galvanic current vs. immersion time plots for the couples presented in **Table** 7-5. As expected the SS304 couple exhibited current values close to nil. In addition, the rest couples exhibit positive current density values indicating that the SS304 substrate is less noble when compared to the various coatings. The CNT doped epoxy presents the highest galvanic effect with the substrate, whilst the epoxy reinforced by CF presents the lowest galvanic effect. This finding is unexpected, since the CNTs are expected to increase the conductivity of the polymer [10-12] and hence decrease the galvanic effect between a neat polymer and a (highly conductive) metal. However, this high galvanic effect is compatible with the fact that the conductivity of composites with identical filler concentration seems to vary, with some

exceptions, by one or two orders of magnitude for identical matrices and by ten or more orders of magnitude for different concentrations. A major reason for this is the existence of polymer tunnelling barriers between CNTs in the form of sheathing layers around the nanotubes, which result in the decrease of the overall composite conductivity.

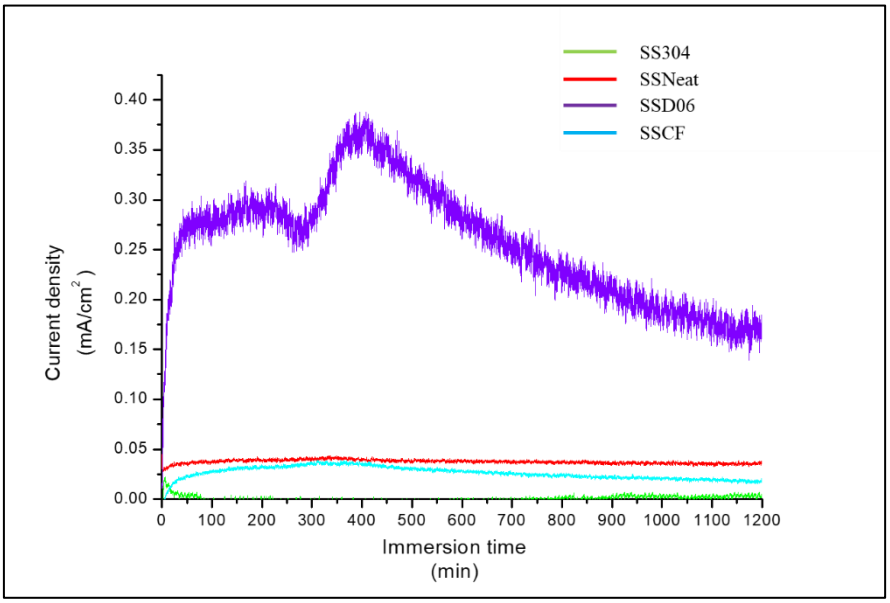

Figure 7-4 Galvanic current vs. time for the couples: ss304-ss304, ss304-resin neat, ss304-resin doped 0.6 wt.% and ss304-composite neat.

7.2.5. Conclusions

The overall assessment of the nano-reinforcement, indicated that the inclusion of CNTs leads to beneficial results, on the anti-corrosive performance. The incorporation of CNTs in the epoxy magnifies the galvanic effect between epoxy and metallic substrates, either aluminium or steel. Nevertheless, it promotes corrosion resistance from both a kinetic and thermodynamic standpoint, whilst magnifying the resistance to localized corrosion.

7.3. Effect of multi-scale reinforcement.

Aluminium 2024-T3 (Al2024) alloy is one of the most widely used alloys in the aerospace industry due to its relatively low weight, high strength and fatigue resistance. Typical uses of Al2024-T3 include fuselage and wing skins, cowls and internal structures. One of the key disadvantages of Al2024-T3 is its low corrosion resistance hence in aerospace applications, it is used after anodizing processes followed by sealing with epoxy paints/coatings [299][300]. The anodization process enhances the adhesion between the aluminium substrate and the epoxy

coating, however due to electrical conductivity mismatches, in the event of a coating failure (scratches), the aluminium corrosion process can be accelerated leading to catastrophic failures [301].

In order to further enhance adhesion and alleviate the mismatches, several studies have been conducted in employing nano-modified epoxies employing mainly graphitic structures like carbon nano tubes (CNTs) [302,303]. Apart from the improved adhesion, CNTs can also reduce the ingress of water in the epoxy due to their hydrophobic nature and high specific area resulting in more tortuous paths for the absorption and diffusion of water further enhancing the performance of the joint structure [219,304–306]. In addition, the CNTs can significantly enhance the electrical conductivity of the insulating epoxy, thus abating the conductivity mismatch between aluminium substrate and coating. In [307], Yu et.al., employed CNTs in various weight contents towards an improved adhesive for aluminium bonding. The thermal and electrical properties of the novel adhesive were investigated along with the adhesive strength in terms of Boeing wedge testing. Thermal gravimetric analysis results showed increased thermal degradation resistance with the onset of decomposition temperature occurring at higher temperatures when compared to a neat adhesive. The surface electrical resistivity results of the modified adhesives exhibited a very low percolation threshold at 0.5%w.w. with more than 5 order of magnitude drop and the resistivity values were further reduced when the CNTs weight content was increased up to 5.0%w.w. In terms of bonding strength and durability it was shown that the incorporation of CNTs filler led to significant improvements and optimum performance was achieved in the case of the 1.0%w.w. filled epoxy.

A recent approach on epoxy resins reinforcement is via the inclusion of multiple filler types like amorphous graphite (AG) or carbon nano tubes (CNTs), in order to exploit synergistic effects between the fillers. When the different fillers belong to various scale sizes, it is possible to even exploit synergistic effects further enhancing performance and material properties [308]. Sumfleth et. al. simultaneously employed CNTs and carbon black towards electrically conductive epoxy nanocomposites. The results showed similar electrical properties between the binary Multi Walled CNTs (MWCNTs) and the ternary MWCNTs/CB nanocomposites. Interestingly though it was shown that in the ternary composites, the percolation threshold as well as the conductivity was preserved when half of the amount of MWCNTs was replaced with CB [309]. In a similar approach Ma et.al., employed CNTs and CB and examined both of the electrical and mechanical properties of the developed ternary nanocomposites. It was shown

that the combined inclusion of the two filler types led to a more effective electrically conductive network with the CB particles interconnecting the gaps among the CNTs particles at a very low percolation. The synergistic effects were also evident in the enhanced ductility, fracture toughness and flexural strength results which were attributed to the distinct geometric and aspect ratio characteristics of the two filler types.

In an event of corrosion initiation, an indication could prevent catastrophic failures. Recently, many research efforts have been focused on non-destructive (NDT) on line inspection techniques that can characterize and monitor aluminium corrosion phenomena[310,311]. One of the studied techniques is that of Acoustic emission (AE) which can monitor transient elastic propagating waves caused by a rapid release of energy within a material under stress [312,313]. AE has already been extensively employed in a wide range of engineering materials like metallic alloys [314–316], fibre reinforced polymers (FRPs) [317], reinforced concrete [318,319] and recently, some efforts were focused on applying AE as a corrosion monitoring technique for steel alloys with promising results been presented. Different corrosion phenomena, like interganullar corrosion [320], uniform [321,322] localized or pitting corrosion [316], have been successfully correlated with specific AE indices. A specific, for the aviation sector, advantage of AE as a corrosion monitoring technique, is that AE can also provide information on the structural integrity of FRPs which gradually are replacing traditional metallic alloys [323,324]. Thus being a “multi-purpose”-on line monitoring tool leading to reduced cost of inspection.

Based on the aforementioned considerations, this chapter is dedicated to the presentation of open circuit and cyclic polarization tests coupled with AE measurements. One of the major indicators of aluminium corrosion is the creation of hydrogen as a by-product of aluminium oxide development. The coupled measurements were targeted on identifying changes in specific AE indices that could be associated with the creation of hydrogen bubbles and/or other aluminium corrosion phenomena. The employed aluminium specimens were either as-received, anodized or coated with neat and modified with carbon allotropes (i.e. carbon nano tubes (CNTS), milled carbon (MC) and combination (Ternary)) epoxies so as to discriminate water vapor bubble phenomena from the corrosion phenomena (general corrosion, pitting corrosion etc.) and correlate these phenomena with characteristic AE signal descriptors.

7.3.1. Experimental

The effect of the multi-scale reinforcement on the anti-corrosive properties of epoxy coatings has been studied. Specimens employing anodized Al2024 substrates and binary MWCNTs, binary CB and ternary epoxy coatings were manufactured according to 2.3.11 and 2.3.9.1.

AE measurements were coupled with the electrochemical measurements according to 2.3.9.4. The capabilities of AE as a corrosion monitoring tool were assessed via correlations among corrosion phenomena and AE indices.

7.3.2. Results and Discussion

7.3.2.1. Interpretation of polarization behaviour of anodized aluminium

Figure 2-1 presents the cyclic polarization behaviour of an as received specimen as recorded during cyclic polarization curves while **Table** 7-7 summarizes all extracted potential values for the as-received, anodized and coated specimens.

Table 7-7 Potensiodynamic polarization values exported from the respective curves.

	E_{corr} (mV)	E_{cp} (mV)	E_b (mV)	E_{pseudo} (mV)
Bare	-946	-940	-644	-578
Anodized	-653	-524	139	-428
Neat	-633	-692	$1{,}58x10^{-6}$	-333
CNTs	-779	-794	$1{,}88x10^{-6}$	-400
CB	-722	-701	$2{,}66x10^{-6}$	-517
Ternary	-590	-735	$7{,}35x10^{-5}$	-306

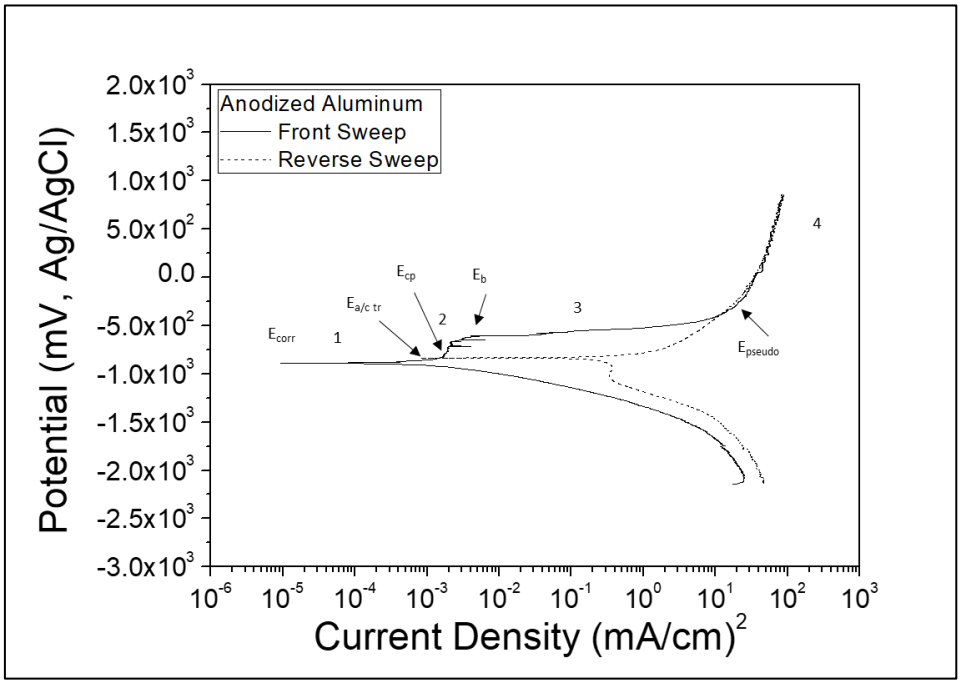

Figure 7-5 Cyclic polarization curves for an anodized aluminium

As seen from the positive hysteresis loop (i.e. reverse currents greater than forward currents for the same potential), the aluminium alloy has been subjected to localized corrosion. This can also be seen by the sharp increase in the current density (i) by almost four orders of magnitude, at potentials higher than the breakdown potential (E_b).

In detail, the forward anodic polarization curve of anodized Al2024 is divided in four stages:

Stage 1a (E_{cp}-E_{corr}): Anodic oxidation of Al occurs at the structural defects of the anodization film, according to the generalized reaction [325]:

$$Al + 3H_2O \rightarrow Al(OH)_3 + 3H^+ + 3e^- \quad (1)$$

Stage 2a: Al 2024 exhibits passivation in the potential range E_{cp}: to E_b due to the phosphoric treatment. The active sites of stage 1 are covered by the long been known bi-layered structure of the passive film on aluminium: the inner layer is a compact amorphous layer whilst the outer layer is a permeable hydrated oxide layer [326].

Stage 3a (E_{pseud}-E_b): Passivation ends at E_b, as shown by the flat gradient sustained for almost four orders of magnitude current density increase. The breakdown of passivity may be attributed to deficient sealing of the porous upper layer of the anodic film. Full sealing by immersion in boiling water following anodization in H_3PO_4, was not applied, since it would decrease the ability of the anodic film to anchor organic coatings [327]. As the anodization film is composed of an inner denser barrier layer and an outer looser porous layer, the chloride ions can access the barrier layer through the pores. When the chloride ion concentration at the bottom of the porous layer reaches a critical level, the barrier layer begins to dissolve. Completely or partially sealing of the tubular pores will reduce both the chlorine ion speed and concentration at the bottom of the porous layer. As the anodic overpotential increases, the chlorine concentration on the barrier layer also increases. Hence, the greater the range of passive overpotentials and the lower the passive current densities, the higher the corrosion resistance of the anodization film. Nevertheless, the fact that the pitting potential is ~400 mV nobler than the corrosion potential demonstrates the efficiency of the anodizing process; as for non-surface treated Al 2024, the pitting potential and corrosion potential values almost coincide.

As soon as Cl^- accesses the Al substrate having surpassed the obstructions of the anodization overlayer, localized corrosion of Al takes place. Four steps are generally accepted to be involved in the localized corrosion of aluminium [328]: (

1) The adsorption of the reactive anions on localized sites of the surface film of aluminium (i.e. sites where the film presents inhomogeneities [329]).

(2) The chemical reaction of the adsorbed anion with the aluminium ion in the aluminium oxide/hydroxide lattice.

(3) The thinning of the oxide film by dissolution. This dissolution is a flaw assisted/ flaw centered process. (The passive film on Al-alloys exhibits semi-conductive properties owing to the non-stoichiometry of composition and local structural inhomogeneities [329]).

(4) The direct attack of the exposed metal by the anion possibly assisted by an anodic potential.

On the above grounds, stage 3 is interpreted as follows:

(1) Once aggressive anion adsorption on the aluminium oxide surface film at the defective site occurs, an active center is developed. In the case of Al2024, the usual film defective site is

the interface between Al and S-phase (Al_2CuMg) [330]. The latter is less noble than Al. The active center was then the site for accelerated film thinning [331].

(2) Once the film is sufficiently thinned, direct attack of the exposed metallic substrate occurs. Because the film is thinned locally, the attack on the metal is also concentrated. Due to the electrochemical potential difference between Al and S-phase [332], localized dissolution of the anodic S-phase should occur**.** Nevertheless, the dissolution characteristics of the S phase are complex and have been shown to incorporate a dealloying mechanism, leading to localized Cu enrichment. It may be assumed that the S-phase does not dissolve as a unique entity, but may undergo a dealloying process leading to selective dissolution of the Mg and Al components of the intermetallic. The resultant Cu enrichment may allow for the intermetallic to behave as a local cathode after some unknown time that eventually leads to dissolution of adjacent Al. As a consequence, small pits are formed.

(3) As the pits are getting deeper, differential aeration cells are formed between the bottom of the pits and the pit walls.

Stage 4a ($E>E_{pseudo}$): The hydrolysis of Al in microscopic and macroscopic heterogeneities according to reaction (1), results in reduction of pH and consequently further dissolution of Al. Diffusion of Cl^- follows into the flaws to maintain electro-neutrality. The agile chlorine ions induce further hydrolysis reactions which may lead to the formation of more $Al(OH)_3$ or $Al(OH)^{2+}$. Thus, further decrease in the electrolyte pH in the flawed areas occurs, stimulating further and faster aluminium dissolution. With raising potential above E_{pseudo}, the chlorine concentration in the flawed regions increases. As a consequence, the pH falls to such low values, that Al hydroxides/ oxyhydroxides become unstable [333]. At $E>E_{pseudo}$, the rate of formation of Al hydroxides/ oxyhydroxides is greater than the rate of their dissolution leading to pseudopassive stage 4.

Although these films are heavily hydrated and soluble, as shown by the very high current densities, they seem to protect the Al substrate due to their thickness, as the negative hysteresis loop upon reverse polarization through stage 4 shows. As reverse scanning passes below E_{pseudo}, the unstable films dissolve and pits reopen. Thereafter, hysteresis becomes negative. The potential of anodic to cathodic transition ($E_{a/c\ tr}$) is nobler than E_{corr}, suggesting that any current limiting process upon anodic polarisation is reduced or even absent at the corrosion potential [331,334].

7.3.2.2. Polarization behaviour of coated aluminium substrates

Figure 7-6 presents the cyclic potensiodynamic polarization curves for all as received, anodized, neat epoxy coated and modified epoxy coated aluminium substrates.

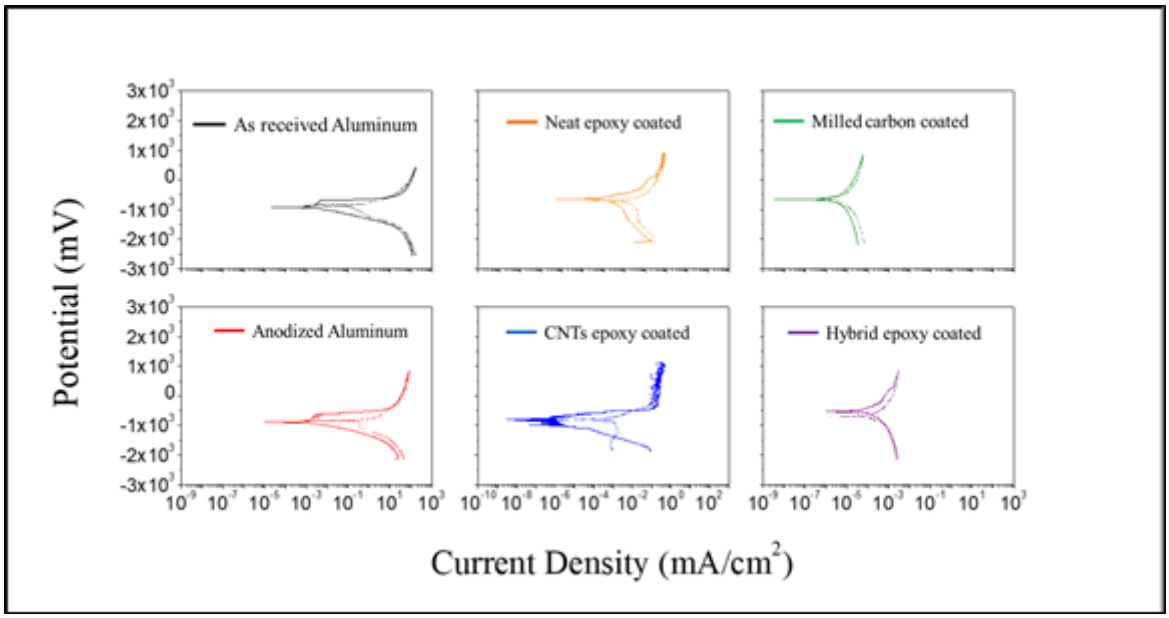

Figure 7-6 Potentiodynamic polarization curves for all the tested specimens

As can be seen in **Figure** 7-6 and **Table** 7-7, the application of the epoxy coatings significantly enhanced corrosion protection to the aluminium substrates. This behaviour is indicated from the less negative rest potential, corrosion potential, breakaway potential and anodic-to-cathodic potential values. Furthermore it is seen that the steep flattening of the gradient at the breakaway potential is almost absent in all coated specimens. The anodic-to-cathodic potential as compared to the corrosion potential indicates a less active surface than in the case of the as received and anodized substrates. Furthermore, we can see that the current density values are significantly lower (orders of magnitude) when compared to the uncoated anodized aluminium.

All the doped resin coatings demonstrate a conductive behaviour attributed to the conductive nature of the carbon allotropic fillers. The observed differences on the respective curves, indicated that the electrolyte didn't penetrate the resin coatings. The modified resin coatings present nobler, as in the case of CNTs, or the same, as in the case of MC coatings, anodic-to-cathodic potential as compared to the corrosion potential and the current density values are

significantly lower when compared to the un-coated specimens. The slightly higher current density values during the reverse polarization may be attributed to water adsorption [316].

In the case of the CNTs coatings, it is seen that the polarization curve is not as smooth as in the case of the MC or ternary ones, exhibiting a "ladder" like pattern with pseudo-passivation steps. This behaviour can be attributed to the ingress of water in the vast number of interfaces between CNT particles and epoxy matrix. The water could have penetrated into the interfacial areas activating the surface thus increasing current density. Saturation and consequent swelling of the interfaces led to passivation of a specific area while subsequently the ingress of water could have taken place in different areas and so on. When observing the three modified coatings curves, it is evident that the Ternary coating curve presents an intermediate behaviour when compared with the CNTs and MC coatings. This behaviour could be an indication of synergistic effects between the fillers like the ones observed in [304].

7.3.2.3. Acoustic emission and polarization curves

Figure 7-7, **Figure** 7-8, **Figure** 7-9 and **Figure** 7-10 present cumulative AE hits, signal amplitude, average frequency and peak frequency respectively with current density vs time curves respectively.

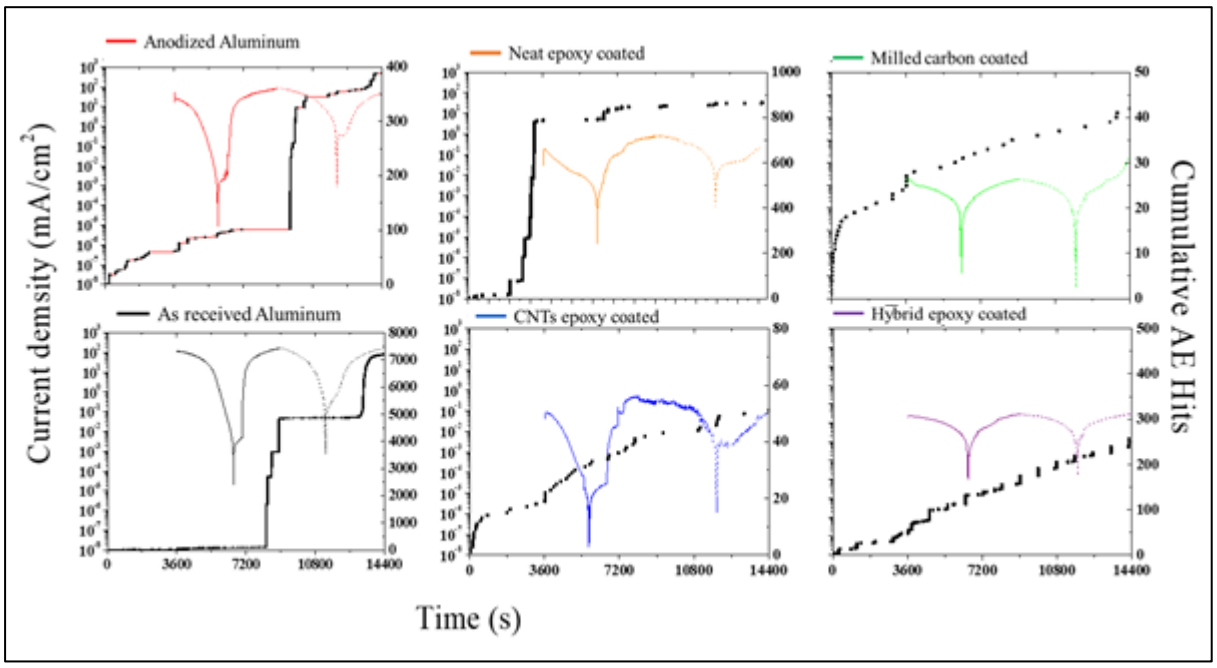

Figure 7-7 Current density and cumulative AE hits vs time curves for all tested specimens un-coated and coated.

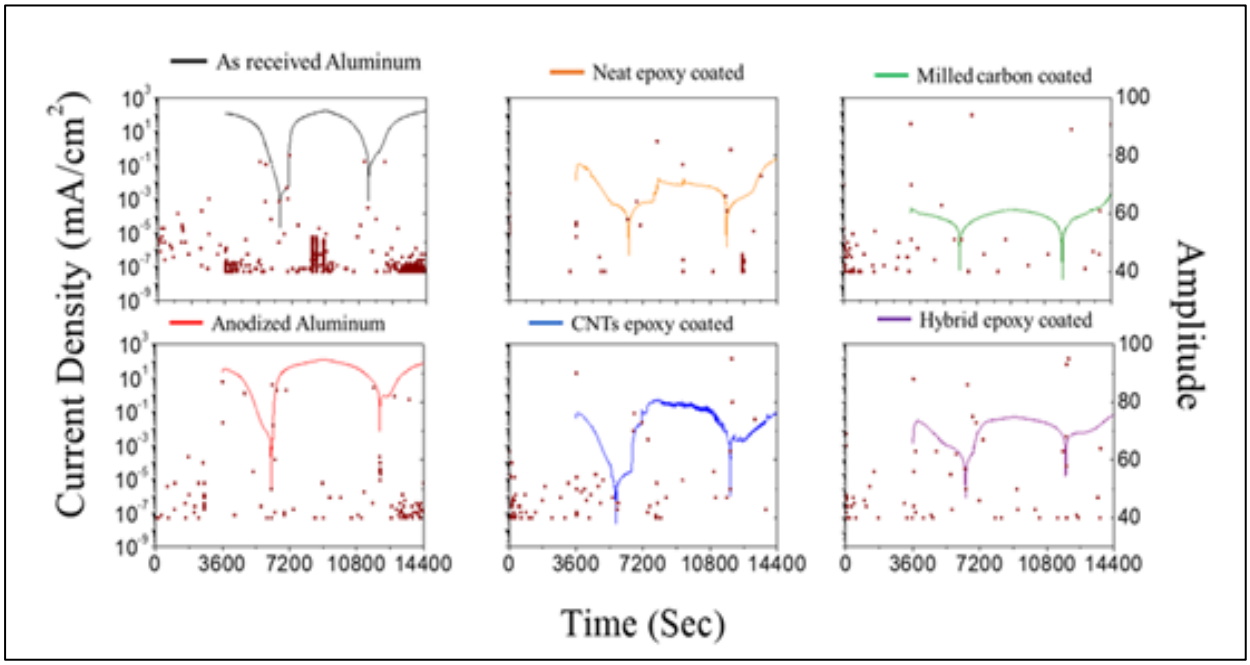

Figure 7-8 Current density and amplitude vs time curves for all tested specimens un-coated and coated.

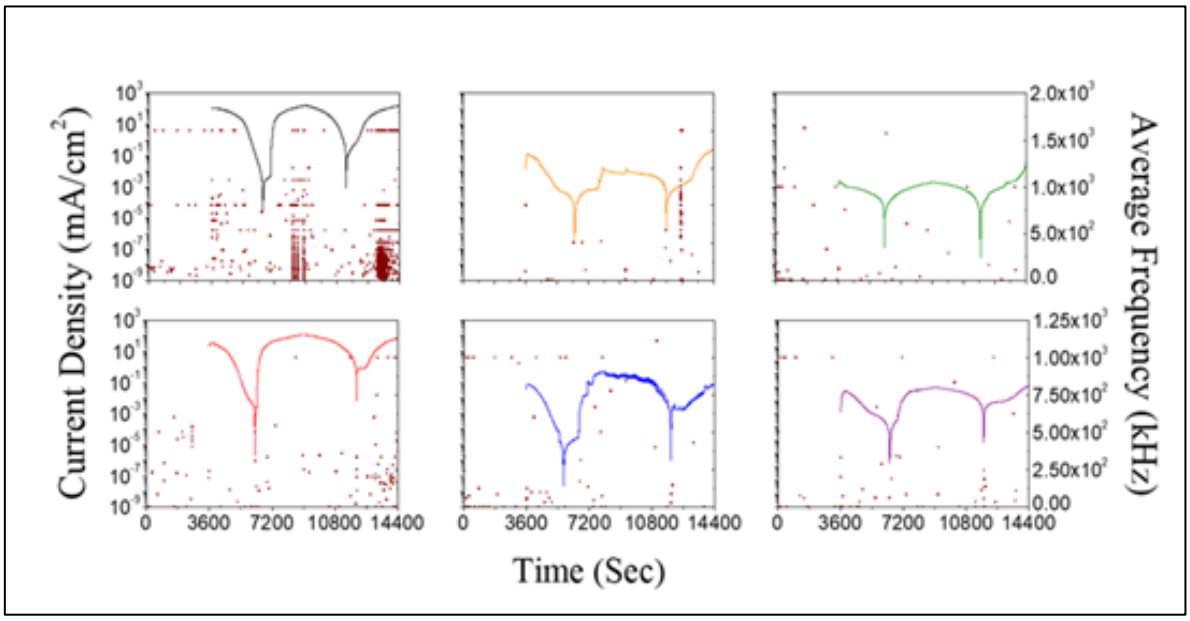

Figure 7-9 Current density and average frequency vs time curves for all tested specimens uncoated and coated.

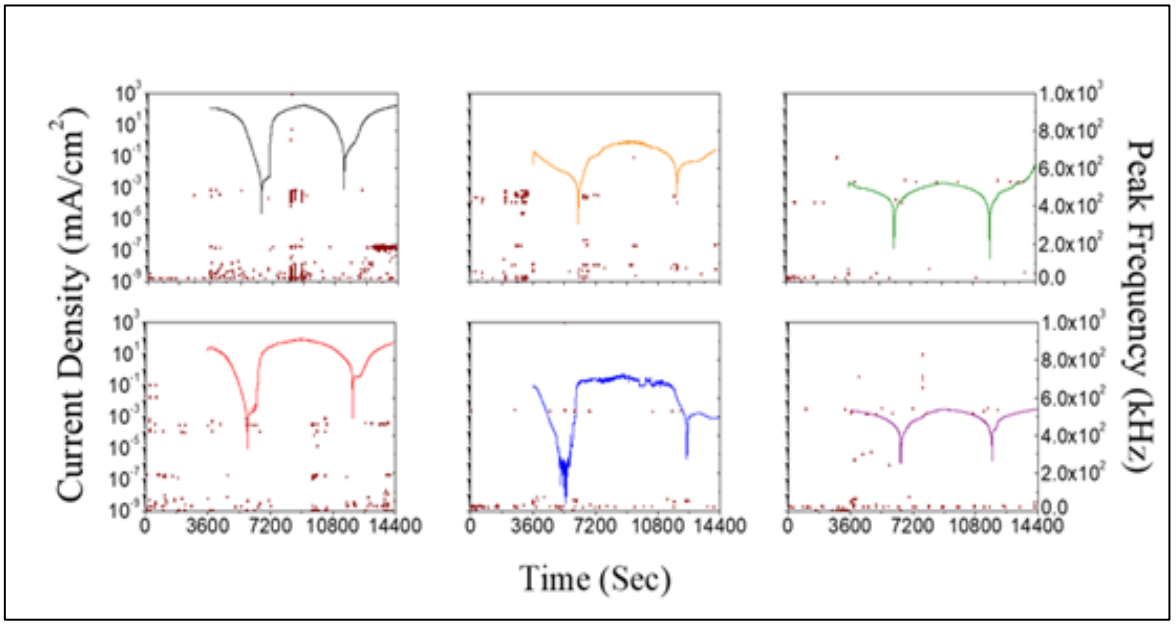

Figure 7-10 Current density and peak frequency vs time curves for all tested specimens un-coated and coated.

As it can be observed, the open circuit step of the testing resulted in insignificant AE activity (first hour in all AE/cyclic polarization curves). The various corrosion stages during polarization have been noted in **Figure** 7-5 for a clearer correlation of the AE activity and corrosion process namely (where 'a' denotes the anodic stage and 'c' the cathodic stage):

Stage 1c: cathodic forward polarization – hydrogen reduction: $2H^+ + 2e^- \rightarrow H_2$ (2)

Stage 2c: cathodic forward polarization –oxygen reduction: $O_2 + 2H_2O + 4e^- \rightarrow 4OH^-$ (3)

Stage 1a: anodic forward polarization- oxidation of Al according to reaction (1)

Stage 2a: anodic forward polarization-passivation at defects of anodizing film

Stage 3a: anodic forward polarization-pitting at the interface between Al and S-phase

Stage 4a: anodic forward polarization + anodic reverse polarization -pseudopassivation by deposition of heavily hydrated alumina films on pits

Stage 5a: anodic reverse polarization-dissolution of films-pit reopening

Stage 6c: cathodic reverse polarization–oxygen reduction (reaction 3)

Stage 7c: cathodic reverse polarization– hydrogen reduction (reaction 2)

A noticeable increase in the AE activity can be observed after 2.5 hours of testing which corresponds roughly to the end of stage 2a where the passivation of the anodizing film occurs at the oxide layer defects sites. It is established that near the corrosion potential, the only

cathodic reaction that occurs in 3.5% NaCl is the reduction of oxygen (reaction 3) [334].Up to this point insignificant amount of AE events are recorded (approximately 200 hits) which can be associated to the oxidation reactions 1 to 3. The first noticeable increase in the AE activity occurs during anodic polarization during stages 2a and 3a. This increase most likely corresponds to hydrogen bubble formation due to the hydrogen reduction reaction (2), where aluminium pitting corrosion occurs. The above postulation is enhanced by the gradual decrease and plateau of AE activity during stage 4a where the anodic reverse polarization stage initiates and pseudopassivation occurs. During stages 5a and 6c it is observed that no significant AE activity is recorded up to the initiation of stage 7c. During stage 5a though it is known that dissolution of the oxide films occurs during anodic reverse polarization hence it would be expected that AE would be significantly increased. Despite this fact though it is observed that during the cathodic reverse stages 6c and 7c, AE is capable of effectively recording the collapse of the film and the pits reopening.

The observed abrupt increase in the AE activity at the pseudo-passive stage (stage 4a) lasts up to the beginning of reverse anodic polarization. This AE activity corresponds to the deposition of heavily hydrated and highly instable alumina films on pits. The AE activity further increases for a third time during stage 7c, which corresponds to the hydrogen reduction process (reaction 2).Pitting of Al can be detected with difficulty by AE, under the applied parameters, since it is a localized phenomenon. Similarly, the first passive stage (stage 2a), is hardly detected by AE, possibly due to the fine thickness of the passive film and its localized deposition on the structural defects of the anodizing film. However, few signals of rising amplitude and peak frequency are discerned during stage 2a that may be ascribed to true passivation.

In terms of signal amplitude in **Figure** 7-8 it is observed that during the first hour (open circuit measurements), the detected signals are scattered in the range from 40db to 60db. During stages 1c and 2c a cluster of low amplitude signals (40-45db) are detected which can be associated to hydrogen and oxygen reduction according to **Equation**s 2 and 3. The oxidation of aluminium and the subsequent passivation of the surface during stages 1a and 2a cannot be detected accurately by the AE, however during pitting of aluminium at stage 3a and the subsequent pseudo-passivation at stage 4a, can be detected. As it is observed during these stages the recorded signals are clustered in the range between 40-50db. During this stage hydrogen bubbles were generated inside the pits as a by-product of aluminium oxidation. It is possible that the recorded AE hits are the result of the bubbles sliding on the specimen surface

and their subsequent rupture. Finally at the second abrupt increase at stages 6c and 7c the recorded signals lay at the same range as with the case of stages 1c and 2c. As stated, at this point the aluminium oxide film collapses while oxygen and hydrogen reduction takes place with the generation of hydrogen and hydroxyl. It can be postulated that the recorded signals in the range between 40db to 50 can be again associated with hydrogen bubbles, a byproduct of the oxide film dissolution.

The same signal ranges, can be observed at the anodized specimens in **Figure** 7-8. The significant differences in the anodized specimen curve, is the significantly less recorded AE activity and the fact that the detected signals in stages 2a and 3a for the as received aluminium, were recorded during stage 4a. By observing the current density curve, it is seen that the breakdown potential was reached earlier while the stabilization of the current density values (stage 4a) lasted longer when compared to the as received aluminium. Hence it is possible that aluminium pitting corrosion was delayed up to stage 5a where the dissolution of the oxide was initiated. During stages 6c and 7c the same amplitude signals as with the case of the as received aluminium but in a smaller population.

Similar patterns were also observed in the average frequency curves (**Figure** 7-9) for the as received and anodized aluminium. Clusters in the frequency range between 1-250 kHz with some scattered hits at higher frequency values (1000 kHz) are present in both aluminium types for all corrosion stages. The latter ones could be classified as environmental or electrical noise however further study should be conducted. The only differentiation that is present, can be seen during stages 6c and 7c, where in the case of the anodized specimen the recorded signals in the range from 1 to 250 kHz are absent. This pattern can be associated with the anodized film which effectively delayed aluminium pitting and general corrosion degradation In the case of the as received specimen during the latter stages of the measurement, it is observed that a significant number of AE hits are present n the range 0-250 kHz. These signals could be an indication of the collapse of the total degradation of the aluminium surface which takes place during these stages.

The above mentioned observations regarding the observed patterns in AE indices, give strong evidence that specific corrosion phenomena can be correlated to combinations of indices of the AE activity. The discrimination of these characteristics depend on the nature of the various corrosion related phenomena on the aluminium substrates and further studies could give a stronger indication for such a correlation.

When observing the combined potensiodynamic and AE indices curves, it is clear that AE activity was significantly affected by the applied epoxy coatings. All epoxy coatings exhibited significantly less AE activity when compared with the as received aluminium with the AG coating been the one with the fewest AE hits. In contrast Ternary coating exhibited a far greater number of AE hits with the CNTs being in the middle. This phenomena can be attributed to the increased number of interfaces that were present in the Ternary coating. Another interesting phenomena is the fact that in the neat epoxy coating, exhibited almost double the AE events were recorded when compared with the anodized specimen and the Ternary coating. It is also interesting that the vast majority of the recorded AE hits, where detected during the open circuit stage and during the polarization measurement very few AE events occurred. This phenomena could be associated with the ingress of water that can cause swelling of the epoxy which in turn can lead to the generation of micro cracks in the surface, up to a saturation point. Both CNTs and Ternary coating exhibited a similar trend in the recorded AE hits with a steadily increasing rate throughout the measurements. The observed "staircase step-like" behaviour could be an indication that water was being absorbed at filler/matrix interfaces activating the surface with subsequent swelling and deactivation. Given that AG coating didn't exhibited such a behaviour, this pattern can be attributed to the CNTs particles.

In terms of signals amplitude, apart from the neat coating, all recorded AE events, were scattered in the range between 40db and 50db with no specific pattern emerging. This behaviour further enhances our postulation of a "general corrosion" performance for the modified coatings. A small cluster in the range of 40db-50db was only present in the neat coating roughly at the end of the open circuit measurement which could be a further indication of the formation of micro cracks in the coating surface due to the ingress of water and swelling of the epoxy. The latter postulation could be further enhanced if we observe the average frequency curve of the neat coating. As can be seen, the cluster of signals lay in the range between 100-750 kHz, a range that in the case of the as received and anodized specimens, is present in the polarization measurement stages. This could be an indication of different phenomena between the three and an additional evidence of the AE capabilities as a corrosion monitoring tool.

More pronounced differences between the uncoated and coated specimens can be observed in **Figure** 7-9. It can be seen that the as received in the aforementioned stages exhibited signals in the frequency ranges from 1 kHz to 150kHz, 200 kHz and 500 kHz. As stated, these signals that were present for the anodized specimen also, can be associated to the various corrosion

phenomena and the by-products associated with them. In contrast, the coated specimens signals at low frequencies (up to 50 kHz) and high frequencies (500 kHz). The medium frequencies around 200 kHz are completely absent from the coating specimens. In combination with the aforementioned patterns of behaviour for the other AE indices, it can be postulated that the observed signals can be associated with water vapor bubbles and epoxy degradation phenomena.

7.3.3. Conclusions

The following corrosion processes were identified by AE during cathodic and anodic polarization of anodized Al2024: a) hydrogen reduction during cathodic polarization, b) pseudo passivation by deposition of heavily hydrated alumina films on pits upon anodic polarization to high overpotentials. The likelihood of hydrogen evolution persistence during the final stage of current stabilization due to underlying pitting was raised. Based on the changes in the AE indices between the as received, anodized and coated substrates, hydrogen bubbles could be associated with low amplitude and medium peak frequency signals; pseudo passivation in terms of heavily hydrated films could be associated with low amplitude and high peak frequency signals; epoxy degradation phenomena like swelling and micro cracking could be associated with low amplitude and high peak frequency signals; reinforcement/epoxy interfacial water transport and likely degradation may be associated with a uniform and sporadic AE amplitude/average frequency signals. In general, the obtained experimental results, give a strong indication that AE can be an effective monitoring tool for aluminium corrosion studies. It has to be stated though that further investigation should be conducted so as to fully differentiate characteristic AE indices and correlate them with corrosion, epoxy and interfacial degradation phenomena.

8. References

[1] N. Domun, H. Hadavinia, T. Zhang, T. Sainsbury, G.H. Liaghat, S. Vahid, Improving the fracture toughness and the strength of epoxy using nanomaterials – a review of the current status, Nanoscale. 7 (2015) 10294–10329. https://doi.org/10.1039/C5NR01354B.

[2] A.P. Mouritz, Review of z-pinned composite laminates, Composites Part A: Applied Science and Manufacturing. 38 (2007) 2383–2397. https://doi.org/10.1016/j.compositesa.2007.08.016.

[3] A.P. Mouritz, Fire resistance of aircraft composite laminates, Journal of Materials Science Letters. 22 (2003) 1507–1509. https://doi.org/10.1023/A:1026103231041.

[4] A.P. Mouritz, E. Gellert, Review of advanced composite structures, Composite Structures. (2001).

[5] S.J. Tucker, B. Fu, S. Kar, S. Heinz, J.S. Wiggins, Ambient cure POSS–epoxy matrices for marine composites, Composites Part A: Applied Science and Manufacturing. 41 (2010) 1441–1446. https://doi.org/10.1016/j.compositesa.2010.06.005.

[6] F.L. Jin, X. Li, S.J. Park, Synthesis and application of epoxy resins: A review, Journal of Industrial and Engineering Chemistry. 29 (2015) 1–11. https://doi.org/10.1016/j.jiec.2015.03.026.

[7] M.J. Yoo, S.H. Kim, S.D. Park, W.S. Lee, J.-W. Sun, J.-H. Choi, S. Nahm, Investigation of curing kinetics of various cycloaliphatic epoxy resins using dynamic thermal analysis, European Polymer Journal. 46 (2010) 1158–1162. https://doi.org/10.1016/j.eurpolymj.2010.02.001.

[8] X. Yang, W. Huang, Y. Yu, Synthesis, characterization, and properties of silicone-epoxy resins, J. Appl. Polym. Sci. 120 (2011) 1216–1224. https://doi.org/10.1002/app.33108.

[9] Z. Wang, J. Jiang, D. Zhang, R. Cheng, Synthesis and characterization of high-performance epoxy resin based on disiloxane and 4,4′-oxybis(benzoic acid) ester, J. Appl. Polym. Sci. 123 (2012) 2485–2491. https://doi.org/10.1002/app.34813.

[10] X. Wang, Q. Zhang, Synthesis, characterization, and cure properties of phosphorus-containing epoxy resins for flame retardance, European Polymer Journal. 40 (2004) 385–395. https://doi.org/10.1016/j.eurpolymj.2003.09.023.

[11] S.-J. Park, F.-L. Jin, Thermal stabilities and dynamic mechanical properties of sulfone-containing epoxy resin cured with anhydride, Polymer Degradation and Stability. 86 (2004) 515–520. https://doi.org/10.1016/j.polymdegradstab.2004.06.003.

[12] R.A. Parıldar, A.A.B. Ibik, Characterization of tertiary amine and epoxy functional all-acrylic coating system, Progress in Organic Coatings. 76 (2013) 955–958. https://doi.org/10.1016/j.porgcoat.2012.10.019.

[13] D. Foix, X. Ramis, A. Serra, M. Sangermano, UV generation of a multifunctional hyperbranched thermal crosslinker to cure epoxy resins, Polymer. 52 (2011) 3269–3276. https://doi.org/10.1016/j.polymer.2011.05.029.

[14] M. Fan, J. Liu, X. Li, J. Cheng, J. Zhang, Curing behaviors and properties of an extrinsic toughened epoxy/anhydride system and an intrinsic toughened epoxy/anhydride system, Thermochimica Acta. 554 (2013) 39–47. https://doi.org/10.1016/j.tca.2012.12.007.

[15] Y. Wang, J. Zhao, Y. Yuan, S. Liu, Z. Feng, Y. Zhao, Synthesis of maleimido-substituted aromatic s-triazine and its application in flame-retarded epoxy resins, Polymer Degradation and Stability. 99 (2014) 27–34. https://doi.org/10.1016/j.polymdegradstab.2013.12.015.

[16] A. Toldy, B. Szolnoki, Gy. Marosi, Flame retardancy of fibre-reinforced epoxy resin composites for aerospace applications, Polymer Degradation and Stability. 96 (2011) 371–376. https://doi.org/10.1016/j.polymdegradstab.2010.03.021.

[17] T. Iijima, N. Yoshioka, M. Tomoi, Effect of cross-link density on modification of epoxy resins with reactive acrylic elastomers, European Polymer Journal. 28 (1992) 573–581. https://doi.org/10.1016/0014-3057(92)90025-W.

[18] J. Hu, J. Shan, D. Wen, X. Liu, J. Zhao, Z. Tong, Flame retardant, mechanical properties and curing kinetics of DOPO-based epoxy resins, Polymer Degradation and Stability. 109 (2014) 218–225. https://doi.org/10.1016/j.polymdegradstab.2014.07.026.

[19] N.-M. Barkoula, J. Gremmels, J. Karger-Kocsis, Dependence of solid particle erosion on the cross-link density in an epoxy resin modified by hygrothermally decomposed polyurethane, Wear. 247 (2001) 100–108. https://doi.org/10.1016/S0043-1648(00)00529-9.

[20] S. Alessi, G. Pitarresi, G. Spadaro, Effect of hydrothermal ageing on the thermal and delamination fracture behaviour of CFRP composites, Composites Part B: Engineering. 67 (2014) 145–153. https://doi.org/10.1016/j.compositesb.2014.06.006.

[21] S.-J. Park, F.-L. Jin, J.-R. Lee, Synthesis and characterization of a novel silicon-containing epoxy resin, Macromol. Res. 13 (2005) 8–13. https://doi.org/10.1007/BF03219009.

[22] J.R. Lee, F.L. Jin, S.J. Park, J.M. Park, Study of new fluorine-containing epoxy resin for low dielectric constant, Surface and Coatings Technology. 180–181 (2004) 650–654. https://doi.org/10.1016/j.surfcoat.2003.10.111.

[23] M. Flores, X. Fernández-Francos, F. Ferrando, X. Ramis, À. Serra, Efficient impact resistance improvement of epoxy/anhydride thermosets by adding hyperbranched polyesters partially modified with undecenoyl chains, Polymer. 53 (2012) 5232–5241. https://doi.org/10.1016/j.polymer.2012.09.031.

[24] Y. Miyano, M. Nakada, N. Sekine, Accelerated testing for long-term durability of GFRP laminates for marine use, Composites Part B: Engineering. 35 (2004) 497–502. https://doi.org/10.1016/j.compositesb.2003.11.006.

[25] H. Miyagawa, L.T. Drzal, Thermo-physical and impact properties of epoxy nanocomposites reinforced by single-wall carbon nanotubes, Polymer. 45 (2004) 5163–5170. https://doi.org/10.1016/j.polymer.2004.05.036.

[26] X. Jiang, H. Kolstein, F. Bijlaard, X. Qiang, Effects of hygrothermal aging on glass-fibre reinforced polymer laminates and adhesive of FRP composite bridge: Moisture diffusion characteristics, Composites Part A: Applied Science and Manufacturing. 57 (2014) 49–58. https://doi.org/10.1016/j.compositesa.2013.11.002.

[27] S. Lu, C. Tian, X. Wang, D. Chen, K. Ma, J. Leng, L. Zhang, Health monitoring for composite materials with high linear and sensitivity GnPs/epoxy flexible strain sensors, Sensors and Actuators A: Physical. 267 (2017) 409–416. https://doi.org/10.1016/j.sna.2017.10.047.

[28] F. Hussain, M. Hojjati, M. Okamoto, R.E. Gorga, Review article: Polymer-matrix Nanocomposites, Processing, Manufacturing, and Application: An Overview, Journal of Composite Materials. 40 (2006) 1511–1575. https://doi.org/10.1177/0021998306067321.

[29] S. Liu, V.S. Chevali, Z. Xu, D. Hui, H. Wang, A review of extending performance of epoxy resins using carbon nanomaterials, Composites Part B: Engineering. 136 (2018) 197–214. https://doi.org/10.1016/j.compositesb.2017.08.020.

[30] R.F. Gibson, A review of recent research on mechanics of multifunctional composite materials and structures, Composite Structures. 92 (2010) 2793–2810. https://doi.org/10.1016/j.compstruct.2010.05.003.

[31] P. Pissis, G. Georgousis, C. Pandis, P. Georgiopoulos, A. Kyritsis, E. Kontou, M. Micusik, K. Czanikova, M. Omastova, Strain and Damage Sensing in Polymer Composites and Nanocomposites with Conducting Fillers, Procedia Engineering. 114 (2015) 590–597. https://doi.org/10.1016/j.proeng.2015.08.109.

[32] K.J. Loh, J. Kim, J.P. Lynch, Self-sensing and power harvesting carbon nanotube-composites based on piezoelectric polymers, Taylor & Francis Group. (2008) 3329–3336.

[33] F. Inam, B.R. Bhat, N. Luhyna, T. Vo, Comparison of structural health assessment capabilities in epoxy – carbon black and epoxy – carbon nanotube nanocomposites, Express Polym. Lett. 8 (2014) 55–61. https://doi.org/10.3144/expresspolymlett.2014.7.

[34] M.R. Ayatollahi, S. Shadlou, M.M. Shokrieh, Fracture toughness of epoxy/multi-walled carbon nanotube nano-composites under bending and shear loading conditions, Materials & Design. 32 (2011) 2115–2124. https://doi.org/10.1016/j.matdes.2010.11.034.

[35] A.L. Gerson, H.A. Bruck, A.R. Hopkins, K.N. Segal, Curing effects of single-wall carbon nanotube reinforcement on mechanical properties of filled epoxy adhesives, Composites Part A: Applied Science and Manufacturing. 41 (2010) 729–736. https://doi.org/10.1016/j.compositesa.2010.02.002.

[36] M.H. Al-Saleh, Electrical and mechanical properties of graphene/carbon nanotube hybrid nanocomposites, Synthetic Metals. 209 (2015) 41–46. https://doi.org/10.1016/j.synthmet.2015.06.023.

[37] N. Domun, K.R. Paton, B.R.K. Blackman, C. Kaboglu, S. Vahid, T. Zhang, J.P. Dear, A.J. Kinloch, H. Hadavinia, On the extent of fracture toughness transfer from 1D/2D nanomodified epoxy matrices to glass fibre composites, J Mater Sci. 55 (2020) 4717–4733. https://doi.org/10.1007/s10853-019-04340-8.

[38] A. Joshi, S. Datar, Carbon nanostructure composite for electromagnetic interference shielding, Pramana - J Phys. 84 (2015) 1099–1116. https://doi.org/10.1007/s12043-015-1005-9.

[39] J.-M. Thomassin, C. Jérôme, T. Pardoen, C. Bailly, I. Huynen, C. Detrembleur, Polymer/carbon based composites as electromagnetic interference (EMI) shielding materials, Materials Science and Engineering: R: Reports. 74 (2013) 211–232. https://doi.org/10.1016/j.mser.2013.06.001.

[40] A. Mostofizadeh, Y. Li, B. Song, Y. Huang, Synthesis, Properties, and Applications of Low-Dimensional Carbon-Related Nanomaterials, Journal of Nanomaterials. 2011 (2011) 1–21. https://doi.org/10.1155/2011/685081.

[41] J.R. Potts, D.R. Dreyer, C.W. Bielawski, R.S. Ruoff, Graphene-based polymer nanocomposites, Polymer. 52 (2011) 5–25. https://doi.org/10.1016/j.polymer.2010.11.042.

[42] L. Vertuccio, F. De Santis, R. Pantani, K. Lafdi, L. Guadagno, Effective de-icing skin using graphene-based flexible heater, Composites Part B: Engineering. 162 (2019) 600–610. https://doi.org/10.1016/j.compositesb.2019.01.045.

[43] B. Ahmadi-Moghadam, Influence of graphene nanoplatelets on modes I, II and III interlaminar fracture toughness of fiber-reinforced polymer composites, Engineering Fracture Mechanics. (2015) 11.

[44] S. Chandrasekaran, N. Sato, F. Tölle, R. Mülhaupt, B. Fiedler, K. Schulte, Fracture toughness and failure mechanism of graphene based epoxy composites, Composites Science and Technology. 97 (2014) 90–99. https://doi.org/10.1016/j.compscitech.2014.03.014.

[45] S. Ijima, Helical microtubules of graphitic carbon, Nature. 354 (1991) 56–58.

[46] S. Yoshimura, R.P.H. Chang, Supercarbon: synthesis, properties and applications, Springer Science & Business Media, 2013.

[47] F. Gojny, M. Wichmann, B. Fiedler, K. Schulte, Influence of different carbon nanotubes on the mechanical properties of epoxy matrix composites – A comparative study, Composites Science and Technology. 65 (2005) 2300–2313. https://doi.org/10.1016/j.compscitech.2005.04.021.

[48] M.B. Jakubinek, B. Ashrafi, Y. Zhang, Y. Martinez-Rubi, C.T. Kingston, A. Johnston, B. Simard, Single-walled carbon nanotube–epoxy composites for structural and conductive aerospace adhesives, Composites Part B: Engineering. 69 (2015) 87–93. https://doi.org/10.1016/j.compositesb.2014.09.022.

[49] F.H. Gojny, M.H.G. Wichmann, U. Köpke, B. Fiedler, K. Schulte, Carbon nanotube-reinforced epoxy-composites: enhanced stiffness and fracture toughness at low nanotube content, Composites Science and Technology. 64 (2004) 2363–2371. https://doi.org/10.1016/j.compscitech.2004.04.002.

[50] S. Ullah, F. Ahmad, A.M. Shariff, M.R. Raza, P.J. Masset, The role of multi-wall carbon nanotubes in char strength of epoxy based intumescent fire retardant coating, Journal of Analytical and Applied Pyrolysis. 124 (2017) 149–160. https://doi.org/10.1016/j.jaap.2017.02.011.

[51] P.-C. Ma, M.-Y. Liu, H. Zhang, S.-Q. Wang, R. Wang, K. Wang, Y.-K. Wong, B.-Z. Tang, S.-H. Hong, K.-W. Paik, J.-K. Kim, Enhanced Electrical Conductivity of Nanocomposites Containing Hybrid Fillers of Carbon Nanotubes and Carbon Black, ACS Appl. Mater. Interfaces. 1 (2009) 1090–1096. https://doi.org/10.1021/am9000503.

[52] P.S. Karthik, A.L. Himaja, S.P. Singh, Carbon-allotropes: synthesis methods, applications and future perspectives, Carbon Letters. 15 (2014) 219–237. https://doi.org/10.5714/CL.2014.15.4.219.

[53] P. Mohan, A Critical Review: The Modification, Properties, and Applications of Epoxy Resins, Polymer-Plastics Technology and Engineering. 52 (2013) 107–125. https://doi.org/10.1080/03602559.2012.727057.

[54] A.K. Chakraborty, T. Plyhm, M. Barbezat, A. Necola, G.P. Terrasi, Carbon nanotube (CNT)–epoxy nanocomposites: a systematic investigation of CNT dispersion, J Nanopart Res. 13 (2011) 6493–6506. https://doi.org/10.1007/s11051-011-0552-3.

[55] G. Gkikas, N.-M. Barkoula, A.S. Paipetis, Effect of dispersion conditions on the thermo-mechanical and toughness properties of multi walled carbon nanotubes-reinforced epoxy, Composites Part B: Engineering. 43 (2012) 2697–2705. https://doi.org/10.1016/j.compositesb.2012.01.070.

[56] M. Chapartegui, N. Markaide, S. Florez, C. Elizetxea, M. Fernandez, A. Santamaría, Specific rheological and electrical features of carbon nanotube dispersions in an epoxy matrix, Composites Science and Technology. 70 (2010) 879–884. https://doi.org/10.1016/j.compscitech.2010.02.008.

[57] A. Montazeri, M. Chitsazzadeh, Effect of sonication parameters on the mechanical properties of multi-walled carbon nanotube/epoxy composites, Materials & Design (1980-2015). 56 (2014) 500–508. https://doi.org/10.1016/j.matdes.2013.11.013.

[58] B. Krause, T. Villmow, R. Boldt, M. Mende, G. Petzold, P. Pötschke, Influence of dry grinding in a ball mill on the length of multiwalled carbon nanotubes and their dispersion and percolation behaviour in melt mixed polycarbonate composites, Composites Science and Technology. 71 (2011) 1145–1153. https://doi.org/10.1016/j.compscitech.2011.04.004.

[59] I.D. Rosca, S.V. Hoa, Highly conductive multiwall carbon nanotube and epoxy composites produced by three-roll milling, Carbon. 47 (2009) 1958–1968. https://doi.org/10.1016/j.carbon.2009.03.039.

[60] S.G. Prolongo, A. Jiménez-Suárez, B.G. Melitón, M. Campo, A. Ureña, Optimum Dispersion Technique of Carbon Nanotubes in Epoxy Resin as a Function of the Desired Behaviour, JNanoR. 26 (2013) 177–186. https://doi.org/10.4028/www.scientific.net/JNanoR.26.177.

[61] A. Toscano, G. Pitarresi, M. Scafidi, M. Di Filippo, G. Spadaro, S. Alessi, Water diffusion and swelling stresses in highly crosslinked epoxy matrices, Polymer Degradation and Stability. 133 (2016) 255–263. https://doi.org/10.1016/j.polymdegradstab.2016.09.004.

[62] T. Glaskova-Kuzmina, A. Aniskevich, A. Martone, M. Giordano, M. Zarrelli, Effect of moisture on elastic and viscoelastic properties of epoxy and epoxy-based carbon fibre reinforced plastic filled with multiwall carbon nanotubes, Composites Part A: Applied Science and Manufacturing. 90 (2016) 522–527. https://doi.org/10.1016/j.compositesa.2016.08.026.

[63] S. Popineau, C. Rondeau-Mouro, C. Sulpice-Gaillet, M.E.R.R. Shanahan, Free/bound water absorption in an epoxy adhesive, Polymer. 46 (2005) 10733–10740. https://doi.org/10.1016/j.polymer.2005.09.008.

[64] G. Gkikas, D.D. Douka, N.M. Barkoula, A.S. Paipetis, Nano-enhanced composite materials under thermal shock and environmental degradation: A durability study, Composites Part B: Engineering. 70 (2015) 206–214. https://doi.org/10.1016/j.compositesb.2014.11.008.

[65] R.C. Newman, D. Ghidaoui, S.E. Faidi, A. Lekatou, S.B. Lyon, S.E. Faidi, D. Ghidaoui, S.B. Lyon, R.C. Newman, Effect of water and its activity on transport properties of glass/epoxy particulate composites, Composites Part A: Applied Science and Manufacturing. 28 (1997) 223–236. https://doi.org/10.1016/S1359-835X(96)00113-3.

[66] A. Lekatou, S.E. Faidi, S.B. Lyon, R.C. Newman, I. Introduction, Elasticity and fracture in particulate composites with strong and degraded interfaces, Journal of Materials Research. 11 (1996) 1293–1304.

[67] S. Firdosh, H.N. Narasimha Murthy, R. Pal, G. Angadi, N. Raghavendra, M. Krishna, Durability of GFRP nanocomposites subjected to hygrothermal ageing, Composites Part B: Engineering. 69 (2015) 443–451. https://doi.org/10.1016/j.compositesb.2014.09.028.

[68] G. Gkikas, D. Douka, N. Barkoula, A.S. Paipetis, Interlaminar shear strength and thermo-mechanical properties of nano-enhanced composite materials under thermal shock, 8689 (2013) 1–8. https://doi.org/10.1117/12.2009974.

[69] G. Pitarresi, M. Scafidi, S. Alessi, M. Di Filippo, C. Billaud, G. Spadaro, Absorption kinetics and swelling stresses in hydrothermally aged epoxies investigated by photoelastic image analysis, Polymer Degradation and Stability. 111 (2015) 55–63. https://doi.org/10.1016/j.polymdegradstab.2014.10.019.

[70] G. Gkikas, a. Paipetis, a. Lekatou, N.M.M. Barkoula, D. Sioulas, B. Canflanca, S. Florez, Corrosion and environmental degradation of bonded composite repair, International Journal of Structural Integrity. 4 (2013) 67–77. https://doi.org/10.1108/17579861311303636.

[71] M. Wang, X. Xu, J. Ji, Y. Yang, J. Shen, M. Ye, The hygrothermal aging process and mechanism of the novolac epoxy resin, Composites Part B: Engineering. 107 (2016) 1–8. https://doi.org/10.1016/j.compositesb.2016.09.067.

[72] J.M. Tomasi, I.D. Helman, W.A. Pisani, D.R. Klimek-McDonald, S. Chinkanjanarot, I. Miskioglu, J.A. King, G.M. Odegard, Accelerated hydrothermal aging of cycloaliphatic epoxy/graphene nanoparticle composites, Polymer Degradation and Stability. 133 (2016) 131–135. https://doi.org/10.1016/j.polymdegradstab.2016.08.009.

[73] O. Starkova, S.T. Buschhorn, E. Mannov, K. Schulte, A. Aniskevich, Water transport in epoxy/MWCNT composites, European Polymer Journal. 49 (2013) 2138–2148. https://doi.org/10.1016/j.eurpolymj.2013.05.010.

[74] R.K. Prusty, D.K. Rathore, B.C. Ray, Water-induced degradations in MWCNT embedded glass fiber/epoxy composites: An emphasis on aging temperature: Research Article, J. Appl. Polym. Sci. 135 (2018) 45987. https://doi.org/10.1002/app.45987.

[75] S.G. Prolongo, M.R. Gude, A. Ureña, Water uptake of epoxy composites reinforced with carbon nanofillers, Composites Part A: Applied Science and Manufacturing. 43 (2012) 2169–2175. https://doi.org/10.1016/j.compositesa.2012.07.014.

[76] J. Shen, W. Huang, L. Wu, Y. Hu, M. Ye, The reinforcement role of different amino-functionalized multi-walled carbon nanotubes in epoxy nanocomposites, Composites Science and Technology. 67 (2007) 3041–3050. https://doi.org/10.1016/j.compscitech.2007.04.025.

[77] J. Wu, K. Yu, K. Qian, Y. Jia, One step fabrication of multi-walled carbon nanotubes/graphene nanoplatelets hybrid materials with excellent mechanical property, Fibers Polym. 16 (2015) 1540–1546. https://doi.org/10.1007/s12221-015-5207-z.

[78] M.A. Ramadan, R. Reda, CNTs, Al2O3 and SiO2 Reinforced Epoxy: Tribological Properties of Polymer Nanocomposites, Tribol. Ind. 39 (2017) 357–363. https://doi.org/10.24874/ti.2017.39.03.11.

[79] G. Mittal, V. Dhand, K.Y. Rhee, S.-J. Park, W.R. Lee, A review on carbon nanotubes and graphene as fillers in reinforced polymer nanocomposites, Journal of Industrial and Engineering Chemistry. 21 (2015) 11–25. https://doi.org/10.1016/j.jiec.2014.03.022.

[80] W. Qin, C. Chen, J. Zhou, J. Meng, Synergistic Effects of Graphene/Carbon Nanotubes Hybrid Coating on the Interfacial and Mechanical Properties of Fiber Composites, Materials. 13 (2020) 1457. https://doi.org/10.3390/ma13061457.

[81] U. Szeluga, B. Kumanek, B. Trzebicka, Synergy in hybrid polymer/nanocarbon composites. A review, Composites Part A: Applied Science and Manufacturing. 73 (2015) 204–231. https://doi.org/10.1016/j.compositesa.2015.02.021.

[82] A.R. Ravindran, R.B. Ladani, S. Wu, A.J. Kinloch, C.H. Wang, A.P. Mouritz, Multi-scale toughening of epoxy composites via electric field alignment of carbon nanofibres and short carbon fibres, Composites Science and Technology. 167 (2018) 115–125. https://doi.org/10.1016/j.compscitech.2018.07.034.

[83] I. Kranauskaitė, J. Macutkevič, A. Borisova, A. Martone, M. Zarrelli, A. Selskis, A. Aniskevich, J. Banys, Enhancing electrical conductivity of multiwalled carbon nanotube/epoxy composites by graphene nanoplatelets, Physics. 57 (2018). https://doi.org/10.3952/physics.v57i4.3602.

[84] S.-Y. Yang, W.-N. Lin, Y.-L. Huang, H.-W. Tien, J.-Y. Wang, C.-C.M. Ma, S.-M. Li, Y.-S. Wang, Synergetic effects of graphene platelets and carbon nanotubes on the mechanical and thermal properties of epoxy composites, Carbon. 49 (2011) 793–803. https://doi.org/10.1016/j.carbon.2010.10.014.

[85] P.-N. Wang, T.-H. Hsieh, C.-L. Chiang, M.-Y. Shen, Synergetic Effects of Mechanical Properties on Graphene Nanoplatelet and Multiwalled Carbon Nanotube Hybrids Reinforced Epoxy/Carbon Fiber Composites, Journal of Nanomaterials. 2015 (2015) 1–9. https://doi.org/10.1155/2015/838032.

[86] A. Mohanty, V.K. Srivastava, Tribological Behavior of Particles and Fiber-Reinforced Hybrid Nanocomposites, Tribology Transactions. 58 (2015) 1142–1150. https://doi.org/10.1080/10402004.2015.1039681.

[87] R. Nadiv, R.M.F. Fernandes, G. Ochbaum, J. Dai, M. Buzaglo, M. Varenik, R. Biton, I. Furó, O. Regev, Polymer nanocomposites: Insights on rheology, percolation and molecular mobility, Polymer. 153 (2018) 52–60. https://doi.org/10.1016/j.polymer.2018.07.079.

[88] M.H.G. Wichmann, J. Sumfleth, F.H. Gojny, M. Quaresimin, B. Fiedler, K. Schulte, Glass-fibre-reinforced composites with enhanced mechanical and electrical properties – Benefits and limitations of a nanoparticle modified matrix, Engineering Fracture Mechanics. 73 (2006) 2346–2359. https://doi.org/10.1016/j.engfracmech.2006.05.015.

[89] ASTM Standards, D 5045 - Standard Test Methods for Plane-Strain Fracture Toughness and Strain Energy Release, (1999) 1–9.

[90] A. Khanam, B. Mordina, R. Tiwari, Statistical evaluation of the effect of carbon nanofibre content on tribological properties of epoxy nanocomposites, Journal of

Composite Materials. 49 (2015) 2497–2507. https://doi.org/10.1177/0021998314549615.

[91] J. Karger-Kocsis, J. Gremmels, Use of hygrothermal decomposed polyester-urethane waste for the impact modification of epoxy resins, (n.d.) 13.

[92] J. Gremmels, Use of Hygrothermal Decomposed Polyester – Urethane, (2000) 1139–1151.

[93] American Society for Testing and Materials, ASTM D 3933 - Preparation of aluminum surfaces for structural adhesives bonding, (1998).

[94] D. Baltzis, S. Orfanidis, A. Lekatou, A.S. Paipetis, Stainless steel coupled with carbon nanotube-modified epoxy and carbon fibre composites: Electrochemical and mechanical study, Plastics, Rubber and Composites. 45 (2016) 95–105. https://doi.org/10.1080/14658011.2016.1144339.

[95] K.B. Katnam, L.F.M. Da Silva, T.M. Young, Bonded repair of composite aircraft structures: A review of scientific challenges and opportunities, Progress in Aerospace Sciences. 61 (2013) 26–42. https://doi.org/10.1016/j.paerosci.2013.03.003.

[96] A.A. Baker, P.J. Callus, S. Georgiadis, P.J. Falzon, S.E. Dutton, K.H. Leong, An affordable methodology for replacing metallic aircraft panels with advanced compositesq, (2002) 10.

[97] W.K. Chiu, Z. Zhou, J. Wang, A. Baker, Battle damage repair of a helicopter composite main rotor blade, Composites Part B: Engineering. 43 (2012) 739–753. https://doi.org/10.1016/j.compositesb.2011.07.014.

[98] H.C.H. Li, J. Wang, A. Baker, Rapid composite bonded repair for helicopter tail drive shafts, Composites Part B: Engineering. 43 (2012) 1579–1585. https://doi.org/10.1016/j.compositesb.2011.08.012.

[99] M. Shamsuddoha, M.M. Islam, T. Aravinthan, A. Manalo, K. Lau, Effectiveness of using fibre-reinforced polymer composites for underwater steel pipeline repairs, Composite Structures. 100 (2013) 40–54. https://doi.org/10.1016/j.compstruct.2012.12.019.

[100] X.-L. Zhao, L. Zhang, State-of-the-art review on FRP strengthened steel structures, Engineering Structures. 29 (2007) 1808–1823. https://doi.org/10.1016/j.engstruct.2006.10.006.

[101] T.-C. Nguyen, Y. Bai, X.-L. Zhao, R. Al-Mahaidi, Curing effects on steel/CFRP double strap joints under combined mechanical load, temperature and humidity, Construction and Building Materials. 40 (2013) 899–907. https://doi.org/10.1016/j.conbuildmat.2012.11.035.

[102] J.-S. Lee, Y.-S. Ryu, N.-I. Kim, B.-J. Kim, Y.-K. Kim, M.-H. Kim, Stud welding for fixation of cryogenic insulation of membrane tanks in LNG ship building, Transactions of Nonferrous Metals Society of China. 19 (2009) s271–s275. https://doi.org/10.1016/S1003-6326(10)60283-X.

[103] K.C. Warren, R.A. Lopez-Anido, S.S. Vel, H.H. Bayraktar, Progressive failure analysis of three-dimensional woven carbon composites in single-bolt, double-shear bearing, Composites Part B: Engineering. 84 (2016) 266–276. https://doi.org/10.1016/j.compositesb.2015.08.082.

[104] M. Gholami, A.R.M. Sam, J.M. Yatim, M.M. Tahir, A review on steel/CFRP strengthening systems focusing environmental performance, Construction and Building Materials. 47 (2013) 301–310. https://doi.org/10.1016/j.conbuildmat.2013.04.049.

[105] T. Yu, D. Fernando, J.G. Teng, X.L. Zhao, Experimental study on CFRP-to-steel bonded interfaces, Composites Part B: Engineering. 43 (2012) 2279–2289. https://doi.org/10.1016/j.compositesb.2012.01.024.

[106] C. Wu, X. Zhao, W. Hui Duan, R. Al-Mahaidi, Bond characteristics between ultra high modulus CFRP laminates and steel, Thin-Walled Structures. 51 (2012) 147–157. https://doi.org/10.1016/j.tws.2011.10.010.

[107] I. Yoshitake, H. Tsuda, J. Itose, N. Hisabe, Effect of discrepancy in thermal expansion coefficients of CFRP and steel under cold temperature, Construction and Building Materials. 59 (2014) 17–24. https://doi.org/10.1016/j.conbuildmat.2014.02.051.

[108] Y.J. Kim, J. LaBere, I. Yoshitake, Hybrid epoxy-silyl modified polymer adhesives for CFRP sheets bonded to a steel substrate, Composites Part B: Engineering. 51 (2013) 233–245. https://doi.org/10.1016/j.compositesb.2013.03.026.

[109] A. Baldan, Adhesively-bonded joints and repairs in metallic alloys, polymers and composite materials: Adhesives, adhesion theories and surface pretreatment, Journal of Materials Science. 39 (2004) 1–49. https://doi.org/10.1023/B:JMSC.0000007726.58758.e4.

[110] U.A. Khashaba, A.A. Aljinaidi, M.A. Hamed, Analysis of adhesively bonded CFRE composite scarf joints modified with MWCNTs, Composites Part A: Applied Science and Manufacturing. 71 (2015) 59–71. https://doi.org/10.1016/j.compositesa.2015.01.004.

[111] E. Jarry, R.A. Shenoi, Performance of butt strap joints for marine applications, International Journal of Adhesion and Adhesives. 26 (2006) 162–176. https://doi.org/10.1016/j.ijadhadh.2005.01.010.

[112] Ch.V. Katsiropoulos, A.N. Chamos, K.I. Tserpes, Sp.G. Pantelakis, Fracture toughness and shear behavior of composite bonded joints based on a novel aerospace adhesive, Composites Part B: Engineering. 43 (2012) 240–248. https://doi.org/10.1016/j.compositesb.2011.07.010.

[113] M.T. Kim, K.Y. Rhee, J.H. Lee, D. Hui, A.K.T. Lau, Property enhancement of a carbon fiber/epoxy composite by using carbon nanotubes, Composites Part B: Engineering. 42 (2011) 1257–1261. https://doi.org/10.1016/j.compositesb.2011.02.005.

[114] B. Wang, J. Yin, L. Wang, Structure and properties of aeronautical composites using carbon nanotubes/epoxy dispersion as nanocomposite matrix, Polym. Compos. 34 (2013) 1690–1697. https://doi.org/10.1002/pc.22570.

[115] G. Gkikas, A. Paipetis, A. Lekatou, N.M. Barkoula, D. Sioulas, B. Canflanca, S. Florez, Corrosion and environmental degradation of bonded composite repair, Int Jnl of Struct Integrity. 4 (2013) 67–77. https://doi.org/10.1108/17579861311303636.

[116] D. Schnerch, M. Dawood, S. Rizkalla, E. Sumner, K. Stanford, Bond Behavior of CFRP Strengthened Steel Structures, Advances in Structural Engineering. 9 (2006) 805–817. https://doi.org/10.1260/136943306779369464.

[117] L. Yue, G. Pircheraghi, S.A. Monemian, I. Manas-Zloczower, Epoxy composites with carbon nanotubes and graphene nanoplatelets – Dispersion and synergy effects, Carbon. 78 (2014) 268–278. https://doi.org/10.1016/j.carbon.2014.07.003.

[118] J.-M. Park, D.-S. Kim, S.-J. Kim, P.-G. Kim, D.-J. Yoon, K.L. DeVries, Inherent sensing and interfacial evaluation of carbon nanofiber and nanotube/epoxy composites using electrical resistance measurement and micromechanical technique, Composites Part B: Engineering. 38 (2007) 847–861. https://doi.org/10.1016/j.compositesb.2006.12.004.

[119] J.S. Fenner, I.M. Daniel, Hybrid nanoreinforced carbon/epoxy composites for enhanced damage tolerance and fatigue life, Composites Part A: Applied Science and Manufacturing. 65 (2014) 47–56. https://doi.org/10.1016/j.compositesa.2014.05.023.

[120] G. Gkikas, D. Sioulas, A. Lekatou, N.M. Barkoula, A.S. Paipetis, Enhanced bonded aircraft repair using nano-modified adhesives, Materials & Design. 41 (2012) 394–402. https://doi.org/10.1016/j.matdes.2012.04.052.

[121] V.K. Srivastava, Effect of carbon nanotubes on the strength of adhesive lap joints of C/C and C/C–SiC ceramic fibre composites, International Journal of Adhesion and Adhesives. 31 (2011) 486–489. https://doi.org/10.1016/j.ijadhadh.2011.03.006.

[122] G. Gkikas, A. Lekatou, D. Sioulas, A.S. Paipetis, Effect of carbon nanotube enhanced adhesives on degradation of bonded joints in corrosive environments, Plastics, Rubber and Composites. 43 (2014) 322–329. https://doi.org/10.1179/1743289814Y.0000000085.

[123] G. Gkikas, D.-D. Douka, N.-M. Barkoula, A.S. Paipetis, Nano-enhanced composite materials under thermal shock and environmental degradation: A durability study, Composites Part B: Engineering. 70 (2015) 206–214. https://doi.org/10.1016/j.compositesb.2014.11.008.

[124] R. Ireland, L. Arronche, V. La Saponara, Electrochemical investigation of galvanic corrosion between aluminum 7075 and glass fiber/epoxy composites modified with carbon nanotubes, Composites Part B: Engineering. 43 (2012) 183–194. https://doi.org/10.1016/j.compositesb.2011.08.001.

[125] A. Kausar, I. Rafique, B. Muhammad, Significance of Carbon Nanotube in Flame-Retardant Polymer/CNT Composite: A Review, Polymer-Plastics Technology and Engineering. 56 (2017) 470–487. https://doi.org/10.1080/03602559.2016.1233267.

[126] J. Chen, J. Han, Comparative performance of carbon nanotubes and nanoclays as flame retardants for epoxy composites, Results in Physics. 14 (2019) 102481. https://doi.org/10.1016/j.rinp.2019.102481.

[127] A. Toldy, G. Szebényi, K. Molnár, L. Tóth, B. Magyar, V. Hliva, T. Czigány, B. Szolnoki, The Effect of Multilevel Carbon Reinforcements on the Fire Performance, Conductivity, and Mechanical Properties of Epoxy Composites, Polymers. 11 (2019) 303. https://doi.org/10.3390/polym11020303.

[128] C.-F. Kuan, W.-J. Chen, Y.-L. Li, C.-H. Chen, H.-C. Kuan, C.-L. Chiang, Flame retardance and thermal stability of carbon nanotube epoxy composite prepared from sol–gel method, Journal of Physics and Chemistry of Solids. 71 (2010) 539–543. https://doi.org/10.1016/j.jpcs.2009.12.031.

[129] J.-S. Wang, Y. Liu, H.-B. Zhao, J. Liu, D.-Y. Wang, Y.-P. Song, Y.-Z. Wang, Metal compound-enhanced flame retardancy of intumescent epoxy resins containing

ammonium polyphosphate, Polymer Degradation and Stability. 94 (2009) 625–631. https://doi.org/10.1016/j.polymdegradstab.2009.01.006.

[130] L. Becker, D. Lenoir, G. Matuschek, A. Kettrup, Thermal degradation of halogen-free flame retardant epoxides and polycarbonate in air, Journal of Analytical and Applied Pyrolysis. 60 (2001) 55–67. https://doi.org/10.1016/S0165-2370(00)00118-2.

[131] W. Zhang, X. He, T. Song, Q. Jiao, R. Yang, The influence of the phosphorus-based flame retardant on the flame retardancy of the epoxy resins, Polymer Degradation and Stability. 109 (2014) 209–217. https://doi.org/10.1016/j.polymdegradstab.2014.07.023.

[132] B. Perret, B. Schartel, K. Stöß, M. Ciesielski, J. Diederichs, M. Döring, J. Krämer, V. Altstädt, Novel DOPO-based flame retardants in high-performance carbon fibre epoxy composites for aviation, European Polymer Journal. 47 (2011) 1081–1089. https://doi.org/10.1016/j.eurpolymj.2011.02.008.

[133] M.S.S. Martins, B. Schartel, F.D. Magalhães, C.M.C. Pereira, The effect of traditional flame retardants, nanoclays and carbon nanotubes in the fire performance of epoxy resin composites: FIRE PERFORMANCE OF EPOXY RESIN COMPOSITES, Fire Mater. 41 (2017) 111–130. https://doi.org/10.1002/fam.2370.

[134] T.A. Nguyen, Q.T. Nguyen, T.P. Bach, Mechanical Properties and Flame Retardancy of Epoxy Resin/Nanoclay/Multiwalled Carbon Nanotube Nanocomposites, Journal of Chemistry. 2019 (2019) 1–9. https://doi.org/10.1155/2019/3105205.

[135] C. Li, N.-J. Kang, S.D. Labrandero, J. Wan, C. González, D.-Y. Wang, Synergistic Effect of Carbon Nanotube and Polyethersulfone on Flame Retardancy of Carbon Fiber Reinforced Epoxy Composites, Ind. Eng. Chem. Res. 53 (2014) 1040–1047. https://doi.org/10.1021/ie403378w.

[136] S. Liu, Z. Fang, H. Yan, H. Wang, Superior flame retardancy of epoxy resin by the combined addition of graphene nanosheets and DOPO, RSC Adv. 6 (2016) 5288–5295. https://doi.org/10.1039/C5RA25988F.

[137] S.K. Lee, B.C. Bai, J.S. Im, S.J. In, Y.-S. Lee, Flame retardant epoxy complex produced by addition of montmorillonite and carbon nanotube, Journal of Industrial and Engineering Chemistry. 16 (2010) 891–895. https://doi.org/10.1016/j.jiec.2010.09.014.

[138] G. Barra, L. Guadagno, L. Vertuccio, B. Simonet, B. Santos, M. Zarrelli, M. Arena, M. Viscardi, Different Methods of Dispersing Carbon Nanotubes in Epoxy Resin and Initial Evaluation of the Obtained Nanocomposite as a Matrix of Carbon Fiber Reinforced Laminate in Terms of Vibroacoustic Performance and Flammability, Materials. 12 (2019) 2998. https://doi.org/10.3390/ma12182998.

[139] J.S. Im, S.K. Lee, S.J. In, Y.-S. Lee, Improved flame retardant properties of epoxy resin by fluorinated MMT/MWCNT additives, Journal of Analytical and Applied Pyrolysis. 89 (2010) 225–232. https://doi.org/10.1016/j.jaap.2010.08.003.

[140] A. Godara, L. Mezzo, F. Luizi, A. Warrier, S.V. Lomov, A.W. van Vuure, L. Gorbatikh, P. Moldenaers, I. Verpoest, Influence of carbon nanotube reinforcement on the processing and the mechanical behaviour of carbon fiber/epoxy composites, Carbon. 47 (2009) 2914–2923. https://doi.org/10.1016/j.carbon.2009.06.039.

[141] N. Prasad, C. Tola, M. Coulaud, M. Claes, S.V. Lomov, I. Verpoest, L. Gorbatikh, Carbon Fiber Composites Based on Multi-Phase Epoxy/PES Matrices with Carbon Nanotubes: Morphology and Interlaminar Fracture Toughness Characterization: Carbon

Fiber Composites Based on Multi-Phase Epoxy/PES Matrices…, Adv. Eng. Mater. 18 (2016) 2040–2046. https://doi.org/10.1002/adem.201600153.

[142] N.W. Khun, B.C.R. Troconis, G.S. Frankel, Effects of carbon nanotube content on adhesion strength and wear and corrosion resistance of epoxy composite coatings on AA2024-T3, Progress in Organic Coatings. 77 (2014) 72–80. https://doi.org/10.1016/j.porgcoat.2013.08.003.

[143] P.-C. Ma, N.A. Siddiqui, G. Marom, J.-K. Kim, Dispersion and functionalization of carbon nanotubes for polymer-based nanocomposites: A review, Composites Part A: Applied Science and Manufacturing. 41 (2010) 1345–1367. https://doi.org/10.1016/j.compositesa.2010.07.003.

[144] W. Bauhofer, J.Z. Kovacs, A review and analysis of electrical percolation in carbon nanotube polymer composites, Composites Science and Technology. 69 (2009) 1486–1498. https://doi.org/10.1016/j.compscitech.2008.06.018.

[145] J.Z. Kovacs, R.E. Mandjarov, T. Blisnjuk, K. Prehn, M. Sussiek, J. Müller, K. Schulte, W. Bauhofer, On the influence of nanotube properties, processing conditions and shear forces on the electrical conductivity of carbon nanotube epoxy composites, Nanotechnology. 20 (2009) 155703. https://doi.org/10.1088/0957-4484/20/15/155703.

[146] G.C. Papanicolaou, K.P. Papaefthymiou, A.F. Koutsomitopoulou, D.V. Portan, S.P. Zaoutsos, Effect of dispersion of MWCNTs on the static and dynamic mechanical behavior of epoxy matrix nanocomposites, J Mater Sci. 47 (2012) 350–359. https://doi.org/10.1007/s10853-011-5804-1.

[147] A. Toldy, P. Anna, I. Csontos, A. Szabó, Gy. Marosi, Intrinsically flame retardant epoxy resin – Fire performance and background – Part I, Polymer Degradation and Stability. 92 (2007) 2223–2230. https://doi.org/10.1016/j.polymdegradstab.2007.04.017.

[148] T.-C. Nguyen, Y. Bai, X.-L. Zhao, R. Al-Mahaidi, Durability of steel/CFRP double strap joints exposed to sea water, cyclic temperature and humidity, Composite Structures. 94 (2012) 1834–1845. https://doi.org/10.1016/j.compstruct.2012.01.004.

[149] N.R. Paluvai, S. Mohanty, S.K. Nayak, Synthesis and Modifications of Epoxy Resins and Their Composites: A Review, Polymer-Plastics Technology and Engineering. 53 (2014) 1723–1758. https://doi.org/10.1080/03602559.2014.919658.

[150] J. Li, P.C. Ma, W.S. Chow, C.K. To, B.Z. Tang, J.-K. Kim, Correlations between Percolation Threshold, Dispersion State, and Aspect Ratio of Carbon Nanotubes, Adv. Funct. Mater. 17 (2007) 3207–3215. https://doi.org/10.1002/adfm.200700065.

[151] I. Alig, P. Pötschke, D. Lellinger, T. Skipa, S. Pegel, G.R. Kasaliwal, T. Villmow, Establishment, morphology and properties of carbon nanotube networks in polymer melts, Polymer. 53 (2012) 4–28. https://doi.org/10.1016/j.polymer.2011.10.063.

[152] D. Baltzis, D.G. Bekas, G. Tzachristas, A. Parlamas, M. Karabela, N.E. Zafeiropoulos, A.S. Paipetis, Multi-scaled carbon reinforcements in ternary epoxy composite materials: Dispersion and electrical impedance study, Composites Science and Technology. 153 (2017) 7–17. https://doi.org/10.1016/j.compscitech.2017.09.035.

[153] D. Baltzis, A.S. Paipetis, Hybrid ternary epoxy nano-composites for improved electrical and mechanical properties, in: Rhodes, GR, 2016: p. 2.

[154] N.R. Paluvai, S. Mohanty, S.K. Nayak, Synthesis and Modifications of Epoxy Resins and Their Composites: A Review, Polymer-Plastics Technology and Engineering. 53 (2014) 1723–1758. https://doi.org/10.1080/03602559.2014.919658.

[155] F.L. Jin, X. Li, S.J. Park, Synthesis and application of epoxy resins: A review, Journal of Industrial and Engineering Chemistry. 29 (2015) 1–11. https://doi.org/10.1016/j.jiec.2015.03.026.

[156] R.F. Gibson, A review of recent research on mechanics of multifunctional composite materials and structures, Composite Structures. 92 (2010) 2793–2810. https://doi.org/10.1016/j.compstruct.2010.05.003.

[157] A.S. Paipetis, V. Kostopoulos, Carbon Nanotube Enhanced Aerospace Composite Materials, Solid Mechanics and Its Applications. 188 (2013). https://doi.org/10.1007/978-94-007-4246-8.

[158] Z. Spitalsky, D. Tasis, K. Papagelis, C. Galiotis, Carbon nanotube–polymer composites: Chemistry, processing, mechanical and electrical properties, Progress in Polymer Science. 35 (2010) 357–401. https://doi.org/10.1016/j.progpolymsci.2009.09.003.

[159] G. Pandey, E.T. Thostenson, Carbon Nanotube-Based Multifunctional Polymer Nanocomposites, Polymer Reviews. 52 (2012) 355–416. https://doi.org/10.1080/15583724.2012.703747.

[160] G. Mittal, V. Dhand, K.Y. Rhee, S.-J. Park, W.R. Lee, A review on carbon nanotubes and graphene as fillers in reinforced polymer nanocomposites, Journal of Industrial and Engineering Chemistry. 21 (2015) 11–25. https://doi.org/10.1016/j.jiec.2014.03.022.

[161] A. Hernández-Pérez, F. Avilés, A. May-Pat, A. Valadez-González, P.J. Herrera-Franco, P. Bartolo-Pérez, Effective properties of multiwalled carbon nanotube/epoxy composites using two different tubes, Composites Science and Technology. 68 (2008) 1422–1431. https://doi.org/10.1016/j.compscitech.2007.11.001.

[162] I. Burmistrov, N. Gorshkov, I. Ilinykh, D. Muratov, E. Kolesnikov, S. Anshin, I. Mazov, J.P. Issi, D. Kusnezov, Improvement of carbon black based polymer composite electrical conductivity with additions of MWCNT, Composites Science and Technology. 129 (2016) 79–85. https://doi.org/10.1016/j.compscitech.2016.03.032.

[163] J.S. Fenner, I.M. Daniel, Hybrid nanoreinforced carbon/epoxy composites for enhanced damage tolerance and fatigue life, Composites Part A: Applied Science and Manufacturing. 65 (2014) 47–56. https://doi.org/10.1016/j.compositesa.2014.05.023.

[164] M. Ayatollahi, M. Shokrieh, S. Shadlou, A. Kefayati, M. Chitsazzadeh, Mechanical and electrical properties of epoxy/multi-walled carbon nanotube/nanoclay nanocomposites, Iran Polym J. c (2011) 835–843.

[165] S. Chandrasekaran, N. Sato, F. Tölle, R. Mülhaupt, B. Fiedler, K. Schulte, Fracture toughness and failure mechanism of graphene based epoxy composites, Composites Science and Technology. 97 (2014) 90–99. https://doi.org/10.1016/j.compscitech.2014.03.014.

[166] T. Subhani, M. Latif, I. Ahmad, S.A. Rakha, N. Ali, A.A. Khurram, Mechanical performance of epoxy matrix hybrid nanocomposites containing carbon nanotubes and nanodiamonds, Materials & Design. 87 (2015) 436–444. https://doi.org/10.1016/j.matdes.2015.08.059.

[167] M.R. Zakaria, H. Md. Akil, M.H. Abdul Kudus, A.H. Kadarman, Improving flexural and dielectric properties of MWCNT/epoxy nanocomposites by introducing advanced hybrid filler system, Composite Structures. 132 (2015) 50–64. https://doi.org/10.1016/j.compstruct.2015.05.020.

[168] D. Baltzis, S. Orfanidis, A. Lekatou, A.S. Paipetis, Stainless steel coupled with carbon nanotube- modified epoxy and carbon fibre composites : Electrochemical and mechanical study Stainless steel coupled with carbon nanotube- modified epoxy and carbon fibre composites :, Plastics, Rubber and Composites. 8011 (2016) 95–105. https://doi.org/10.1080/14658011.2016.1144339.

[169] A. Papadopoulos, G. Gkikas, A.S. Paipetis, N.M. Barkoula, Effect of CNTs addition on the erosive wear response of epoxy resin and carbon fibre composites, Composites Part A: Applied Science and Manufacturing. 84 (2016) 299–307. https://doi.org/10.1016/j.compositesa.2016.02.012.

[170] G. Gkikas, N.M. Barkoula, A.S. Paipetis, Effect of dispersion conditions on the thermo-mechanical and toughness properties of multi walled carbon nanotubes-reinforced epoxy, Composites Part B: Engineering. 43 (2012) 2697–2705. https://doi.org/10.1016/j.compositesb.2012.01.070.

[171] M.H.G. Wichmann, J. Sumfleth, B. Fiedler, F.H. Gojny, K. Schulte, Multiwall carbon nanotube/epoxy composites produced by a masterbatch process, Mechanics of Composite Materials. 42 (2006) 395–406. https://doi.org/10.1007/s11029-006-0050-3.

[172] G. Nadia, L. Joachim, O. Regev, C.E. Koning, Toolbox for Dispersing Carbon Nanotubes into Polymers To Get Conductive Nanocomposites, Chemistry Materials. 18 (2006) 1089–1099. https://doi.org/10.1021/tx050106d.

[173] A.K. Chakraborty, T. Plyhm, M. Barbezat, A. Necola, G.P. Terrasi, Carbon nanotube (CNT)–epoxy nanocomposites: a systematic investigation of CNT dispersion, Journal of Nanoparticle Research. 13 (2011) 6493–6506. https://doi.org/10.1007/s11051-011-0552-3.

[174] P. Taylor, G. Pandey, E.T. Thostenson, Carbon Nanotube-Based Multifunctional Polymer Nanocomposites Carbon Nanotube-Based Multifunctional Polymer, (2012) 37–41. https://doi.org/10.1080/15583724.2012.703747.

[175] W. Zhang, A.A. Dehghani-Sanij, R.S. Blackburn, Carbon based conductive polymer composites, Journal of Materials Science. 42 (2007) 3408–3418. https://doi.org/10.1007/s10853-007-1688-5.

[176] G. Pandey, E.T. Thostenson, Carbon Nanotube-Based Multifunctional Polymer Nanocomposites, Polymer Reviews. 52 (2012) 355–416. https://doi.org/10.1080/15583724.2012.703747.

[177] M.M. Rueda, M.-C. Auscher, R. Fulchiron, T. Périé, G. Martin, P. Sonntag, P. Cassagnau, Rheology and applications of highly filled polymers: A review of current understanding, Progress in Polymer Science. 66 (2017) 22–53. https://doi.org/10.1016/j.progpolymsci.2016.12.007.

[178] G. Barra, L. Vertuccio, U. Vietri, C. Naddeo, H. Hadavinia, L. Guadagno, Toughening of Epoxy Adhesives by Combined Interaction of Carbon Nanotubes and Silsesquioxanes, Materials. 10 (2017) 1131. https://doi.org/10.3390/ma10101131.

[179] N.A. Siddiqui, S.U. Khan, P.C. Ma, C.Y. Li, J.-K. Kim, Manufacturing and characterization of carbon fibre/epoxy composite prepregs containing carbon nanotubes, Composites Part A: Applied Science and Manufacturing. 42 (2011) 1412–1420. https://doi.org/10.1016/j.compositesa.2011.06.005.

[180] Y.S. Song, J.R. Youn, Influence of dispersion states of carbon nanotubes on physical properties of epoxy nanocomposites, Carbon. 43 (2005) 1378–1385. https://doi.org/10.1016/j.carbon.2005.01.007.

[181] S.C. Schulz, G. Faiella, S.T. Buschhorn, L.A.S.A. Prado, M. Giordano, K. Schulte, W. Bauhofer, Combined electrical and rheological properties of shear induced multiwall carbon nanotube agglomerates in epoxy suspensions, European Polymer Journal. 47 (2011) 2069–2077. https://doi.org/10.1016/j.eurpolymj.2011.07.022.

[182] S.S. Rahatekar, K.K.K. Koziol, S.A. Butler, J.A. Elliott, M.S.P. Shaffer, M.R. Mackley, A.H. Windle, Optical microstructure and viscosity enhancement for an epoxy resin matrix containing multiwall carbon nanotubes, Journal of Rheology. 50 (2006) 599–610. https://doi.org/10.1122/1.2221699.

[183] M. Quaresimin, K. Schulte, M. Zappalorto, S. Chandrasekaran, Toughening mechanisms in polymer nanocomposites-From experiments to modelling, Composites Science and Technology. 123 (2016) 187–204. https://doi.org/10.1016/j.compscitech.2015.11.027.

[184] M.J. Green, Analysis and measurement of carbon nanotube dispersions: Nanodispersion versus macrodispersion, Polymer International. 59 (2010) 1319–1322. https://doi.org/10.1002/pi.2878.

[185] U. Szeluga, B. Kumanek, B. Trzebicka, Synergy in hybrid polymer/nanocarbon composites. A review, Composites Part A: Applied Science and Manufacturing. 73 (2015) 204–231. https://doi.org/10.1016/j.compositesa.2015.02.021.

[186] T. Wei, L. Song, C. Zheng, K. Wang, J. Yan, B. Shao, Z.J. Fan, The synergy of a three filler combination in the conductivity of epoxy composites, Materials Letters. 64 (2010) 2376–2379. https://doi.org/10.1016/j.matlet.2010.07.061.

[187] J. Sumfleth, X.C. Adroher, K. Schulte, Synergistic effects in network formation and electrical properties of hybrid epoxy nanocomposites containing multi-wall carbon nanotubes and carbon black, Journal of Materials Science. 44 (2009) 3241–3247. https://doi.org/10.1007/s10853-009-3434-7.

[188] K. Friedrich, Routes for achieving multifunctionality in reinforced polymers and composite structures, Elsevier Inc., 2015. https://doi.org/10.1016/B978-0-323-26434-1.00001-5.

[189] A.D.B.L. Ferreira, P.R.O. N??voa, A.T. Marques, Multifunctional Material Systems: A state-of-the-art review, Composite Structures. 151 (2016) 3–35. https://doi.org/10.1016/j.compstruct.2016.01.028.

[190] S. Pavlopoulou, S.A. Grammatikos, E.Z. Kordatos, K. Worden, A.S. Paipetis, T.E. Matikas, C. Soutis, Continuous debonding monitoring of a patch repaired helicopter stabilizer: Damage assessment and analysis, Composite Structures. 127 (2015) 231–244. https://doi.org/10.1016/j.compstruct.2015.03.014.

[191] G. Gkikas, Ch. Saganas, S.A. Grammatikos, D.G. Aggelis, A.S. Paipetis, Simultaneous acoustic and dielectric real time curing monitoring of epoxy systems, Proc. of SPIE Vol.

8346, Smart Sensor Phenomena, Technology, Networks, and Systems Integration. 8346 (2012) 1–7. https://doi.org/10.1117/12.915481.

[192] C.A. Martin, J.K.W. Sandler, M.S.P. Shaffer, M.K. Schwarz, W. Bauhofer, K. Schulte, A.H. Windle, Formation of percolating networks in multi-wall carbon-nanotube-epoxy composites, Composites Science and Technology. 64 (2004) 2309–2316. https://doi.org/10.1016/j.compscitech.2004.01.025.

[193] G. Gkikas, A.S. Paipetis, Optimisation and analysis of the reinforcement effect of carbon nanotubes in a typical matrix system, (2015) 461–478. https://doi.org/10.1007/s11012-014-9915-z.

[194] Z. Fan, S.G. Advani, Rheology of multiwall carbon nanotube suspensions, Journal of Rheology. 51 (2007) 585–604. https://doi.org/10.1122/1.2736424.

[195] P. Garg, B.P. Singh, G. Kumar, T. Gupta, I. Pandey, R.K. Seth, R.P. Tandon, R.B. Mathur, Effect of dispersion conditions on the mechanical properties of multi-walled carbon nanotubes based epoxy resin composites, Journal of Polymer Research. 18 (2011) 1397–1407. https://doi.org/10.1007/s10965-010-9544-8.

[196] J.K.W. Sandler, J.E. Kirk, I.A. Kinloch, M.S.P. Shaffer, A.H. Windle, Ultra-low electrical percolation threshold in carbon-nanotube-epoxy composites, Polymer. 44 (2003) 5893–5899. https://doi.org/10.1016/S0032-3861(03)00539-1.

[197] J. Sandler, M.S.P. Shaffer, T. Prasse, W. Bauhofer, K. Schulte, A.H. Windle, Development of a dispersion process for carbon nanotubes in an epoxy matrix and the resulting electrical properties, Polymer. 40 (1999) 5967–5971. https://doi.org/10.1016/S0032-3861(99)00166-4.

[198] J.P. Peng, H. Zhang, L.C. Tang, Y. Jia, Z. Zhang, Dielectric properties of carbon nanotubes/epoxy composites, Journal of Nanoscience and Nanotechnology. 13 (2013) 964–969. https://doi.org/10.1166/jnn.2013.6041.

[199] P. P??tschke, M. Abdel-Goad, I. Alig, S. Dudkin, D. Lellinger, Rheological and dielectrical characterization of melt mixed polycarbonate-multiwalled carbon nanotube composites, Polymer. 45 (2004) 8863–8870. https://doi.org/10.1016/j.polymer.2004.10.040.

[200] J. Sandler, M.S.P. Shaffer, T. Prasse, W. Bauhofer, K. Schulte, A.H. Windle, Development of a dispersion process for carbon nanotubes in an epoxy matrix and the resulting electrical properties, 40 (1999) 5967–5971.

[201] P.D. Fazzino, K.L. Reifsnider, P. Majumdar, Impedance spectroscopy for progressive damage analysis in woven composites, Composites Science and Technology. 69 (2014) 2008–2014. https://doi.org/10.1016/j.compscitech.2009.05.007.

[202] J. Mijovi??, J.M. Kenny, A. Maffezzoli, A. Trivisano, F. Bellucci, L. Nicolais, The principles of dielectric measurements for in situ monitoring of composite processing, Composites Science and Technology. 49 (1993) 277–290. https://doi.org/10.1016/0266-3538(93)90109-T.

[203] M. Monti, I. Armentano, G. Faiella, V. Antonucci, J.M. Kenny, L. Torre, M. Giordano, Toward the microstructure-properties relationship in MWCNT/epoxy composites: Percolation behavior and dielectric spectroscopy, Composites Science and Technology. 96 (2014) 38–46. https://doi.org/10.1016/j.compscitech.2014.03.008.

[204] C.L. Poh, M. Mariatti, A. Fauzi, M. Noor, O. Sidek, T.P. Chuah, S.C. Chow, Dielectric properties of surface treated multi-walled carbon nanotube / epoxy thin fi lm composites, Composites Part B. 85 (2016) 50–58. https://doi.org/10.1016/j.compositesb.2015.09.024.

[205] D. Bekas, G. Georgios, G.M. Maistros, A.S. Paipetis, On the use of dielectric spectroscopy for the real time assessment of the dispersion of carbon nanotubes in epoxy, (2016). https://doi.org/10.1039/C6RA15594D.

[206] D.G. Bekas, A.S. Paipetis, Study of the Effect of Damage on the Electrical Impedance of Carbon Nanotube Reinforced Epoxy Nanocomposites, Journal of Sensors. (2015). https://doi.org/10.1155/2015/805303.

[207] D.G. Bekas, A.S. Paipetis, Damage monitoring in nanoenhanced composites using impedance spectroscopy, Composites Science and Technology. 134 (2016) 96–105. https://doi.org/10.1016/j.compscitech.2016.08.013.

[208] H. Search, C. Journals, A. Contact, M. Iopscience, I.P. Address, Improvement of toughness and electrical properties of epoxy composites with carbon nanotubes prepared by industrially, 125702 (n.d.). https://doi.org/10.1088/0957-4484/22/12/125702.

[209] A. Allaoui, N. Bounia, Rheological and Electrical Transitions in Carbon Nanotube/Epoxy Suspensions, CNANO. 6 (2010) 158–162. https://doi.org/10.2174/157341310790945669.

[210] A.N. Wilkinson, I.A. Kinloch, R.N. Othman, Low viscosity processing using hybrid CNT-coated silica particles to form electrically conductive epoxy resin composites, Polymer. 98 (2016) 32–38. https://doi.org/10.1016/j.polymer.2016.06.009.

[211] T. Yokozeki, S. Carolin Schulz, S.T. Buschhorn, K. Schulte, Investigation of shear thinning behavior and microstructures of MWCNT/epoxy and CNF/epoxy suspensions under steady shear conditions, European Polymer Journal. 48 (2012) 1042–1049. https://doi.org/10.1016/j.eurpolymj.2012.03.013.

[212] P. Pötschke, M.A. Abdel-goad, Rheological and dielectrical characterization of melt mixed polycarbonate-multiwalled carbon nanotube composites . Polymer polycarbonate-multiwalled carbon nanotube composites, (2004). https://doi.org/10.1016/j.polymer.2004.10.040.

[213] J. Rubinson, Y. Kayinamura, Charge transport in conducting polymers: insights from impedance spectroscopy., Chem. Soc. Rev. 38 (2009) 3339–3347. https://doi.org/10.1039/b904083h.

[214] Y. Sun, H. Da Bao, Z.X. Guo, J. Yu, Modeling of the electrical percolation of mixed carbon fillers in polymer-based composites, Macromolecules. 42 (2009) 459–463. https://doi.org/10.1021/ma8023188.

[215] H.D. Wagner, P.M. Ajayan, K. Schulte, Nanocomposite toughness from a pull-out mechanism, Composites Science and Technology. 83 (2013) 27–31. https://doi.org/10.1016/j.compscitech.2013.04.017.

[216] J.-Y. Wang, H.J. Ploehn, Dynamic mechanical analysis of the effect of water on glass bead–epoxy composites, Applied Polymer Science. 59 (1996) 345–357.

[217] S. Bocchini, G. Fornasieri, L. Rozes, S. Trabelsi, J. Galy, N.E. Zafeiropoulos, M. Stamm, J.-F. Gérard, C. Sanchez, New hybrid organic–inorganic nanocomposites based

on functional [Ti16O16(OEt)24(OEMA)8] nano-fillers, Chem. Commun. (2005) 2600. https://doi.org/10.1039/b502434j.

[218] I. Srikanth, S. Kumar, A. Kumar, P. Ghosal, C. Subrahmanyam, Effect of amino functionalized MWCNT on the crosslink density , fracture toughness of epoxy and mechanical properties of carbon – epoxy composites, Composites Part A: Applied Science and Manufacturing. 43 (2012) 2083–2086. https://doi.org/10.1016/j.compositesa.2012.07.005.

[219] D. Baltzis, D. Bekas, K. Tsirka, A. Parlamas, A. Ntaflos, N. Zafeiropoulos, A.G. Lekatou, A.S. Paipetis, Multi-scaled carbon epoxy composites underwater immersion: A durability study, Composites Science and Technology. 199 (2020) 108373. https://doi.org/10.1016/j.compscitech.2020.108373.

[220] G. Foteinidis, K. Tsirka, L. Tzounis, D. Baltzis, A.S. Paipetis, The Role of Synergies of MWCNTs and Carbon Black in the Enhancement of the Electrical and Mechanical Response of Modified Epoxy Resins, Applied Sciences. 9 (2019) 3757. https://doi.org/10.3390/app9183757.

[221] F.-L. Jin, X. Li, S.-J. Park, Synthesis and application of epoxy resins: A review, Journal of Industrial and Engineering Chemistry. 29 (2015) 1–11. https://doi.org/10.1016/j.jiec.2015.03.026.

[222] A.P. Mouritz, A.G. Gibson, Fire properties of polymer composite materials, Springer, Dordrecht, 2006.

[223] Y. Miyano, M. Nakada, N. Sekine, Accelerated testing for long-term durability of GFRP laminates for marine use, Composites Part B: Engineering. 35 (2004) 497–502. https://doi.org/10.1016/j.compositesb.2003.11.006.

[224] H. Miyagawa, L.T. Drzal, Thermo-physical and impact properties of epoxy nanocomposites reinforced by single-wall carbon nanotubes, Polymer. 45 (2004) 5163–5170. https://doi.org/10.1016/j.polymer.2004.05.036.

[225] X. Jiang, H. Kolstein, F. Bijlaard, X. Qiang, Effects of hygrothermal aging on glass-fibre reinforced polymer laminates and adhesive of FRP composite bridge: Moisture diffusion characteristics, Composites Part A: Applied Science and Manufacturing. 57 (2014) 49–58. https://doi.org/10.1016/j.compositesa.2013.11.002.

[226] T. Glaskova-Kuzmina, A. Aniskevich, A. Martone, M. Giordano, M. Zarrelli, Effect of moisture on elastic and viscoelastic properties of epoxy and epoxy-based carbon fibre reinforced plastic filled with multiwall carbon nanotubes, Composites Part A: Applied Science and Manufacturing. 90 (2016) 522–527. https://doi.org/10.1016/j.compositesa.2016.08.026.

[227] S. Popineau, C. Rondeau-Mouro, C. Sulpice-Gaillet, M.E.R. Shanahan, Free/bound water absorption in an epoxy adhesive, Polymer. 46 (2005) 10733–10740. https://doi.org/10.1016/j.polymer.2005.09.008.

[228] G. Gkikas, D.-D. Douka, N.-M. Barkoula, A.S. Paipetis, Nano-enhanced composite materials under thermal shock and environmental degradation: A durability study, Composites Part B: Engineering. 70 (2015) 206–214. https://doi.org/10.1016/j.compositesb.2014.11.008.

[229] A. Lekatou, S.E. Faidi, S.B. Lyon, R.C. Newman, Elasticity and fracture in particulate composites with strong and degraded interfaces, J. Mater. Res. 11 (1996) 1293–1304. https://doi.org/10.1557/JMR.1996.0164.

[230] A. Lekatou, S.E. Faidi, D. Ghidaoui, S.B. Lyon, R.C. Newman, Effect of water and its activity on transport properties of glass/epoxy particulate composites, Composites Part A: Applied Science and Manufacturing. 28 (1997) 223–236. https://doi.org/10.1016/S1359-835X(96)00113-3.

[231] M.M. Sakka, Z. Antar, K. Elleuch, J.F. Feller, Tribological response of an epoxy matrix filled with graphite and/or carbon nanotubes, Friction. 5 (2017) 171–182. https://doi.org/10.1007/s40544-017-0144-z.

[232] S. Alessi, M. Di Filippo, G. Pitarresi, M. Scafidi, A. Toscano, Fracture Toughness of Hydrothermally Aged Epoxy Systems with Different Crosslink Density, Procedia Engineering. 109 (2015) 507–516. https://doi.org/10.1016/j.proeng.2015.06.257.

[233] S. Firdosh, H.N. Narasimha Murthy, R. Pal, G. Angadi, N. Raghavendra, M. Krishna, Durability of GFRP nanocomposites subjected to hygrothermal ageing, Composites Part B: Engineering. 69 (2015) 443–451. https://doi.org/10.1016/j.compositesb.2014.09.028.

[234] A. Toscano, G. Pitarresi, M. Scafidi, M. Di Filippo, G. Spadaro, S. Alessi, Water diffusion and swelling stresses in highly crosslinked epoxy matrices, Polymer Degradation and Stability. 133 (2016) 255–263. https://doi.org/10.1016/j.polymdegradstab.2016.09.004.

[235] G. Pitarresi, M. Scafidi, S. Alessi, M. Di Filippo, C. Billaud, G. Spadaro, Absorption kinetics and swelling stresses in hydrothermally aged epoxies investigated by photoelastic image analysis, Polymer Degradation and Stability. 111 (2015) 55–63. https://doi.org/10.1016/j.polymdegradstab.2014.10.019.

[236] M. Wang, X. Xu, J. Ji, Y. Yang, J. Shen, M. Ye, The hygrothermal aging process and mechanism of the novolac epoxy resin, Composites Part B: Engineering. 107 (2016) 1–8. https://doi.org/10.1016/j.compositesb.2016.09.067.

[237] S. Alessi, G. Pitarresi, G. Spadaro, Effect of hydrothermal ageing on the thermal and delamination fracture behaviour of CFRP composites, Composites Part B: Engineering. 67 (2014) 145–153. https://doi.org/10.1016/j.compositesb.2014.06.006.

[238] L. Vertuccio, L. Guadagno, G. Spinelli, S. Russo, G. Iannuzzo, Effect of carbon nanotube and functionalized liquid rubber on mechanical and electrical properties of epoxy adhesives for aircraft structures, Composites Part B: Engineering. 129 (2017) 1–10. https://doi.org/10.1016/j.compositesb.2017.07.021.

[239] L. Guadagno, C. Naddeo, M. Raimondo, G. Barra, L. Vertuccio, S. Russo, K. Lafdi, V. Tucci, G. Spinelli, P. Lamberti, Influence of carbon nanoparticles/epoxy matrix interaction on mechanical, electrical and transport properties of structural advanced materials, Nanotechnology. 28 (2017) 094001. https://doi.org/10.1088/1361-6528/aa583d.

[240] N.M. Zulfli, A.A. Bakar, W. Chow, Mechanical and water absorption behaviors of carbon nanotube reinforced epoxy/glass fiber laminates, Journal of Reinforced Plastics and Composites. 32 (2013) 1715–1721. https://doi.org/10.1177/0731684413501926.

[241] I. Srikanth, S. Kumar, A. Kumar, P. Ghosal, Ch. Subrahmanyam, Effect of amino functionalized MWCNT on the crosslink density, fracture toughness of epoxy and

mechanical properties of carbon–epoxy composites, Composites Part A: Applied Science and Manufacturing. 43 (2012) 2083–2086. https://doi.org/10.1016/j.compositesa.2012.07.005.

[242] A. Allaoui, N. El Bounia, How carbon nanotubes affect the cure kinetics and glass transition temperature of their epoxy composites? – A review, Express Polym. Lett. 3 (2009) 588–594. https://doi.org/10.3144/expresspolymlett.2009.73.

[243] M.M. Rahman, S. Zainuddin, M.V. Hosur, C.J. Robertson, A. Kumar, J. Trovillion, S. Jeelani, Effect of NH2-MWCNTs on crosslink density of epoxy matrix and ILSS properties of e-glass/epoxy composites, Composite Structures. 95 (2013) 213–221. https://doi.org/10.1016/j.compstruct.2012.07.019.

[244] O. Starkova, S. Chandrasekaran, L.A.S.A. Prado, F. Tölle, R. Mülhaupt, K. Schulte, Hydrothermally resistant thermally reduced graphene oxide and multi-wall carbon nanotube based epoxy nanocomposites, Polymer Degradation and Stability. 98 (2013) 519–526. https://doi.org/10.1016/j.polymdegradstab.2012.12.005.

[245] A. Nemati Giv, M.R. Ayatollahi, S.H. Ghaffari, L.F.M. da Silva, Effect of reinforcements at different scales on mechanical properties of epoxy adhesives and adhesive joints: a review, The Journal of Adhesion. 94 (2018) 1082–1121. https://doi.org/10.1080/00218464.2018.1452736.

[246] V. Kumar, S.K. Sinha, A.K. Agarwal, Tribological studies of epoxy composites with solid and liquid fillers, Tribology International. 105 (2017) 27–36. https://doi.org/10.1016/j.triboint.2016.09.010.

[247] M.F. Ashby, Y.J.M. Bréchet, Designing hybrid materials, Acta Materialia. 51 (2003) 5801–5821. https://doi.org/10.1016/S1359-6454(03)00441-5.

[248] F.U. Buehler, J.C. Seferis, Effect of reinforcement and solvent content on moisture absorption in epoxy composite materials, Composites Part A: Applied Science and Manufacturing. 31 (2000) 741–748. https://doi.org/10.1016/S1359-835X(00)00036-1.

[249] H. Alamri, I.M. Low, Effect of water absorption on the mechanical properties of nano-filler reinforced epoxy nanocomposites, Materials & Design. 42 (2012) 214–222. https://doi.org/10.1016/j.matdes.2012.05.060.

[250] W. Liu, S. Hoa, M. Pugh, Fracture toughness and water uptake of high-performance epoxy/nanoclay nanocomposites, Composites Science and Technology. 65 (2005) 2364–2373. https://doi.org/10.1016/j.compscitech.2005.06.007.

[251] L. Schlagenhauf, B. Kianfar, T. Buerki-Thurnherr, Y.-Y. Kuo, A. Wichser, F. Nüesch, P. Wick, J. Wang, Weathering of a carbon nanotube/epoxy nanocomposite under UV light and in water bath: impact on abraded particles, Nanoscale. 7 (2015) 18524–18536. https://doi.org/10.1039/C5NR05387K.

[252] P. Nogueira, C. Ramirez, A. Torres, M.J. Abad, J. Cano, J.L. Pez, I.L. Pez-Bueno, L. Barral, Effect of water sorption on the structure and mechanical properties of an epoxy resin system, Journal of Applied Polymer Science. 80 (2000) 71–80.

[253] M. Harsch, J. Karger-Kocsis, M. Holst, Influence of fillers and additives on the cure kinetics of an epoxy/anhydride resin, European Polymer Journal. 43 (2007) 1168–1178. https://doi.org/10.1016/j.eurpolymj.2007.01.025.

[254] H. Düzcükoğlu, Ş. Ekinci, Ö.S. Şahin, A. Avci, M. Ekrem, M. Ünaldi, Enhancement of Wear and Friction Characteristics of Epoxy Resin by Multiwalled Carbon Nanotube and

Boron Nitride Nanoparticles, Tribology Transactions. 58 (2015) 635–642. https://doi.org/10.1080/10402004.2014.998358.

[255] L.C. Zhang, I. Zarudi, K.Q. Xiao, Novel behaviour of friction and wear of epoxy composites reinforced by carbon nanotubes, Wear. 261 (2006) 806–811. https://doi.org/10.1016/j.wear.2006.01.033.

[256] R. Selzer, K. Friedrich, Mechanical properties and failure behaviour of carbon fibre-reinforced polymer composites under the influence of moisture, Composites Part A: Applied Science and Manufacturing. 28 (1997) 595–604. https://doi.org/10.1016/S1359-835X(96)00154-6.

[257] N. Guermazi, A. Ben Tarjem, I. Ksouri, H.F. Ayedi, On the durability of FRP composites for aircraft structures in hygrothermal conditioning, Composites Part B: Engineering. 85 (2016) 294–304. https://doi.org/10.1016/j.compositesb.2015.09.035.

[258] D.G. Bekas, A.S. Paipetis, Damage monitoring in nanoenhanced composites using impedance spectroscopy, Composites Science and Technology. 134 (2016) 96–105. https://doi.org/10.1016/j.compscitech.2016.08.013.

[259] P.D. Fazzino, K.L. Reifsnider, P. Majumdar, Impedance spectroscopy for progressive damage analysis in woven composites, Composites Science and Technology. 69 (2009) 2008–2014. https://doi.org/10.1016/j.compscitech.2009.05.007.

[260] S.P. Zaoutsos, M.C. Zilidou, Influence of extreme low temperature conditions on the dynamic mechanical properties of carbon fiber reinforced polymers, IOP Conf. Ser.: Mater. Sci. Eng. 276 (2017) 012024. https://doi.org/10.1088/1757-899X/276/1/012024.

[261] S.-Y. Fu, Y.-W. Mai, B. Lauke, C.-Y. Yue, Synergistic effect on the fracture toughness of hybrid short glass fiber and short carbon fiber reinforced polypropylene composites, Materials Science and Engineering: A. 323 (2002) 326–335. https://doi.org/10.1016/S0921-5093(01)01383-1.

[262] M. Fotouhi, P. Suwarta, M. Jalalvand, G. Czel, M.R. Wisnom, Detection of fibre fracture and ply fragmentation in thin-ply UD carbon/glass hybrid laminates using acoustic emission, Composites Part A: Applied Science and Manufacturing. 86 (2016) 66–76. https://doi.org/10.1016/j.compositesa.2016.04.003.

[263] N. De Greef, L. Gorbatikh, S.V. Lomov, I. Verpoest, Damage development in woven carbon fiber/epoxy composites modified with carbon nanotubes under tension in the bias direction, Composites Part A: Applied Science and Manufacturing. 42 (2011) 1635–1644. https://doi.org/10.1016/j.compositesa.2011.07.013.

[264] B. Dhiman, V. Guleria, P. Sharma, Applications and Future Trends of Carbon Fiber Reinforced Polymer Composites: A Review, 07 (2020) 7.

[265] P.F. Liu, J. Yang, B. Wang, Z.F. Zhou, J.Y. Zheng, A Study on the Intralaminar Damage and Interlaminar Delamination of Carbon Fiber Composite Laminates Under Three-Point Bending Using Acoustic Emission, J Fail. Anal. and Preven. 15 (2015) 101–121. https://doi.org/10.1007/s11668-014-9901-8.

[266] A. Godara, L. Gorbatikh, G. Kalinka, A. Warrier, O. Rochez, L. Mezzo, F. Luizi, A.W. van Vuure, S.V. Lomov, I. Verpoest, Interfacial shear strength of a glass fiber/epoxy bonding in composites modified with carbon nanotubes, Composites Science and Technology. 70 (2010) 1346–1352. https://doi.org/10.1016/j.compscitech.2010.04.010.

[267] K. Sravanthi, Influence of micro and nano carbon fillers on impact behavior of GFRP composite materials, Materials Today. (n.d.) 4.

[268] J. Karger-Kocsis, H. Mahmood, A. Pegoretti, All-carbon multi-scale and hierarchical fibers and related structural composites: A review, Composites Science and Technology. 186 (2020) 107932. https://doi.org/10.1016/j.compscitech.2019.107932.

[269] F.H. Gojny, M.H.G. Wichmann, B. Fiedler, W. Bauhofer, K. Schulte, Influence of nano-modification on the mechanical and electrical properties of conventional fibre-reinforced composites, Composites Part A: Applied Science and Manufacturing. 36 (2005) 1525–1535. https://doi.org/10.1016/j.compositesa.2005.02.007.

[270] R. Shrivastava, K.K. Singh, Interlaminar Fracture Toughness Characterization of Laminated Composites: A Review, Polymer Reviews. 60 (2020) 542–593. https://doi.org/10.1080/15583724.2019.1677708.

[271] X. Liu, T. Sun, Z. Wu, H. He, Mode II interlaminar fracture toughness of unidirectional fiber-reinforced polymer matrix composites with synthetic boehmite nanosheets at room temperature and low temperature, Journal of Composite Materials. 52 (2018) 945–952. https://doi.org/10.1177/0021998317716529.

[272] H. Ning, Y. Li, J. Li, N. Hu, Y. Liu, L. Wu, F. Liu, Toughening effect of CB-epoxy interleaf on the interlaminar mechanical properties of CFRP laminates, Composites Part A: Applied Science and Manufacturing. 68 (2015) 226–234. https://doi.org/10.1016/j.compositesa.2014.09.030.

[273] G.W. Beckermann, K.L. Pickering, Mode I and Mode II interlaminar fracture toughness of composite laminates interleaved with electrospun nanofibre veils, Composites Part A: Applied Science and Manufacturing. 72 (2015) 11–21. https://doi.org/10.1016/j.compositesa.2015.01.028.

[274] S. Hamer, H. Leibovich, A. Green, R. Avrahami, E. Zussman, A. Siegmann, D. Sherman, Mode I and Mode II fracture energy of MWCNT reinforced nanofibrilmats interleaved carbon/epoxy laminates, Composites Science and Technology. 90 (2014) 48–56. https://doi.org/10.1016/j.compscitech.2013.10.013.

[275] M. Yasaee, I.P. Bond, R.S. Trask, E.S. Greenhalgh, Mode I interfacial toughening through discontinuous interleaves for damage suppression and control, Composites Part A: Applied Science and Manufacturing. 43 (2012) 198–207. https://doi.org/10.1016/j.compositesa.2011.10.009.

[276] K. Bilisik, G. Erdogan, E. Sapanci, S. Gungor, Fracture Toughness (Mode-II) of Nanostitched Composites, Procedia Structural Integrity. 21 (2019) 146–153. https://doi.org/10.1016/j.prostr.2019.12.096.

[277] A.P. Mouritz, L.K. Jain, Interlaminar Fracture Properties of Stitched Fibreglass Composites, (1997) 12.

[278] K. Bilisik, G. Erdogan, E. Sapanci, S. Gungor, Mode-II toughness of nanostitched carbon/epoxy multiwall carbon nanotubes prepreg composites: Experimental investigation by using end notched flexure, Journal of Composite Materials. 53 (2019) 4249–4271. https://doi.org/10.1177/0021998319857462.

[279] M. Arai, Y. Noro, K. Sugimoto, M. Endo, Mode I and mode II interlaminar fracture toughness of CFRP laminates toughened by carbon nanofiber interlayer, Composites

Science and Technology. 68 (2008) 516–525. https://doi.org/10.1016/j.compscitech.2007.06.007.

[280] A. Korjakin, R. Rikards, F.-G. Buchholz, H. Wang, A.K. Bledzki, A. Kessler, Comparative study of interlaminar fracture toughness of GFRP with different fiber surface treatments, Polym. Compos. 19 (1998) 793–806. https://doi.org/10.1002/pc.10154.

[281] M.S. Chaudhry, A. Czekanski, Z.H. Zhu, Characterization of carbon nanotube enhanced interlaminar fracture toughness of woven carbon fiber reinforced polymer composites, International Journal of Mechanical Sciences. 131–132 (2017) 480–489. https://doi.org/10.1016/j.ijmecsci.2017.06.016.

[282] S. Wu, R.B. Ladani, A.R. Ravindran, J. Zhang, A.P. Mouritz, A.J. Kinloch, C.H. Wang, Aligning carbon nanofibres in glass-fibre/epoxy composites to improve interlaminar toughness and crack-detection capability, Composites Science and Technology. 152 (2017) 46–56. https://doi.org/10.1016/j.compscitech.2017.09.007.

[283] E. Borowski, E. Soliman, U. Kandil, M. Taha, Interlaminar Fracture Toughness of CFRP Laminates Incorporating Multi-Walled Carbon Nanotubes, Polymers. 7 (2015) 1020–1045. https://doi.org/10.3390/polym7061020.

[284] Y. Arooj, Y. Zhao, X. Han, T. Bao, Y. Wang, Combined effect of graphene oxide and MWCNTs on microwave absorbing performance of epoxy composites: MICROWAVE ABSORBING PERFORMANCE OF EPOXY COMPOSITES, Polym. Adv. Technol. 26 (2015) 620–625. https://doi.org/10.1002/pat.3496.

[285] D.C. Davis, B.D. Whelan, An experimental study of interlaminar shear fracture toughness of a nanotube reinforced composite, Composites Part B: Engineering. 42 (2011) 105–116. https://doi.org/10.1016/j.compositesb.2010.06.001.

[286] S.R. Shahbaz, Ö.B. Berkalp, Effect of MWCNTs addition, on the mechanical behaviour of FRP composites, by reinforcement grafting and matrix modification, Journal of Industrial Textiles. 50 (2020) 205–223. https://doi.org/10.1177/1528083718825317.

[287] N. De Greef, L. Gorbatikh, A. Godara, L. Mezzo, S.V. Lomov, I. Verpoest, The effect of carbon nanotubes on the damage development in carbon fiber/epoxy composites, Carbon. 49 (2011) 4650–4664. https://doi.org/10.1016/j.carbon.2011.06.047.

[288] S. Lili, Z. Yan, D. Yuexin, Z. Zuoguang, Interlaminar Shear Property of Modified Glass Fiber-reinforced Polymer with Different MWCNTs, Chinese Journal of Aeronautics. 21 (2008) 361–369. https://doi.org/10.1016/S1000-9361(08)60047-3.

[289] K.K. Panchagnula, Improvement in the mechanical properties of neat GFRPs with multi-walled CNTs, (n.d.) 11.

[290] M.-C. Yip, Y.-C. Lin, C.-L. Wu, Effect of Multi-Walled Carbon Nanotubes Addition on Mechanical Properties of Polymer Composites Laminate, Polymers and Polymer Composites. 19 (2011) 131–140. https://doi.org/10.1177/0967391111019002-313.

[291] H. Qian, E.S. Greenhalgh, M.S.P. Shaffer, A. Bismarck, Carbon nanotube-based hierarchical composites: a review, J. Mater. Chem. 20 (2010) 4751. https://doi.org/10.1039/c000041h.

[292] M. Hosur, T. Mahdi, S. Jeelani, Studies on the performance of multi-phased carbon/epoxy composites with nanoclay and multi-walled carbon nanotubes, Multiscale

and Multidiscip. Model. Exp. and Des. 1 (2018) 255–268. https://doi.org/10.1007/s41939-018-0017-9.

[293] J.R. Pothnis, D. Kalyanasundaram, S. Gururaja, Enhancement of open hole tensile strength via alignment of carbon nanotubes infused in glass fiber – epoxy - CNT multi-scale composites, (n.d.) 33.

[294] V.-T. Hoang, Y.-J. Yum, Optimization of the fabrication conditions and effects of multi-walled carbon nanotubes on the tensile properties of various glass fibers/unsaturated polyester resin composites, E-Polymers. 18 (2018) 441–451. https://doi.org/10.1515/epoly-2018-0033.

[295] A. Jiménez-Suárez, M. Campo, S.G. Prolongo, M. Sánchez, A. Ureña, Effect of filtration in functionalized and non-functionalized CNTs and surface modification of fibers as an effective alternative approach, Composites Part B: Engineering. 94 (2016) 286–291. https://doi.org/10.1016/j.compositesb.2016.02.063.

[296] A. Tugrul Seyhan, M. Tanoglu, K. Schulte, Mode I and mode II fracture toughness of E-glass non-crimp fabric/carbon nanotube (CNT) modified polymer based composites, Engineering Fracture Mechanics. 75 (2008) 5151–5162. https://doi.org/10.1016/j.engfracmech.2008.08.003.

[297] Y.C. Shin, W.I. Lee, H.S. Kim, Mode II interlaminar fracture toughness of carbon nanotubes/epoxy film-interleaved carbon fiber composites, Composite Structures. 236 (2020) 111808. https://doi.org/10.1016/j.compstruct.2019.111808.

[298] D. Baltzis, O. Evaggelou, A.G. Lekatou, A.S. Paipetis, Acoustic Emission Feasibility Study for Carbon Epoxy Coated Aluminum Corrosion Monitoring, Int J Metall Mater Eng. 4 (2018). https://doi.org/10.15344/2455-2372/2018/143.

[299] S.M. Fekih, A. Albedah, F. Benyahia, M. Belhouari, B. Bachir Bouiadjra, A. Miloudi, Optimisation of the sizes of bonded composite repair in aircraft structures, Materials & Design. 41 (2012) 171–176. https://doi.org/10.1016/j.matdes.2012.04.025.

[300] A. Vagask??, E. Fechov??, P. Michal, M. Gomb??r, The influence of input factors of aluminium anodizing process on resulting thickness and quality of aluminium oxide layer, Procedia Engineering. 149 (2016) 512–519. https://doi.org/10.1016/j.proeng.2016.06.699.

[301] G. Gkikas, D. Sioulas, A. Lekatou, N.M. Barkoula, A.S. Paipetis, Enhanced bonded aircraft repair using nano-modified adhesives, Materials and Design. 41 (2012) 394–402. https://doi.org/10.1016/j.matdes.2012.04.052.

[302] A. Fereidoon, N. Kordani, Y. Rostamiyan, D.D. Ganji, M.G. Ahangari, Effect of CNTs on adhesion strength of glass/epoxy composite with alloy aluminum surface, (n.d.).

[303] N.W. Khun, B.C.R. Troconis, G.S. Frankel, Effects of carbon nanotube content on adhesion strength and wear and corrosion resistance of epoxy composite coatings on AA2024-T3, Progress in Organic Coatings. 77 (2014) 72–80. https://doi.org/10.1016/j.porgcoat.2013.08.003.

[304] D. Baltzis, D.G. Bekas, G. Tzachristas, A. Parlamas, M. Karabela, N.E. Zafeiropoulos, A.S. Paipetis, Multi-scaled carbon reinforcements in ternary epoxy composite materials: Dispersion and electrical impedance study, Composites Science and Technology. 153 (2017) 7–17. https://doi.org/10.1016/j.compscitech.2017.09.035.

[305] U.A. Khashaba, A.A. Aljinaidi, M.A. Hamed, Analysis of adhesively bonded CFRE composite scarf joints modified with MWCNTs, Composites Part A: Applied Science and Manufacturing. 71 (2015) 59–71. https://doi.org/10.1016/j.compositesa.2015.01.004.

[306] U.A. Khashaba, A.A. Aljinaidi, M.A. Hamed, Nanofillers modification of Epocast 50-A1/946 epoxy for bonded joints, Chinese Journal of Aeronautics. 27 (2014) 1288–1300. https://doi.org/10.1016/j.cja.2014.08.007.

[307] S. Yu, M.N. Tong, G. Critchlow, Use of carbon nanotubes reinforced epoxy as adhesives to join aluminum plates, Materials & Design. 31 (2010) S126–S129. https://doi.org/10.1016/j.matdes.2009.11.045.

[308] U. Szeluga, B. Kumanek, B. Trzebicka, Synergy in hybrid polymer/nanocarbon composites. A review, Composites Part A: Applied Science and Manufacturing. 73 (2015) 204–231. https://doi.org/10.1016/j.compositesa.2015.02.021.

[309] J. Sumfleth, X.C. Adroher, K. Schulte, Synergistic effects in network formation and electrical properties of hybrid epoxy nanocomposites containing multi-wall carbon nanotubes and carbon black, J Mater Sci. 44 (2009) 3241–3247. https://doi.org/10.1007/s10853-009-3434-7.

[310] F. Bellenger, H. Mazille, H. Idrissi, Use of acoustic emission technique for the early detection of aluminum alloys exfoliation corrosion, NDT & E International. 35 (2002) 385–392. https://doi.org/10.1016/S0963-8695(02)00011-7.

[311] H. Idrissi, J. Derenne, H. Mazille, L.D.P. Industrielle, Detection of Pitting Corrosion of Aluminium Alloys By Acoustic Emission Technique, (n.d.) 299–306.

[312] M. Boinet, J. Bernard, M. Chatenet, F. Dalard, S. Maximovitch, Understanding aluminum behaviour in aqueous alkaline solution using coupled techniques. Part II: Acoustic emission study, Electrochimica Acta. 55 (2010) 3454–3463. https://doi.org/10.1016/j.electacta.2009.06.038.

[313] S. Caines, F. Khan, J. Shirokoff, A. Arora, S. Gholizadeh, Z. Leman, B.T.H.T. Baharudin, M.G.R.R. Sause, A. Gribov, A.R. Unwin, S. Horn, E. Maillet, N. Godin, M. R'Mili, P. Reynaud, J. Lamon, G. Fantozzi, M. Boinet, J. Bernard, M. Chatenet, F. Dalard, S. Maximovitch, M.G.R.R. Sause, F. Haider, S. Horn, J. Bernard, M. Boinet, M. Chatenet, F. Dalard, F. Bellenger, H. Mazille, H. Idrissi, H. Chang, E.H. Han, J.Q. Wang, W. Ke, Use of acoustic emission technique for the early detection of aluminum alloys exfoliation corrosion, NDT and E International. 72 (2012) 3454–3463. https://doi.org/10.1016/j.patrec.2011.09.018.

[314] M. Perrin, M.L. Pastor, H. Welemane, A. Cantarel, M. Karama, V. Munoz, B. Valès, M. Perrin, M.L. Pastor, H. Welemane, A. Cantarel, M. Karama, Damage detection in CFRP by coupling acoustic emission and infrared thermography, Composites Part B: Engineering. 85 (2016) 68–75. https://doi.org/10.1016/j.compositesb.2015.09.011.

[315] M. Strantza, D. Van Hemelrijck, P. Guillaume, D.G. Aggelis, Acoustic emission monitoring of crack propagation in additively manufactured and conventional titanium components, Mechanics Research Communications. 84 (2017) 8–13. https://doi.org/10.1016/j.mechrescom.2017.05.009.

[316] M. Fregonese, H. Idrissi, H. Mazille, Monitoring pitting corrosion of AISI 316L austenitic stainless steel by acoustic emission technique: Choice of representative

acoustic parameters, Journal of Materials Science. 36 (2001) 557–563. https://doi.org/10.1023/A:1004891514836.

[317] S. Masmoudi, A. El Mahi, R. El Guerjouma, Mechanical behaviour and health monitoring by acoustic emission of sandwich composite integrated by piezoelectric implant, Composites Part B: Engineering. 67 (2014) 76–83. https://doi.org/10.1016/j.compositesb.2014.05.032.

[318] A. Zaki, H.K. Chai, D.G. Aggelis, N. Alver, Non-Destructive Evaluation for Corrosion Monitoring in Concrete: A Review and Capability of Acoustic Emission Technique, Sensors. 15 (2015) 19069. https://doi.org/10.3390/s150819069.

[319] A. Farhidzadeh, A.C. Mpalaskas, T.E. Matikas, H. Farhidzadeh, D.G. Aggelis, Fracture mode identification in cementitious materials using supervised pattern recognition of acoustic emission features, Construction and Building Materials. 67 (2014) 129–138. https://doi.org/10.1016/j.conbuildmat.2014.05.015.

[320] J. Xu, X. Wu, E.-H. Han, Acoustic emission response of sensitized 304 stainless steel during intergranular corrosion and stress corrosion cracking, Corrosion Science. 73 (2013) 262–273. https://doi.org/10.1016/j.corsci.2013.04.014.

[321] W. Hwang, S. Bae, J. Kim, S. Kang, N. Kwag, B. Lee, Acoustic emission characteristics of stress corrosion cracks in a type 304 stainless steel tube, Nuclear Engineering and Technology. 47 (2015) 454–460. https://doi.org/10.1016/j.net.2015.04.001.

[322] K.H.W. Seah, C.H. Chew, S.H. Teoh, The correlation of acoustic emission with rate of corrosion, 34 (1993) 1–7.

[323] K.M. Bak, K. Kalaichelvan, A. Jothilingam, K. Mohamed Bak, K. Kalaichelvan, A. Jothilingam, S. RajendraBoopathy, K.M. Bak, K. Kalaichelvan, A. Jothilingam, K. Mohamed Bak, K. Kalaichelvan, A. Jothilingam, S. RajendraBoopathy, Acoustic emission characterization of failure modes of single-lap joints in glass/epoxy specimens, Journal of Composite Materials. 50 (2016) 3–23. https://doi.org/10.1177/0021998315569749.

[324] K.M. Bak, K. Kalaichelvan, V. Arumugam, A novel approach for classification of failure modes in single lap joints using acoustic emission data, Journal of Composite Materials. 48 (2014) 3003–3017. https://doi.org/10.1177/0021998313504323.

[325] M. Schutze, R.W. Cahn, P. Haasen, E.J. Kramer, Corrosion and Environmental Degradation, 2000.

[326] F.P. Hunter M. S., Naturally and thermally formed oxide films on aluminum, Journal of Electrochemical Society. 103 (1956) 482–485.

[327] D. Altenpohl, Aluminum: Technology, Applications and Environment: A Profile of a Modern Metal Aluminum from Within, 6th ed., 1998.

[328] R.T. Foley, Localized Corrosion of Aluminum Alloys—A Review, CORROSION. 42 (1986) 277–288. https://doi.org/10.5006/1.3584905.

[329] Z. Szklarska-Smialowska, Pitting corrosion of aluminum, Corrosion Science. 41 (1999) 1743–1767.

[330] J.A. DeRose, A. Bałkowiec, J. Michalski, T. Suter, K.J. Kurzydlowski, P. Schmutz, Microscopic and Macroscopic Characterisation of an Aerospace Aluminium Alloy (AA2024), in: J.A. DeRose, T. Suter, T. Hack, R.A. Adey (Eds.), WIT Transactions on

State of the Art in Science and Engineering, 1st ed., WIT Press, 2012: pp. 23–38. https://doi.org/10.2495/978-1-84564-752-0/03.

[331] E.M. Rosen, D.C. Silverman, Corrosion Prediction from Polarization Scans Using an Artificial Neural Network Integrated with an Expert System, CORROSION. 48 (1992) 734–745. https://doi.org/10.5006/1.3315994.

[332] B. N., B. R.G., Electrochemical characteristics of intermetallic phases in aluminum alloys: an experimental survey and discussion, Journal of Electrochemical Society. 125 (2005) 140–151.

[333] A. Lekatou, A.K. Sfikas, A.E. Karantzalis, D. Sioulas, Microstructure and corrosion performance of Al-32%Co alloys, Corrosion Science. 63 (2012) 193–209. https://doi.org/10.1016/j.corsci.2012.06.002.

[334] E. McCafferty, Validation of corrosion rates measured by the Tafel extrapolation method, Corrosion Science. 47 (2005) 3202–3215. https://doi.org/10.1016/j.corsci.2005.05.046.

9. Outro

9.1. Conclusions

The presented research efforts involved the modification of a commercially available epoxy resin via the multi-scaled reinforcing approach. Towards that end, carbonaceous fillers from the nano- and micro- scaled were introduced in the epoxy matrix using the industry proven high shear forces dispersion method. Reference studies were conducted in order to optimize the dispersion parameters in relation to the MWCNTs and MC fillers weight contents. The resulting ternary formulations were studied and compared to the neat and binary ones via selected experimental procedures targeting electrical, mechanical, thermomechanical, physical and wear resistance properties. The durability of the ternary composites was assessed via hydrothermal exposure experiments. In a parallel study, the neat, binary and ternary formulations were employed as metallic substrate protective coatings and their electrochemical and anti-corrosive performance was assessed. AE measurements were coupled with the electrochemical experimental procedures, so as to explore the technique's corrosion monitoring capabilities.

The results indicated that the multi-scaled reinforcing approach exhibits significant advantages over the 'one filler' approach. The combined introduction of the nano- and micro-scaled fillers led to superior electrical, mechanical and physical performance when compared to both neat epoxy and binary composites. Mitigation of water ingress degradation was evident at the hydrothermal performance of the ternary composites. The superior characteristics of the ternary composites were also evident in the anti-corrosive study as well. Specimens with ternary coatings exhibited significantly lower electrochemical values and more stable performance than their neat and binary counterparts.

The observed results were attributed to the formation of a hybrid 3D network of MWCNTs and MC interconnected particles. This hybrid network was far more effective in facilitating electrical flow while hindering crack initiation and propagation. The stiffer particles were able to reduce chain mobility and facilitate cross linking leading to improved thermomechanical properties. Furthermore, mitigation of the detrimental effects of water ingress evident in all studied durability related properties.

AE exhibited significant capabilities for real-time corrosion monitoring regardless the employed coating formulation. AE activity successfully tracked the evolution of corrosion

process while specific AE indices were successfully correlated with distinctive corrosion degradation phenomena.

9.2. Suggestions for future work.

Within the scope of this thesis, the multi-scaled approach proved to be a reliable route towards epoxy based composites with superior performance. Studies on the ternary composites could extend to other material properties either at the epoxy composite level of FRCs level. Ballistic tests, bending and/or fatigue tests, could reveal capabilities for extending the application range of epoxies. Studies with other carbonaceous filler combinations like graphene/CB or MWCNTs/graphene could identify capabilities for even greater enhancements in final properties. Although in such studies the dispersion parameters should also be adjusted accordingly.

In terms of anti-corrosive performance, a coating thickness optimization study could follow in order to find the limits of the ternary coatings. Ternary coatings could be applied to other metallic materials that are susceptible to corrosion to verify the observed performance, and extend the knowledge base for the new formulations. Such a study could be coupled with AE measurements to further explore corrosion monitoring capabilities and validate the results from the presented efforts.

10. Publications

10.1. Publications in peer-reviewed journals

[1]. **D. Baltzis**, D. Bekas, K. Tsirka, A. Parlamas, A. Ntaflos, N. Zafeiropoulos, A.G. Lekatou, A.S. Paipetis, Multi-scaled carbon epoxy composites underwater immersion: A durability study, Composites Science and Technology. 199 (2020) 108373. https://doi.org/10.1016/j.compscitech.2020.108373.

[2] G. Foteinidis, K. Tsirka, L. Tzounis, **D. Baltzis**, A.S. Paipetis, The Role of Synergies of MWCNTs and Carbon Black in the Enhancement of the Electrical and Mechanical Response of Modified Epoxy Resins, Applied Sciences. 9 (2019) 3757. https://doi.org/10.3390/app9183757.

[3] M. Kosarli, D.G. Bekas, K. Tsirka, **D. Baltzis**, D.T. Vaimakis-Tsogkas, S. Orfanidis, G. Papavassiliou, A.S. Paipetis, Microcapsule-based self-healing materials: Healing efficiency and toughness reduction vs. capsule size, Composites Part B: Engineering. 171 (2019) 78–86. https://doi.org/10.1016/j.compositesb.2019.04.030.

[4] D.G. Bekas, Z. Sharif-Khodaei, **D. Baltzis**, M.H.F. Aliabadi, A.S. Paipetis, Quality assessment and damage detection in nanomodified adhesively-bonded composite joints using inkjet-printed interdigital sensors, Composite Structures. 211 (2019) 557–563. https://doi.org/10.1016/j.compstruct.2019.01.008.

[5] **D. Baltzis**, O. Evaggelou, A.G. Lekatou, A.S. Paipetis, Acoustic Emission Feasibility Study for Carbon Epoxy Coated Aluminum Corrosion Monitoring, Int J Metall Mater Eng. 4 (2018). https://doi.org/10.15344/2455-2372/2018/143.

[6] **D. Baltzis**, D.G. Bekas, G. Tzachristas, A. Parlamas, M. Karabela, N.E. Zafeiropoulos, A.S. Paipetis, Multi-scaled carbon reinforcements in ternary epoxy composite materials: Dispersion and electrical impedance study, Composites Science and Technology. 153 (2017) 7–17. https://doi.org/10.1016/j.compscitech.2017.09.035.

[7] D.G. Bekas, **D. Baltzis**, A.S. Paipetis, Nano-reinforced polymeric healing agents for vascular self-repairing composites, Materials & Design. 116 (2017) 538–544. https://doi.org/10.1016/j.matdes.2016.12.049.

[8] D.G. Bekas, **D. Baltzis**, K. Tsirka, D. Exarchos, T. Matikas, A. Meristoudi, S. Pispas, A.S. Paipetis, Self-healing polymers: evaluation of self-healing process via non-destructive

techniques, Plastics, Rubber and Composites. 45 (2016) 147–156. https://doi.org/10.1080/14658011.2016.1151987.

[9] **D. Baltzis**, S. Orfanidis, A. Lekatou, A.S. Paipetis, Stainless steel coupled with carbon nanotube-modified epoxy and carbon fibre composites: Electrochemical and mechanical study, Plastics, Rubber and Composites. 45 (2016) 95–105. https://doi.org/10.1080/14658011.2016.1144339.

[10] D.G. Bekas, K. Tsirka, **D. Baltzis**, A.S. Paipetis, Self-healing materials: A review of advances in materials, evaluation, characterization and monitoring techniques, Composites Part B: Engineering. 87 (2016) 92–119. https://doi.org/10.1016/j.compositesb.2015.09.057.

[11] S. Hamilakis, **D. Balgis**, K. Milonakou-Koufoudaki, C. Mitzithra, C. Kollia, Z. Loizos, Electrodeposition of CdSe photoabsorber thin films in the presence of selected organic additives, Materials Letters. 145 (2015) 11–14. https://doi.org/10.1016/j.matlet.2015.01.052.

10.2. Selected papers in peer-reviewed conference proceedings

[1] S. Orfanidis, D. Baltzis, A. Lekatou, A. Paipetis, The study of mechanical and electrochemical integrity of Invar bonded with nano-modified epoxy resin, in proceedings of the 6th Pan-Hellenic Conference on Metallic Materials, Greece, 2016.

[2] D. Baltzis, A. Lekatou, A. Paipetis, Corrosion monitoring of anodized aluminium with acoustic emission, in proceedings of the 6th Pan-Hellenic Conference on Metallic Materials, Greece, 2016.

[3] D. Baltzis, A. Paipetis, Hybrid ternary epoxy nano-composites for improved electrical and mechanical properties, in proceedings of the 17th International Conference on Experimental Mechanics – ICEM 17, Greece, 2016

[4] D. Baltzis, A. Paipetis, Carbon Nano Tubes inclusion in an epoxy resin: A study for improved fire resistance, in proceedings of 7th Panhellenic Conference on Thermal Analysis and Calorimetry.

[5] D. Baltzis, A. Lekatou, A. Paipetis, Nano modified epoxy resins for carbon fiber reinforced composites applied in aerospace aluminium sheet patched repairs, in proceedings of the 4th International Conference of Engineering Against Failure (ICEAF IV), Greece, 2015.

11. Apendix – Supplementary information

Table 11-1 Epoxy resin final properties.

	Cure cycle	
Glass transition temperature (^{0}C)	1 day at 23^{0}C+4h at 100^{0}C	120-134
Tensile strength (MPa)	8h at 80^{0}C	84-86
Elongation at tensile strength (%)	8h at 80^{0}C	5.-5.9
Tensile modulus (MPa)	8h at 80^{0}C	3000-3200
Bend notch fracture toughness (MPa√m)	8h at 80^{0}C	0.77-0.83
Bend notch fracture energy (J/m^2)	8h at 80^{0}C	192-212

Dispersion methodology operational principle

The dispersions presented were conducted using a commercially available shear mixer, namely Dispermat, model AE. Two dispersion modules were available (i) an impeller disk module and (ii) a bead mill module (Torus Mill module).

(i) The impeller module, employs a toothed steel disk at the end of the rotation shaft. By applying high rotation speeds, the impeller disk creates a vortex that violently stirs the solution. Deagglomaration takes places at the impeller's teeth proximity while the vortex constantly mix the solution. Dispersions with impeller disks are a common practise in the paints and coatings industry.

(ii) (ii) The bead mill module is comprised of a small inner bucket with zirconia beads and a small stirring wheel connected to the main shaft. An impeller disk is also connected to the lower end of the rotating shaft. During dispersion, the lower impeller disk creates a vertical flow forcing the liquid into the bead mill bucket. Inside the bead mill bucket, the zirconia bead break down the agglomerates. The bead mill stirring wheel forces the mixture to the bottom of the dispersion bucket to close the loop. The bead mill module was employed in

the preliminary experiments of this thesis. Evidence of filler particles breakage and reduction in aspect ratio values, led to the replacement with the impeller disk.

UL 94 fire rate classification

As related to plastic materials, there are 6 flame classifications that can be assigned to materials based on the open flame results. These classifications can be further divided in surface, vertical and horizontal groups.

- UL 94-5VA Surface Burn; Burning stops within 60 seconds and test specimens should not have a burn-through (no hole). This is the highest (most flame retardant) UL94 rating and can be achieved via special flame retardant formulations.
- UL 94-5VB Surface Burn; Burning stops within 60 seconds, test specimens could exhibit a burn-through (a hole may be present).
- UL 94 V-0 Vertical Burn; burning stops within 10 seconds while no flaming drips are allowed.
- UL 94 V-1 Vertical Burn; burning stops within 60 seconds while no flaming drips are allowed
- UL 94 V-2 Vertical Burn; burning stops within 60 seconds while flaming drips are allowed.
- UL 94 H-B Horizontal Burn; Slow horizontal burn test (H-B) are considered "self-extinguishing".

Especially for the HB classification a series of requirements should also be met:

- There are no visible signs of combustion after the ignition source is removed.
- Or the flame front does not pass the 25 mm reference mark
- Or the flame front passes the 25 mm reference mark but does not reach the 100 mm reference mark,
- Or the flame front reaches the 100 mm reference mark and the linear burning rate does not exceed 40 mm/min for specimens having a thickness between 3 and 13 mm or 75 mm/min for specimens having a thickness less than 3 mm.